TRANSPORTATION RESEARCH RECORD 888

Structural Performance of Pavement Systems

TRANSPORTATION RESEARCH BOARD

NATIONAL RESEARCH COUNCIL

NATIONAL ACADEMY OF SCIENCES
WASHINGTON, D.C. 1982

Transportation Research Record 888
Price $11.20
Edited for TRB by Scott C. Herman

modes
1 highway transportation
4 air transportation

subject area
24 pavement design and performance

Library of Congress Cataloging in Publication Data
National Research Council. Transportation Research Board.
Structural performance of pavement systems.

(Transportation research record; 888)
1. Pavements--Addresses, essays, lectures. I. Title.
II. Series.
TE7.H5 no. 888 [TE250] 380.5s [625.8] 83-8030
ISBN 0-309-03500-7 ISSN 0361-1981

Sponsorship of the Papers in This Transportation Research Record

GROUP 2--DESIGN AND CONSTRUCTION OF TRANSPORTATION FACILITIES
R. V. LeClerc, consultant, Olympia, Washington, chairman

Pavement Design Section
W. Ronald Hudson, University of Texas at Austin, chairman

Committee on Rigid Pavement Design
Richard A. McComb, Federal Highway Administration, chairman
Ernest J. Barenberg, Kenneth J. Boedecker, Jr., William E. Brewer, Albert J. Bush III, William J. Carson, Richard N. Cochrane, Bert E. Colley, Donald K. Emery, Jr., Raymond A. Forsyth, James L. Greene, Yang H. Huang, Ronald L. Hutchinson, Michael P. Jones, Richard W. Kinchen, T. J. Larsen, B. Frank McCullough, Robert G. Packard, Dwight E. Patton, Karl H. Renner, Surendra K. Saxena, Jens E. Simonsen, T. Paul Teng, Paul J. Witkiewicz, William A. Yrjanson

Committee on Flexible Pavement Design
R. G. Hicks, Oregon State University, chairman
Leon M. Noel, Federal Highway Administration, secretary
Ernest J. Barenberg, Robert A. Crawford, R. N. Doty, W. B. Drake, Fred N. Finn, Wade L. Gramling, William Bryan Greene, Roger V. LeClerc, Dallas N. Little, J. W. Lyon, Jr., Frank P. Nichols, Jr., Adrian Pelzner, Dale E. Peterson, William A. Phang, James A. Sherwood, James F. Shook, Eugene L. Skok, Jr., William T. Stapler, Hisao Tomita, Harvey J. Treybig, Harry H. Ulery, Jr., Loren M. Womack, Richard J. Worch

Committee on Pavement Rehabilitation Design
Gordon W. Beecroft, Oregon Department of Transportation, chairman
James F. Shook, The Asphalt Institute, secretary
Edward Aikman, Walter R. Barker, Martin L. Cawley, W. G. Davison, Paul J. Diethelm, Fred N. Finn, Wade L. Gramling, William Bryan Greene, W. J. Head, James W. Hill, Ali S. Kemahli, Edwin C. Lokken, Richard W. May, Carl L. Monismith, Gene R. Morris, Lawrence L. Smith, Richard L. Stewart, R. N. Stubstad, Harvey J. Treybig, Hugh L. Tyner, Matthew W. Witczak, Loren M. Womack

Committee on Strength and Deformation Characteristics of Pavement Sections
Amir N. Hanna, Portland Cement Association, chairman
Richard D. Barksdale, Stephen F. Brown, George R. Cochran, Gaylord Cumberledge, Jim W. Hall, Jr., R. G. Hicks, Robert K. H. Ho, Ignat V. Kalcheff, William J. Kenis, Thomas W. Kennedy, Erland Lukanen, Kamran Majidzadeh, Lufti Raad, J. Brent Rauhut, Quentin L. Robnett, Jatinder Sharma, Gary Wayne Sharpe, James F. Shook, Eugene L. Skok, Jr., T. Paul Teng, Mian-Chang Wang

Lawrence F. Spaine, Transportation Research Board staff

Sponsorship is indicated by a footnote at the end of each report. The organizational units, officers, and members are as of December 31, 1981.

Contents

Authors of the Papers in This Record

Bandyopadhyay, Sudipta S., Advanced Technology Section, National Soil Services, Inc., 5814 Heffernan Street, Houston, TX 77087

Chen, Nan Jim, Arizona Transportation Research Center, Arizona Department of Transportation, 206 South Seventeenth Avenue, Phoenix, AZ 85007

Ciolko, A.T., Transportation Development Department, Construction Technology Laboratories, Portland Cement Association, 5420 Old Orchard Road, Skokie, IL 60077

Colley, B.E., Transportation Development Department, Construction Technology Laboratories, Portland Cement Association, 5420 Old Orchard Road, Skokie, IL 60077

Di Vito, Joseph A., Arizona Transportation Research Center, Arizona Department of Transportation, 206 South Seventeenth Avenue, Phoenix, AZ 85007

Friberg, Bengt F., Consulting Engineer, 2 Downey Lane, St. Louis, MO 63132

Kennedy, Thomas W., Department of Civil Engineering, University of Texas at Austin, Austin, TX 78712

Luhr, David, College of Engineering, University of Texas at Austin, Austin, TX 78712

Lytton, Robert L., Department of Civil Engineering, Texas A&M University, College Station, TX 77840

MacLeod, D.R., Department of Civil Engineering, Carleton University, Ottawa, Ontario, Canada K1S 5B6

McCullough, B. Frank, Department of Civil Engineering, College of Engineering, University of Texas at Austin, Austin, TX 78712

Molenaar, A.A.A., Department of Civil Engineering, Laboratory for Road and Railroad Research, Delft University of Technology, 4 Stevinweg, 2628 CN Delft, The Netherlands

Monismith, C.L., Department of Civil Engineering, University of California-Berkeley, Berkeley, CA 94720

Morris, Gene R., Arizona Transportation Research Center, Arizona Department of Transportation, 206 South Seventeenth Avenue, Phoenix, AZ 85007

Nussbaum, P.J., Transportation Development Department, Construction Technology Laboratories, Portland Cement Association, 5420 Old Orchard Road, Skokie, IL 60077

Rauhut, J. Brent, Brent Rauhut Engineering, Inc., 912 Prairie Trail, Austin, TX 78758

Stanek, Floyd J., Office of Research, HRS-14, Federal Highway Administration, 400 7th Street, S.W., Washington, DC 20590

Tayabji, S.D., Transportation Development Department, Construction Technology Laboratories, Portland Cement Association, 5420 Old Orchard Road, Skokie, IL 60077

Uzan, Jacob, Department of Civil Engineering, Technion—Israel Institute of Technology, Haifa, Israel

Van Gurp, Ch. A.P.M., Department of Civil Engineering, Laboratory for Road and Railroad Research, Delft University of Technology, 4 Stevinweg, 2628 CN Delft, The Netherlands

Wang, M.C., Department of Civil Engineering, Pennsylvania State University, 212 Sackett Building, University Park, PA 16802

Yandell, W.O., School of Civil Engineering, University of New South Wales, P.O. Box 1, Kensington, New South Wales, Australia 2033

Prestressed Pavement Joint Designs

P.J. NUSSBAUM, S.D. TAYABJI, AND A.T. CIOLKO

Four transverse joint designs for prestressed concrete pavements are presented. Items considered in developing the designs include slab length, tendon force, tendon size, tendon spacing, desired midslab prestress, allowable joint movement, and use of one or two active joints between adjacent main slabs. Proper attention must be given to joint hardware design because a large number of items such as anchors, strands, load-transfer devices, infiltration-prevention devices, reinforcement, and positioning bars are located within a few inches of the joint. Therefore, detailing of joint hardware is a critical element of design. Designs I, II, and III are for an 8-in-thick pavement with main slab lengths of 350 ft. A short prestressed gap slab and a single active joint are used between the main slabs. Design IV is for a 7-in-thick pavement with main slab lengths of 250 ft. A tied concrete shoulder is used. Gap slabs are 10 in thick, conventionally reinforced, with an active joint at each end.

The objective of the Federal Highway Administration (FHWA) Research Project 5E, Premium Pavements for Zero Maintenance, is to exploit modern materials and technology in developing zero-maintenance pavements for warranted use. As a portion of this research project, an investigation has been conducted by Construction Technology Laboratories, a division of the Portland Cement Association. The objective of the investigation was to develop design and construction techniques for prestressed concrete pavements.

Prestressed pavement design includes the determination of required pavement thickness and joint hardware. Joint hardware is determined based on anticipated slab movement and length. Figure 1 shows the basic steps involved in prestressed pavement design.

As shown in Figure 1, the prestressed pavement design process is iterative and involves the interaction of many factors. The process starts with the selection of an initial slab thickness. Then, for joint hardware design, trial main slab length and

Figure 1. Prestressed pavement design process.

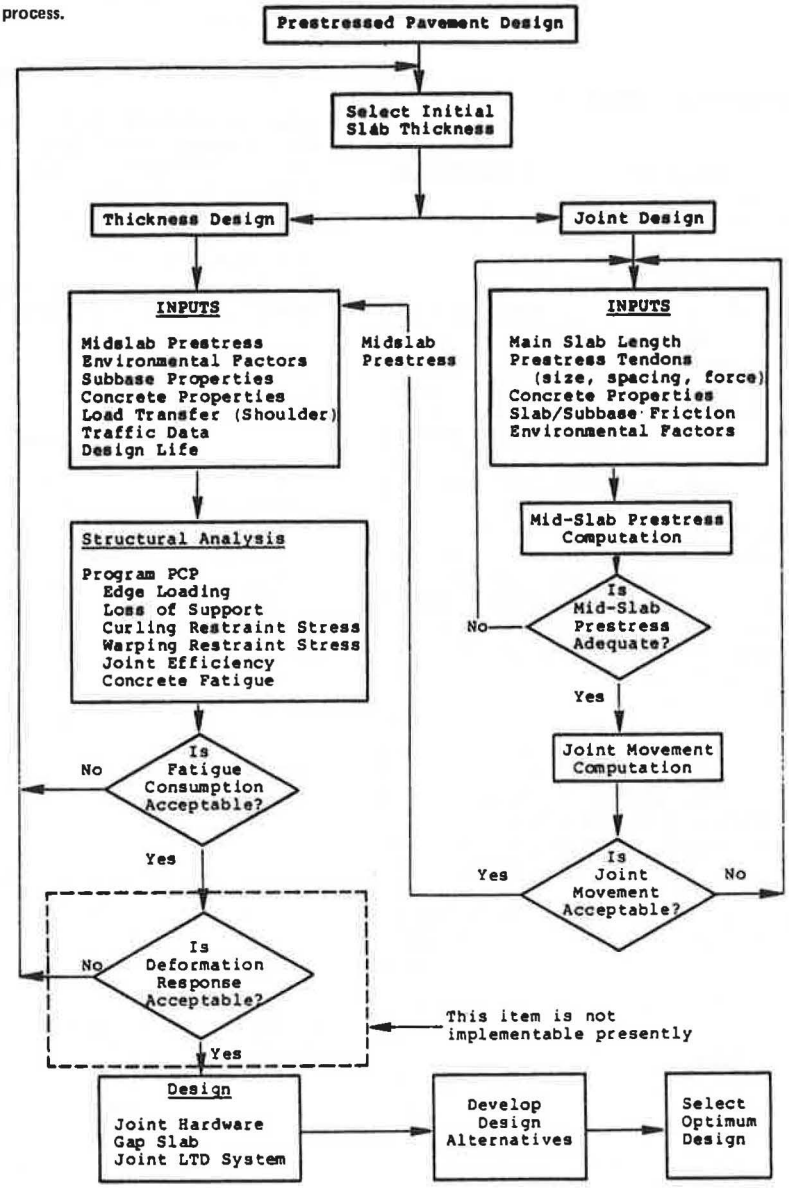

prestress tendon size, spacing, and force are selected. Effective midslab prestress is computed. A minimum of about 50-psi midslab prestress should be obtained. If it is not obtained, slab length, tendon size, spacing, or force is varied until the desired midslab prestress is obtained.

When the midslab prestress criterion is satisfied, anticipated maximum joint movement is computed. Selection of an appropriate joint infiltration-prevention device such as a strip seal, compression seal, or steel cover plate depends on the magnitude of total joint movement. Total movement may be accommodated at one or two active joints between adjacent slabs. Slab length is varied until computed joint movement can be accommodated by the device selected.

After slab length, midslab prestress level, and joint hardware are established, a structural analysis is performed. This analysis requires a value of effective midslab prestress as an input. The structural analysis computes fatigue consumption due to edge stresses at midslab. If fatigue consumption is more than 100 percent, the design process is repeated by using a larger slab thickness.

This paper presents transverse joint designs for prestressed pavements. Further design details are given elsewhere (1).

JOINT DESIGN STEPS

Joint design for prestressed pavements involves the following steps:

1. Determination of required pavement thickness;
2. Selection of slab length;
3. Determination of prestressing tendon size, spacing, and force; and
4. Detailing of joint hardware.

Proper attention must be given to joint hardware design because a large number of items such as anchors, strands, load-transfer devices, infiltration-prevention devices, reinforcement, and positioning bars are located within a few inches of the joint. Detailing of joint hardware is, therefore, a critical element of design. Detailing requirements also put a limit on the practical minimum slab thickness that can be used for construction.

Prestressed pavement thickness is determined by using the computer program presented in Tayabji and others (2). This program considers the case of loads applied at or near a longitudinal edge. Bottom fiber stresses due to load, temperature differentials, moisture differentials, and midslab prestress are determined and summed for different magnitudes of traffic load. The resultant stress for each loading consumes a portion of the pavement's fatigue resistance. The design thickness is that for which fatigue consumption generally ranges between 60 and 100 percent. By using this procedure, a small compressive stress is maintained in the slab.

Thickness design is based on edge loading; consideration is given to stresses due to temperature, moisture, edge support loss, and the presence or absence of a tied concrete shoulder. On this basis, thickness requirements were 7 and 8 in for zero-maintenance pavements with and without a tied shoulder, respectively (2).

Selection of slab length and tendon force, size, and spacing is influenced by the desired minimum prestress level at midslab and the allowable joint movement. As noted previously, this selection process is iterative. Several trial selections are required before a satisfactory solution is achieved. A brief discussion of factors considered in computing midslab prestress and joint movement follows.

PRESTRESS REQUIREMENTS

End prestress must be sufficient to provide a minimum midslab prestress of about 50 psi after subtracting losses due to tendon friction, concrete shrinkage, concrete creep, steel relaxation, and subbase friction restraint. Equations for computing losses are given elsewhere (1).

Equations for computing prestress losses require the use of an end prestress value. This means an initial value is assumed and a final value is determined by an iterative process. One method of shortening this process is to make judgment assumptions regarding tendon diameter, spacing, and stress level. For example, if 0.6-in-diameter tendons are stressed to 70 percent of ultimate, the allowable tendon force is 41 000 lb. For tendons spaced at 18-in centers in an 8-in-thick pavement, initial end prestress is 285 psi. This procedure was used to compute losses for examples shown in Table 1. Coefficients and other values required for computations are listed in Table 2.

SLAB END MOVEMENTS

Slab end movements result from daily and seasonal temperature variations and concrete drying shrinkage and creep.

Temperature-Associated Movements

Temperature-associated movements are functions of the concrete coefficient of thermal expansion and local temperature variations. Movements are affected by seasonal as well as daily temperature effects. Seasonal movements take place over a long period of time; therefore, it is assumed that slab-to-subbase friction does not restrict movement (3). Daily movements due to temperature variation are affected by slab-to-subbase friction; therefore, daily

Table 1. Prestress calculations.

Item	General Calculations	
	Slab 7 in Thick	Slab 8 in Thick
Slab length (ft)	250	350
Strand diameter (in)	0.6	0.6
Strand force (kips)	41	44
Strand spacing (in)	24	18
End of slab prestress (psi)	244	306
Prestress losses (psi)		
Shrinkage	6	6
Creep	4	6
Relaxation	20	31
Strand friction	39	66
Subbase friction	100	140
Total	169	249
Midslab prestress (psi)	75	57

Table 2. Prestress loss computation coefficients.

Item	Magnitude
Tendon ultimate strength (psi)	270 000
Area, 0.6-in-diameter tendon (in^2)	0.217
Concrete creep coefficient	2.5
Concrete shrinkage strain (millionths)	150
Strand relaxation coefficient	
70 percent of ultimate stress	0.08
75 percent of ultimate stress	0.10
Wobble friction coefficient per foot	0.0014
Subbase friction factor	0.8
Modulus of elasticity of steel (million psi)	28
Modulus of elasticity of concrete (million psi)	5

movements are corrected for subbase frictional restraint.

During winter, slab concrete is more moist than in the summer. This results in a concrete coefficient of thermal expansion that is about 15 percent lower than that for concrete in a drier state (4). This factor is considered for computation of daily temperature-associated movements for winter months.

Seasonal slab movement is given by the following equation:

$$d_1 = \alpha(\Delta t)L \quad (1)$$

where

d_1 = slab movement associated with seasonal temperature changes,
α = coefficient of thermal expansion of concrete,
Δt = seasonal variation in average concrete temperature, and
L = slab length (ft).

Maximum daily slab movement during the summer months is given by the following equation:

$$d_2 = \alpha(\Delta t_s)L - d_f \quad (2)$$

where

d_2 = slab movement associated with daily temperature variation during summer,
Δt_s = summer maximum temperature less summer average temperature, and
d_f = slab movement restrained by subbase friction, i.e.,

$$d_f = (\sigma_f/2E_c)L \quad (3)$$

where σ_f is the maximum subbase friction restraint stress, and E is the modulus of elasticity.

Maximum daily slab movement during the winter months is given by the following equation:

$$d_3 = 0.85\,\alpha(\Delta t_w)L - d_f \quad (4)$$

where d_3 is the slab movement associated with daily temperature variation during winter and Δt_w is the winter average temperature less winter minimum temperature.

Shrinkage

Shrinkage strain is influenced by amount of mixing water, water-cement ratio, aggregate type, and curing conditions. For concrete prisms drying from all faces, long-term shrinkage strain varies from 100 to 500 millionths (5). For slabs drying only from the top, a value of 250 millionths has been assumed. About 100 millionths of this strain takes place within the first month. Because gap slabs are not placed until about one month after main slabs are cast, only 150 millionths strain needs to be considered in computing future slab shortening.

Slab shrinkage is given by the following equation:

$$d_4 = \epsilon_s L \quad (5)$$

where d_4 is the slab shortening due to shrinkage and ϵ_s is the concrete shrinkage strain.

Concrete Creep

Creep is the long-term shortening of concrete subjected to sustained stress. The relation between concrete creep strain (ϵ_k) and elastic strain is expressed by the following equation (6):

$$\epsilon_k = C_u(f_{av}/E_c) \quad (6)$$

where f_{av} is the average prestress along the slab length (psi) and C_u is the ultimate creep coefficient.

Slab shortening due to creep (d_5) is then given by the following equation:

$$d_5 = \epsilon_k L \quad (7)$$

Creep magnitude varies with gradation of concrete aggregates, particle shape, aggregate type, cement content, water-cement ratio, concrete density, curing, age at loading, load intensity, and concrete element size. A creep coefficient of 2.5 is suggested for computing creep-associated shortening of prestressed pavements.

Two examples of slab end movement computations are presented for the four joint designs presented in this paper. Coefficients, weather information, and other factors used in the calculations are listed in Table 3.

Designs I, II, and III

Computations are for an 8-in-thick pavement with 350-ft-long main slabs. One active joint is used at the gap slab. The movements are as follows:

d_1 = 1.32 in,
d_2 = 0.38 in,
d_3 = 0.62 in,
d_4 = 0.64 in, and
d_5 = 0.32 in.

The total movement at an active joint equals $d_1 + d_2 + d_3 + d_4 + d_5$ = 3.28 in.

Design IV

Computations are made for a 7-in-thick pavement with 250-ft-long main slabs. Two active joints are used at the gap slab. The movements are as follows:

d_1 = 0.47 in,
d_2 = 0.14 in,
d_3 = 0.22 in,
d_4 = 0.22 in, and
d_5 = 0.12 in.

The total movement at each active joint equals $d_1 + d_2 + d_3 + d_4 + d_5$ = 1.17 in.

Knowledge of slab end movements is essential to setting the initial opening at active joints of gap slabs. It is also important in selecting the size of compression seals, width of cover plates, and ex-

Table 3. End movement computation coefficients.

Item	Magnitude
Modulus of elasticity of concrete (million psi)	5
Concrete creep coefficient	2.5
Coefficient of thermal expansion, summer (in/in/°F)	0.000 005 0
Coefficient of thermal expansion, winter (in/in/°F)	0.000 004 3
Concrete shrinkage strain (millionths)	150
Slab-to-subbase friction factor	0.8
Summer avg concrete temperature (°F)	93
Winter avg concrete temperature (°F)	30
Seasonal variation in avg concrete temperature (°F)	63
Summer maximum concrete temperature (°F)	114
Winter minimum concrete temperature (°F)	-8
Summer maximum temperature excess of avg (°F)	21
Winter minimum temperature less than avg (°F)	38
Avg slab prestress for 7-in-thick pavement (psi)	165
Avg slab prestress for 8-in-thick pavement (psi)	160

tensibility requirements of compressive and strip seals.

The average concrete temperature during placement of gap slabs is used to determine the initial width of active joints. From design I calculations, it is seen that a joint width set at 93°F would be expected to close 0.38 in due to daily summer temperature variation. Extrapolation shows that for a placement temperature of 72°F, closure would be 0.76 in. Thus, the joint width set for the latter condition would be double that required for the first.

Table 4. Joint design parameters.

Item	General Parameters	
	Slab 8 in Thick	Slab 7 in Thick
Main slab length (ft)	350	250
Gap slab thickness (in)	8	10
Gap slab length (in)	59	59
Design condition	Free edge	Tied shoulder
No. of active joints	1	2
Tendon diameter (in)	0.6	0.6
Tendon spacing (in)	18	24
Tendon load (kips)	44	41
End of slab prestress (psi)	306	244
Midslab prestress (psi)	57	75
Movement at each joint (in)	3.3	1.2

JOINT DESIGNS

Four transverse joint designs are presented. Designs I, II, and III are for an 8-in-thick pavement with main slab lengths of 350 ft. A single active joint between adjacent main slabs is used for these designs. Design IV is for a 7-in-thick pavement with a tied concrete shoulder. Main slab lengths are 250 ft. Two active joints between adjacent main slabs are used for this design.

Gap spaces are left between ends of main slabs to accommodate posttensioning operations. Gap slabs are cast in these spaces approximately 30 days after

Figure 2. Design I, overall view.

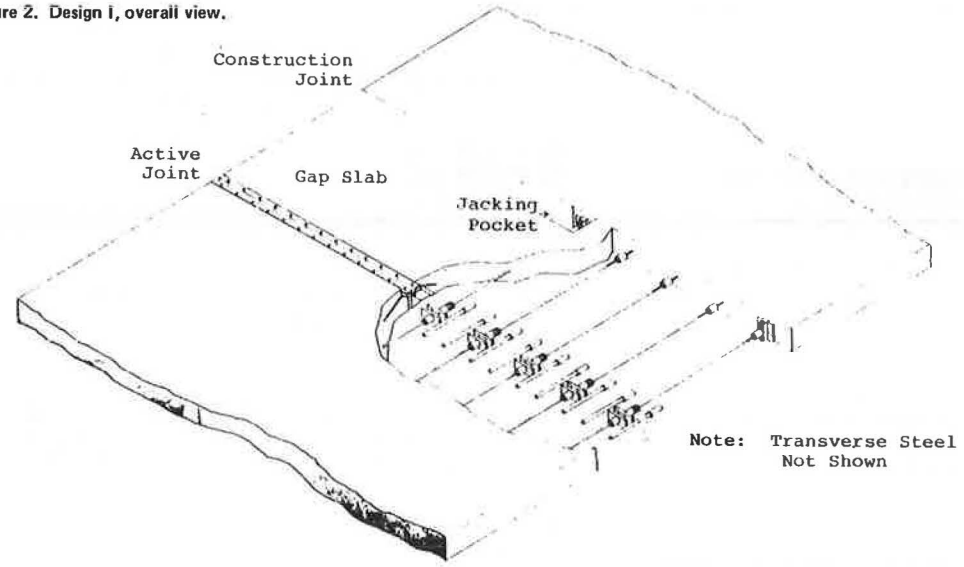

Figure 3. Design I, plan.

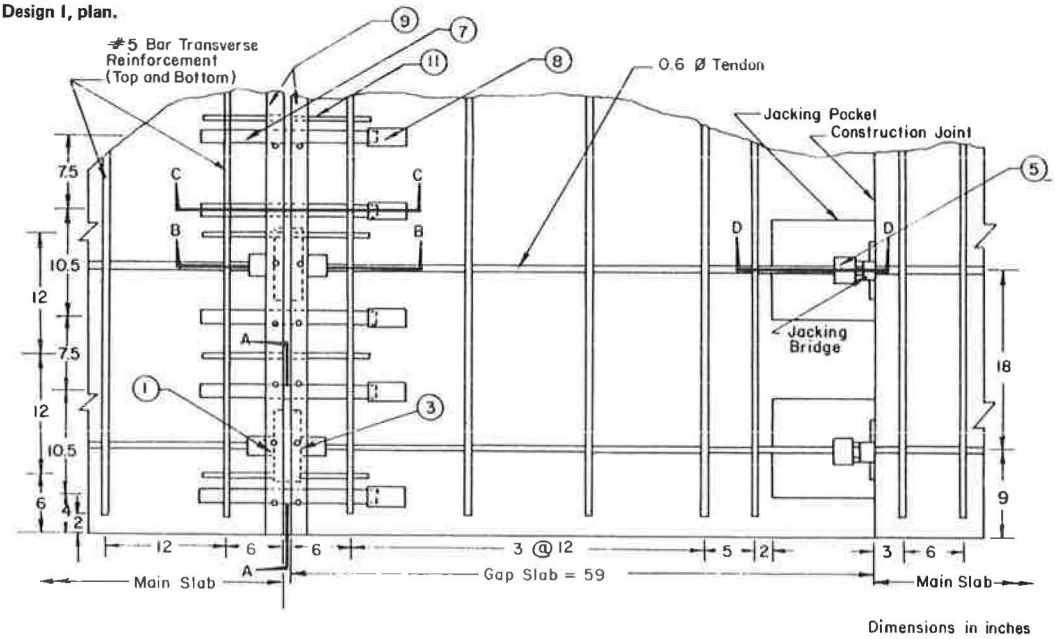

Figure 4. Section B-B, design I.

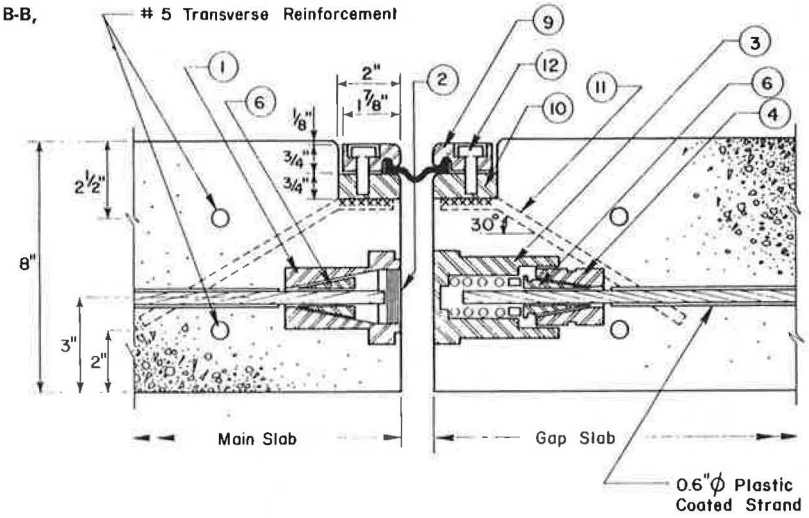

Figure 5. Section D-D, design I.

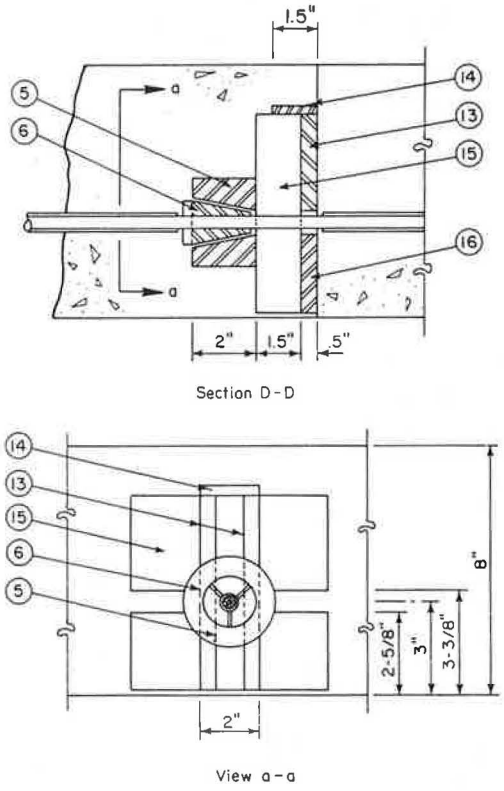

Table 5. Joint hardware for design I.

Item	Description	Dimension
1	Combined chuck anchor bodies (Figure 6)	For 0.6-in strand
2	Stainless-steel caps to fit anchor body (Figure 4)	
3	Automatic seating anchors (Figure 7)	For 0.6-in strand
4	Externally threaded chucks	For 0.6-in strand
5	Barrel chucks for temporary prestressing and stress transfer (Figure 5)	2.75x2 in long
6	Three-jawed wedges (Figure 4)	For 0.6-in strand
7	Stainless-steel dowels (Figure 3)	1.25 in thick, 18 in long
8	Dowel caps (Figure 3)	1.3125 in inside diameter by 4 in
9	Extrusions for upper portion of seal holder with holes for bolts (Figure 4)	6 ft long, 0.75x1.875 in
10	Extrusions for lower portion of seal holder drilled and tapped (Figure 4)	6 ft long, 0.75x2 in
11	No. 3 deformed bars welded to lower seal holder extrusion (Figure 4)	9 in long[a]
12	Bolts (Figure 4)	0.5 in
13	Steel plates (Figure 5)	6.25x2.75x0.5 in
14	Steel plates (Figure 5)	2x1.5x0.25 in
15	Steel plates (Figure 5)	6x3x0.5 in
16	Steel plates (Figure 5)	6x2.5x0.5 in

[a]Bent as shown in Figure 6.

main slab placement. Prestressed pavement construction details are given elsewhere (7). Joint design parameters used for this paper are listed in Table 4.

Design I: Strand Prestressed Gap Slab

An overall view of a joint designed for an 8-in-thick pavement with main slab lengths of 350 ft is shown in Figure 2. For clarity of viewing, the transverse steel located near the ends of main slabs and in the gap slab is not shown.

In this design, main slab prestress is applied at construction and active joint faces. Tendons from the construction joint face are continued to anchorage devices located at the active joint. Jacking pockets are provided at the construction joint for posttensioning the gap slab. Gap slab tensioning is accomplished by using a jacking system that grasps the construction joint chuck and advances the tendon into the anchorage device. The anchorage device automatically grips the strand as it is advanced. A more descriptive account of each step in the process, together with details concerning jacking equipment and procedures, is given in the construction manual (7).

A plan view of design I is shown in Figure 3. Additional details of joint hardware locations and dimensions are shown in Figures 4 and 5 for sections B-B and D-D. Circled numbers on the drawings refer to the parts that are listed (with dimensions) in Table 5.

Tendon anchors, load-transfer devices, and methods of preventing infiltration are major joint hardware. These items are discussed separately.

Anchors

Two types of permanent anchors were designed for use at active joints. One type, which is located in the main slab, combines the anchor body and chuck into one casting. Bearing is provided close to the joint

Conventional anchors are used in jacking pockets located at the construction joint face. Tendons and anchors are positioned below slab middepth to reduce upward warping of slab ends. Tendon centers are located 5 in below the slab surface.
face. Tendons and wedges are protected from corrosion by a stainless-steel cap threaded into the anchor after completion of tensioning. A sectional view of this anchor is shown in Figure 4. Details are shown in Figure 6.

The second type of permanent anchor is located at the active joint face of the gap slab. The anchor body is threaded internally to accept an externally threaded chuck. Anchors are provided with springs to prevent wedges from moving toward the joint face during gap slab prestressing. Sufficient space is provided within the anchor body to permit strand extension during prestressing operations. These springs also provide positive seating of wedges. A sectional view of this anchor is shown in Figure 4. Details are presented in Figure 7.

Load Transfer

Stainless-steel dowels 1.25 in in diameter are located on each side of the anchors. Transverse spacing is shown in Figure 3. Dowels are embedded in the concrete of the main slabs at active joint ends. That portion of the dowel that extends into the gap slabs are greased, and caps are placed over dowel ends to assure unrestrained slab end movements.

Infiltration Prevention

Premolded nylon-reinforced neoprene-strip seals are used to prevent joint infiltration. Strip-seal holders consist of upper and lower steel extrusions, as shown in Figure 4. Dimensions of top elements are 1.875x0.75 in. One side is shaped to hold the longitudinal edge of the strip seals. The tops of the extrusions are set 0.125 in below the concrete surface for protection from snowplow blades.

Top extrusions are drilled and countersunk to recess 0.5-in bolts used for clamping the upper sealholder extrusion to the lower extrusion. Bolt spacing is 6 in on centers. The lower extrusion is drilled and tapped at spacings to match those in the upper extrusion. The lower extrusion is anchored in the slab by No. 4 deformed bars.

Several different diaphragms or strip seals can be used with this joint design. Generally, diaphragm or strip seals are premolded extruded neoprene or natural rubber folds that extend the length of the joint. They are mechanically anchored to each side of the joint. Normally, 0.125- to 0.375-in-thick neoprene is used. The neoprene is usually reinforced with fibers to provide tensile strength and resist puncturing.

Design II: Rod Prestressed Gap Slab

An overall view of design II is shown in Figure 8. This design is for an 8-in-thick pavement with main slab lengths of 350 ft. Rods and nuts are used to prestress the gap slab from jacking pockets. Splice chucks located in these pockets join tendons and rods. Jacking in the pocket advances the rod into the anchor. The rod nut located at the gap slab active joint face is tightened to maintain prestress. This system eliminates the need for the temporary jacking bridge used at the construction joint face of the main slab in design I. In addition, the specially designed anchors used at active joints in design I are not required. Dowels are used at the active joint to transfer load. Additional details of joint hardware locations and dimensions are given elsewhere (1).

Figure 6. Permanent anchor.

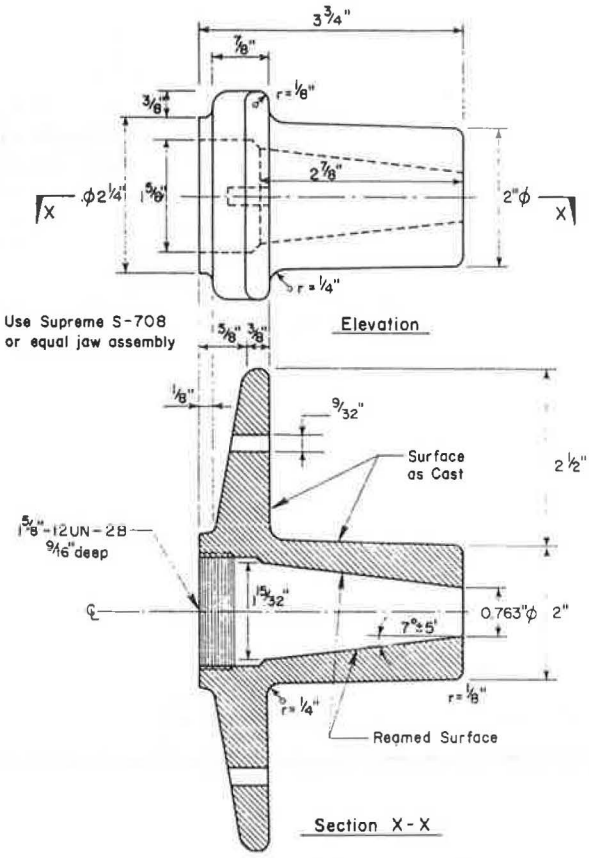

Figure 7. Automatic seating anchor.

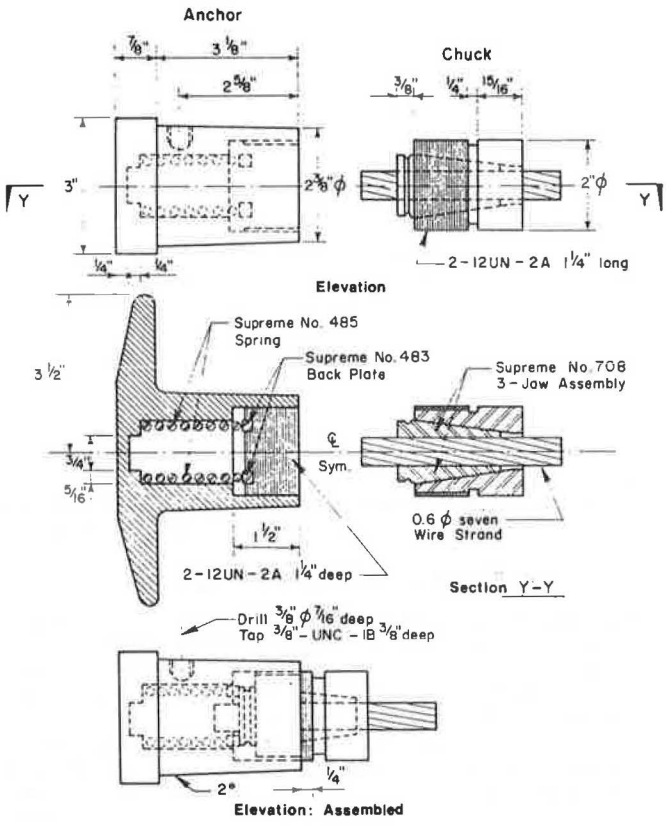

Figure 8. Design II, overall view.

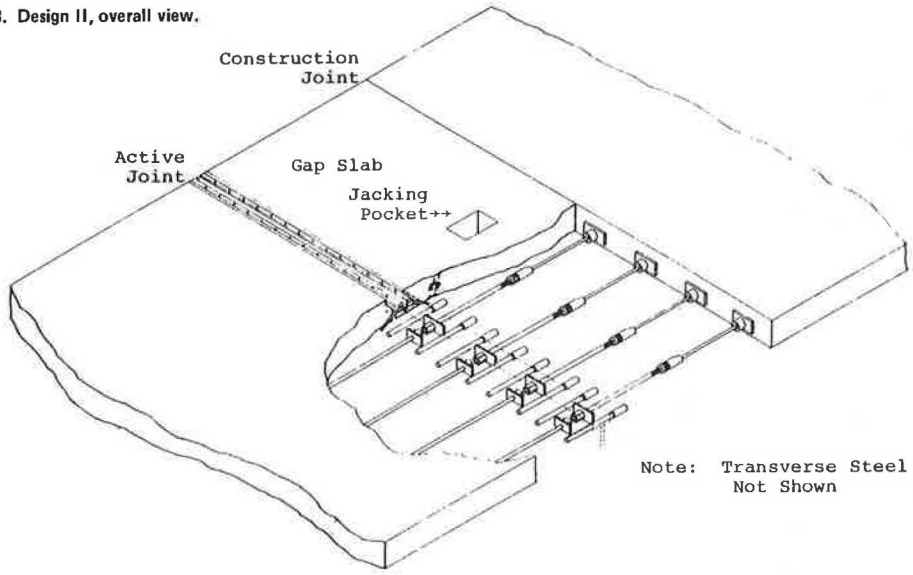

Figure 9. Design III, overall view.

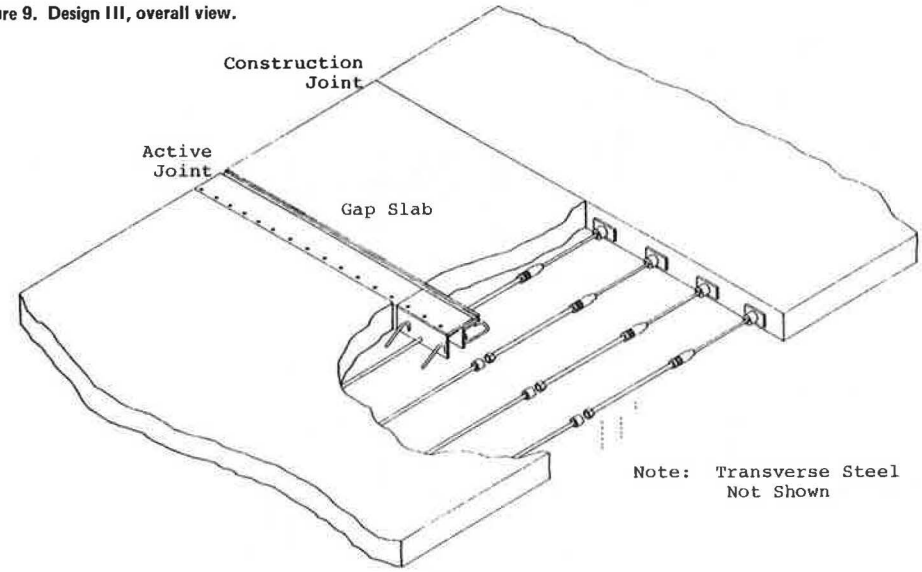

Design III: Cover Plate Joint

An overall view of design III is shown in Figure 9. This design, which is for an 8-in-thick pavement with main slab lengths of 350 ft, also uses a rod-and-nut system to prestress the gap slab. However, posttensioning is accomplished by manual torquing of the nut located at the active joint face. Thus, jacking pockets are not required. The steel cover plate joint serves as bearing for tensioning tendons and nuts at the active joint. In addition, cover plates contribute to load transfer.

Additional details of joint hardware locations and dimensions are given elsewhere (1).

Design IV: Compression Seal Joint

An overall view of design IV is shown in Figure 10. This design is for a 7-in-thick pavement with main slab lengths of 250 ft. Main slab pavement thickness is reduced because a tied concrete shoulder is used. Prestressing is terminated at main slab ends. Gap slabs are 10 in thick and are conventionally reinforced. An active joint is provided at each end of the gap slab. Dowels provide load transfer at active joints.

A plan view of design IV is shown in Figure 11. Additional details of joint hardware and dimensions are shown in Figures 12 and 13. Items designated by circled numbers are described in Table 6.

As shown in Figure 12, a compression seal is used at the active joint. Seals must accommodate an anticipated joint opening of 1.2 in. Concrete shoulders prevent downward seal movement. Stainless-steel dowels spaced at 12-in centers are located 4 in below the slab surface. Tendon anchors are "off-the-shelf" models. Anchor faces are recessed to provide space for grout corrosion protection.

SUMMARY

Four joint designs for use with prestressed pavements are presented. Details are provided for 7- and 8-in-thick pavements. These thicknesses are computed to be satisfactory for zero-maintenance designs developed for heavily trafficked freeways. For less-heavy traffic, smaller thicknesses may be

Figure 10. Design IV, overall view.

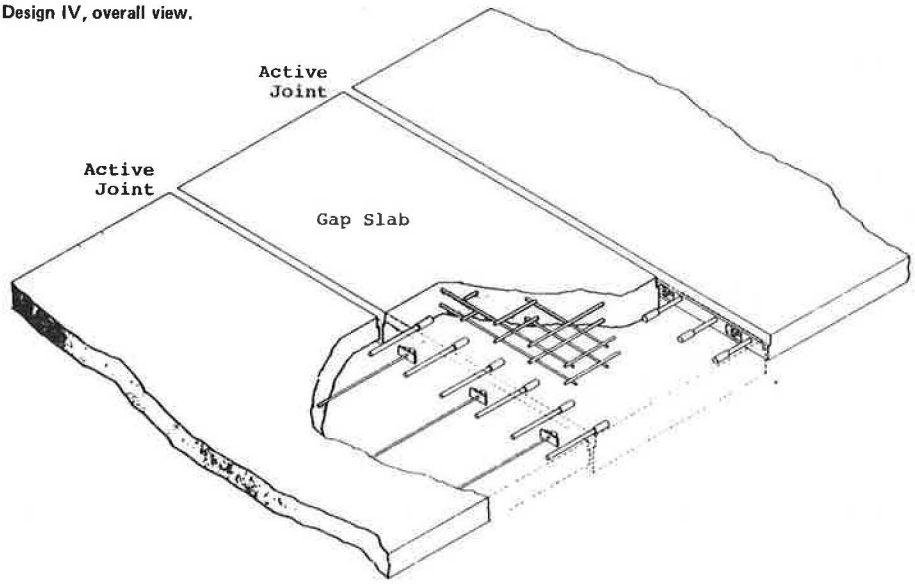

Figure 11. Design IV, plan.

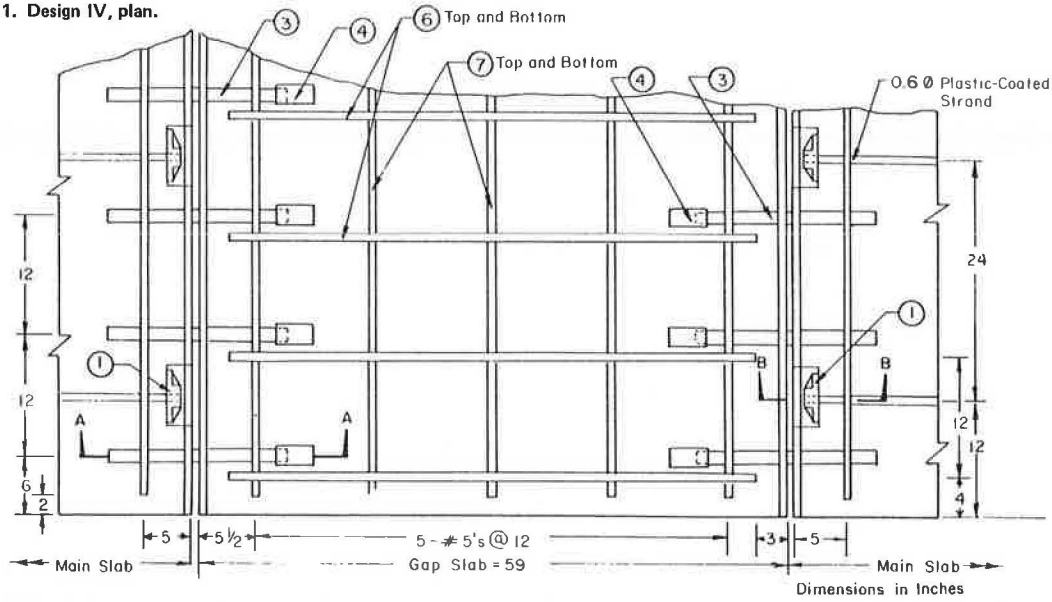

Figure 12. Section A-A, design IV.

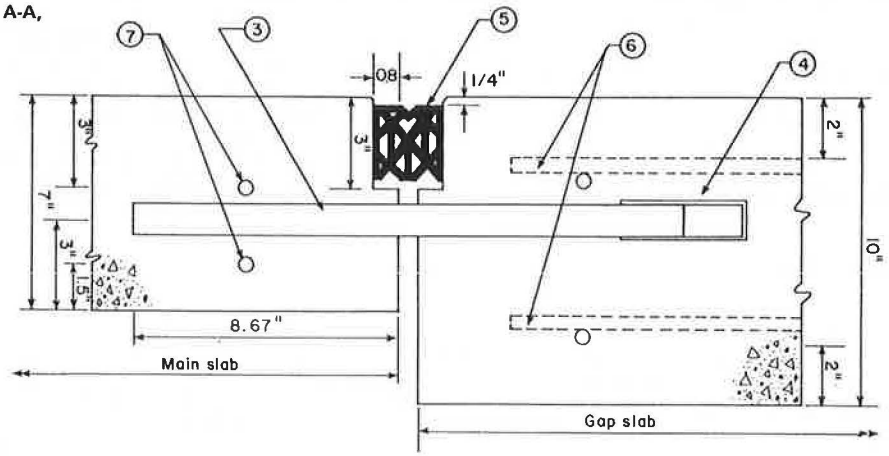

ciated with these neoprene strips since their installation in 1975, including the design for fastening the edges to the slabs.

4. The method of posttensioning the gap slab in design I is the same concept as was used in the design and construction of the prestressed pavement near Harrisburg, Pennsylvania, in 1976. This method is presented in the PCA report (8). The valuable research information and knowledge obtained from this first-of-its-kind method constructed in the United States identified ways to improve the procedural techniques for posttensioning the gap slab. Joint design II merely presents another procedural technique for performing this posttensioning operation.

5. The use of the cover plate in design III for the 8-in, 350-ft slab is the same concept used in the two German airfield pavements in 1959 and 1960 (8, Figures 26 and 27, pp. 51-52).

6. The paper states that the length of the pavement slab is varied until the computed joint movements can be accommodated by the joint device selected. This is contrary to the procedure practiced heretofore by well-known designers and contributors who first determine (or select) the length of the pavement slab and then design the joint to accommodate the predesigned slab. The paper offers no explanation or reason as to why it recommends this reversal in design procedure from current practice.

7. In the discussion of joint design IV, it is stated that a 7-in pavement thickness can be used because the pavement is tied to the shoulder. The paper does not explain how this partial transfer of the vehicle load to the shoulder is to be achieved or, equally important, how this tie with the shoulder may influence the slab end movements and the design of the gap slab.

8. The paper states that tendons and anchors are positioned below slab middepth to reduce upward warping of slab ends. But yet no explanation is given as to how this eccentric prestressing, as recognized and used in current practice, will influence or effect the design of the slab.

9. The paper states that the design process starts with the selection of an initial slab thickness based on a minimum midslab prestress of only 50 psi. Other designers and contributors to prestressed pavement technology claim and substantiate their midslab prestress of 200 psi or more can be maintained in slab lengths of 400-500 ft. For the two slab thicknesses of 7 and 8 in, the paper presents slab lengths of only 250 and 350 ft, respectively.

10. The paper does not give any explanation or rationale as to why only one active joint is proposed for the longer slab but two active joints are proposed for the shorter slab, wherein the joint must accommodate end movements due to half of the slab length only.

11. In the section on slab end movements, the paper discusses long-term creep but does not discuss the seasonal effects of moisture. Among others, the potential benefits of moisture effects were substantiated in previous work conducted in 1956-1959 at the University of Missouri at Rolla. The potential benefits of moisture effects are reported in the literature by Teller and Sutherland (9), Friberg (10), and Kelley (11). Application of these findings indicates that the slab end movements presented in the paper may be reduced by as much as 1 in.

(Note: This discussion paper reflects my views only and does not necessarily reflect the official views or position of FHWA.)

Authors' Closure

We thank Stanek for his review of the paper. We are pleased that he acknowledges our appreciation of the fine pioneering work done in prestressed pavements by other researchers. A detailed review of this pioneering work is included in our first report on the project (8).

As Stanek states in his comments 1-5, we were guided by the past work of others in developing joint systems that are engineered to provide the required levels of performance.

The approach we used in determining the design slab length for the examples presented in the paper was based primarily on two considerations. First, the commercial availability of joint seals that can accommodate large joint movements influences the allowable magnitude of joint movement, and thus slab length. Second, the maximum joint opening is limited to about 3-4 in to prevent tire ingress into joints. This procedure is not a reversal from current practice. It is the established practice for joint designs that involve large openings.

With regard to provisions for a tied shoulder, we recommend use of a prestressed tied shoulder. Mainline lanes and the shoulder are cast in the same paving operation and prestressed at the same time. Thus, differential length changes between main-line pavement and shoulder are avoided. A weakened-plane longitudinal joint is provided between the outside lane and the shoulder.

Although additional prestressing is developed due to eccentric placement of tendons, this effect exists only at slab ends. As a simple analysis of a semi-infinite slab on elastic foundation shows, the effect of the moment developed due to tendon eccentricity dissipates rapidly away from slab ends. Therefore, although tendon eccentricity reduces upward-warping deformation at slab ends, it does not contribute to stresses in the interior portion of the slab.

Our approach to prestressed pavement design is not to provide as much midslab prestress as possible. It is rather to provide a minimum level of prestress to ensure that early cracks that may develop remain tightly closed. We do not object to the use of higher prestress levels, but we believe that higher prestress should be used to increase slab lengths or to provide an added factor of safety. However, unless satisfactory slab deformation response is assured, higher midslab prestress should not be used just to reduce slab thickness.

It should be noted that the calculated design midslab prestress level for the Arizona demonstration project was 42 psi (12). In addition, the measured midslab prestress at the Mississippi demonstration project, immediately after final prestressing, was 60 psi for sections that incorporated two layers of polyethylene under the slab (13).

Single active joints between main slabs are used to reduce the number of active joints. For design IV, use was made of shorter slab lengths and two active joints to permit use of compression seals. Design IV illustrates an economical option for joint hardware.

With regard to the influence of moisture effects, we believe that slab lengthening during winter months is not substantial at the slab surface. The reason the slab top does not lengthen as much as the bottom is due to drying shrinkage at the surface. This drying shrinkage is not fully recoverable and, in addition, slab shortening due to temperature is greater at the pavement surface.

Figure 13. Section B-B, design IV.

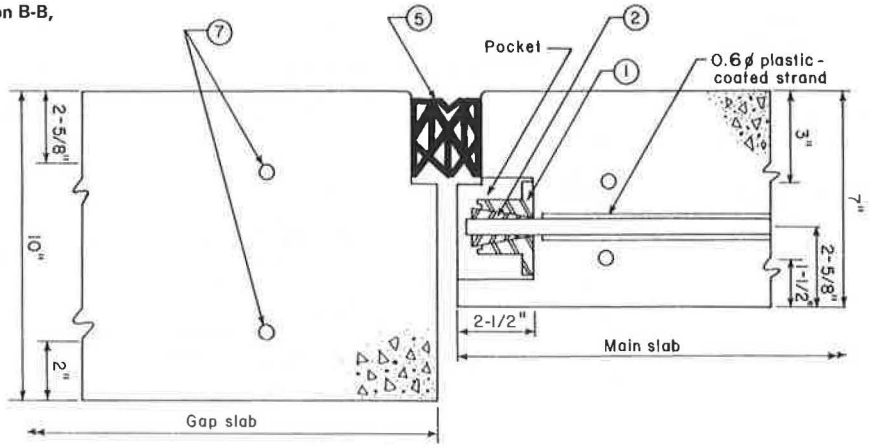

Table 6. Joint hardware for design II.

Item	Description	Dimension
1	Standard anchors (Figure 11)	3x5.25 in for 0.6-in strand
2	Three-jawed wedges (Figure 13)	For 0.6-in strand
3	Stainless-steel dowels (Figure 12)	18 in long, 1.125 in
4	Dowel caps (Figure 12)	4 in long to fit over 1.125-in dowel
5	Compression seal ACMASEAL (K-400) (Figure 12)	36 ft long, nominal uncompressed 2.5 in high, 3.4 in wide
6	No. 5 bar longitudinal reinforcement (Figure 12)	54 in long
7	No. 5 bar transverse reinforcement (Figure 11)	35 ft long

satisfactory. Joint design details in this paper can be easily adapted to other thicknesses by making the necessary dimensional changes.

ACKNOWLEDGMENT

The work was conducted by the Transportation Development Department of Construction Technology Laboratories under the direction of Bert E. Colley. W.G. Corley, director, Engineering Development Division, reviewed the text of this paper and made valuable suggestions.

Bengt F. Friberg acted as a principal consultant and contributed to all phases of the study. His participation is gratefully acknowledged. In addition, Wolfgang Krahl also served as a consultant and contributed to many phases of the study. T.F. McMahon and W. Kenis of FHWA provided technical coordination. Their cooperation and suggestions are gratefully acknowledged.

The opinions and findings expressed or implied in the paper are ours. They are not necessarily those of FHWA.

Discussion

Floyd J. Stanek

The comments in this discussion paper were formulated from information received while I served as technical monitor and coordinator for two studies of prestressed pavements sponsored by the Office of Research, FHWA. One study was a coordinated study by three state highway agencies to conduct an on-site inspection for the study, Performance of Prestressed Pavements in Four States. The representative members of this inspection team are Wade L. Gramling, Pennsylvania Department of Transportation (DOT); Gene Morris, Arizona DOT; and T. Paul Teng, Mississippi State Highway Department.

The other study was a follow-up research study of the Prestressed Pavement Demonstration Project, which was constructed in 1971-1972 near Dulles International Airport, Loudoun County, Virginia. This study was conducted by Bengt Friberg, one of the principal contributors to the original design and construction of this project. I served as monitor of this project for the Office of Research, FHWA, since 1972 and was closely associated with Friberg during the past 18 months for the completion of this study. A research report for each of these two studies is scheduled for future publication by FHWA.

For proper assessment, the subject paper, Prestressed Pavement Joint Design, should be viewed in the context of the following specific comments.

1. Several designs of previous contributors are presented in a report by the Portland Cement Association (PCA) (8). This report gives a summary account of the expansion joints used in the prestressed pavement demonstration projects constructed in the early 1970s in Virginia and Pennsylvania and also of the joints in roadways and airfield pavements constructed in Germany during the 1950s.

2. The design of the load-transfer mechanism for joint design I for an 8-in, 350-ft slab is similar to the dowel design in the 6-in-thick prestressed pavement constructed near Dulles International Airport. This dowel design is shown in the PCA report (8, Figure 33, p. 61). Stainless-steel dowels were not available during the scheduled construction of this project. The initial dowels of ordinary steel were replaced with stainless-steel dowels in 1975. The valuable research information and knowledge obtained from this demonstration project support the recommendation that stainless-steel dowels should be used.

3. Similarly, except for the technique of fastening the edges to the pavement slab, the neoprene-strip seals in design I are the same as those initially recommended for the design of the Dulles Prestressed Pavement Demonstration Project. At the time of construction during the winter of 1971-1972, there was some question of long-term reliability of the particular design proposed for fastening the edges to the pavement slab. Polyurethane foam was installed initially, but it was later replaced with neoprene strips. There has been no problem asso-

Figure 1. Prestress pavement design process.

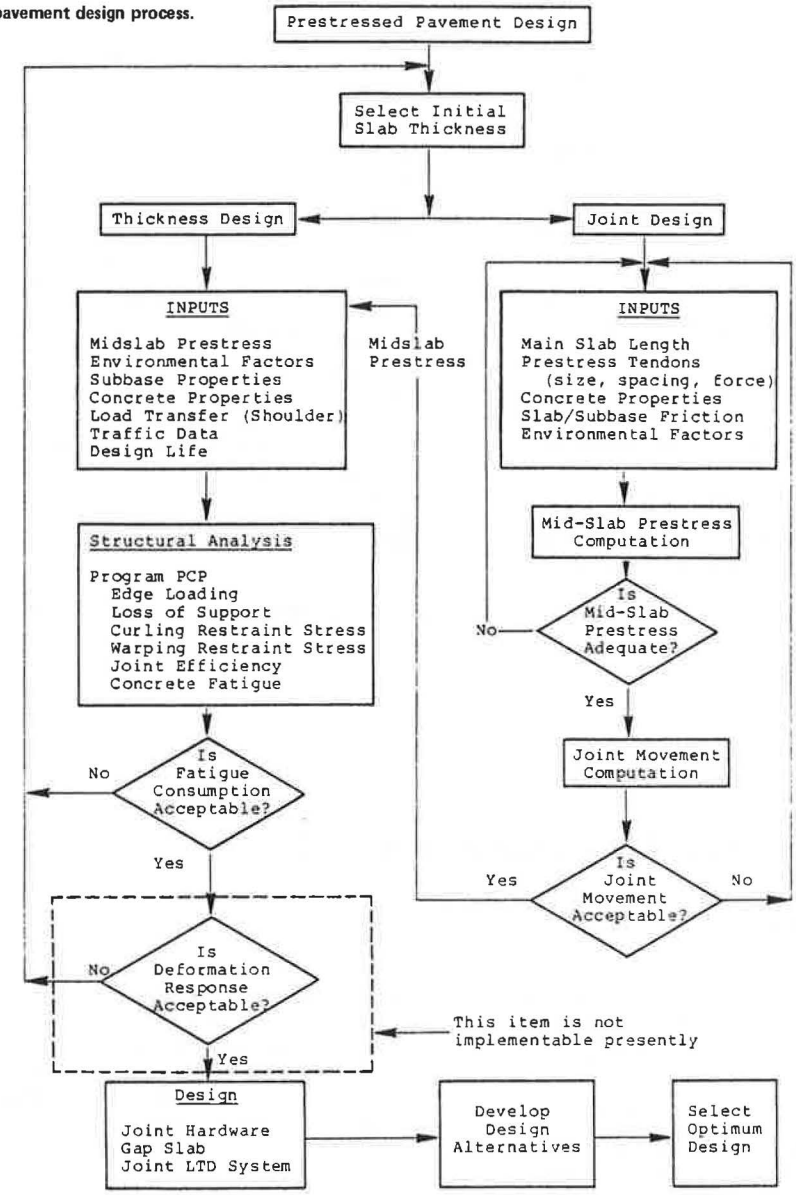

of effective midslab prestress as an input. Alternatively, a minimum level of the midslab prestress value may be assumed for the structural analysis. Structural analysis computes fatigue consumption due to edge stresses at midslab. If fatigue consumption is more than 100 percent, the design process is repeated by using a larger slab thickness.

It is assumed that fatigue consumption or damage is additive and that calculated fatigue consumption of 100 percent or more would result in structural failure of the slab. In practice, structural failure (i.e., cracking) in the slab does not result in immediate functional failure. Concrete pavements continue to provide satisfactory performance even if cracked. However, because of the zero-maintenance requirements of prestressed concrete pavements, the stringent criterion of 100 percent fatigue consumption is used to define failure.

This paper presents a thickness design procedure for prestressed concrete pavements. Factors considered in developing the procedure include traffic loading; temperature and moisture variations in the concrete slab; loss of subbase support; properties of concrete, subbase, and subgrade; and effective midslab prestress.

DESIGN PROCEDURE

A computerized program for thickness design of prestressed pavements is presented. Required pavement thickness is a function of stresses that result from traffic loads, temperature and moisture variations, loss of subbase support, and midslab effective prestress. The summation of these stresses is balanced against fatigue consumed to obtain a pavement designed to resist bottom flexural cracking.

An acceptable criterion for a design based on deflection is not available. Therefore, deflections are not computed. However, it is recognized that prestressed concrete pavements are thinner than conventional concrete pavements. For this reason, it is recommended that high-quality stabilized subbases be specified for use with prestressed pavements.

Procedures used for computing stresses and decisions regarding inputs for the computer program are briefly discussed. A detailed discussion, a program user's manual, and a program listing are presented elsewhere (1).

REFERENCES

1. P.J. Nussbaum, S.D. Tayabji, and A.T. Ciolko. Prestressed Pavement Joint Designs. FHWA, June 1981.
2. S.D. Tayabji, B.E. Colley, and P.J. Nussbaum. Prestressed Pavement Thickness Design. FHWA, June 1981.
3. B.F. Friberg. Prestressed Pavements--Theory into Practice. Proc., International Conference on Concrete Pavement Design, Purdue Univ., West Lafayette, IN, 1977.
4. J.H. Emanual and J.L. Hulsey. Prediction of the Thermal Coefficient of Expansion of Concrete. Journal of the American Concrete Institute, April 1977.
5. Design and Control of Concrete Mixtures. Portland Cement Association, Skokie, IL, 1979.
6. T.C. Hansen and A.H. Mattock. Influence of Size and Shape of Member on the Shrinkage and Creep of Concrete. Journal of the American Concrete Institute, Vol. 63, No. 2, Feb. 1966.
7. P.J. Nussbaum, B.F. Friberg, A.T. Ciolko, and S.D. Tayabji. Prestressed Pavement Construction Manual. FHWA, June 1981.
8. A.N. Hanna, P.J. Nussbaum, T. Arriyavat, J. Tseng, and B.F. Friberg; Portland Cement Association. Technological Review of Prestressed Pavements. FHWA, Rept. FHWA-RD-77-8, Dec. 1976.
9. L.W. Teller and E.C. Sutherland. The Structural Design of Concrete Pavements. Public Roads, Vol. 23, No. 8, April-June 1943, pp. 167-212.
10. B.F. Friberg. Investigations of Prestressed Concrete Pavements. HRB, Bull. 332, 1962, pp. 40-94.
11. E.F. Kelley. Structural Design of Concrete Pavements. Journal of the American Concrete Institute, Vol. 35, Supplement, Sept. 1939.
12. G.R. Morris and H.C. Emery. The Design and Construction of Arizona's Prestressed Concrete Pavement. Research Section, Highway Division, Arizona Department of Transportation, Phoenix, Jan. 1978.
13. G.E. Albritton. Prestressed Concrete Highway Pavement: Performance During Construction. Paper presented at 57th Annual Meeting, Transportation Research Board, Washington, DC, Jan. 1978.

Publication of this paper sponsored by Committee on Rigid Pavement Design.

Prestressed Pavement Thickness Design

S.D. TAYABJI, B.E. COLLEY, AND P.J. NUSSBAUM

A computerized procedure for thickness design of zero-maintenance prestressed concrete pavements is presented. Factors considered in developing the design procedure include traffic loading, temperature and moisture variation in the concrete slab, loss of subbase support, properties of concrete, properties of subbase, properties of subgrade, and effective midslab prestress. The procedure is based on flexural stress analysis and prevention of bottom transverse cracking that may initiate from the longitudinal edge of the slab in the vicinity of midslab. Inputs for the computer program include number and magnitude of axle loadings, wheel placement, traffic volume distribution during a 24-h day, temperature data, load transfer effectiveness, and effective prestress at midslab. Program output is in terms of total fatigue consumption at the end of design life. If fatigue consumption is less than 100 percent, then the thickness meets design criteria. A design example is presented for a rural four-lane highway in Illinois.

The objective of the Federal Highway Administration (FHWA) Research Project 5E, Premium Pavements for Zero Maintenance, is to exploit modern materials and technology in developing zero-maintenance pavements for warranted use. As a portion of this research project, an investigation has been conducted by Construction Technology Laboratories, a division of the Portland Cement Association. The objective of the investigation was to develop design and construction techniques for prestressed concrete pavements.

Conventional concrete pavements are designed on the basis of concrete's relatively low modulus of rupture without effectively using the natural advantage of its high compressive strength. In prestressed pavements, precompression in the concrete due to prestressing increases allowable stress in the flexural zone. Precompression causes the reduction or elimination of cracking and a large decrease in the number of transverse joints. Consequently, a more comfortable riding surface is provided and maintenance costs are reduced.

Prestressed pavement design includes the determination of required pavement thickness and joint hardware. Joint hardware is determined based on anticipated slab movement and length. Figure 1 shows the basic steps involved in prestressed pavement design.

As shown in Figure 1, the design process is iterative and involves the interaction of many factors. The process starts with the selection of an initial slab thickness. Then, for joint hardware design, trial main slab length and prestress tendon size, spacing, and force are selected. Effective midslab prestress is computed. A minimum of about 50-psi midslab prestress should be obtained. If it is not obtained, slab length, tendon size, spacing, or force is varied until the desired midslab prestress is obtained. A minimum prestress is desirable to ensure that the early shrinkage cracks that may develop remain tightly closed. Thus, load transfer across possible cracks is improved due to aggregate interlock.

When the midslab prestress criterion is satisfied, anticipated maximum joint movement is computed. Selection of an appropriate joint infiltration-prevention device such as a strip seal, compression seal, or steel cover plate depends on the magnitude of total joint movement. Total movement may be accommodated at one or two active joints between adjacent slabs. Slab length is varied until the computed joint movement can be accommodated by the device selected.

After slab length, midslab prestress level, and joint hardware are established, a structural analysis is performed. This analysis requires the value

Figure 2. Tandem axle load configuration.

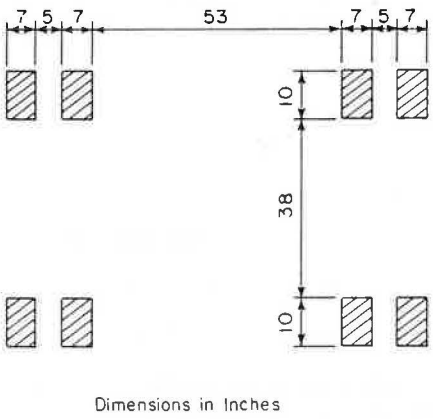

Figure 3. Load placement coefficients, C_e.

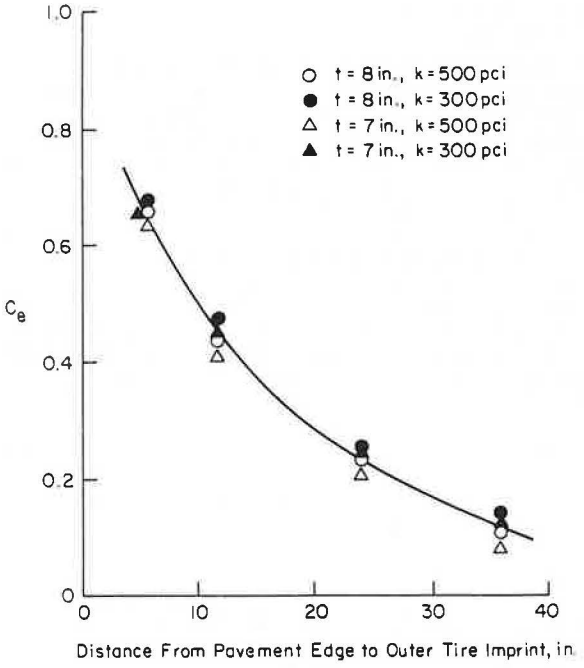

Traffic Load Stresses

A finite-element computer program for analysis of slabs on a Winkler (liquid) foundation was used to compute moments for the case of edge loading (2). These moments, expressed as a function of the radius of relative stiffness (1), are stored in this computer program. They are used together with a coefficient to determine edge stresses that result from loads located at or inward from the pavement edge. The program also considers optional use of a tied concrete shoulder with a variable input for load-transfer efficiency at the longitudinal joint.

Either a single- or a tandem-axle load configuration may be selected as input. Wheel imprint dimensions and wheel and axle spacings used in the program are shown in Figure 2. For single-axle loading, the wheel imprint size and spacings are the same.

Moments at the pavement edge due to loads at the edge are given by the following equations. For an 18-kip single-axle load,

$$M = 483.4(l)^{0.571} \text{ in-lb} \quad (1)$$

where M is the bending moment at edge, and l is the radius of relative stiffness of pavement (in), i.e.,

$$l = \sqrt[4]{Eh^3/[12(1-u^2)k]} \quad (2)$$

where

E = modulus of elasticity of concrete (psi),
h = slab thickness (in),
u = Poisson's ratio = 0.15, and
k = modulus of subgrade reaction (psi).

For a 36-kip tandem-axle load,

$$M = 185.1(l)^{0.820} \text{ in-lb} \quad (3)$$

Moment equations are based on the assumption of loss of subbase support for a 20-in distance inward from the pavement edge. This adjustment is made to recognize upward slab warping due to moisture differentials in the pavement.

Load stress (f_L) is determined by the following equation:

$$f_L = (6M/h^2)(P/18\,000\,n)\,C_e \text{ psi} \quad (4)$$

where

P = single- or tandem-axle load (lb),
n = 1 for single-axle load and 2 for tandem-axle load, and
C_e = load placement coefficient.

The load placement coefficients shown in Figure 3 are provided as program input. These coefficients are used to reduce stress at the pavement edge when loads are applied in wheel paths located inward from the edge.

Equation 4 for load stress (f_L) can be further modified to incorporate the contribution of a tied shoulder. This is done by using the following equation:

$$f_L = (6M/h^2)(P/18\,000\,n)C_e[1/(1+JE)] \text{ psi} \quad (4a)$$

where JE is joint efficiency, i.e., JE = deflection at shoulder side of joint divided by deflection at main pavement side of joint.

Traffic Characteristics

Axle loads and lateral placement of loads across the pavement during different periods of a 24-h day are program inputs. Curling stresses vary during the day, and maximum curling stresses exist for only short durations of time. Therefore, the traffic distribution during the entire day is required to equate maximum stresses to the number of load applications during selected time periods. Time periods and traffic during the selected periods are program inputs.

States accumulate traffic loadometer data in the format used in FHWA W4 loadometer tables. These tables tabulate the number of axles observed within load groups and are generally reported for 2000-lb increments. For concrete pavements, traffic projections are made for design periods that usually range from 20 to 40 years.

A recommended lateral distribution of traffic is shown in the table below:

Distance from Outside Wheel to Pavement Edge (in)	Truck Traffic (%)
0-6	20
6-12	20
12-18	25
18-24	15
24-30	10
30-36	5

These values were selected based on information obtained by Emery (3). Traffic volume is subdivided with respect to time of day. A recommended distribution is given in the user's manual.

Temperature Effects

Curling stresses develop in a slab when temperatures vary with depth. During daytime when the top surface is warmer than the bottom, tensile stresses develop at the slab bottom. During nighttime when temperature gradients are reversed, tensile stresses develop at the slab top. For stress calculations, it is generally assumed that the temperature gradient is linear. The maximum gradient is assumed to be about 3°F/in during daytime and about 1°F/in during nighttime. In practice, the temperature distribution is usually nonlinear and constantly changing. Also, maximum daytime and nighttime temperature differentials exist for short time durations.

Because the daily variation of air temperature follows an approximately sinusoidal cycle, temperature variations at the slab surface can be assumed to be sinusoidal. This variation can be represented as follows (4,5):

$$\theta_T = \theta_o \sin(2\pi t/T) \quad (5)$$

where

θ_T = temperature at surface of slab,
θ_o = constant = amplitude of the temperature cycle at slab surface,
t = time of day (24-h clock), and
T = 24 h.

Equation 5 represents daytime conditions well but gives an incorrect distribution for nighttime conditions. For nighttime, the amplitude is about one-third of that computed by using this equation. Therefore, for nighttime conditions, θ_o is replaced by θ_o' which is equal to $\theta_o/3$. Accuracy of the nighttime temperature distribution is not as critical because these stresses are subtracted from the load stresses.

For homogeneous semi-infinite solids whose surface temperature varies sinusoidally, the temperature (θ_z) at any time t on a plane at depth z below the surface is given by

$$\theta_z = \theta_o \exp(-\beta) \cdot \sin[(2\pi t/T) - \beta] \quad (6)$$

where

$\beta = (z/\psi^2)\sqrt{\pi/T}$,
ψ^2 = diffusivity of the material (in^2/h) = $\lambda/\gamma c$,
λ = thermal conductivity of the material (Btu/h-ft-°F),
γ = weight per unit volume of the material (lb/ft), and
c = specific heat of the material (Btu/lb-°F).

For a concrete slab resting on earth or subbase, Equation 6 is applicable, as diffusivities of the materials are similar. For concrete,

λ = 1.20 Btu/h-ft-°F,
γ = 145 lb/ft^3,
c = 0.22 Btu/lb-°F, and
ψ^2 = 542 in^2/h.

By using this procedure, calculated variations in temperature distribution with time for concrete pavement thicknesses of as much as 10 in are shown in Figure 4. These data are more representative of measured field data than the assumption of a linear temperature distribution. For example, temperature distributions shown in Figure 4 agree well with those measured at the American Association of State Highway Officials (AASHO) Road Test (6).

Average slab temperature (θ_M) at time t is obtained by integrating Equation 6 for θ_z between 0 and the slab thickness (H) and dividing by H. The difference (θ_D) between average slab temperature and slab bottom temperature (θ_B) is given by

$$\theta_D = \theta_M - \theta_B \quad (7)$$

Curling stress at the bottom of the edge of a long slab is given by

$$f_c = \alpha E \theta_D \quad (8)$$

where α is the coefficient of thermal expansion. This nonlinear temperature distribution formulation is used in the computerized design procedure to calculate curling stresses.

Its use requires an input value for θ_o shown in Equation 5. For U.S. conditions, a recommended value is 30°F; however, other values may be substituted where local information is available and conditions are substantially different.

Moisture Effects

Top-to-bottom variations in pavement moisture con-

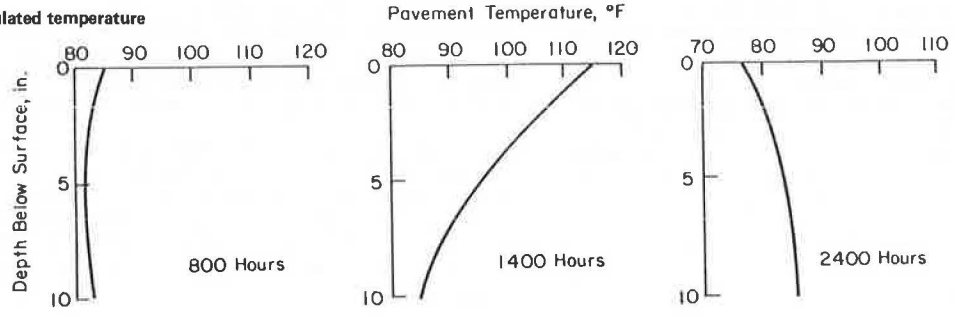

Figure 4. Calculated temperature distribution.

tent result in bottom fiber compressive stresses. Ideally, these stresses would be calculated for cyclical seasonal changes in moisture content. Calculated stresses would then be used in the thickness design procedure in the same manner as temperature stresses. However, only limited data are available regarding top-to-bottom moisture distribution, seasonal moisture variation, or stress magnitude.

Friberg (7) and Nagataki (8) report that restrained warping strain at the slab bottom may be about 150 millionths. These data are valuable and serve to direct future research. However, it is assumed currently that warping stresses for 7- and 8-in-thick pavements are 190 and 220 psi, respectively.

Warping also results in loss of support along the pavement edge. Loss of support causes an increase in edge stress associated with traffic loading. Effects of upward warping on load stress calculations are included in Equations 1 and 3.

Subbase Support

Pavement performance is related to the quality of subbase and subgrade support. Ideally, as shown in Figure 1, a thickness design procedure should incorporate allowable subbase and subgrade deformations as limiting criteria. For a concrete pavement in contact with the subbase at a corner or edge, these deformations could be related to slab deflection. However, measured concrete pavement deflections are influenced by temperature and moisture gradients in the concrete at the time of testing. Therefore, sufficient data are not available to develop criteria for correlating subbase and subgrade deformations with pavement deflection.

For given load conditions, prestressed concrete pavements are thinner than conventional concrete pavements. Thus, subbase support requirements are more critical. For zero-maintenance projects, it is recommended that a high-quality subbase be used with prestressed pavements. Modulus of subgrade reaction at the top of the subbase should be about 500 lb/in³.

Fatigue of Concrete

Flexural fatigue research on concrete has shown that as the ratio of flexural stress to modulus of rupture decreases, the number of stress repetitions to failure increases (9). Allowable load repetitions for stress ratios between 0.50 and 0.85 are given by the following equation (10):

$$\log(NN) = 11.83 - 12.20(f_T/MR) \quad (9)$$

where

NN = allowable stress repetitions,
f_T = total flexural stress, and
MR = concrete modulus of rupture (psi).

The above equation is used in the program. However, at the designer's option, other fatigue equations may be used as program input.

Midslab Prestress

Midslab prestress is computed by accounting for prestress losses due to tendon friction, concrete shrinkage, concrete creep, steel relaxation, and subbase friction restraint. A minimum of about 50-psi midslab prestress should be available. This is achieved by properly selecting slab length and tendon force, size, and spacing. Selection is an iterative process. Several trial calculations are generally required before the desired value of midslab prestress is obtained. Details of midslab prestress computation are given in the following discussion.

Tendon Friction

Tendon friction results from curvature and wobble. Curvature is due to intentional and wobble to unintentional tendon profile variations. Tendon friction (f_t) is determined from the following equation:

$$f_t = f_{pe}\left(1 - \exp\left\{-[ux + (KL/2)]\right\}\right) \text{ psi} \quad (10)$$

where

f_{pe} = end prestress (psi),
u = curvature friction coefficient,
x = angular change of tendon from jacking end to midslab (radians),
K = wobble friction coefficient per foot, and
L = slab length (ft).

For straight portions of pavements, intentional angular changes are negligible. Therefore, tendon friction can be obtained from the following equation:

$$f_t = f_{pe}\left\{1 - \exp[-(KL/2)]\right\} \text{ psi} \quad (11)$$

Concrete Shrinkage

Prestress loss due to concrete shrinkage (f_s) is given by the following equation:

$$f_s = \epsilon_s E_s (A_s/A_c) \text{ psi} \quad (12)$$

where

ϵ_s = concrete shrinkage strain,
E_s = modulus of elasticity of tendon steel (psi),
A_s = area of tendon per unit width of slab (in²), and
A_c = area of slab per unit width of slab (in²).

Concrete Creep

Prestress loss due to concrete creep (f_{cr}) is given by the following equation:

$$f_{cr} = C_u(E_s/E_c)f_{pe}(A_s/A_c) \text{ psi} \quad (13)$$

where C_u is the ultimate creep coefficient and E_c is the modulus of elasticity of concrete (psi).

Steel Relaxation

Prestress loss due to steel relaxation (f_r) is given by the following equation:

$$f_r = \rho f_{pe} \text{ psi} \quad (14)$$

where ρ is the relaxation coefficient for the appropriate stress level.

Subbase Friction

Prestress loss due to subbase friction (f_f) is given by the following equation:

$$f_f = [(U_s \gamma^L)/288] \text{ psi} \quad (15)$$

where U_s is the slab-to-subbase friction factor,

Table 1. Prestress calculations.

Item	General Calculations	
	Slab 7 in Thick	Slab 8 in Thick
Slab length (ft)	250	350
Strand diameter (in)	0.6	0.6
Strand force (kips)	41	41
Strand spacing (in)	24	18
End of slab prestress (psi)	244	285
Prestress losses (psi)		
Shrinkage	6	6
Creep	4	6
Relaxation	20	23
Strand friction	39	62
Subbase friction	100	140
Total	169	237
Midslab prestress (psi)	75	48

Note: For the 8-in-thick design, actual tendon force selected is 44 kips. This results in an end of slab prestress of 306 psi and midslab prestress of 57 psi.

Table 2. Prestress loss computation coefficients.

Item	Magnitude
Tendon ultimate strength (psi)	270 000
Area, 0.6-in-diameter tendon (in^2)	0.217
Concrete creep coefficient	2.5
Concrete shrinkage strain (millionths)	150
Strand relaxation coefficient	
70 percent of ultimate stress	0.08
75 percent of ultimate stress	0.10
Wobble friction coefficient per foot	0.0014
Subbase friction factor	0.8
Modulus of elasticity of steel (million psi)	28
Modulus of elasticity of concrete (million psi)	5

and γ is the concrete unit weight (lb/ft^3).

Effective midslab prestress (f_p) is given by the following equation:

$$f_p = f_{pe} - f_t - f_s - f_{cr} - f_r - f_f \quad (16)$$

Example calculations for computing prestress losses and midslab prestress are given in Table 1. Coefficients and other values used for computations are listed in Table 2.

PROGRAM FORMULATION

Total flexural stress at the midslab edge is computed by using the following equation:

$$f_{T_{ijkl}} = f_{L_{ijkl}} + f_{C_{jkl}} - f_p - f_{W_{kl}} \quad (17)$$

where

$f_{T_{ijkl}}$ = total flexural stress for the ith axle group at the jth period of the day of kth month of lth year,
$f_{L_{ijkl}}$ = traffic load stress due to the ith axle group at the jth period of day of kth month of lth year,
$f_{C_{jkl}}$ = curling stress at the jth period of day of kth month of lth year,
f_p = effective prestress at midslab at the jth period of day of kth month of lth year, and
$f_{W_{kl}}$ = warping stress during kth month of lth year.

The anticipated number of repetitions (N_i) of stress of magnitude $f_{T_{ijkl}}$ is determined. Then, the allowable number of stress repetitions (NN_i) of magnitude $f_{T_{ijkl}}$ is calculated by using the fatigue model. Fatigue consumption (F_i) due to repeated stress applications of magnitude $f_{T_{ijkl}}$ is obtained as follows:

$$F_i = N_i/NN_i \quad (18)$$

Total fatigue consumption (F_{TOT}) during the design period is obtained by summing fatigue consumed by load repetitions for each stress level and is given by

$$F_{TOT} = \Sigma F_i \quad (19)$$

If total fatigue consumption at the end of the design period is less than 100 percent, the thickness obtained meets structural design criteria.

DESIGN EXAMPLE

The thickness design of a prestressed pavement for a heavily trafficked highway in central Illinois is presented. The high volume of heavy loads used is representative of traffic at locations where the concept of zero-maintenance pavements is applicable. The concept of zero maintenance implies use of a premium pavement at locations where higher first-cost is justified by a reduction in future costs due to repairs, user travel delays, and increased potential for accidents.

The design procedure may be used to determine the pavement thickness for any traffic mix. However, use of a thickness less than 6 in may not be practical, as space requirements for placing joint hardware such as anchors, seal holders, load-transfer devices, reinforcement, and positioning bars may not be available.

1. Project traffic data: The traffic distribution used was obtained from data gathered from field surveys and interviews by Darter and Barenberg (11). Average daily traffic (ADT) for the design period was selected as 6000 vehicles/day, the design life is 20 years, and the single-axle load distribution for the design lane during the design period is given in the table below:

Axle Load (kips)	No.
18-20	80 422
20-22	62 144
22-24	25 589
24-26	8 530
26-28	3 656
28-30	1 219
30-32	609
32-34	183

The tandem-axle load distribution for the design lane during the design period is as follows:

Axle Load (kips)	No.
38-40	29 244
40-42	11 576
42-44	4 874
44-46	3 656
46-48	1 828
48-50	1 219
50-52	1 219
52-54	609
54-56	183

2. The material properties are as follows: concrete modulus of elasticity, 5 million psi; concrete modulus of rupture, 700 psi; modulus of subbase reaction, 500 lb/in^3; diffusivity of

concrete, 5.24 in^2/h; and coefficient of thermal expansion of concrete, 0.000 005 in/in/°F.

3. The effective midslab prestress is 50 psi.

4. Warping restraint stress values are as follows: stress for a 7-in-thick slab is 190 psi, and stress for an 8-in-thick slab is 220 psi.

5. The results obtained by using the computer program are presented below:

Slab Thickness (in)	Edge Load Transfer Efficiency (%)	Fatigue Consumed (%)
7	0	2070
7	60	1
8	0	36

Based on above results, a 7-in-thick concrete pavement with a tied concrete shoulder or an 8-in-thick pavement without a tied concrete shoulder may be used.

SUMMARY

A computerized design procedure for prestressed concrete pavement is presented. The procedure is based on flexural stress analysis and prevention of bottom transverse cracking at the slab edge. Currently, only limited data are available to determine values for temperature cycle amplitude (θ_o) and warping restraint stress. Therefore, recommended design values may be used. The design procedure is simple to use and can be implemented immediately.

When prestressed and conventional pavements are compared for alternate designs, it is recommended that other factors in addition to first-costs be considered in the evaluation. These factors include a large reduction in the number of joints, which results in an improved riding surface and reduced number of lane closures for maintenance and repair.

ACKNOWLEDGMENT

Work was conducted by the Transportation Development Department of the Construction Technology Laboratories under the direction of Bert E. Colley. W.G. Corley, director, Engineering Development Division, reviewed the text of this paper and made valuable suggestions.

Bengt F. Friberg acted as a principal consultant and contributed to all phases of the study. His participation is gratefully acknowledged. T.F. McMahon and W. Kenis of FHWA provided technical coordination. Their cooperation and suggestions are gratefully acknowledged.

The opinions and findings expressed or implied in the paper are ours. They are not necessarily those of FHWA.

Discussions

Floyd J. Stanek

The comments presented in this discussion paper were formulated from information received while I served as technical monitor and coordinator for two studies of prestressed pavements sponsored by the Office of Research, FHWA. One study was a coordinated study by three state highway agencies to conduct an on-site inspection for the study, Performance of Prestressed Pavements in Four States. The representative members of this inspection team are as follows: Wade L. Gramling, Pennsylvania Department of Transportation (DOT); Gene Morris, Arizona DOT; and T. Paul Teng, Mississippi State Highway Department.

The other study was a follow-up research study of the Prestressed Pavement Demonstration Project, constructed in 1971-1972, near Dulles International Airport, Loudoun County, Virginia. This study was conducted by Bengt Friberg, one of the principal contributors to the original design and construction of this project. I served as monitor of this project for the FHWA Office of Research since 1972 and was closely associated with Friberg during the past 18 months for the completion of this study. A research report for each of these two studies is scheduled for future publication by FHWA.

For proper assessment, the subject paper, Prestressed Pavement Thickness Design, should be viewed in context of the following specific comments.

1. The paper deviates from the current practice of prestressing concrete pavements, which places the stressing tendons below midplane of the thickness of the pavement slab. This deviation will have a tremendous influence and effect on resistance to vehicle loads, fatigue properties, and other significant design advantages.

2. It is incorrect to use fatigue consumption as the design criteria based on bottom surface stresses at midslab only. The paper states that prestressing concrete increases the allowable stress in the flexural zone. It is statistically incorrect to use results from fatigue tests conducted on early-age, presumably 28-day-old, plain concrete for the design of prestressed pavements for a 20-year life. Prestressing improves material properties and the structural behavior of concrete pavements by preventing microcracking and maintaining internal stresses at advantageous levels. Fatigue properties of advanced-aged prestressed concrete are not currently available.

3. The design calculations for the one illustrative example presented are based on the assumption that only 50-psi prestress is available at midslab. Other designers and contributors to prestressed pavement technology claim midslab prestress of 200 psi or more can be maintained in slab lengths of 400 to 500 ft. For the two slab thicknesses of 7 and 8 in, the paper considers only slab lengths of 250 and 350 ft, respectively.

4. In the discussion of the temperature effects, the paper assumes a maximum daytime temperature gradient of 3°F. It is not clear as to how the design procedure evaluates and incorporates the corresponding time duration that this maximum gradient is imposed on the pavement. At any rate, previous contributors claim and substantiate that a temperature gradient of 3°F occurs in concrete pavements for only 1.73 percent of the time. This is less than a half-hour during each daily cycle. A comprehensive account of the time duration and corresponding temperature gradients through concrete pavements is presented by Swanberg (12). The paper also states that the accuracy of nighttime temperature is not as critical because these stresses are subtracted from load stresses. This is overconservative when fatigue consumption is used as the only design criteria.

5. The paper does not identify or characterize the serviceability requirements for a zero-maintenance pavement. But for the one prestressed zero-maintenance pavement presented, the paper recommends only a 7-in-thick slab tied to the shoulder or an 8-in-thick slab if not tied to the shoulder.

6. The vehicle load for the example presented is assumed to be 6000 ADT, whereas a traffic load of 21 000-27 000 ADT is assumed in an illustrative design of a zero-maintenance pavement presented elsewhere (11).

7. The paper states that the concept of zero maintenance is characterized primarily on economical and safety considerations on heavily traveled highways. But, the paper does not explain how these considerations are accounted for in the computerized program presented.

8. The paper's treatment of tendon relaxation behavior is not consistent with design aspects of prestressing pavement slabs or with the research results presented by Maguire, Sozen, and Siess (13). The inconsistencies are twofold, as stated herein and in comment 9. The paper assumes an initial prestressing force of only 70 percent of the strand's ultimate strength, whereas 80 percent is permitted by the American Concrete Institute (ACI) building code and has been used successfully by previous designers. This higher prestressing force increases the minimum prestress at midslab an additional 30-40 psi, permits longer slab lengths of 400 to 500 ft, and also becomes most advantageous for prestressing the gap slab as is done in some current designs.

9. The paper assumes that the relaxation coefficient for strands stressed to 70 percent of the ultimate strength remains constant along the length of the slab. In accordance with the values presented for the 7- and 8-in slabs in Tables 1 and 2, the stressing force at midslab due to strand frictional losses is only 59 and 55 percent of the ultimate strength, respectively. This will reduce the magnitude of the relaxation coefficient along the length of the slab substantially, perhaps by as much as 50 percent, at midslab.

10. A summary account of the performance, road tests, and measurements conducted on prestressed pavements constructed prior to 1976 in the United States, France, Holland, Switzerland, Belgium, Austria, and Germany is presented in a report by the Portland Cement Association (PCA) (14, pp. 68-103). Three of the five prestressed pavement demonstration projects constructed during the 1970s in four states with slab thickness of only 6 in are described in this report. An on-site inspection of these five projects was conducted during 1981 by the coordinated four-person team identified in the beginning of this discussion paper. The performance report by this inspection team is scheduled to be published in a future FHWA report.

11. In the results for the one design example presented, the paper states that a 7-in-thick concrete pavement may be used if tied to a concrete shoulder with a joint efficiency of 60 percent. In accordance with Equation 4a, a joint efficiency of 60 percent is equivalent to transferring 37.5 percent of the vehicle load to the shoulder. The paper does not explain how this partial transfer of the vehicle load is to be achieved or how this will affect the design and cost of the shoulder. Also, no accounting is presented as to how this tie with the shoulder will influence and effect the longitudinal stresses and movements of the slab due to temperature and moisture effects.

12. In the discussion of the example presented, the paper states that a slab thickness of less than 6 in may not be practical because of space requirements. No such problems have been reported for the prestressed pavements described in the PCA report (14) or in any of the highway prestressed pavements constructed with thicknesses of 6 in or less.

13. The paper's treatment of the frictional forces between pavement slab and subbase is not consistant with currently known technology as explained herein and in comment 14. In the design example presented, the paper does not state what friction-reducing medium was assumed between the pavement and the subbase. In Table 2, the paper shows a subbase friction factor of 0.8. This value is not correlated with the range of 0.3 to 0.8 for polyethylene sheets that could reduce to as low as 0.13 with special additives in accordance to the values presented in the PCA report (14, Table 14, pp. 164, 168).

14. In Table 1, the paper treats subbase friction as a prestress loss of 100 and 140 psi at midslab for the 7- and 8-in slabs, respectively. Previous contributors have shown and substantiated that the influence of the subbase friction can be either a positive or a negative effect, depending on whether the slab is expanding with warmer temperatures during the daytime (a positive effect) or is contracting with colder temperatures during the nighttime (a negative effect). For the values shown in Table 1, this could increase the midslab prestress an additional 200-240 psi for the daytime when the traffic volume is the highest. This phenomenon becomes most critical and important when the design criterion is based on fatigue consumption. In addition to others, this phenomenon has been reported and discussed in the literature (12;14, reference 87, p. 179; 15).

15. In the discussion of moisture effects, the paper acknowledges cyclic seasonal changes (7,8), but then apparently treats warping as a constant flexural stress with compressive stresses of 190 and 220 psi in the bottom of the 7- and 8-in slabs, respectively. The paper then states that the warping stresses cause a loss of support along the pavement edge, presumably to describe the effect in the lateral direction. The paper does not explain if and how this lateral effect influences or becomes combined with the corresponding flexural stresses in the longitudinal direction. All effects contributing to this combination must be time coordinated accurately when fatigue consumption is the only governing design criterion.

(Note: This discussion paper reflects my views and does not necessarily reflect the official views or position of FHWA.)

Bengt F. Friberg

The paper by Tayabji, Colley, and Nussbaum bases the determination of the thickness of prestressed pavements on a fatigue analysis for traffic loads for a 20-year period with an assumed strength of concrete given as a flexural strength of 700 psi. The paper includes a computer program for determining pavement thickness. Without more data from the computer program than are given, the results must be judged from the two examples presented: a 7-in-thick slab 250 ft long with edge load transfer in the transverse direction from the edge or an 8-in slab 350 ft long without edge load transfer.

These are relatively short and thick prestressed slabs compared with designs for recent prestressed U.S. highway projects that used greased posttensioned steel strands in extruded plastic tubing. The two design examples are believed to be the result of using a low limiting strand stress as well as high values of strand friction and subgrade friction. These and other conservative assumptions in fatigue stress analyses should be covered in other discussions.

It is desired to limit this discussion to the items of warping, length changes, and creep in concrete pavements, especially as they are evidenced in prestressed slabs where they appear to result in valuable and favorable distribution of prestress on the full-restrained sections. Such developments are

shown elsewhere (7), yet none of the applicable data have been included in the project reports. The reasons may be an unwillingness to accept that a pavement slab may grow, either seasonally or progressively. Evidence of growth is present in some slabs [the Rolla investigation (7)]. This information, along with similar information from other highway research, has been omitted from the reports.

Progressive growth of concrete pavements and the seasonal length change is shown in Figure 5, which was obtained in the pioneering work at the Bureau of Public Roads by Teller and Sutherland and furnished by E. C. Sutherland, and which covers the entire period that the pavement existed from 1930 to 1942. The seasonal length change would compensate for about 30°F of the annual temperature cycle.

The relatively high moisture content near the bottom is recognized as a permanent condition in pavement slabs. Figure 6 shows the moisture gradients from top to bottom of a 7-in road slab in Oregon for one year (16). Full saturation is 4.8 percent. The top of the slab dried out rapidly. No values were shown for the first inch of depth because its values varied from day to day or even hourly; however, at a 2-in depth, the slowly drying trend in the upper part is clear. The bottom 2 in show a continuing high moisture content at about 100 percent of saturation. These data are in agreement with observations by Carlson (17).

Tests of creep in concrete have been under way since before 1920 (18), including cylinders to 10-in diameter, different stress levels, and dry or moist storage for up to 30 years under load. The creep is measured in relation to unloaded control specimens

Figure 5. Progressive and seasonal length changes of 40-ft slabs.

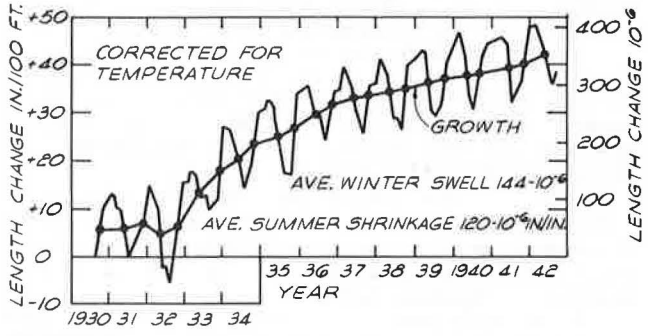

Figure 6. Moisture contents at 2 to 6 in depth in 7-in road slab in Oregon during the first year.

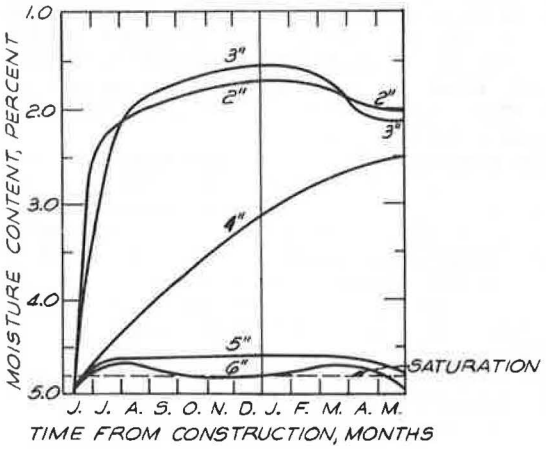

at the same storage. For storage at 100 percent relative humidity, cylinders showed swelling from 100×10^{-6} at 10 years to near 200×10^{-6} at 20 to 30 years of storage.

These and other creep data have been analyzed in accordance with theories by Ross, as published in the United States by Lorman (19), which give comprehensive coverage of the variables involved. A simple hyperbolic relation between creep strain (e_c) and time (t) in days under stress (f) by using a creep coefficient (M) defines the ultimate creep as strain per unit of stress, and a creep time constant of N days is used as follows:

$$e_c = [Mt/(N + t)]\, f \quad (20)$$

The so-called sustained modulus includes creep strain plus initial strain. By its use, stress information can be estimated at any time. Modulus of resistance is the term used elsewhere (7, Figure 11, Table 6).

Each value of the sustained modulus in the report by Friberg (7, Figure 11) is based on observations of six slabs, one dense and one air-entrained for prestress of 100, 300, and 500 psi. Good agreement and linearity can be seen. In each case, the sustained modulus at top is less than one-half of the sustained modulus at the bottom of the slabs. Lorman (19) shows creep coefficients increasing with decreasing moisture content and doubling as the relative humidity decreased from 100 to less than 70 percent. For the Rolla slabs, the creep coefficients at top and bottom were 0.5 and 0.2×10^{-6} in the 8-in slabs and 0.7 and 0.3×10^{-6}/psi in the 5.5-in slabs.

Because of the normal moisture gradients in pavements, differential shrinkage must be present as a common behavior in all slabs, including swelling at the bottom. Upward-warping deflections at the ends and edges is the result, so that the moment of the corresponding pavement weight redistribution may overcome the warping curvature that is unrestrained at the ends and that must be fully restrained in long slabs.

With a lower sustained modulus at the top than at the bottom, the flexural neutral axis can no longer be at middepth. Equal strains at the top and bottom section would mean unequal stress and lack of moment equilibrium. The simplest approximation is that the modulus varies linearly from top to bottom; the neutral axis can then be found for the trapezoidal stress areas.

In the paper, the neutral axis is assumed at middepth. A moisture gradient flexural restraint stress of 190 psi in 7-in slabs and 220 psi in 8-in slabs at bottom has been assumed, but the relation to the prestress, creep, and steel stress relaxation has not been explained. The restrained warping strain at the bottom of 150×10^{-6}, attributed to Friberg (7), is not clear. Nagataki shows that, for a warping unprestressed slab 284 in long and 10 in thick, strain differences between the end section and the fully restrained midsection of $+180 \times 10^{-6}$ at top and -130×10^{-6} at bottom, with the neutral axis well below middepth (8).

On the available data, compression stress at the bottom of 7-in slabs must be in excess of -480 and -550 psi in the 8-in slabs. The midlength effective prestress would be from 100 psi lower at night to 100 psi higher in daytime in the 7-in slab, with daily variations of ±140 psi in the 8-in slab.

If the lower sustained modulus that can naturally be expected at the surface had been recognized in the paper, an even more favorable effective prestress would have been computed. As indicated elsewhere (7, Figure 12), for 280-psi prestress on

the 8-in thickness, the stress at bottom is about -800 psi at two years, subject only to adjustment for steel stress relaxation.

Authors' Closure

We thank the discussants for their review of the paper. We believe there are many factors that influence concrete pavement performance that are not well understood and cannot be quantified. Also, because prestressed concrete pavements are thinner than conventional concrete pavements, deformation responses became more important. A significant amount of distress in concrete pavements is related to deformation. However, no practical criteria exist for including deformations in the design of concrete pavements. Therefore, the approach taken in formulating the design procedure has been to make assumptions that provide a reasonable margin of safety.

Design slab thickness is highly dependent on the number of repetitions and weight of the heaviest truck axles. We chose to provide a design example that uses heavy truck traffic. For less heavy traffic, a slab thickness of 6 in may be satisfactory. The design example should not be misinterpreted to mean all prestressed pavement should be 8 in thick or 7 in thick with tied shoulders. However, we believe that for zero-maintenance primary system highways, slab thickness should not be less than 6 in.

With regard to continued concrete growth with time, the information available seems to contradict Friberg's contention. Cracked and jointed concrete pavements do exhibit overall lengthening or growth. However, this growth is primarily due to the intrusion of incompressible material into cracks and joints. In addition, concrete slabs may exhibit growth if the concrete contains reactive aggregates. With regard to Figure 5, the concrete growth of about 350×10^{-6} in/in in the 40-ft slab that contained a midslab joint was measured by a micrometer at the slab surface. Thus, the data of Figure 5 represent slab growth of 350×10^{-6} in/in at the slab surface. We agree that concrete placed in a highly moist environment will exhibit growth. This growth, as discussed by Friberg, is only about 200×10^{-6} in/in for concrete cured continuously at 100 percent relative humidity from the time of casting up to a period of 20 years (18,20).

For a slab on grade, some growth due to moist conditions might be expected at the slab bottom. However, the slab surface would be expected to show drying shrinkage. Furthermore, this drying shrinkage at the slab surface is never fully recoverable under field conditions. This difference in moisture content between slab top and bottom is illustrated in Figure 6. Therefore, we cannot accept the application of the data of Figure 5 without serious reservations. In one of the 10-year reports on six experimental projects undertaken during the 1940s, Paxson, in describing the results of the Oregon studies, stated that "there is apparently no slab growth in the sense of a swell of the concrete due to physical or chemical change in the concrete itself. There is some evidence that shrinkage has been taking place" (21).

Similarly, results of the 10-year studies in other states indicate that, with few exceptions, all contraction joints experienced a gradual progressive increase in width during the first few years and very little increase in residual opening thereafter (22). In a recent National Cooperative Highway Research Program (NCHRP) report on joint-related distress in portland cement concrete (PCC) pavement, it is stated that the pavement lengthens due to infiltration and accumulation of incompressibles in joints and notes that "there is no permanent increase in the length of individual slabs" (23). Therefore, there is no clear consensus regarding continual growth of concrete in pavement slabs.

We do consider the effect of differential shrinkage on slab stresses. However, because of limited data, empirically derived values for warping restraint stresses are used.

The usual approach to thickness design of prestressed pavements is not to provide as much midslab prestress as possible. It is rather to provide a minimum level of prestress to ensure that any early cracks that may develop remain tightly closed. If a large midslab prestress is made available, then theoretically one could determine a design thickness of 4 to 5 in. However, balance must be maintained between theoretical calculations and practicability of construction. We do not object to use of higher prestressing levels but believe that higher prestress levels should be used to increase slab lengths or be used to provide an added factor of safety. Unless a satisfactory slab deformation response is assured, higher midslab prestress levels should not be used to result in significant slab thickness reductions.

With regard to comments by Stanek on pavement thickness, it is obvious to us that Stanek has overlooked the fact that the paper does recommend use of slab thicknesses of 6 in for prestressed concrete pavements. However, we do not recommend the use of thicknesses less than 6 in for reasons discussed in the paper and in this closure. Thus, the use of 6-in slab thickness for the demonstration projects is not contradictory to the paper. Responses to Stanek's specific comments follow.

1. For the four designs presented, tendons are placed about 0.5-1 in below slab middepth. Because of this steel location, the slab will retain better contact with the subgrade. This is an accepted practice and was followed on the Mississippi and Arizona demonstration projects (24,25).

2. We do not understand Stanek's comment on fatigue considerations. Because traffic loading on a pavement is of a repeated nature, the use of the fatigue considerations that we employed is general practice in pavement design.

3. As discussed previously, we do not have objections to use of higher midslab prestress. However, we do believe that prestress is primarily used to ensure that early non-load-related cracking is minimized.

As a point of interest, the calculated design midslab prestress for the Arizona demonstration project was 42 psi (25). The measured midslab prestress at the Mississippi demonstration project immediately after final prestressing was 60 psi for sections that incorporated two layers of polyethylene sheets under the slab (24).

4. The thickness design procedure does not use a linear temperature distribution for the slab as Stanek contends. As the discussion under temperature effect verifies, the design procedure uses a nonlinear temperature distribution. In addition, curling restraint stresses are computed for different periods of the day. This ensures a more realistic consideration of curling restraint stresses.

5. For the purpose of thickness design, the requirement for zero-maintenance pavements was that no load-associated cracking take place and that any early cracks remain tightly closed.

6. In the design procedure, ADT, axle load, and placement of axles are variables. The design example in the paper used the following vehicle parameters:

ADT (vehicles) = 6000,
Percentage of trucks = 11,
Percentage of directional distribution = 50,
Percentage of trucks in design lane = 100,
Mean axles per truck = 2.529, and
Percentage of trucks at edge = 20.

This results in 6 092 580 axles in the design lane in 20 years with 1 218 516 of these axles along the edge. This is a high level of truck axle loading and is equivalent to 22 000 ADT by using the vehicle parameters given elsewhere (11). As design engineers are aware, the number of axle loads at the edge is a more significant number than the ADT value.

7. The primary warrants for zero maintenance include reduced maintenance and user safety. These considerations are subjective and can only be established by each highway agency. However, the prestressed pavement design does ensure that a primary cause of maintenance activities, such as joint and crack-related distress, would be greatly minimized.

8. The paper does not put a limit of 70 percent of ultimate strength on the prestressing force in the tendons. The design process is iterative and use of tendon force of 70 percent of ultimate strength is made for the first trial. In fact, for the 8-in-thick design, although Table 1 shows trial calculations that use a 70 percent value, the final design value is 75 percent (26).

For the Arizona demonstration project, a 75 percent value was used. ACI Building Code 318-77 recommends use of a value of 70 percent after elastic shortening and anchorage slip losses have taken place but before time-dependent losses due to shrinkage, creep, and relaxation occur.

9. Stanek's comment on the relaxation coefficient for strands is not clear. As Table 1 indicates, losses due to steel relaxation are only 20 and 23 psi for the 7- and 8-in-thick pavements, respectively. Also, steel stresses at midslab immediately after prestressing are about 84 and 78 percent of that at slab ends for the 7- and 8-in-thick pavements, respectively. Steel stresses are not 59 and 55 percent as reported by Stanek. Reduction in computed prestress loss due to relaxation by using a nonuniform stress along the length of the tendons would be negligible.

10. As discussed previously, we do not recommend use of slab thicknesses less than 6 in. Thus, use of 6-in-thick prestressed slabs for low-volume and low-axle-weight loading is not contradictory to our presentation.

As a guide, the following thicknesses as related to traffic may be considered for pavements without a tied shoulder:

Truck Traffic Level	Slab Thickness (in)
Heavy	8
Medium	7
Light	6

11. At the pavement edge, load transfer is achieved by tieing the shoulder to the main slab by using deformed bars. The main slab and shoulder are placed in the same paving operation and prestressed at the same time. Thus, differential length changes would not occur.

12. Use of slab thickness less than 6 in is not considered practical because of difficulties that would be encountered during construction. In addition, use by medium to heavy truck traffic would result in significant levels of deformation-based distress. Also, Morris (27) of the Arizona DOT has reported that, from a construction standpoint, it is not desirable to have a prestressed pavement less than 6 in thick.

13. Stanek's view on the subbase friction reduction that can be achieved by using polyethylene sheets is not practical. Although laboratory tests on small specimens indicate lower values when using oil between two layers of polyethylene sheets, this method is not practical, is not used, and therefore cannot be recommended. Also, longer sections have differences in grade that result in larger frictional restraint values than those measured in the laboratory. The measured coefficient of subbase friction at the Mississippi demonstration project was about 0.6 when two sheets of polyethylene were used (24).

14. Prestress loss due to subbase friction is to account for frictional resistance encountered at the time of prestressing. It is not to account for the effect of decreasing slab temperature. Thus, once a stable slab-to-subbase interface condition is reached, decreasing temperature results in additional loss of effective prestress at midslab. Similarly, increasing temperatures result in compressive bottom frictional restraint stress.

The incorporation of frictional restraint stress due to the average slab temperature variation results in a more conservative design. Tensile frictional restraint stress during decreasing temperatures is of more significance to design than compressive frictional restraint stress during increasing temperature.

15. Cyclic seasonal changes do result in variations in warping restraint stresses. In fact, the computer program does consider monthly variations of warping restraint stresses. It should be noted, however, that during periods when the pavement surface is continually moist, warping restraint stresses may be lower due to smaller moisture differentials between the slab top and bottom.

With regard to the effect of loss of support due to warping, Equations 1 and 3 were developed by using a finite-element computer program that includes loss of support along the pavement edge. The net effect of loss of support is to increase traffic load associated stresses in the longitudinal direction.

REFERENCES

1. S.D. Tayabji, B.E. Colley, and P.J. Nussbaum. Prestressed Pavement Thickness Design. FHWA, June 1981.
2. S.D. Tayabji and B.E. Colley. Analysis of Jointed Concrete Pavements. FHWA, Oct. 1981.
3. D.K. Emery, Jr. Paved Shoulder Encroachment and Transverse Lane Displacement for Design Trucks on Rural Freeways. Paper presented to Committee on Shoulder Design, Transportation Research Board, Washington, DC, Jan. 1974.
4. J. Thomlinson. Temperature Variations and Consequent Stresses Produced by Daily and Seasonal Temperature Cycles in Concrete Slabs. Concrete and Construction Engineering, June 1940.
5. S.G. Bergstrom. Temperature Stresses in Concrete Pavements. Swedish Cement and Concrete Research Institute, Royal Institute of Technology, Stockholm, 1950.
6. The AASHO Road Test: Report 5, Pavement Research. TRB, Special Rept. 61E, 1962.
7. B.F. Friberg. Investigations of Prestressed

Concrete for Pavements. HRB, Bull. 332, 1962, pp. 40-94.
8. S. Nagataki. Shrinkage and Shrinkage Restraints in Concrete Pavements. Journal of the Structural Division, ASCE, July 1970.
9. J.W. Murdock. A Critical Review of Research on Fatigue of Plain Concrete. Engineering Experiment Station, Univ. of Illinois, Urbana, Bull. 475, 1965.
10. Thickness Design for Concrete Pavements. Portland Cement Association, Skokie, IL, 1966.
11. M.I. Darter and E.J. Barenberg. Design of Zero Maintenance Plain Jointed Concrete Pavement: Vol. II, Design Manual. FHWA, Rept. FHWA-RD-77-112, June 1977.
12. J.H. Swanberg. Temperature Variation in a Concrete Pavement and the Underlying Subgrade. HRB, Proc., Vol. 25, 1945, pp. 69-180.
13. B.M. Maguire, M.A. Sozen, and C.P. Siess. A Study of Stress Relaxation in Prestressing Reinforcement. Journal of the Portland Cement Association, April 1964, pp. 13-57.
14. A.N. Hanna, P.J. Nussbaum, T. Arriyavat, J. Tseng, and B.F. Friberg; Portland Cement Association. Technological Review of Prestressed Pavements. FHWA, Rept. FHWA-RD-77-8, Dec. 1976.
15. E.F. Kelley. Structural Design of Concrete Pavement. Journal of the American Concrete Institute, Vol. 35, Supplement, Sept. 1939.
16. G.S. Paxson. Investigational Concrete Pavement in Oregon. HRB, Res. Rept. 3B, 1945, pp. 77-89.
17. R.W. Carlson. Drying Shrinkage of Large Concrete Members. Journal of the American Concrete Institute, Jan.-Feb. 1937, pp. 327-336.
18. G.E. Troxell, J.M. Raphael, and R.E. Davis. Long-Time Creep and Shrinkage Tests of Plain and Reinforced Concrete. Proc., ASTM, Vol. 58, 1958, pp. 1101-1120.
19. W.R. Lorman. The Theory of Concrete Creep. Proc., ASTM, Vol. 40, 1940, pp. 1082-1102.
20. A.M. Neville. Properties of Concrete. Pitman Publishing, Ltd., London, 1981.
21. G.S. Paxson. Report on Experimental Project in Oregon. HRB, Res. Rept. 17B, 1956, pp. 151-155.
22. E.C. Sutherland. Analysis of Data from State Reports. HRB, Res. Rept. 17B, 1965, pp. 1-11.
23. Joint-Related Distress in PCC Pavement: Cause, Prevention, and Rehabilitation. NCHRP, Synthesis of Highway Practice 56, 1979.
24. G.E. Albritton. Prestressed Concrete Highway Pavement: Performance During Construction. Paper presented at 57th Annual Meeting, Transportation Research Board, Washington, DC, Jan. 1978.
25. G.R. Morris and H.C. Emery. The Design and Construction of Arizona's Prestressed Concrete Pavement. Research Section, Highway Division, Arizona Department of Transportation, Phoenix, Jan. 1978.
26. P.J. Nussbaum, S.D. Tayabji, and A.T. Ciolko. Prestressed Pavement Joint Design. FHWA, June 1981.
27. G.R. Morris. Full-Depth, Full-Width Designs and Prestressed Concrete Pave the Way for Arizona's Highways. Civil Engineering, ASCE, March 1978.

Publication of this paper sponsored by Committee on Rigid Pavement Design.

Comparison of Solutions for Stresses in Plain Jointed Portland Cement Concrete Pavements

D. R. MacLEOD AND C. L. MONISMITH

A number of existing models to compute the stresses in plain jointed portland cement concrete (PCC) pavements due to traffic loads are examined, and those that show the most promise are recommended. Solutions examined include (a) plate on dense-liquid subgrades, closed form and finite elements; (b) plate on elastic solid, closed form and finite element; and (c) layered elastic system, closed form and finite element (two-dimensional and three-dimensional representations). Although the three-dimensional finite-element analysis for the layered elastic solid is probably the most representative of the methods examined, the associated computer costs preclude its use on a routine basis at this time. The study does show that a two-dimensional finite-element analysis for the same representation is suitable for determining load-associated stresses in plain jointed PCC pavements. Changes in the engineering properties of materials, climate variations, and loading conditions can be accommodated. The maximum tensile stress—the controlling factor in the fatigue life of PCC pavements—occurs near the edge of the PCC at the midslab position. A finite-element analysis, which allows for the consideration of the strengths of the cement-stabilized layer (not accounted for in a dense-liquid subgrade type of analysis), has demonstrated that the stiffness of the cement-stabilized layer has an important effect on the fatigue life of PCC pavements. This analysis has indicated that different cracking-behavior patterns can be identified with different stabilized layer stiffnesses. A detailed traffic analysis, with allowances for thermal stresses and material variabilities, has indicated that there is a common fatigue relation for PCC pavements when the failure criteria $N_f = 225\,000\,(MR/\sigma)^4$ is used.

It has long been recognized that cracking in portland cement concrete (PCC) pavements cannot be related to traffic alone, but such factors as climate, pavement material stiffnesses, strengths, and thicknesses are significant in establishing pavement behavior as well. To date, mechanistic models have not been able to deal satisfactorily with these factors. This paper examines some of the existing models that have been used to analyze the development of load-associated cracking in plain jointed PCC pavements. Based on these analyses, those representations that have promise are recommended for use, recognizing that a satisfactory predictive model for PCC pavement cracking should

1. Predict the location, type, and severity of distress;
2. Be adaptable to various climatic conditions;
3. Allow for changes in the engineering properties of materials (in particular, the model should realistically reflect the influence of various stabilized subbases on performance);
4. Allow for changes in loading conditions (this

Table 1. Transverse and longitudinal first-stage cracking patterns for pavements with 8-in concrete layers, San Francisco Bay area.

Route No.	Transverse Cracking (%)	Longitudinal Cracking (%)
CTS designs		
US-101, Marin and Sonoma Counties	97	3
I-80, Alameda and Contra Costa Counties	90	10
CA-17, Santa Clara and Alameda Counties	84	16
CTB designs		
US-101, Marin and Sonoma Counties	40	60
I-680, Alameda and Contra Costa Counties	52	48

Figure 1. Load position and traffic distribution.

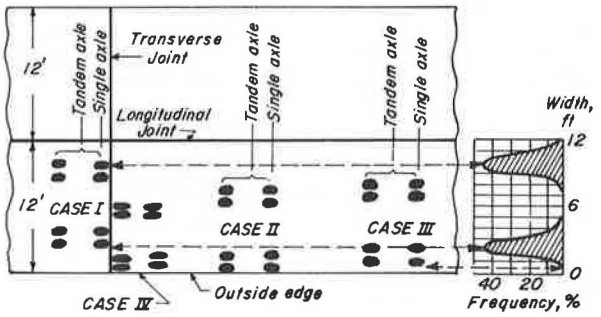

is particularly important in evaluating changes in legal axle-load limits); and

5. Permit a rational approach for the design of overlays for PCC pavements.

LOCATION AND TYPE OF DISTRESS

For a plain jointed PCC pavement, the initial crack (first-stage crack) may be a transverse crack across the middle of the slab or it may be a longitudinal crack that initiates at the transverse joint and propagates in the direction of traffic.

Darter (1) has reported that, based on study of pavements in the American Association of State Highway Officials (AASHO) Test Road and the Michigan Test Road, longitudinal cracking occurred in PCC pavements less than about 8 in in thickness and that transverse cracking occurred in pavements thicker than 8 in.

An analysis of pavements with 8-in-thick concrete layers in the San Francisco Bay area (2) indicated that cracking patterns were dependent on the strength of the cement-stabilized base directly underneath the PCC layer. Two different materials were used: one a cement-treated subgrade (CTS) and the other a cement-treated base (CTB), with CTS being weaker than CTB. The data given in Table 1 indicate that pavements that contain CTS cracked transversely at midslab, while pavements with CTB exhibited considerably more longitudinal cracking. These longitudinal cracks generally started in the inner wheel path of the outer lane at the transverse joint and progressed away from the joint until the slab was completely cracked.

For concrete slab design, a number of locations have been considered for determination of stress. Four such locations are shown in Figure 1 (3).

For case I, stresses at the transverse joint between two adjacent slabs are determined. This location is used as the critical location in both the Portland Cement Association (PCA) (3) and the California Department of Transportation (Caltrans) (4) design procedures. For this situation, the maximum flexural stress is assumed to occur at the underside of the slabs and to act parallel to the transverse joint; this would lead to longitudinal cracking in the wheel path that initiated at the transverse joint edge.

Cases II and III assume that the maximum stress occurs at the pavement lateral edge at midslab length. For both of these cases, Darter (1) concluded from a finite-element analysis that the highest stresses were perpendicular to the transverse joint (i.e., parallel to the longitudinal slab edge) and decreased as the load moved inward. These stresses would lead to transverse cracking in the midpanel position. Distribution of the wheel load across the lane (Figure 1) indicates that case III is probably more critical, since case II occurs only infrequently.

Case IV (corner loading) occurs when the load is located near the transverse and longitudinal joints. This has been neglected in some previous studies because of difficulties in the three-dimensional analysis and the fact that corner cracking is not as common as the longitudinal and transverse cracking for highway-type loading.

STRESS-ANALYSIS PROCEDURES

A number of different procedures are available to estimate stresses and deformations in systems representative of concrete pavement structures. This section briefly summarizes the available methodology, including the procedure selected for this investigation.

Elastic Plate on Dense Liquid Subgrade

Closed-form solutions have been developed for load stresses by Westergaard (5-8) and for temperature-induced stresses by Westergaard (9) and Bradbury (10). Influence charts presented by Pickett and Ray (11) for the load stresses for multiple wheels at various locations in the slab area have been used by PCA (3) and by Caltrans (4), for example, to select slab thicknesses to mitigate fatigue from repetitive traffic loadings for a range in axle loads and for single and tandem axles.

For airfield pavements, PCA (12) and the U.S. Army Corps of Engineers Waterways Experiment Station (USACE-WES) (13) have developed computer solutions for this pavement representation to ascertain stresses (PCA-interior, USACE-WES-edge) for a range in aircraft loads and gear configurations. These programs are currently used for design purposes.

A discrete-element model based on a finite-difference solution (14) has been developed to analyze concrete slabs. The method considers the concrete to be an assemblage of joints, rigid bars, and torsional bars. This analysis is available as a computer program (15).

More recently, finite-element solutions have been developed that can reflect different load-transfer conditions at joints and partial contact between the slab and the dense liquid subgrade (16,17). Computer solutions such as WESLIQUID (18) for stress analysis and JCP (1) for analysis of cumulative damage effects are examples of the methodology.

A major limitation of this pavement representation is that stresses in the materials underlying the concrete cannot be determined. Moreover, it is difficult to assess the influence of the change in stiffness characteristics of materials such as CTB on the response of the concrete to loading.

Elastic Plate on Elastic Foundations

Several solutions have been developed over the years in which the pavement is represented as an elastic

plate resting on an elastic solid [e.g., Hogg (19), Holl (20), Pickett and Ray (11)] or on a layered elastic solid. The finite-element procedure has also been adapted for solution of these situations [Wang and others (21,22) and Huang (23)] and computer solutions are available [e.g., WESLAYER (18)].

Multilayer Elastic Systems

Asphalt concrete pavements have been represented as multilayered elastic solids, and a number of computer programs have been developed to estimate stresses and deformations in such systems, e.g., ELSYM (24), BISAR (25), and CHEVRON, which was developed by H. Warren and W.L. Deickmann in their unpublished report, Numerical Computation of Stresses and Strains in a Multiple-Layer Asphalt Pavement System, which was written for the Chevron Research Corporation in 1963.

Recently, the U.S. Army Corps of Engineers has developed a procedure for concrete pavement design for airfield pavements in which the pavement is expressed as a multilayer elastic solid with full continuity at each of the interfaces (26). This procedure has some disadvantages in that the slab is assumed to be infinite in extent in the horizontal plane. Stresses at the edges have to be increased over those that occur in the interior (the computed stresses) for this analysis procedure.

The finite-element method has some advantage in analyzing this representation in that it has the capability to consider the three-dimensional configurations of concrete slabs. Also, as will be seen, some simplifications can be made to reduce the computational costs associated with finite-element analyses.

Two-Dimensional Finite-Element Models

The applicability of the finite-element solution to pavement problems has been demonstrated in recent years (27-30). Two systems have been used: one an axisymmetric configuration [Figure 2 (27)] and the other a plane strain formulation (Figure 3).

As with the conventional solutions for multilayer elastic systems (e.g., BISAR, ELSYM), the axisymmetric solution is limited, for concrete pavements, to the interior loading condition. The plain strain formulations can be made applicable to determine interior and edge stresses but cannot evaluate corner stresses. An indirect procedure is required in that the interior strip load required to give the same interior stress, as found by axisymmetric or elastic-layer solutions, is determined by trial. This equivalent strip load is then used to calculate edge stresses. Solid SAP (31) and ANSR (32) are representative examples of available computer solutions for two-dimensional problems.

Three-Dimensional Finite-Element Models

One approach to modeling three-dimensional slab configurations is that presented by Wilson and Pretorius (33). It employs a prismatic space finite-element method. The approach is essentially two-dimensional, with the third dimension introduced into the idealization by expressing the load as a Fourier series in this direction. This configuration permits determination of edge but not corner stresses.

The most general method available is the eight-node-brick three-dimensional program (three-dimensional version of Solid SAP). This program permits determination of interior, edge, and corner loadings. It can also accumulate changes in material properties in both the horizontal and the vertical directions.

FINITE-ELEMENT ANALYSES WITH LAYERED ELASTIC SOLID FOUNDATION

Of the analysis methods presented, it was concluded that the finite-element procedure in which the underlying materials are represented as layered elastic solids would be the most appropriate to study the plain jointed concrete pavements used in California.

For this purpose, the Solid SAP three-dimensional program was selected for initial studies. However, time and memory requirements required program modifications. The modifications (2) are based on a procedure used by Otte (34). Symmetry in the x and y directions was used; the concrete slab was divided into four segments, each with a load of P/4 (Figure 4). Superposition of the effects of the fine loads provides the solution. Even with these modifications, the program was very costly to run and required 140 K core memory and central processor time of 8000 s on a CDC 6400 computer.

Figure 5 is a schematic diagram of the loading used. Axle loads of 18 000 lb were used with axle spacings of 7 ft to simulate the principle of tandem axles (in California a 4-ft spacing is more common, but the 7-ft spacing permits the comparison of mid-slab loading and loading at the transverse joint in the same computer analyses).

Two pavement sections on US-101 in the Petaluma area north of San Francisco were analyzed. Each was

Figure 2. Finite-element idealization of a cylinder.

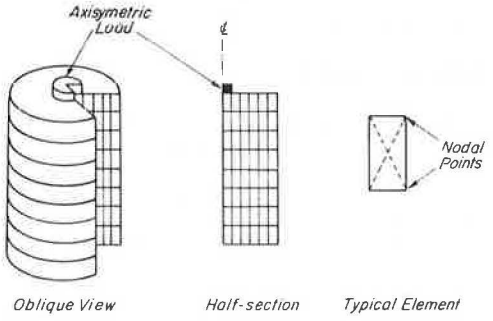

Figure 3. Finite-element idealization of plain strain conditions.

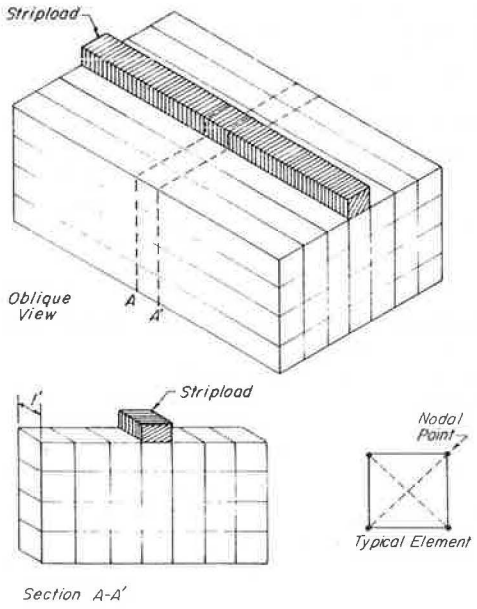

typical of CTS or CTB constructions. Table 2 contains a summary of material properties determined from laboratory tests on recovered samples and from an analysis of construction records. Note that the stiffness characteristics of CTB are about three times that of CTS.

Figures 6, 7, and 8 are plots of S_{xx}, S_{yy}, and the maximum principal stresses for the Petaluma site (pavement with CTS) that used the three-dimensional analysis and assumed no load transfer at the joint. Figure 8 indicates that the maximum stress occurs at the midslab edge, where the principal stress is approximately 10 percent higher than the midslab interior stress. These stresses are larger than the corner stresses and significantly larger than the stresses at the interior wheel at the transverse joint.

It is of interest to note that the S_{xx} stresses are larger than the S_{yy} stresses for the loads located at midslab, which indicates that transverse cracking in the midslab length should be the failure mode. This confirms the observed failure pattern.

Figures 9, 10, and 11 indicate that the Windsor site (pavement with CTB) exhibits much the same stress-distribution patterns, but the stresses are significantly lower in magnitude. Principal stresses at the midslab edge are about 215 psi versus 325 psi at Petaluma. Again, the relative magnitude of the stresses suggests that transverse cracking should be the failure mode. However, the largest value of S_{xx} (180 psi) is only slightly higher than S_{yy} (170 psi). Accordingly, it is possible that, with some load transfer occurring at

Figure 4. Axisymmetric and asymmetric loading conditions.

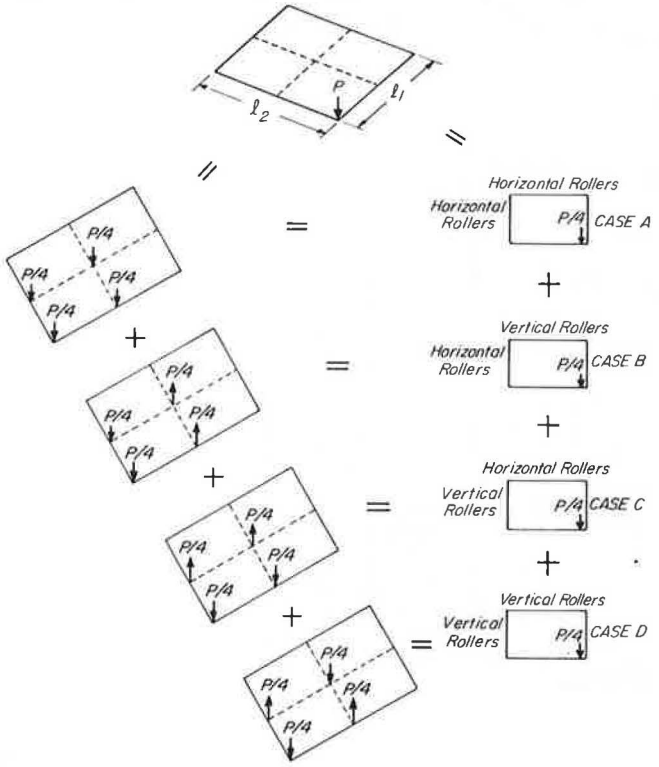

Figure 5. Load positions and stresses considered in fatigue analysis.

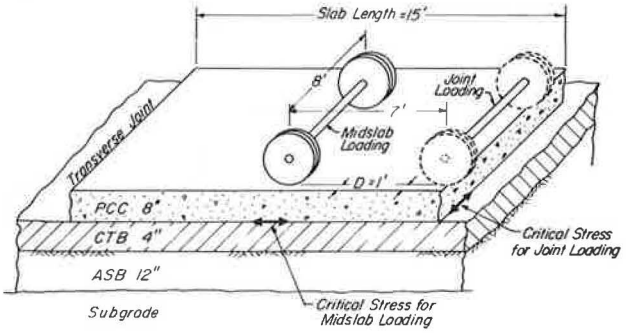

Table 2. Stiffness moduli and layer thicknesses of pavement components.

Component	Stiffness Modulus (psi)		Layer Thickness (in)	
	Windsor (CTB)	Petaluma (CTS)	Windsor (CTB)	Petaluma (CTS)
PCC	4.0×10^6	3.0×10^6	8.0	8.0
Cement-treated layer	1.1×10^6	0.35×10^6	4	4
Aggregate subbase				
Summer	15×10^3	9.0×10^3	12	12
Winter	10×10^3	5.0×10^3		
Subgrade				
Summer	8.0×10^3	7.5×10^3		
Winter	5.0×10^3	4.0×10^3		

Figure 6. S_{xx} stresses on underside of PCC, Petaluma test section.

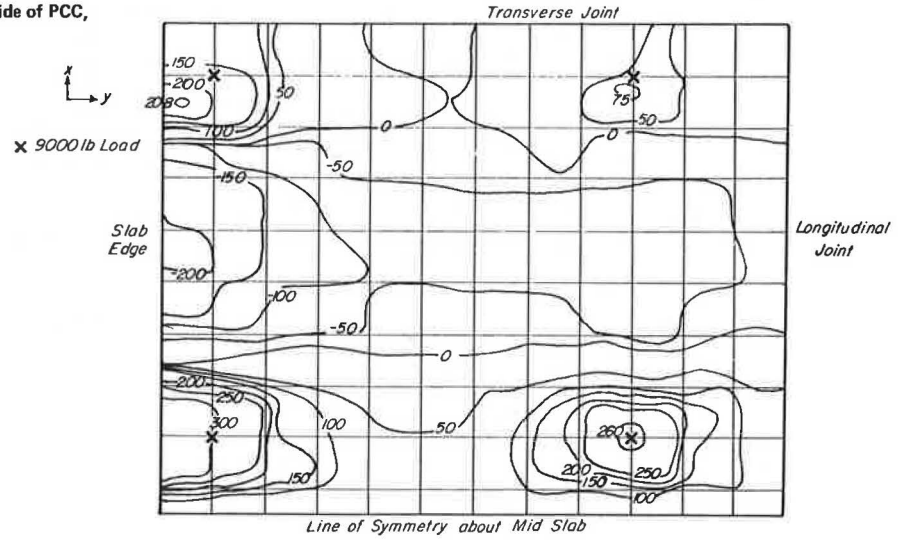

Figure 7. S_{yy} stresses on underside of PCC, Petaluma test section.

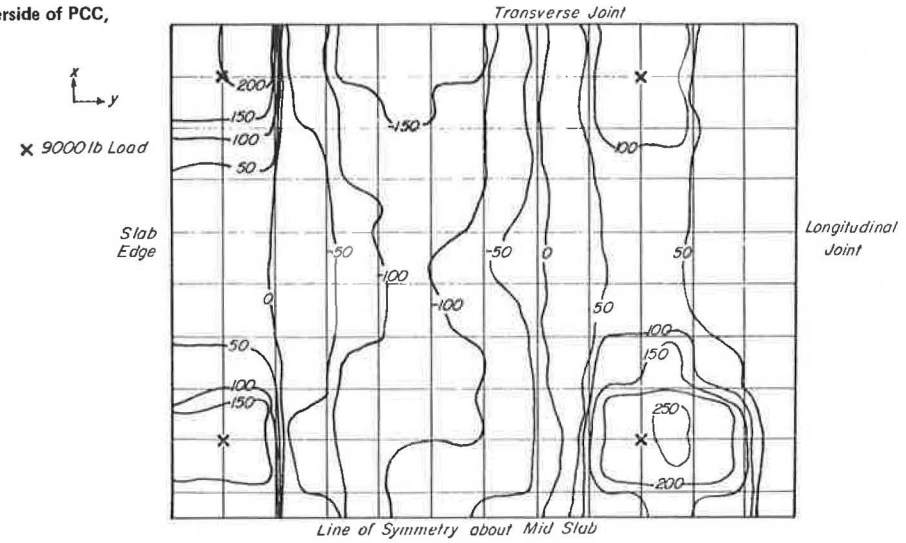

Figure 8. Principal stresses on underside of PCC, Petaluma test section.

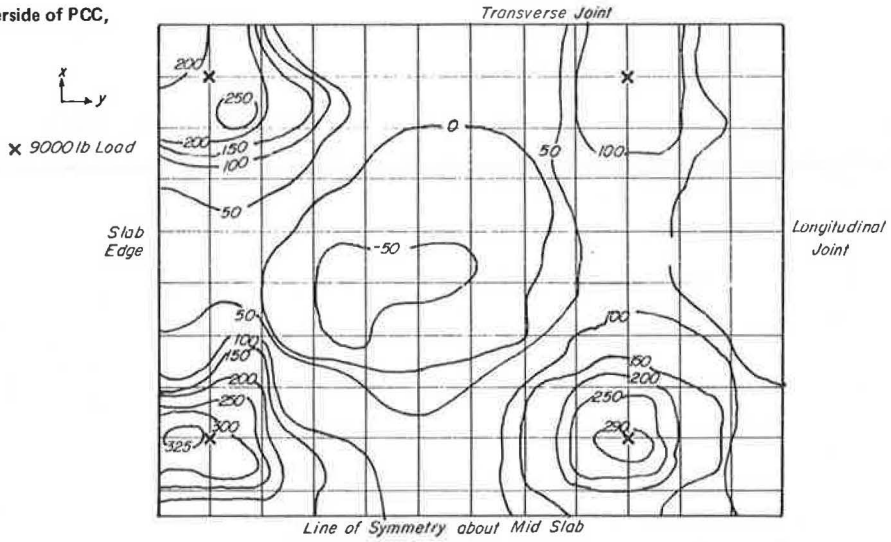

Figure 9. S_{xx} stresses on underside of PCC, Windsor test section.

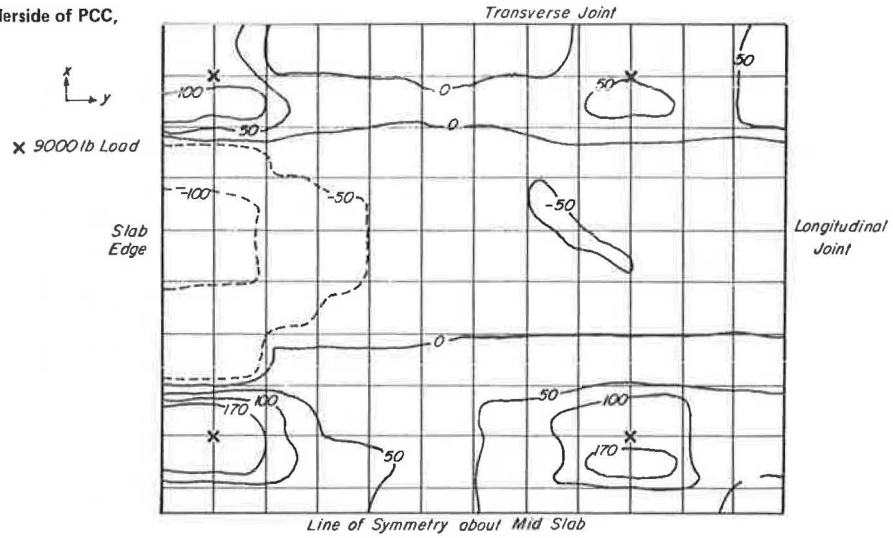

Figure 10. S_{yy} stresses on underside of PCC, Windsor test section.

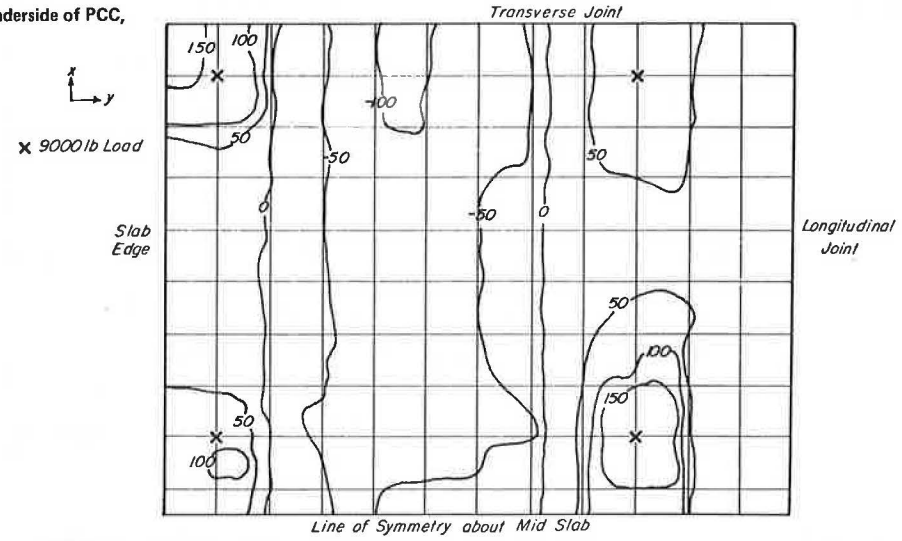

Figure 11. Principal stresses on underside of PCC, Windsor test section.

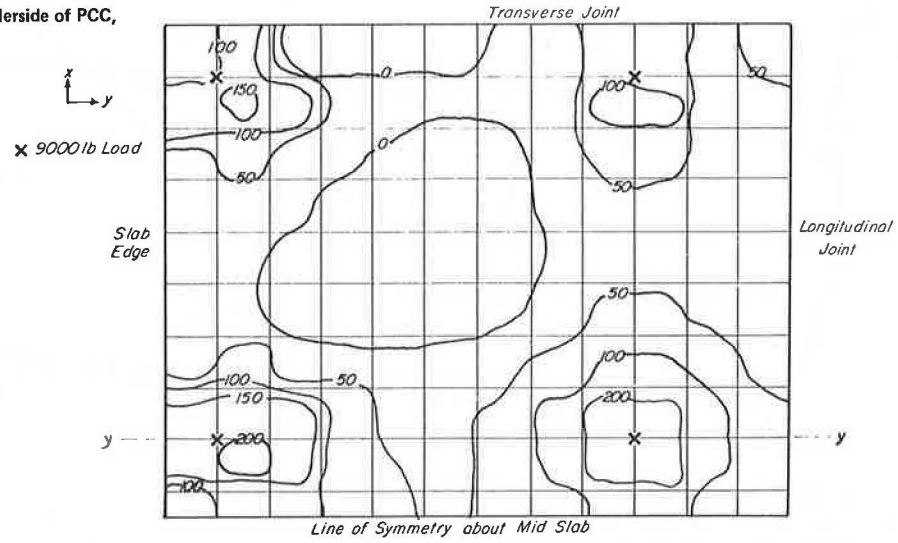

Figure 12. Model used for two-dimensional analysis.

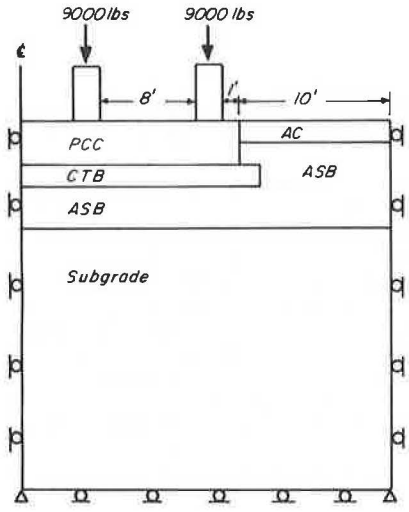

the joints, longitudinal rather than transverse cracking could be obtained and may assist in explaining the observed behavior of more frequent longitudinal cracking with the CTB-type pavements.

The major significance of the three-dimensional analysis is the fact that, in both cases, the maximum principal stresses occur for the midslab loading condition. This suggests that slab response can be analyzed by a simpler two-dimensional finite-element idealization along the y-y axis. Such a situation is representative of stresses caused by an axle at the midslab loading condition or at the transverse joint if full interlock is assumed.

Figure 12 is a schematic diagram of the conditions used for the analyses. Because the two-dimensional model uses a strip load rather than the circular or rectangular loadings employed by the other solutions, it was required to calibrate the solution for the strip load with those obtained for other solutions for the interior loading case where all solutions can be considered equivalent. This was done by adjusting the strip load until it resulted in the same principal stress on the underside of the

Figure 13. Stress distribution for CTB site.

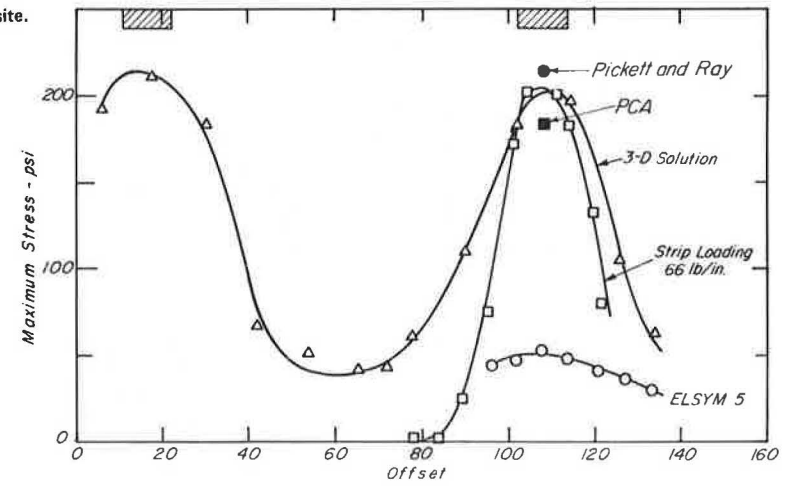

Figure 14. Stress distribution for CTS site.

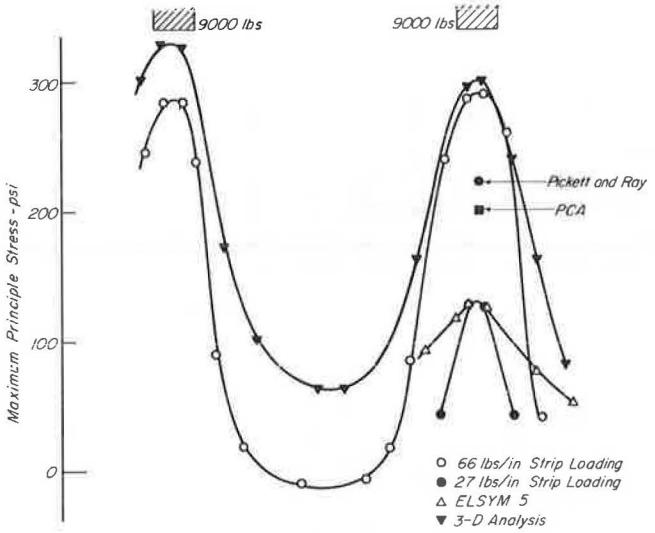

Figure 15. Analysis of pavement components.

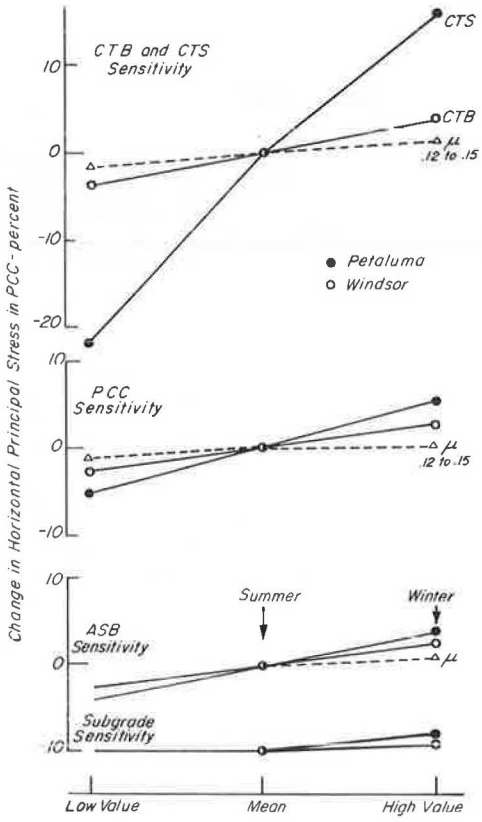

concrete as predicted by the other solutions.

Figures 13 and 14 show the three-dimensional stress distribution and corresponding two-dimensional and ELSYM 5 solutions for the CTB and CTS sites. The strip loading of 66 lb/in agrees with the three-dimensional solution, while a strip loading of 27 lb/in more closely matches the ELSYM 5 solution.

The difference is considerable; the ELSYM 5 solution results in interior stresses of 140 psi while the three-dimensional analysis indicates stresses of 325 psi. There is also a considerable divergence between the three-dimensional and two-dimensional solutions between the loaded wheels. This is not surprising, since previous work with the Solid SAP three-dimensional program (31) indicated that there would be a divergence at lower stresses due to the boundary conditions used. That study indicated, however, that when the stresses were higher, the differences in the calculated stresses would be minimal.

The divergence between the elastic-layer solution was judged significant enough to justify a comparison of estimated stresses by using other procedures [Pickett and Ray (11) influence charts, and the Caltrans (4) method] (k in the range 250 to 300 lb/in^3). The computed values are shown in Figures 13 and 14. For the CTB site (Figure 13), the agreement between three-dimensional Solid SAP, Pickett and Ray, and the PCA method is reasonable, but the elastic-layer solutions (ELSYM and BISAR) indicate much lower stresses.

There is less agreement between solutions for the CTS site, but this is expected, since solutions other than the finite element and elastic layer cannot adequately handle variations in the CTS strength. Comparisons of all solutions indicate that the stresses based on the elastic-layer solutions are too low. Consequently, the two-dimensional strip loadings were adjusted to match the three-dimensional analysis that is believed to be the most accurate. The difference between the elastic-layer solutions (ELSYM 5 and BISAR) and the other solutions remains to be explained.

Results of the two-dimensional finite-element study are summarized in Figure 15 (low value indi-

cates the 10th decile and high values indicate the 90th decile for the stiffness characteristics of the materials analyzed). The steeper the slope of the line in Figure 15, the greater the influence of the parameter on the fatigue life of the pavement. (This is based on the assumption that the horizontal principal stress on the underside of the PCC layer is a determinant of fatigue life.)

Figure 15 indicates that the moduli of the aggregate subbase (ASB) and the subgrade (as well as Poisson's ratio) of these layers have a limited direct influence on the fatigue behavior of the concrete pavement. This is not surprising, since existing design procedures (PCA) have indicated that pavement performance is not changed significantly for minor changes of the modulus of subgrade reaction (k). However, the behavior of the pavement is influenced by the quality of these materials in other than fatigue distress. The better the quality of materials, the better the resistance to pumping, settlement, frost damage, and volume change. This figure does indicate, however, that the expected variations in the CTB have dramatic effects on the performance of the stress level in the concrete layer above it. The results do not imply that the absolute strength of the CTB is more important than the absolute strength of the PCC; it simply indicates that the variations in the strength of CTB that result from a more loosely controlled construction procedure (road mix and acceptance of a wider range of materials) are more significant than the smaller variations in strength of the PCC, which is a more carefully controlled product.

APPLICABILITY OF ANALYSIS TO PREDICT IN-SERVICE PERFORMANCE

To assess the efficacy of this analysis procedure, it was used to predict the performance, as measured by cracking, for both the Windsor and Petaluma sections. In order to do this, it is necessary to simulate the in situ conditions for a range of environmental conditions. In the northern California area in which the pavements are located, the winters are wet and the summers dry. This results in different stiffness moduli for both the untreated subbase and subgrade soils during the year. Table 2 lists representative values for summer and winter conditions.

Daily and monthly variations in temperatures can lead to thermal stresses in the PCC and stabilized bases. When the surface of the PCC is hot and the underside is cooler, this thermal gradient creates tensile stresses on the underside of the PCC. These combine with the load stresses and produce combined tensile stresses on the underside of the pavement. They have a detrimental effect during the hot days and a beneficial effect during the cooler nights.

Thermal stresses can be calculated by using finite-element techniques; however, this study required a more detailed procedure. From weather records, the temperature gradients across the slabs were calculated by using a procedure suggested by Barber (35). The thermal stresses were then determined by the procedure developed by Bradbury (10).

Truck traffic was estimated by the axle group from Caltrans traffic data. This information was further divided into axle weights by using W-4 tables compiled at the weigh stations within the study sections. These data were then classified into five subgroups that represented temperature conditions for noon, midnight, early morning, early evening, and the remaining transition periods. Changes in traffic distribution from month to month were also calculated so that the number of vehicles (n_i) with a given axle weight that had traveled on the particular section of highway could be calculated for each of the applicable thermal conditions.

Because cracking in the PCC is attributable to fatigue, it was necessary to select an appropriate fatigue criterion for the concrete. The relation finally used was that developed by Vesic and Saxena (36):

$$N_f = 225\,000\,(MR/\sigma)^4 \quad (1)$$

where

N_f = number of load applications to failure at stress level σ,
MR = modulus of rupture of concrete, and
σ = tensile stress from traffic load.

Load stresses were combined with the calculated thermal stresses to determine the allowable number of repetitions (N_i) associated with Equation 1. In this instance, since the load stresses are fluctuating and the thermal stresses are constant, it was necessary to use a modified Goodman diagram (30) to determine the allowable number of load repetitions (N_i). Summing the ratios of n_i/N_i for the various subgrade and temperature conditions provides, according to the linear summation of cycle ratios, an indication of the potential for fatigue cracking. The summation should approach unity at failure.

Figure 16 summarizes the cracking data for various segments of the Windsor and Petaluma sections plotted versus n_i/N_i. Note that the procedure is valid for sections that contain both types of cement-stabilized materials.

The same procedure was applied to an additional 1200 lane miles of freeway in various climatic re-

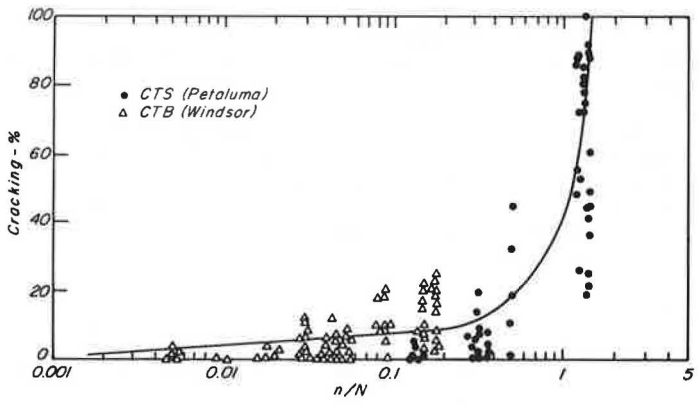

Figure 16. Percentage of total cracking versus n/N, US-101: Marin and Sonoma Counties.

gions of California. The additional analyses supported the validity of the approach (37).

Thus, it would appear that the finite-element procedure, which uses a layered elastic solid rather than the dense liquid subgrade idealization as a representation of the foundation for the PCC, permits a realistic assessment to be made of the influence of properties of the cement-stabilized layer on cracking performance of the concrete.

As an additional consideration, such a procedure is sufficiently general to permit it to be applied to the design of overlays for plain jointed pavements. If the existing concrete slab is not cracked, the thickness of the additional overlay can be determined so that the reduced strains in the existing concrete that result from the overlay will use up the remaining life, which is obtained by subtracting from unity the sum of the n_i/N_i's applied to the time of the overlay.

The finite-element procedure can also be used to examine the development of reflection cracking in the overlay and the use of various treatments to mitigate this phenomenon (38).

CONCLUSIONS

From the material presented in the paper, a few conclusions appear warranted for plain jointed PCC pavements:

1. A two-dimensional finite-element analysis that uses a layered elastic solid rather than a dense liquid subgrade as the idealization of the underlying materials for the concrete layer is suitable for the analysis of the fatigue response. Changes in (a) engineering properties of the foundation materials, (b) loading conditions, and (c) temperature variations can be accommodated.
2. The maximum tensile stress, which is the controlling factor on the fatigue life of this type of pavement, occurs near the edge at the midslab position for the representative highway load configurations examined in the investigation.
3. The finite-element analysis, which permits consideration of different stiffness characteristics of the cement-stabilized layer, has demonstrated that the strength of this layer has a significant influence on the fatigue life of the concrete layer. This analysis has also indicated that different cracking patterns can be identified with different stiffnesses in the cement-stabilized layer.
4. The fatigue relation presented by Vesic and Saxena (36) appears to reasonably predict the cracking performance of the concrete when due consideration is given to the influence of thermal stresses, material variabilities, and traffic repetitions.

ACKNOWLEDGMENT

This study was conducted in cooperation with the Pavement Management System Task Force, Caltrans, and the Federal Highway Administration (FHWA), U.S. Department of Transportation. The contents of this paper reflect our views, and we are responsible for the facts and the accuracy of the data presented herein. The contents do not necessarily reflect the official views or policies of the State of California or FHWA. The paper does not constitute a standard, specification, or regulation.

REFERENCES

1. M.I. Darter. Design of Zero-Maintenance Plain Jointed Concrete Pavement, Vol. 1: Development of Design Procedures. FHWA, Rept. FHWA-RD-77-111, June 1977, 261 pp.
2. D.R. MacLeod. Considerations for Maintenance Strategies for Portland Cement Concrete Pavements. Univ. of California, Berkeley, Ph.D. dissertation, 1979.
3. Thickness Design for Concrete Pavements. Portland Cement Association, Skokie, IL, 1966.
4. Portland Cement Concrete Pavement (7-641). In Highway Design Manual, California Department of Transportation, Sacramento, Dec. 1981.
5. H.M. Westergaard. Computation of Stresses in Concrete Roads. Proc., HRB, Vol. 5, Part I, 1925, pp. 90-112.
6. H.M. Westergaard. Stresses in Concrete Pavements Computed by Theoretical Analysis. Public Roads, Vol. 7, No. 2, April 1926, pp. 25-35.
7. H.M. Westergaard. Stresses in Concrete Runways of Airports. Proc., HRB, Vol. 19, 1939, pp. 197-262.
8. H.M. Westergaard. New Formulas for Stresses in Concrete Pavements of Airfields. Trans., ASCE, Vol. 113, 1948, pp. 425-444.
9. H.M. Westergaard. Analysis of Stresses in Concrete Pavements Due to Variations of Temperature. Proc., HRB, Vol. 6, 1926, pp. 201-215.
10. R.D. Bradbury. Reinforced Concrete Pavements. Wire Reinforcement Institute, Washington, DC, 1938.
11. G. Pickett and G.K. Ray. Influence Charts for Rigid Pavements. Trans., ASCE, Vol. 116, 1951, pp. 49-73.
12. R.G. Packard. Computer Program for Airport Pavement Design (SRO 29.02P). Portland Cement Association, Skokie, IL, 1967.
13. Computerized Aircraft Ground Flotation Analysis, Edge-Loaded Rigid Pavements (H 51). U.S. Army Corps of Engineers Waterways Experiment Station, Vicksburg, MS, 1967.
14. W.R. Hudson and H. Matlock. Analysis of Discontinuous Orthotropic Pavement Slabs Subjected to Combined Loads. HRB, Highway Research Record 131, 1966, pp. 1-48.
15. H.J. Treybig, W.R. Hudson, and A. Abon-Ayyash. Application of Slab Analysis Methods to Rigid Pavement Problems. Center for Highway Research, Univ. of Texas, Austin, Res. Rept. 56-26, May 1972.
16. Y.H. Huang and S.T. Wang. Finite-Element Analysis of Rigid Pavements with Partial Subgrade Contact. TRB, Transportation Research Record 485, 1974, pp. 39-54.
17. A.M. Tabatabaie and E.J. Barenberg. Finite-Element Analysis of Jointed or Cracked Concrete Pavements. TRB, Transportation Research Record 671, 1978, pp. 11-17.
18. Y.T. Chou. Structural Analysis Computer Programs for Rigid Multicomponent Structures with Discontinuities--WESLIQUID and WESLAYER, Report 1: Program Development and Numerical Presentations. U.S. Army Corps of Engineers Waterways Experiment Station, Vicksburg, MS, Tech. Rept. GL-81-6, 1981.
19. A.H.A. Hogg. Equilibrium of a Thin Plate, Symmetrically Loaded, Resting on an Elastic Foundation of Infinite Depth. Philosophical Magazine, Series 7, Vol. 25, 1938, pp. 576-582.
20. D.L. Holl. Thin Plates on Elastic Foundation. In Proc., Fifth International Congress for Applied Mechanics (Cambridge, MA, 1938), Wiley, New York, 1939, pp. 71-74.
21. S.K. Wang, M. Sargious, and Y.K. Cheung. Advanced Analysis of Rigid Pavement. Transportation Engineering Journal, ASCE, Vol. 98, No. TE1, Proc. Paper 8699, Feb. 1972, pp. 37-44.
22. S.K. Wang, M. Sargious, and Y.K. Cheung. Effect of Openings on Stresses in Rigid Pave-

ments. Transportation Engineering Journal, ASCE, Vol. 99, No. TE2, Proc. Paper 9721, May 1973, pp. 255-265.
23. Y.H. Huang. Finite Element Analysis of Slabs on Elastic Solids. Transportation Engineering Journal, ASCE, Vol. 100, No. TE2, May 1974, pp. 403-416.
24. G. Ahlborn. ELSYM Computer Program for Determining Stresses and Deformations in Five Layer Elastic System. Univ. of California, Berkeley, 1972.
25. D.L. DeJong, M.G.F. Peutz, and A.R. Korswagen. Computer Program, BISAR, Layered Systems Under Normal and Tangential Surface Loads. Koninklijke/Shell-Laboratorium, Amsterdam, External Rept. AMSR-0006.73, 1973.
26. F. Parker and others. Development of a Structural Design Procedure for Rigid Airport Pavements. Federal Aviation Administration, Rept. FAA-RD-77-81, 1977.
27. J.M. Duncan, C.L. Monismith, and E.L. Wilson. Finite Element Analysis of Pavements. HRB, Highway Research Record 228, 1968, pp. 11-17.
28. G.L. Dehlen. The Effect of Non-Linear Materials Response on the Behavior of Pavements Subjected to Traffic Loads. Univ. of California, Berkeley, Ph.D. dissertation, 1969.
29. P.E. Fossberg. Load Deformation Characteristics of Three Layer Pavements Containing Cement Treated Base. Univ. of California, Berkeley, Ph.D. dissertation, 1970.
30. P.C. Pretorius. Design Considerations for Pavements Containing Soil-Cement Bases. Univ. of California, Berkeley, Ph.D. dissertation, 1969.
31. E.L. Wilson. Solid SAP: A Static Analysis Program for Three-Dimensional Solid Structures. Univ. of California, Berkeley, Rept. UC-SESM 71-19, 1971.
32. G. Powell and D.P. Monkar. ANSR 1, A General Purpose Program for Analysis of Non-Linear Structural Response. Univ. of California, Berkeley, Rept. EERC-75-37, 1975.
33. E.L. Wilson and P.C. Pretorius. A Computer Program for the Analysis of Prismatic Solids. Univ. of California, Berkeley, Rept. UC-SESM 70-21, 1970.
34. E. Otte. A Structural Design Procedure for Cement Treated Layers in Pavements. Univ. of Pretoria, Pretoria, South Africa, Ph.D. dissertation, 1978.
35. E.S. Barber. Calculation of Maximum Pavement Temperatures from Weather Reports. HRB, Bull. 168, 1957, pp. 1-8.
36. A.S. Vesic and S.K. Saxena. Analysis of Structural Behavior of AASHO Road Test Rigid Pavements. NCHRP, Rept. 97, 1970.
37. D.R. MacLeod and C.L. Monismith. A Cracking Model for Plain Jointed Portland Cement Concrete Pavements. Proc., Second International Conference on Concrete Pavement Design, Purdue Univ., West Lafayette, IN, 1981, pp. 317-330.
38. N.F. Coetzee. Some Considerations on Reflective Cracking for Asphalt Concrete Overlay Pavements. Univ. of California, Berkeley, Ph.D. dissertation, 1979.

Publication of this paper sponsored by Committee on Rigid Pavement Design.

Structural Performance Model and Overlay Design Method for Asphalt Concrete Pavements

A. A. A. MOLENAAR AND CH. A. P. M. VAN GURP

The development of a structural performance model for flexible pavements is described. This model consists of a set of probability-of-survival curves in which the structural deterioration of pavement structures, which are characterized with their equivalent layer thickness, is given with respect to the number of load repetitions. The equivalent layer thickness is calculated according to Odemark's theory. It is shown that the equivalent layer thickness and the survival rate of the pavement can be determined by means of deflection measurements. Furthermore, it is shown how an in situ asphalt concrete fatigue relation can be derived for the construction considered. An overlay design chart based on the equivalent layer thickness concept is given, and an example of how the developed techniques are used for the overlay design of asphalt pavements is presented.

Because the economic recession is restricting the available pavement maintenance and rehabilitation budget, an optimal allocation of this budget for maintenance projects becomes more and more important. It is obvious that, in this situation, engineering judgment alone is not enough to solve overlay design and budget-allocation problems. More emphasis is therefore placed on the so-called rational methods.

This paper describes the efforts of the Laboratory for Road and Railroad Research, Delft University of Technology, on the development of structural performance and overlay design methods. These models are based on deflection measurements that were carried out on several road sections over a three-year period and on a theoretical analysis of three layer pavement systems. An example illustrates the use of these models.

STRUCTURAL PERFORMANCE MODEL: THEORETICAL ANALYSIS

Ninety-three layer structures were analyzed with the BISAR computer program to derive relations between the equivalent layer thickness (h_e) and the maximum strain in the asphalt layer or the vertical compressive strain at the top of the subgrade (1). The equivalent layer thickness is defined as follows:

$$h_e = \sum_{i=1}^{2} 0.9\, h_i \sqrt[3]{E_i/E_3} \quad (1)$$

where

h_e = equivalent layer thickness (m),
h_i = thickness of layer i (m),

E_i = elastic modulus of layer i (N/m²), and
E_3 = elastic modulus of the subgrade (N/m²).

The geometry of the loading system used in the analysis is shown in Figure 1. The results of this analysis are presented in Figure 2. The equivalent layer thickness was used as an independent variable because it is a simple way to describe the bearing capacity of pavement structures. The equivalent-layer-thickness concept was originally developed by Odemark (2) and has been successfully used by Jung and Phang (3) in the assessment of subgrade deflection.

Figure 1. Geometry of loading system.

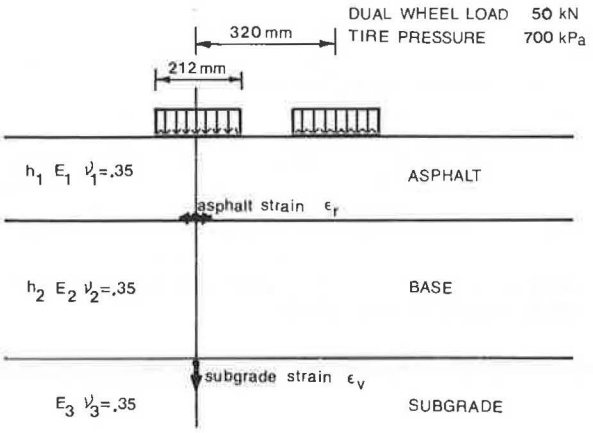

Figure 2. Relations between equivalent layer thickness (h_e) and maximum asphalt strain (ϵ_r) or subgrade strain (ϵ_v).

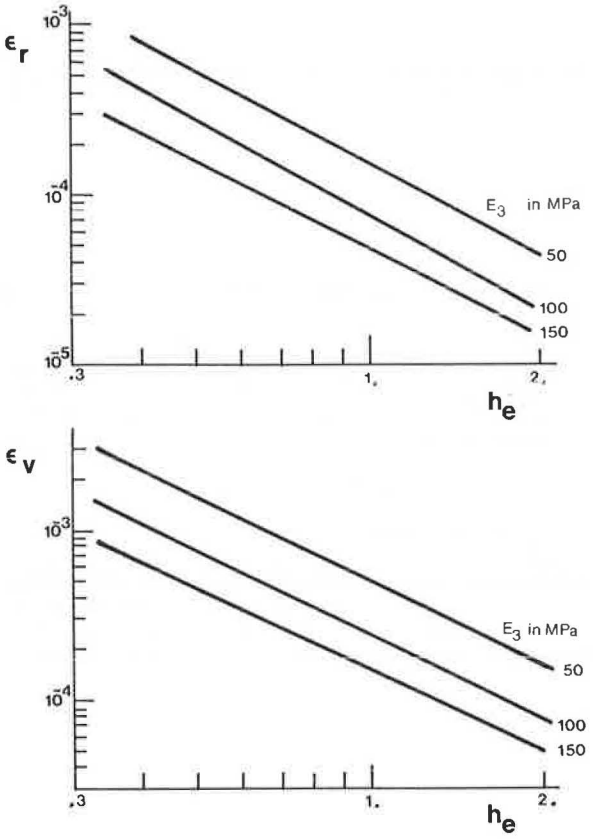

From the relation given in Figure 2 and appropriate fatigue relations for the asphalt mix and the subgrade considered, relations between the equivalent layer thickness and the pavement life expressed as the number of equivalent 100-kN axles could be developed. An example is given in Figure 3. Figure 3a shows the equivalent layer thickness versus asphalt strain relation, while Figure 3b shows the fatigue relation for a gravel-sand asphalt mix. Combining Figures 3a and 3b results in Figure 3c, which gives the relation between the equivalent layer thickness and the pavement life based on the asphalt strain criteria. The same procedure is followed to derive relations between the equivalent layer thickness and the pavement life based on the subgrade strain criteria (Figures 3d, 3e, and 3f).

Finally, the combination of Figure 3c and Figure 3f results in Figure 3g, which shows the overall relation between equivalent layer thickness and pavement life. Figure 3g can be used for pavement design purposes, which means that an equivalent layer thickness can be selected if the design number of load applications is known. The equivalent layer thickness determined in this way can then be split up in layer thicknesses and layer moduli by using Equation 1. In fact, alternative designs can be made very easily by using the procedure described here.

It should be noted that the pavement life determined from Figure 3g is the mean pavement life because it is based on the mean value of material properties, layer thicknesses, and strains. The mean pavement life means that the design has a reliability of 50 percent.

By taking into account the variability of layer thicknesses and material properties, survival curves have been derived from design charts as given in Figure 3. These survival curves give the probability of survival of a given design (h_e) in relation to the number of load applications. An example of such a survival curve is given in Figure 4.

The way in which these probability-of-survival curves were derived is fully described elsewhere (1). However, for the sake of completeness it will be repeated here.

First, the variance of the equivalent layer thickness was assessed from the following equation:

$$S^2_{h_e} = \sum_{i=1}^{L-1} (\delta f/\delta h_i)^2 S^2_{h_i} + \sum_{i=1}^{L} (\delta f/\delta E_i)^2 S^2_{E_i} \quad (2)$$

where

$S^2_{h_i}$ = variance of layer thickness i,
$S^2_{E_i}$ = variance of the elastic modulus of layer i,
L = number of layers,
$f = 0.9 \sum_{i=1} h_i \sqrt[3]{E_i/E_s}$, and
E_s = elastic modulus of the subgrade.

Next, $S^2_{\log \epsilon}$ was calculated from

$$S^2_{\log \epsilon} = d^2 S^2_{\log h_e} + S^2_{\text{l.o.f. } (h_e - \epsilon)} \quad (3)$$

where

$S^2_{\log \epsilon}$ = variance of the estimated strain,
d^2 = slope of the equivalent layer thickness versus strain relation, and

$S^2_{l.o.f.\ (h_e - \epsilon)}$ = variance due to lack of lit of the equivalent layer thickness versus strain relation.

Finally, $S^2_{log\ N}$ was calculated from

$$S^2_{log\ N} = b^2 S^2_{log\ \epsilon} + S^2_{l.o.f.\ (N - \epsilon)} \quad (4)$$

where

$S^2_{log\ N}$ = variance of the estimated number of load repetitions to failure,

b^2 = slope of the used fatigue relation, and

$S^2_{l.o.f.\ (N - \epsilon)}$ = variance due to lack of lit of the strain versus number of repetitions to failure relation (fatigue relation).

Figure 3. Pavement design curves.

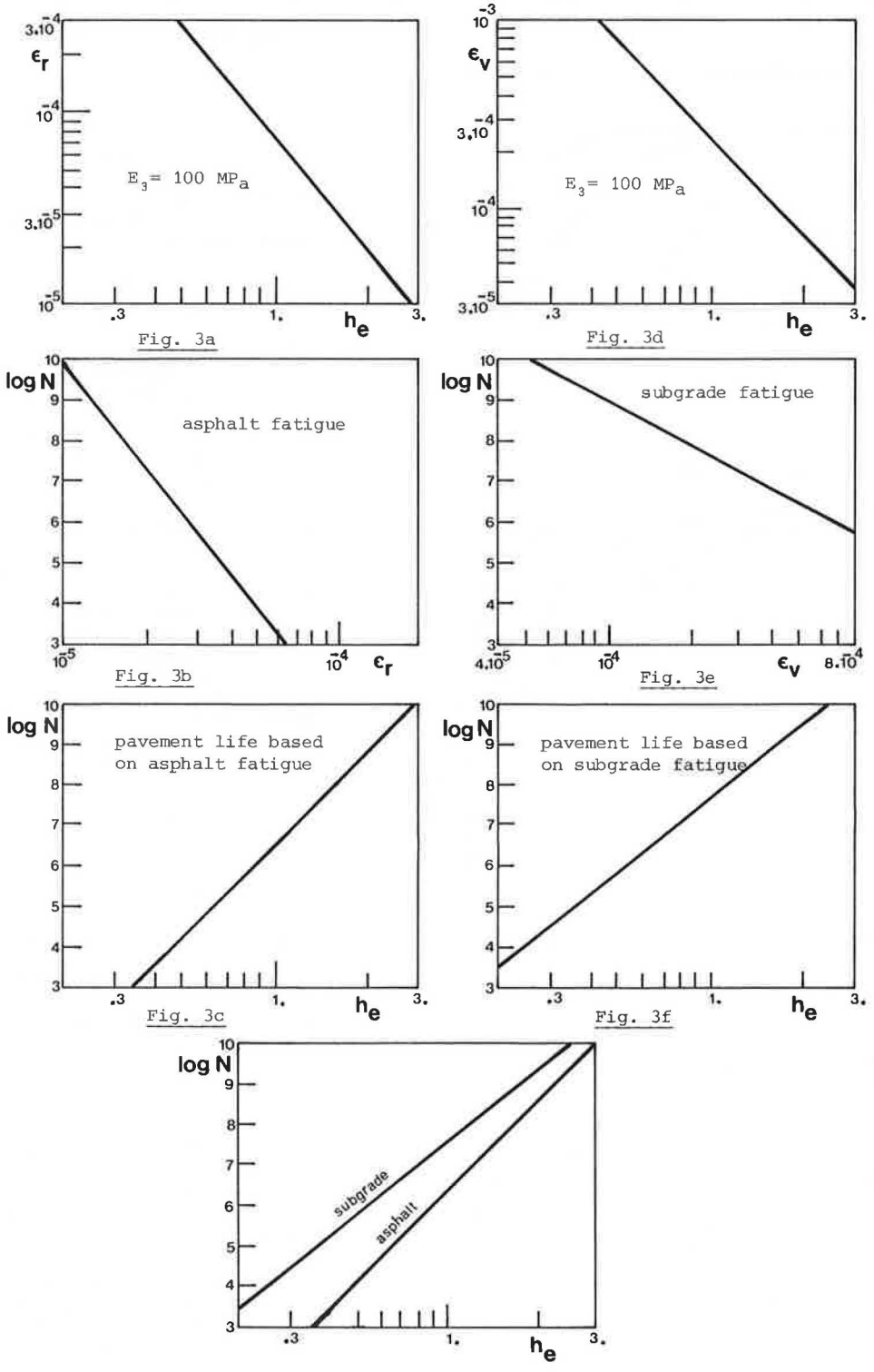

The number of load repetitions to a certain level of reliability (N_p) can now be calculated from

$$\log N_p = \log \bar{N} - U_p S_{\log N} \quad (5)$$

where $\bar{N}$ is the number of load repetitions that have all variables set at their mean value and U_p is the value taken from the normal tables that corresponds with the desired confidence level P. Figure 4 is derived by using an $S_{\log N}$ value of 0.4.

From the foregoing, it will be clear that any value for $S_{\log N}$ can be used by knowing the variations in layer thicknesses and material properties.

Figure 4. Probability-of-survival curves for a given set of equivalent layer thicknesses.

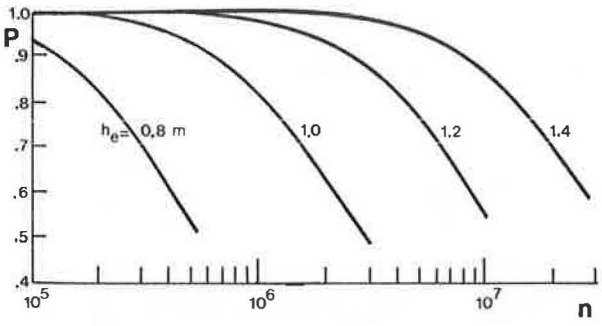

Figure 5. Basic set of survival curves.

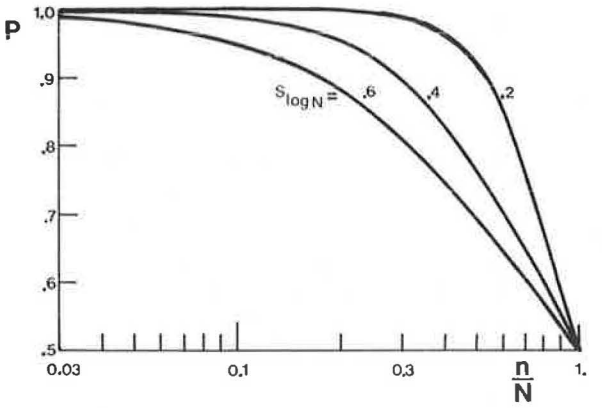

Figure 6. Principles of falling-weight deflection measurements.

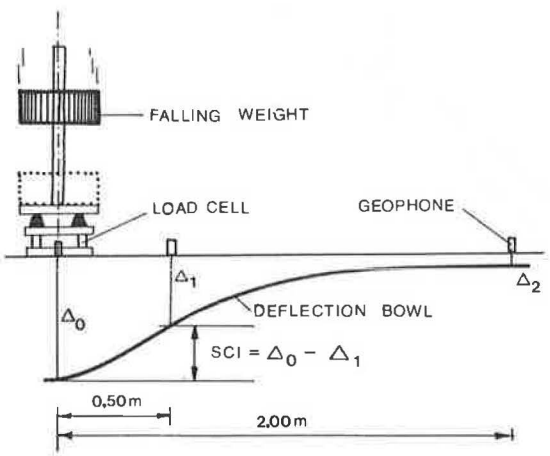

Because the shape of the survival curves depends on the material properties and their variations, a basic set of survival curves was derived, which is shown in Figure 5. Figure 5 was derived simply by using different values for $S_{\log N}$ in Equation 5. Now the probability of survival is given as a function of the ratio of applied number of load applications to allowable number of load applications and $S_{\log N}$.

Later it will be shown how a value for $S_{\log N}$ can be determined from deflection measurements. Then it will be shown how Figure 5 will be used for residual life assessment.

ASSESSMENT OF EQUIVALENT LAYER THICKNESS FROM DEFLECTION MEASUREMENTS

Deflection measurements in this study were taken by means of a falling-weight deflectometer. The basic principle of this device is shown in Figure 6. From BISAR calculations, the following relation could be derived between the surface curvature index measured with the falling-weight device and the equivalent layer thickness:

$$\log h_e = -1.117 - 0.486 \log E_3 - (0.556 - 0.021 \log E_3) \log (21 \times 10^{-6} + 0.6\ SCI) \quad (6)$$

where SCI is the surface curvature index measured with a falling-weight deflectometer (P = 50 kN, t = 0.02 s) (m), and E_3 is the elastic modulus of the subgrade (MN/m^2).

The elastic modulus of the subgrade can be assessed directly from the deflection measured 2 m from the loading center with the following equation:

$$\log E_3 = 3.869 - 1.009 \log \Delta_2 \quad (7)$$

where Δ_2 is the deflection measured at 2 m from the loading center (P = 50 kN, t = 0.02 s).

Temperature corrections should be applied on the calculated h_e in order to get the h_e at the reference temperature of 11°C. This temperature was selected as the reference temperature because it is the weighted mean annual air temperature of 11°C for Dutch conditions (4). It has been shown elsewhere (5) that the temperature correction should be applied in the following way:

$$h_{e_{t=11°C}}^{*} = h_{e_t}^{*} - (11 - t) \cdot 0.014 \quad (8)$$

where

$$h_{e_t}^{*} = h_e \sqrt[3]{E/100}\ (m) \quad (9)$$

and t is the air temperature at the measurements.

The temperature-corrected $h_{e_{t=11°C}}$ is calculated with the following equation:

$$h_{e_{t=11°C}} = h_{e_{t=11°C}}^{*} \sqrt[3]{100/E_3} \quad (10)$$

OBSERVED STRUCTURAL PERFORMANCE

By using the techniques described in the previous sections, the decrease of the h_e in time was determined for a number of road sections by means of deflection measurements that were carried out over a three-year period. Because extensive measurements during and after completion of the construction were carried out by others on a couple of sections (6), the decrease of the h_e from the opening of those sections to traffic could be determined. An example of such a deterioration curve is given in Figure 7a. Figure 7b gives the same deterioration curve, but

Figure 7. Decrease of h_e with respect to (a) time (years) and (b) number of load applications.

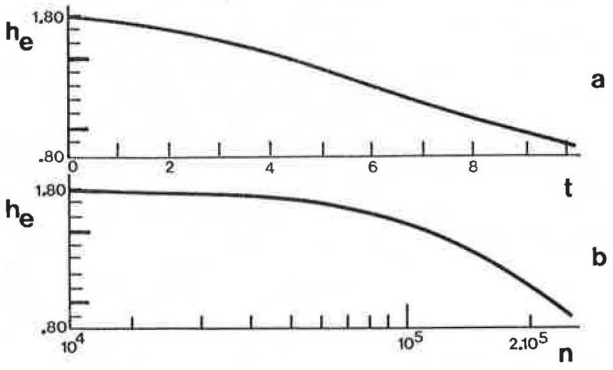

Figure 8. Decrease of K with respect to ratio n/N and β.

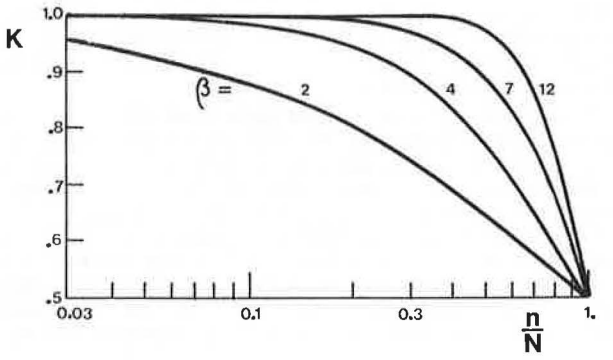

Figure 9. Determination of residual life (1 - n/N) from P and $S_{log\ N}$.

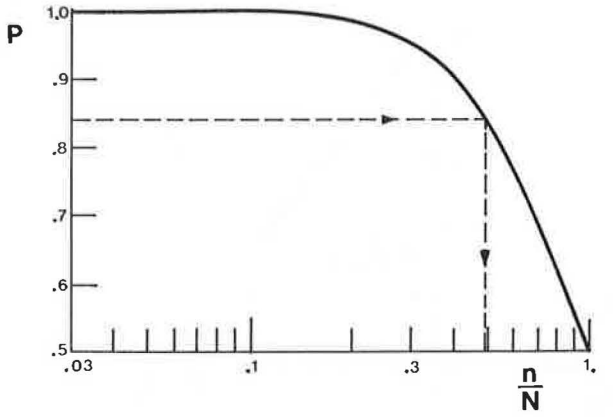

now with respect to the number of equivalent 100-kN single axles that have passed the section considered. For almost all of the sections that were studied, a comparable decrease of h_e was observed. On some sections, the expected decrease of h_e could not be determined.

The decrease of h_e with respect to the ratio n/N (Figure 7b) can be written as follows:

$$K = 1/[1 + \exp(\beta \log n/N)] \quad (11)$$

where

$$K = h_{e_n}/h_{e_o},$$

h_{e_n} = equivalent layer thickness after n load applications,

h_{e_o} = equivalent layer thickness at the beginning of the pavement life (n = 0), and

β = a constant.

A graphical representation of Equation 11 is shown in Figure 8. If one compares Figure 8 (observed structural deterioration) with Figure 5 (theoretically derived structural deterioration), one notices the striking resemblance. Therefore, it is concluded that K (Figure 8) and P (Figure 5) are exchangeable with each other and that P can be determined by means of deflection measurements. Furthermore, it is concluded that a proper value of $S_{log\ N}$ can be determined for each construction from a comparison of β and $S_{log\ N}$ with each other (compare Figures 8 and 5). If the h_e is known for at least two values of n, β can be determined by means of regression techniques.

From our study, we concluded that β (and so $S_{log\ N}$) is dependent on the type of construction. For rather rigid constructions (i.e., constructions with a cement-stabilized base), $S_{log\ N}$ is about 0.3. For full-depth asphalt constructions $S_{log\ N}$ is about 0.4, and for constructions with an unbound granular base $S_{log\ N}$ is about 0.6. Next we will show how one or the other is used in the assessment of the residual life of pavement structures.

RESIDUAL LIFE ASSESSMENT

For reasons of costs and time, it will not be possible to perform regular deflection measurements in order to follow the decrease of h_e in time. These measurements are mostly taken at the moment when one expects that an overlay should be applied on the construction considered. In order to be able to make a proper estimation of K, it is therefore recommended to perform deflection measurements in the wheel tracks and between the wheel tracks. The value of h_e calculated from the measurements between the wheel tracks is thought to be a reasonable estimate for h_{e_o}, since this part of the structure is hardly subjected to traffic loading.

Furthermore, a value for $S_{log\ N}$ can be selected from the type of construction (see previous section). Knowing K and $S_{log\ N}$, the corresponding value for the ratio n/N can be determined (Figure 9), and the pavement life N can be calculated if the applied number of load applications n is known. The residual life, which is defined as N - n, can then easily be calculated. Once again it should be noted that the ratio n/N = 1 corresponds to the mean pavement life and that ratios greater than 1 can occur.

OVERLAY DESIGN

In order to be able to make life predictions for a strengthened construction, one should know the fatigue behavior of the asphalt materials used in the existing construction. Normally, laboratory-determined fatigue relations are used, which are corrected for beneficial effects as rest periods, etc. It is believed, however, that the fatigue behavior in situ can be very different from laboratory-determined fatigue behavior. Therefore, it is suggested that for each construction considered, an in situ fatigue relation should be determined. This is done in the following way.

From the h_{e_o}, which is determined according to the procedure outlined in the previous section, the

initial maximum tensile strain in the asphalt layer is determined by using Figure 2. Because the pavement life N can also be calculated (see previous section), the combination of the calculated ϵ and N will result in a point in the fatigue diagram (Figure 10).

To get a fatigue relation, a line with a slope of -4 is drawn through this fatigue point (Figure 10). A value of -4 is selected for the slope of the fatigue line because it is a reasonable value compared with slope values for in situ fatigue relations reported elsewhere (7,8). This fatigue relation, determined in the above-described way, is used to predict the pavement life N for lower values of ϵ (i.e., higher values of h_e). An example of the process described above is given next.

Figure 10. Determination of an in situ fatigue relation.

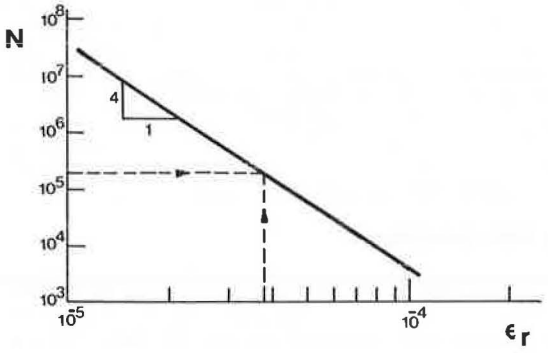

From a construction that consists of a 100-mm-thick asphalt layer on a 350-mm unbound granular base layer, the ratio of h_e in the wheel tracks to h_e between the wheel tracks is determined to be 0.6. Because the construction consists of a rather thick unbound base layer, the value of $S_{\log N}$ is set at 0.6. From Figure 11a it is determined that the ratio n/N is 0.7. Because the number of equivalent 100-kN single axles that have loaded the construction (n) equals 2.1×10^5, the allowable number of equivalent 100-kN single axles is 3×10^5.

The equivalent layer thickness between the wheel tracks is 1000 mm; from Figure 11b it was determined that the initial tensile strain (ϵ_i) is 7.3×10^{-5}. The combination of the calculated ϵ_i and N resulted in the fatigue relation for the construction considered, which is given in Figure 11c. The pavement life for higher values of h_e was calculated, and pavement survival curves were derived for those higher h_e values, assuming that $S_{\log N}$ for these constructions is the same as the $S_{\log N}$ for the construction considered (0.6). These curves are shown in Figure 11d. For the construction considered, it was determined that it should sustain another 7×10^5 equivalent 100-kN single-axle repetitions.

From Figure 11d it can be seen that if the minimum acceptance level for the survival rate is set at 0.65, a construction with h_e = 1270 mm is capable of sustaining the design number of load repetitions. The needed increase in h_e is therefore 270 mm.

Figure 12 shows the overlay design chart that is used to determine by which overlay the needed increase in h_e can be achieved. This figure was derived from BISAR calculations. As can be seen from Figure 12, the overlay in the example can be

Figure 11. Illustration of example problem.

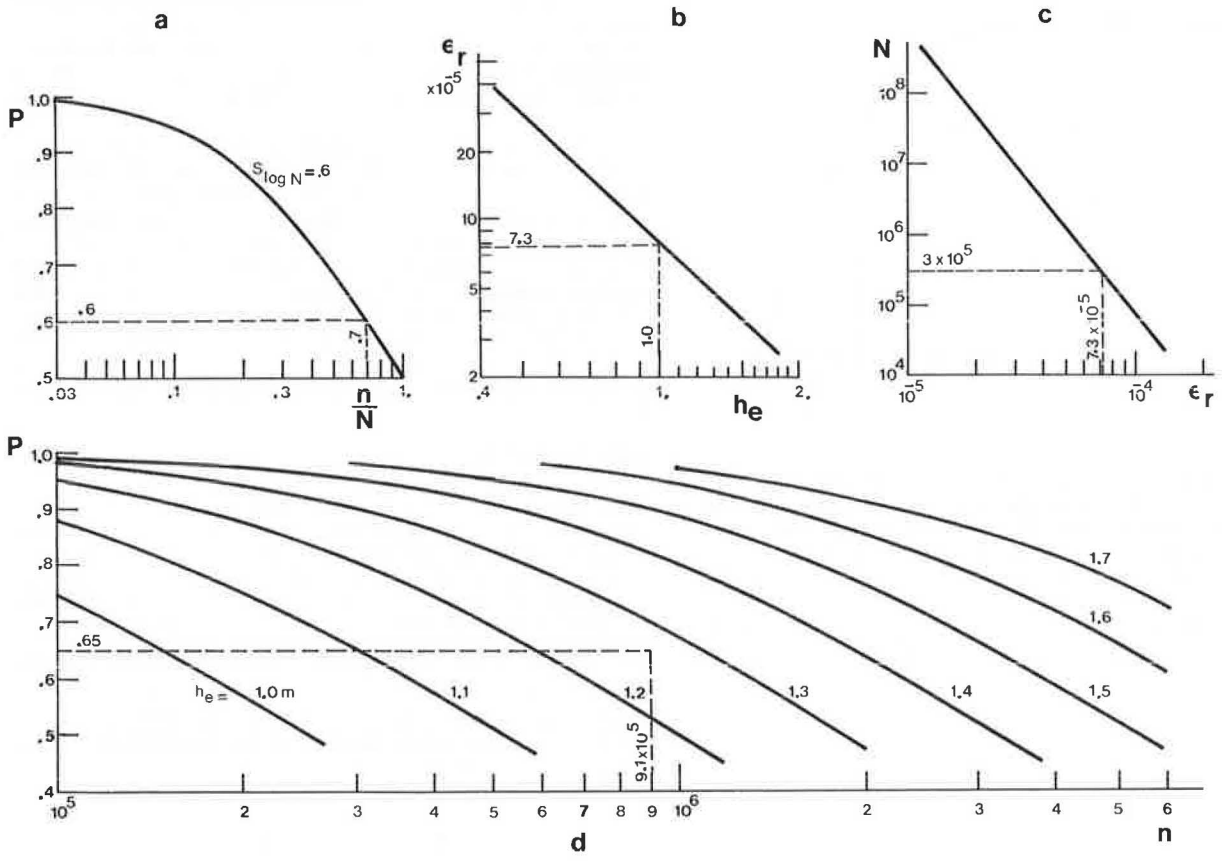

Figure 12. Overlay design graph (overlay thickness in millimeters).

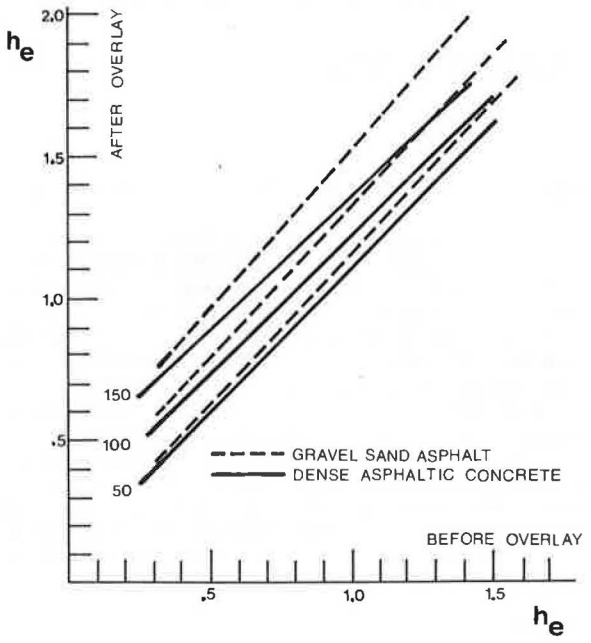

either a 75-mm gravel-sand asphalt layer or a 110-mm dense asphaltic concrete layer. Because of better skid resistance and crack-propagation properties (slower crack propagation), the dense asphaltic concrete solution is selected.

As will be noted, the minimum acceptance level for the survival rate has a rather high influence on the overlay thickness. A value of 0.65 was selected, because accepting lower values of the survival rate will increase the need of routine maintenance because of a worse condition of the pavement surface, especially if rather severe winter conditions occur (9).

CONCLUSIONS

Based on the results of the study presented in this paper, the following conclusions can be drawn:

1. Because the equivalent layer thickness correlates well with the maximum tensile strain in the asphalt layer or the vertical compressive strain at the top of the subgrade, it is an adequate parameter to judge the pavement bearing capacity.
2. The equivalent layer thickness can be easily determined by means of deflection measurements.
3. The probability-of-survival curves derived from observed structural deterioration of pavements can be described with an e-power relation that shows very much resemblance with the theoretically derived probability-of-survival curves.
4. The shape of the survival curve seems to be dependent on the type of construction.
5. The survival rate of the pavement can be determined by means of deflection measurements in and between the wheel tracks.
6. For each pavement section considered, an appropriate in situ fatigue relation can be determined from the equivalent layer thickness determined from deflection measurements taken between the wheel tracks. The precondition is, however, that no cracking be visible in this area.

REFERENCES

1. A.A.A. Molenaar and Ch.A.P.M. van Gurp. Optimization of the Thickness Design of Asphalt Concrete. Proc., 10th Australian Road Research Board Conference, Sydney, Vol. 10, No. 2, 1980.
2. N. Odemark. Investigations as to Elastic Properties and Soils and Design of Pavements According to the Theory of Elasticity. Statens Vaeginstitut, Stockholm, Sweden, 1949.
3. F.W. Jung and W.A. Phang. Elastic Layer Analysis Related to Performance in Flexible Pavement Design. Ministry of Transportation and Communications, Downsview, Ontario, Canada, Rept. RR 191, 1975.
4. Shell Pavement Design Manual: Asphalt Pavements and Overlays for Road Traffic. Shell International Petroleum Company, Ltd., London, 1978.
5. A.A.A. Molenaar and E. Beuving. Deflection Measurements for the Determination of the Structural Deterioration of Pavements. Department of Civil Engineering, Laboratory for Road and Railroad Research, Delft Univ. of Technology, Delft, The Netherlands, Rept. WB-25 (7-80-115-20), 1980.
6. P. van Diggele. Comparative Study on Unbound Gravel Bases of Blast Furnace Slag, Lava, and Red Burnt Colliery Shale. Study Centre for Road Construction, Arnhem, The Netherlands, Publ. I, 1974.
7. P. de Kiewit, P.C. Koning, R.F. Carmichael, and W.R. Hudson. Evaluation and Overlay Design for Flexible Pavements on Low-Volume Roads. Proc., Fourth International Conference on Structural Design of Asphalt Pavements, Univ. of Michigan Ann Arbor, 1977.
8. F. Finn, C. Saraf, R. Kulkarni, K. Nair, W. Smith, and A. Abdullah. The Use of Distress Prediction Subsystems for the Design of Pavement Structures. Proc., Fourth International Conference on Structural Design of Asphalt Pavements, Univ. of Michigan, Ann Arbor, 1977.
9. A.A.A. Molenaar. Measurements on Frost Damage on Provincial Roads in South Holland. In The Winter of 1978-1979, Study Centre for Road Construction, Arnhem, The Netherlands, Publ. N, 1980.

Publication of this paper sponsored by Committee on Pavement Rehabilitation Design.

Structural Performance Evaluation of Recycled Pavements by Using Dynamic Deflection Measurements

SUDIPTA S. BANDYOPADHYAY

A comparative study is presented that concerns the structural performance of recycled pavements, which is based on the Dynaflect deflection measurements on five test sections of Kansas highway KS-96 that were monitored at regular intervals. Central-plant hot-recycling processes and in-place cold-recycling processes (with and without rejuvenating agent) were used to construct the four recycled test sections; the fifth one was a typical overlay section generally used in Kansas. In addition to the five deflection parameters that are associated with the Dynaflect measurements and are thought to be indicative of the structural characteristics of the measured pavement structure, criteria used for the comparative evaluation include the relative variation, with time, of required overlay thickness, pavement life, average pavement modulus, and subgrade modulus. The study reveals that the average values of layer coefficients for recycled materials generally found in the literature do not properly reflect the structural performance of the recycled sections. The study also reveals that the cold-recycled section (without rejuvenating agent) is perhaps superior in structural performance as compared with other sections. However, the typical overlay section and the cold-recycled section (with 2 percent rejuvenating agent) have a structural performance comparable to the previous one. Total pavement thickness is certainly a contributing factor. Gradual development of creep-actuated stiffening properties of the bituminous materials is found to vary widely, depending on the type of material.

The tremendous increase in recent years in the cost of asphalt cement and asphalt paving and an awareness of the need to conserve finite deposits of nonrenewable natural resources have prompted significant interest and investment in pavement recycling. In addition to the conservation of asphalt and aggregate, advantages of pavement recycling include conservation of energy, environmental preservation (reduced mining for new aggregate), and selective rehabilitation (elimination of the need for full-width overlays on multilaned highways).

Although pavement recycling as such is by no means a new concept, the methodology process, as it exists today, is still relatively new and undergoing changes. Thanks to the vigorous interest and participation of government, contractors, and researchers, pavement recycling is becoming a realization.

In general, pavement-recycling approaches can be classified under the following categories: surface recycling, in-place recycling, and central-plant recycling. Each of these three categories can be subdivided further into hot and cold processes.

Surface recycling is the reworking of the top 1 in of the pavement surface and can be achieved by techniques such as heater planing, heater scarifying, cold planing, and cold milling. Although surface recycling is effective in reducing distresses like rutting, shoving, corrugation, and reflection cracking, it produces limited structural improvement. In-place surface and/or base recycling consist of in-place pulverization followed by reshaping and compaction with or without the addition of a stabilizer. The advantages of in-place recycling include significant structural improvement and the ability to treat almost all types of pavement distress in asphalt-surfaced roadways. The problem of quality control is the major disadvantage of in-place recycling. In central-plant recycling, the pavement material is first scarified and removed from the roadway, mixed in a plant, and then laid and compacted to the desired grade. Advantages include improvements in structural capacity and the ability to correct all types of distress. Higher cost (compared with the other two), quality control, and potential air pollution problems are the disadvantages.

Although numerous publications have appeared in the specialized literature on design, construction, and cost analysis of different categories of pavement recycling, including reports of a symposium (1) and a seminar (2) at the national level, very little information, if any, is available concerning the relative performance of recycled pavements. The objective of this paper is to present a comparative structural evaluation of recycled pavements (in-place and central-plant) and analyze the performance of recycled pavements compared with typical pavement overlays. The analysis and evaluation are based on the dynamic deflection measurements obtained by a Dynaflect on different test sections of a reconstructed highway in Kansas.

PROJECT HISTORY

A test section about a mile long was selected on highway KS-96, which is east of Scott City in western Kansas. The original pavement was built in 1954 and was 7 in thick; it was a cold mix composed of sand-gravel with little or no crushed material and put down by blade laying. Conventional seals were added several times subsequently up to the current thickness of 8 in.

A 1952 soil survey report on the project described the soils as colby silt loam. The surface soil was a silt with a small proportion of very fine sand that extended to a depth of about 12-18 in. Underlying the surface soil was found a zone of dark brown weathered material that varied in thickness from 4 to 8 in and was classified as a silty clay. During the original construction, the top 12 in of the subgrade was compacted to a density equal to or greater than 95 percent of the Standard Proctor density.

The predominant type of distress that developed over the years was mainly transverse and some longitudinal cracking. The transverse cracks, which developed in the mat, eventually progressed from a single crack to a series of closely spaced multiple cracks. The mix beneath and adjacent to the cracks then deteriorated to the point where it lost its stability and load-carrying capacity substantially. The deterioration continued despite an extensive crack-sealing maintenance program.

PAVEMENT RECYCLING

The arrangement of the recycled test sections is shown in Figure 1. The decision to keep about 4 in of the existing mat was prompted by the requirement that traffic be allowed during the construction period. Construction was carried out during the last week of August 1979.

Central-Plant Hot Recycling

A CMI-750 Roto Mill, which is capable of cutting a section 12.5 ft wide, was used to mill about 3.5 in off the existing pavement in one pass. For the in-plant hot-recycling process (section A), the milled material was loaded into trucks, hauled, and

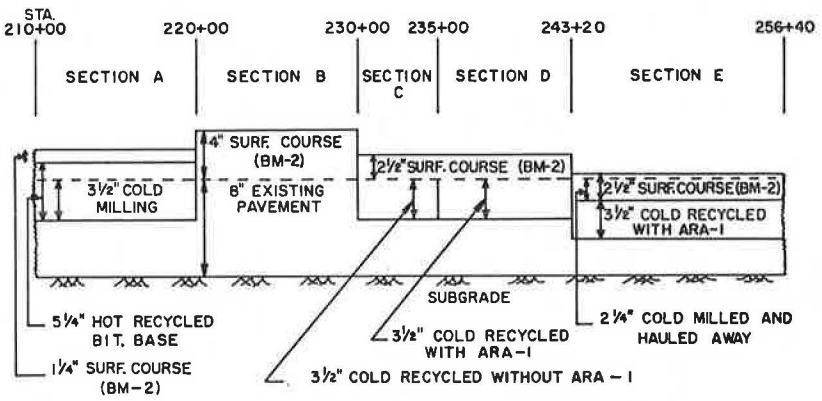

Figure 1. Arrangement of test sections.

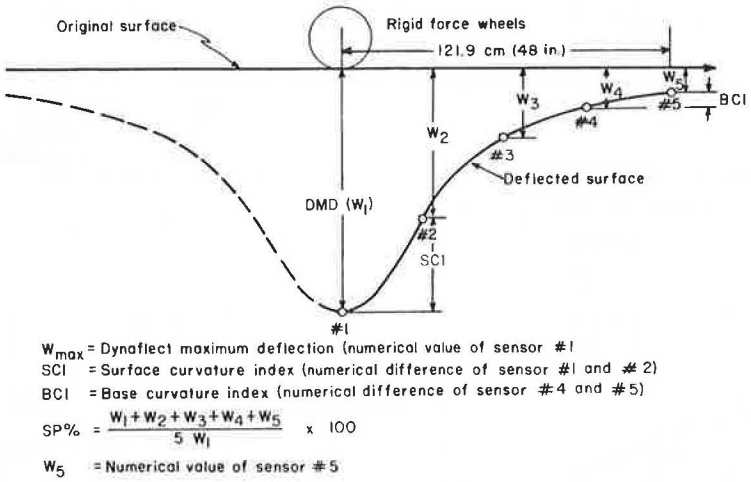

Figure 2. Deflection basin parameters associated with Dynaflect measurements.

stockpiled at the plant site. The reclaimed material was mixed with virgin material on a 50:50 proportion. About 2.5 percent new 120 to 150 penetration-grade asphalt was added. A split feed drum mixer was used, and the virgin aggregate was introduced at the flame end of the drum and superheated to 300°-500°F. The reclaimed material was introduced at about the midpoint of the drum and heated by hot gasses as well as by heat transferred from the superheated virgin aggregate. The combined material was then laid back in two lifts totaling 5.25 in thick on a 30-ft width. It was then topped with a 1.5-in wearing course.

In-Place Cold Recycling

The in-place cold recycling was done with and without a rejuvenating agent. A CMI-750 milled the old roadway 3.5 in deep and 12 ft wide. While milling, except in the no-additive section (section C), a distributor was attached by hose to the front of the PR-750. The rejuvenating agent (ARA-1) was pumped through the PR-750 water spray bar. The milled material formed a windrow about 3 ft high behind the PR-750. A blade followed and cut the turf shoulder down to the depth of the 3.5-in cut. A CMI Clarco Windrow loader, which was pushed by the paver, picked up the windrow and loaded it into the paver. The paver relaid the recycled material 15-ft wide. The recycled mix was then compacted and traffic was allowed on the rolled material. A wearing course was then applied the following day. A detailed account of the cold-recycled section is given elsewhere (3).

DEFLECTION MEASUREMENTS

The deflection basin parameters associated with Dynaflect measurements are shown in Figure 2. The Dynaflect maximum deflection (DMD) is a measure of the structural characteristics of the pavement and support conditions. The surface curvature index (SCI) is predominantly an indicator of the structural integrity of the surface layer. The base curvature index (BCI) measures the base support conditions. The spreadability (SP) measures the load-carrying capacity and stiffness ratio of the pavement structure, and the fifth sensor reading (W_5) has been shown to be an indirect measure of the subgrade modulus. These five parameters, considered either individually or jointly, can provide an estimate of the structural condition of the pavement structure being surveyed. Further information regarding evaluation and application of Dynaflect deflections is given elsewhere (3-12).

Dynaflect deflection measurements were obtained on all sections before and after construction. The results are presented in Table 1. All the parameter values are the average values normalized with respect to a base temperature of 70°F (5,10).

STRUCTURAL PERFORMANCE EVALUATION

Different thicknesses of the structural layers in the test section preclude a direct comparison between them. Therefore, the sections will be evaluated in terms of their structural number (SN). The SN is defined as an index number derived from an analysis of traffic, roadbed soil conditions, and a regional factor that may be converted to thickness

Table 1. Average Dynaflect parameter values.

Section	Date	DMD (mils)	SCI (mils)	BCI (mils)	SP (%)	W_5 (mils)
A	Sept. 15, 1978	1.58	0.49	0.11	50	0.30
	Oct. 23, 1979	1.53	0.21	0.13	61	0.35
	May 7, 1980	1.26	0.29	0.12	58	0.31
	Aug. 20, 1980	1.38	0.33	0.13	57	0.33
B	Sept. 15, 1978	1.58	0.49	0.11	50	0.30
	Oct. 23, 1979	1.31	0.14	0.11	67	0.41
	May 7, 1980	1.05	0.19	0.13	64	0.35
	Aug. 20, 1980	1.13	0.23	0.12	62	0.36
C	Sept. 15, 1978	1.58	0.49	0.11	50	0.30
	Oct. 23, 1979	1.42	0.25	0.12	59	0.33
	May 7, 1980	1.09	0.25	0.12	58	0.25
	Aug. 20, 1980	1.09	0.26	0.12	58	0.28
D	Sept. 15, 1978	1.58	0.49	0.11	50	0.30
	Oct. 23, 1979	1.64	0.30	0.13	59	0.38
	May 7, 1980	1.20	0.32	0.10	57	0.30
	Aug. 20, 1980	1.22	0.36	0.11	56	0.32
E	Sept. 15, 1978	1.58	0.49	0.11	50	0.30
	Oct. 23, 1979	1.58	0.49	0.13	54	0.42
	May 7, 1980	1.50	0.41	0.13	57	0.35
	Aug. 20, 1980	1.49	0.46	0.13	55	0.39

Figure 3. Required overlay thickness before and after reconstruction.

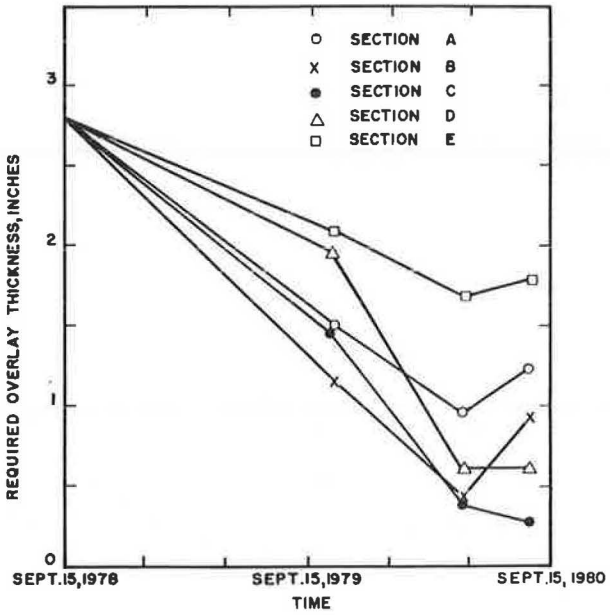

of various flexible-pavement layers through the use of suitable layer coefficients related to the type of material being used in each layer of the pavement structure. The layer coefficient (designated by a_1, a_2, and a_3 for surface, base, and subbase, respectively) is the empirical relation between SN for a pavement structure and layer thickness, which expresses the relative ability of material to function as a structural component of the pavement (13).

Analytically, the SN is given by the following equation:

$$SN = a_1 D_1 + a_2 D_2 + a_3 D_3 \quad (1)$$

where the D_i values are the respective layer thicknesses. A layer coefficient value of 0.44 is generally used for surface course in Kansas. Because layer coefficients for recycled materials have not yet been formulated in Kansas, the following coefficients are selected based on the recommendations by Epps (14):

1. Hot-recycled bituminous base = 0.40,
2. Cold-recycled bituminous base (with ARA-1) = 0.38, and
3. Cold-recycled bituminous base (without ARA-1) = 0.30.

A layer coefficient of 0.15 was selected for the existing mat. The SNs of different sections are then given by the following: section A = 3.33, section B = 2.96, section C = 2.83, section D = 3.11, and section E = 2.73. According to this criteria, section A is supposed to be structurally superior to the other sections and section E represents the weakest section, provided that the values of layer coefficients used are realistic. As will be seen in the following sections, pavements that might be categorized structurally superior according to SN criteria are not necessarily superior in their structural performance.

Overlay Thickness and Pavement Life Criteria

The recorded DMDs on each section were used to determine a representative DMD for the section. At the 95 percent confidence level, the representative DMD equals the following:

$$\text{Representative DMD} = (\overline{DMD} + 1.645\ s) \cdot f \cdot c \quad (2)$$

where

$\overline{DMD}$ = arithmetic mean of the individual values,
s = standard deviation,
f = temperature adjustment factor, and
c = critical period adjustment factor.

The representative DMD was used to compute the overlay thickness and the pavement life according to the Asphalt Institute method (15). An evaluation of f and c factors has been discussed elsewhere (5,10). It should be emphasized that too many extraneous forces affect the condition of the pavement for any method of estimating the overlay thickness and pavement service life accurately. This paper is primarily concerned with the comparative study of solutions and, therefore, comparative values rather than absolute values are mainly significant.

Required overlay thickness and pavement life for each section before and after reconstruction are plotted in Figures 3 and 4, respectively. It is evident from Figures 3 and 4 that, based on overlay thickness and pavement life criteria, section C (SN = 2.83) is superior to the other sections and section E (SN = 2.73) is the weakest section. It should also be noted that the performances of section B (SN = 2.96) and section D (SN = 3.11) are comparable with that of section C. For all sections, the percentage reduction in the required overlay thickness and the percentage increase in the pavement life after reconstruction are given in Table 2.

One important observation that can be made from Figures 3 and 4 is that the performance of all sections after reconstruction improves up to about seven to eight months. After that, except for section C, the performance begins to deteriorate. The rate at which the performance improves or deteriorates can be judged by observing the slope of the lines in Figures 3 and 4. The rate of improvement for sections A and E is much lower than that of the other sections. However, the rate of deterioration of section B is much higher than that of any other section. The performance of section C was steadily improving one year after construction.

The gradual improvement observed after construction in the performance of the recycled sections can

Table 2. Percentage improvement in structural performance of test sections after reconstruction.

Item	Section A			Section B			Section C			Section D			Section E		
	10/23/79	5/7/80	8/20/80	10/23/79	5/7/80	8/20/80	10/23/79	5/7/80	8/20/80	10/23/79	5/7/80	8/20/80	10/23/79	5/7/80	8/20/80
DMD	3	20	13	17	34	28	10	31	31	-4	24	23	0	5	6
SCI	57	41	33	71	61	53	49	49	47	39	35	27	0	16	6
BCI	-18	-9	-18	0	-18	-9	-9	-9	-9	-18	9	0	-18	-18	-18
SP	22	16	14	34	28	24	18	16	16	18	14	12	8	14	10
W_5	-17	-3	-10	-37	-17	-20	-10	17	7	-27	0	-7	-40	-17	-30
Overlay thickness	47	65	56	58	85	67	47	86	90	29	79	78	25	40	36
Pavement life	344	656	489	511	1233	711	344	1256	1444	156	1011	1000	122	256	211
Avg pavement modulus	900	667	600	1733	1733	1233	767	1067	1067	583	633	533	367	567	517
Subgrade modulus	-17	0	-6	-17	3	3	-8	17	17	-17	0	11	-6	3	3

Figure 4. Pavement life before and after reconstruction.

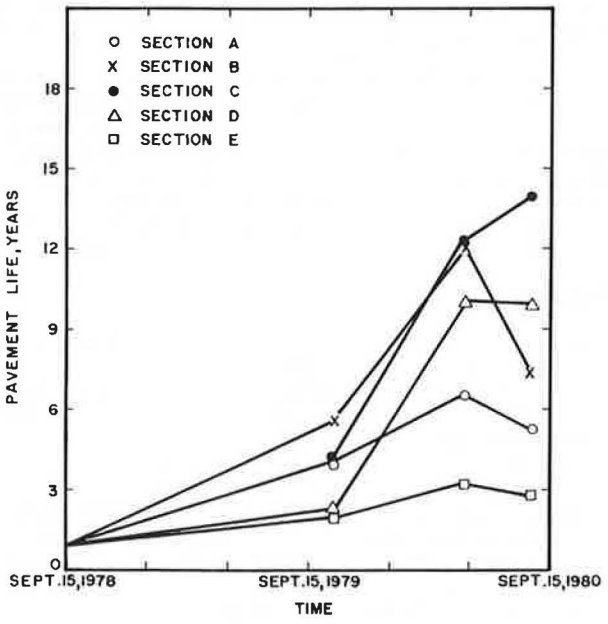

be expected because the deflections taken on a newly laid asphalt pavement a few days after its construction will subsequently decrease in magnitude (up to a certain time). The reasons for this reduction in magnitude are (a) densification of the bituminous material under wheel loads, and (b) gradual development of creep-actuated stiffening properties of the bituminous material. Although the expected densification of the bituminous material due to wheel loads is generally achieved in the first few months of the pavement service period, the development of the full stiffening properties may take some additional time. It is evident that the stiffening properties of section C were still developing one year after its construction, while the stiffening properties of the other sections realized their full potential about seven or eight months after their construction and then started to deteriorate.

Pavement and Subgrade Modulus

To investigate the mechanism of the variation of the stiffening properties with time for the sections, average pavement modulus (average of all the bituminous layers) was computed from the deflection measurements by assuming the pavement structure as a two-layer medium. The pavement modulus values were determined from a consideration of the corresponding average SP and DMD values and assuming a Poisson's ratio value for the pavement and the subgrade equal to 0.45 (16).

The variation with time of section pavement modulus is shown in Figure 5. It can be seen that the average pavement modulus for section A started to decrease almost immediately after construction, while that of section B reached its highest value about four months after construction and then started to decrease drastically. The average pavement modulus value for section C increased to about one year after construction and those of sections D and E increased to about eight months after construction and then slowly began to decrease. The average pavement modulus of section B is substantially larger than that of other sections; the greater thickness of section B, as compared with other sections, may be a contributing factor to its larger value of pavement modulus. Section C has the next largest pavement modulus.

The variation of subgrade modulus with time, computed from corresponding DMD and SP values (16), is shown in Figure 6. Monthly precipitation values are also plotted in Figure 6. It can be seen that, immediately after construction, the subgrade moduli of all the sections decreased and, after that, there was no significant gain in the moduli values, as shown in Table 2. This trend, with respect to values of subgrade modulus, is also substantiated by the BCI and W_5 values, which are indicative of subgrade strength. Substantial amounts of rain at the site during the time of construction may help to explain the reduction in values of subgrade modulus. As can be expected, the subgrade modulus behavior for all the sections is approximately the same. A recent study concludes that there is a statistically significant cross correlation between precipitation and the value of subgrade modulus. Further discussion of this topic is beyond the scope of this paper.

SUMMARY

Five test sections are being monitored on KS-96 near Scott City, Kansas, to study the structural performance characteristics of recycled pavements. Central-plant hot-recycling and in-place cold-recycling processes (with and without rejuvenating agent) were used in the construction of four test sections; the fifth section has a 4-in surface course overlay. A comparative evaluation is presented based on the Dynaflect deflection measurements being obtained at regular intervals on all test sections.

It was found that the structural performance of the different sections is not necessarily directly related to their SN obtained from the recommended values of layer coefficients found in the literature for recycled materials. This would suggest that further studies are needed to evaluate realistic

Figure 5. Variation of pavement modulus of sections with time.

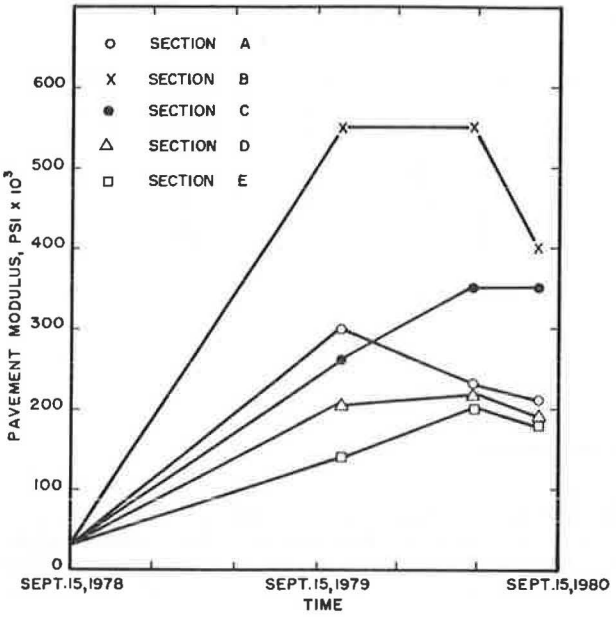

Figure 6. Subgrade modulus and monthly precipitation.

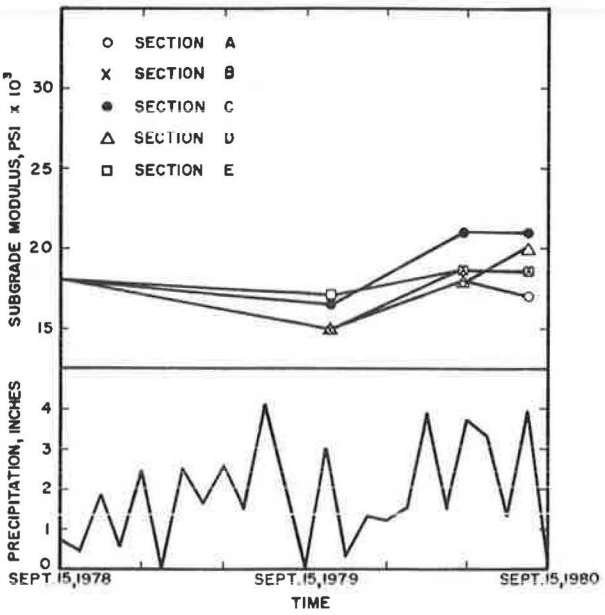

values of layer coefficients for recycled materials, which should adequately reflect their structural performance.

Based on the criteria of required overlay thickness and pavement life, section C, which has a 3.5-in in-place cold-recycled layer (without rejuvenating agent), is found to be superior than the other sections. The performance of section B with 4 in of surface course overlay and of section D with 3.5 in of in-place cold-recycled layers (with 2 percent ARA-1) is comparable to that of section C. Section E, which has structural layers similar to section D but is 2.25 in less in thickness, is the weakest section, thereby accentuating the effect of thickness on structural performance. Section A, which has a 5.25-in hot-recycled bituminous layer and also the highest SN, has a poor structural performance compared with sections B, C, and D.

As far as the average pavement modulus is concerned, section B developed a modulus value initially much higher than those of the other sections. However, after about 7-8 months, the modulus value for this section began to decrease rather abruptly and attained a value only slightly higher than the modulus of section C, which showed a steady gain in magnitude for almost 10-11 months. The average pavement modulus of section A began decreasing almost immediately after the section was built.

Subgrade moduli in all sections showed remarkably similar characteristics, as can be expected, and also exhibited some susceptibility to rain.

ACKNOWLEDGMENT

Most of the work presented in this paper was accomplished while I was with the Geotechnical Section of the Kansas Department of Transportation. The contents of this paper reflect my views, and I am solely responsible for the facts and accuracy of the data presented. The contents do not necessarily reflect the official views or policies of the Kansas Department of Transportation or the Federal Highway Administration. The help received from Darrel D. Steele is readily acknowledged. Partial support from the Professional Development Program at National Soil Services, Inc., is also acknowledged.

REFERENCES

1. Recycling of Bituminous Pavements. ASTM, Special Tech. Publ. 662, 1978.
2. Proceedings of the National Seminar on Asphalt Pavement Recycling. TRB, Transportation Research Record 780, 1980, 141 pp.
3. S.S. Bandyopadhyay. Design and Structural Condition Evaluation of a Cold Recycled Pavement. Symposium on Advances in Pavement Materials Characterization, ASTM, Houston, Dec. 1981.
4. S.S. Bandyopadhyay. Sample Size of Pavement Deflections. Journal of Civil Engineering Design, Vol. 2, No. 4, 1980, pp. 339-346.
5. S.S. Bandyopadhyay. Developing a Functional Subsystem of Overlay Design Using Dynamic Deflections. Journal of Civil Engineering Design, Vol. 2, No. 4, 1980, pp. 443-457.
6. S.S. Bandyopadhyay. Dynamic Deflections of Pavements--Measurements, Interpretations, and Applications. Proc., International Symposium on Bearing Capacity of Roads and Airfields, Norway, June 1982.
7. S.S. Bandyopadhyay. Pavement Deflections--Static and Dynamic. Public Works Journal, Vol. 113, No. 1, Jan. 1982, pp. 48-49.
8. S.S. Bandyopadhyay. Determining Sample Size of Pavement Deflections by Nomograph. Civil Engineering, ASCE (in preparation).
9. S.S. Bandyopadhyay. Pavement Distress Identification and Condition Evaluation. In Civil Engineering for Practicing and Design Engineers, Pergamon Press (in preparation).
10. S.S. Bandyopadhyay. Flexible Pavement Evaluation and Overlay Design. Transportation Engineering Journal, ASCE (in preparation).
11. R.W. Kinchen and W.H. Temple. Asphaltic Concrete Overlays of Rigid and Flexible Pavements, Final Report. Louisiana Department of Transportation and Development, Baton Rouge, Oct. 1980.
12. G. Peterson. Predicting Performance of Pavements by Deflection Measurements. Research and Development Unit, Utah Department of Transportation, Salt Lake City, 1975.

13. Interim Guide for Design of Pavement Structure--1972. AASHO, Washington, DC, 1972.
14. J.A. Epps. State-of-the-Art Cold Recycling. TRB, Transportation Research Record 780, 1980, pp. 68-100.
15. Asphalt Overlays and Pavement Rehabilitation. Asphalt Institute, College Park, MD, Manual Series 17, Nov. 1977.
16. K. Majidzadeh. Dynamic Deflection Study for Pavement Condition Investigation, Final Report. Ohio Department of Transportation, Columbus, June 1974.

Publication of this paper sponsored by Committee on Pavement Rehabilitation Design.

Application of Asphalt Rubber on New Highway Pavement Construction

GENE R. MORRIS, NAN JIM CHEN, AND JOSEPH A. DI VITO

Asphalt rubber has been used for many years as a stress-absorbing membrane (SAM) or stress-absorbing membrane interlayer (SAMI) for both rigid and flexible pavement overlay systems in Arizona with satisfactory performance. In 1977, a new experimental application of asphalt rubber was used to build a low-volume highway pavement between Dewey and I-17 on AZ-169. Several experimental pavement sections were placed. After four years of service, only two sections are still in excellent condition with no cracks or ruts observed to date. One section consisted of a cement-treated base and the other a lime-fly ash-treated base. Each section received a SAMI and a 1-in wearing course. Other test sections failed, and constant patching is required to maintain a minimal level of service. Generally, cement-treated bases will always have shrinkage cracks that easily reflect through any asphalt concrete surface layer if without special treatment to retard crack propagation. A finite-element procedure was used as an aid in explaining why a SAMI can be used effectively to eliminate reflective cracks. It was found that SAMIs can significantly reduce crack tip stresses due to thermal and traffic loads and provide longer service life of the asphalt concrete surface layer.

In the early 1960s, asphalt rubber was originally used as a patching material for alligator-cracking-type failures in Arizona (1,2). Later it was developed as a stress-absorbing membrane (SAM) and stress-absorbing membrane interlayer (SAMI) for rehabilitation and overlay of cracked pavements (3-7). Asphalt rubber has also been used as a joint and crack seal material and as a waterproof membrane for the control of expansive clay subgrades.

Coetzee and Monismith (8) investigated the effectiveness of a SAMI as an overlay system over rigid pavements by inducing thermal and symmetrical traffic loading across a crack. Results of this study concluded that a SAMI can reduce stresses in overlays and can also prolong the service life of a typical overlay.

Many field studies of SAM and SAMI have been undertaken by the Arizona Department of Transportation. In 1977, a new area for application of asphalt rubber was introduced in the construction of a low-volume road with a cement-treated base (CTB). This paper discusses this new asphalt-rubber application.

CONSTRUCTION AND PERFORMANCE

The Dewey project, as it is often referred to, is on AZ-169 between mileposts 4.8 and 14.5 and is located approximately 80 miles north of Phoenix. It was constructed as a new connecting highway between Dewey, Arizona, and I-17. Currently, the average daily traffic (ADT) is approximately 1000 with 6 percent trucks. The embankments and grades were constructed in 1976 and surfacing was placed in August 1977. This project consisted of five test sections and one control section.

The original pavement design (before it was decided to build test pavements) called for stage construction of 6 in of full-depth asphalt concrete with an open-graded asphalt concrete friction course (ACFC) on the compacted subgrade. Initial surfacing was 2 in and the remaining 4 in was designated for future surfacing.

Subgrade material is primarily decomposed granite, clayey sand, and gravel with a plasticity index ranging as high as 69. The average project elevation is approximately 4400 ft, and winter months are often severe.

The characteristics of the control section and the five test sections are as follows:

1. Control section, station 262-520: The subgrade was compacted to 100 percent of maximum density (36-ft width). Two inches of asphalt concrete were placed on the compacted subgrade. Asphalt concrete was made with an AR2000 asphalt.
2. Test section 1, station 520-555, Lime-Fly Ash-Treated Base: Three percent quicklime and 12.5 percent fly ash (by weight of subgrade material) were added to in-place subgrade soil and thoroughly mixed to a depth of 6 in and then compacted to 100 percent of maximum density. An asphalt-rubber membrane was placed across the entire roadway, shoulders, and cut ditches. A 1-in ACFC was placed as a wearing course.
3. Test section 2, station 555-590, CTB: Four and one-half percent (by weight of subgrade material) portland cement was added to the in-place subgrade soil. This was thoroughly mixed to a depth of 6 in and then compacted to 100 percent of maximum density. An asphalt-rubber membrane was placed across the entire roadway, shoulders, and cut ditches. A 1-in ACFC was placed as a wearing course.
4. Test section 3, stations 590-640 and 670-765: The subgrade was compacted to 100 percent of maximum density. Asphalt rubber then was placed across the entire roadway, shoulders, and cut ditches. A 1-in ACFC was placed as a wearing course.
5. Test section 4, station 640-670: Same treatment as test section 3 except that an asphalt-rubber membrane was placed 2 ft down into the subgrade.

6. Test section 5, station 765-780, AR1000, Enzymatic SS: The subgrade was compacted to 100 percent of maximum density by using Enzymatic SS, a compaction aid. Two inches of asphalt concrete were placed on the subgrade as a wearing course. AR1000 asphalt was used in the production of the asphalt concrete.

Test sections 1 and 2 and the lime-fly ash and cement-stabilized sections have served perfectly with no visible problems or defects whatsoever, as shown in Figures 1 and 2. Several pavement cores were taken from these test sections. A typical core is shown in Figure 3. All other test sections, as well as the control section, have experienced some degree of distress; performance of even the best of which has been judged unacceptable. Examples of these sections are shown in Figures 4 and 5. The control section and the other three test sections experienced numerous construction difficulties. The intent was to encapsulate the pavement subgrade to prevent moisture change and, thereby, rely on the inherent strength of a cohesive soil molded at optimum density and moisture content. These sections might have performed better if different construction procedures were followed. The asphalt-rubber membrane was placed directly on the compacted subgrade. During construction, asphalt concrete haul trucks were allowed to travel on the recently completed membrane and very often picked up the membrane. These areas were never patched. As a result, a complete, intact membrane seal was never achieved. During the first winter (which was very wet), it became apparent that these sections were doomed to failure. An asphalt-rubber membrane can be properly placed if construction procedures are controlled to prevent pickup of the membrane from the subgrade.

A great deal was learned from this test project. Although we know stabilized bases will crack, especially CTBs, both of these test sections (sections 1

Figure 1. Test section 1: lime-fly ash subgrade, SAMI, and 1-in ACFC.

Figure 2. Test section 2: CTB, SAMI, and 1-in ACFC.

Figure 3. Pavement core at station 540.

Figure 4. Test section 3.

Figure 5. Test section 5.

Table 1. Range of pavement layer properties.

Item	Elastic Modulus, E (ksi)	Shear Modulus, G (ksi)	Poisson Ratio, μ	Thermal Coefficient α (per °F)	Thickness, t (in)
Asphalt concrete or ACFC	100-500	40-200	0.3	0.000 012 5	1-4
SAMI	0.2-2.0	0.08-0.8	0.35	0.000 015	0.4
CTB	1000-4000	420-1680	0.2	0.000 003 9	6-10
Subgrade	10	4	0.48	0.000 01	40

Figure 6. General configuration of pavement structure with CTB and a crack.

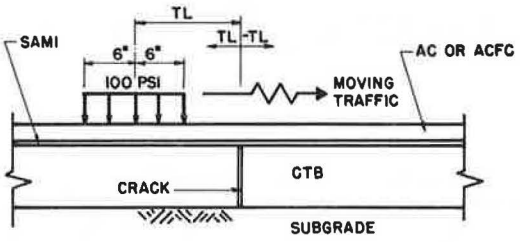

LOADING CASE	A	B	C	D	E	F	G	H	I	H'	G'	F'	E'	D'	C'	B'	A'
TL (IN)	16	14	12	10	8	6	4	2	0	-2	-4	-6	-8	-10	-12	-14	-16

Figure 7. General input pavement temperature profile.

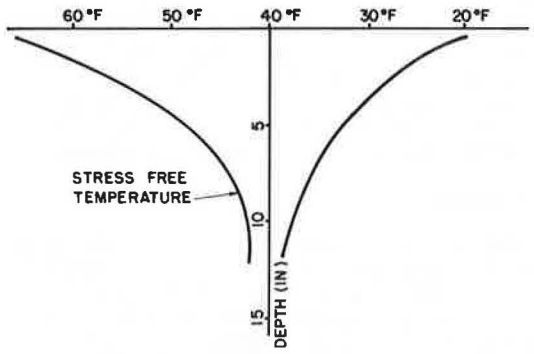

Figure 8. Effects of SAMI on thermal horizontal stress near crack tip.

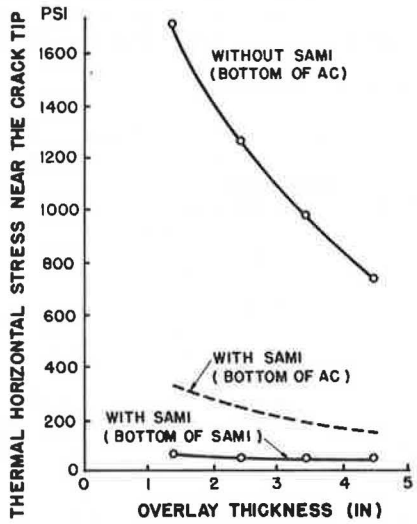

and 2) remain crack-free after four years of service. The SAMI has effectively prevented transmission of the cracks in the stabilized base through to the 1-in-thick surface course.

Asphalt rubber has shown its effectiveness in preventing reflective cracking in overlays over existing pavements, and it was expected that a membrane would do the same on new construction with stabilized bases.

ANALYTICAL STUDIES

An analysis was conducted of the theoretical behavior of the structure to explore the basic reason why the asphalt rubber prevented reflective cracking as well as to provide a method to determine the structural adequacy of the systems.

Several finite-element method (FEM) computer programs were used for the analysis of stresses and strains. The primary computer program used for this study was a slightly modified static-analysis program for solid structures--namely, Solid SAP by Wilson (9). The slight modification of this program was in the calculation of the effective stress, which is defined by using the normal and shear stresses in an orthogonal Cartesian coordinate system, as follows:

$$S_{eff} = (1/\sqrt{2})\,[(S_{11} - S_{22})^2 + (S_{22} - S_{33})^2 + (S_{33} - S_{11})^2 + 6(S_{12}^2 + S_{23}^2 + S_{31}^2)]^{1/2} \quad (1)$$

It is considered to be a realistic determinant for fracture (cracking) under the triaxial stress state that exists in the overlay pavement.

In order to reduce the cost of computer time, a linear elastic plane-strain analysis was assumed with up to 685 nodes and 620 elements. The general configuration of the pavement structure is shown in Figure 6. The range of different layer properties is given in Table 1. This does not exactly model the pavement condition in Dewey. However, the objective of this paper is to provide an analytical explanation for the apparent success of this new asphalt-rubber application.

Computer runs were not arranged as a factorial matrix due to the high cost of each run. Instead, several interesting variables were studied separately.

Thermal Effects

The general temperature profile shown in Figure 7 was used. Results of this study indicate the horizontal tensile stress near the crack tip reduced significantly as a result of the SAMI, as shown in Figure 8. The SAMI will not reduce the overall horizontal stress in asphalt concrete or an ACFC due to thermal expansion or contraction, but it will significantly reduce the stress concentration above the crack tip, thereby minimizing reflective cracking.

Overlay Thickness

Overlay thicknesses from 1 to 4 in were studied. For

Figure 9. Effects of SAMI on effective stress near crack tip.

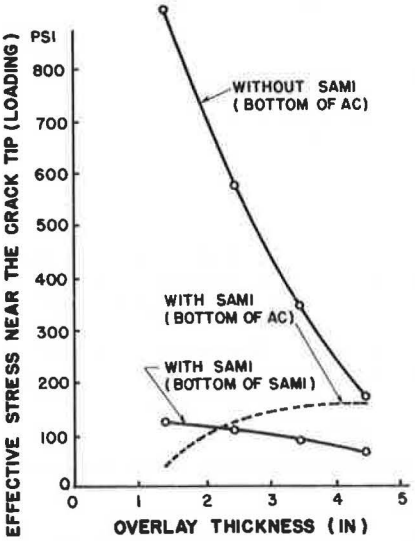

Figure 10. Influence of crack width on stresses.

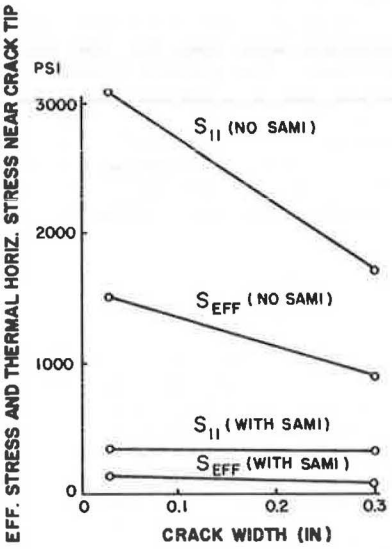

Figure 11. Influence line of effective stress near crack tip due to moving load.

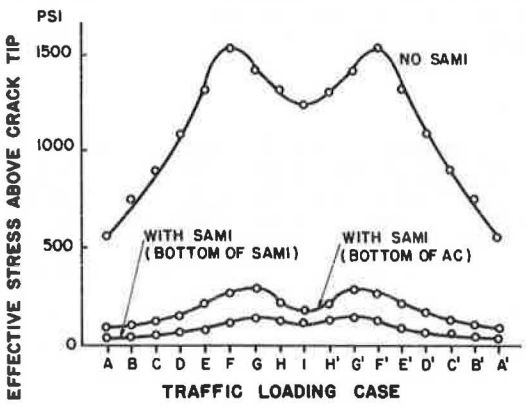

Figure 12. Influence line of shear stress near crack tip due to moving load.

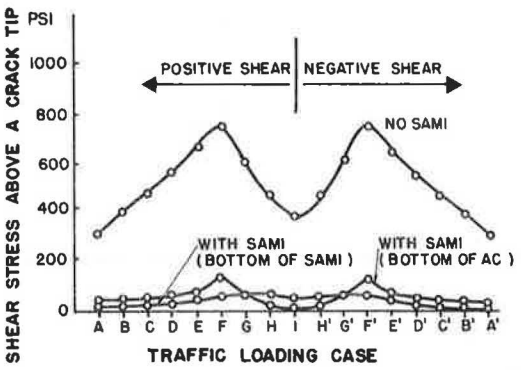

an overlay without a SAMI, stresses were reduced significantly due to increasing thickness (Figures 8 and 9). However, for an overlay with SAMI, stresses were only slightly reduced due to the increasing overlay thickness. This indicates that, from an economical point of view, a thick overlay may not be justified for a reflective overlay design when SAMI is used.

Crack Width

Only two different crack widths were investigated--0.03 and 0.3 in. Results show that when there is not a SAMI in the overlay system, the stress concentration problem is more serious for smaller cracks than larger cracks (Figure 10). For overlays with a SAMI, stresses stay approximately the same no matter what the crack width. It is assumed there is no load-transfer capacity across a crack, which is valid in most cases, depending on the magnitude of the crack width and vertical differential movements.

Effects of Moving Traffic

Traffic loading was represented by a 12-in long, 100-psi load moving from one side of the crack to the other, as shown in Figure 6. Shear and effective stresses are at a maximum when the edge of this simulated traffic load just reaches the location of a crack, as shown in Figures 11 and 12. This study also revealed that a SAMI can reduce effective stress and, more importantly, shear stress in the surface layer, which many researchers believe is one of the major factors that causes reflective cracking.

SUMMARY

1. SAMI can be used for the overlay of flexible and rigid pavements, for new construction, or anywhere else that stress concentration around a crack needs to be reduced.
2. SAMI can reduce stresses due to thermal changes as well as vertical shear stresses due to moving traffic loads.
3. SAMIs can retard (or eliminate) reflective cracks by reducing crack tip stresses. In many cases, crack tip stresses drop to 10 percent or less of the original stresses.
4. A three-dimensional finite-element analysis with more realistic time- and temperature-dependent material properties will provide better results. However, the computer time required may increase 10 to 20 times. The primary purpose of this paper is to report a new area for the application of asphalt rubber as a SAMI in the construction of new pavement and try to provide analytical explanations for the

apparent success of this new approach in pavement design.

5. During the analytical study, it was assumed that there is no load-transfer capability across a crack. This is especially true when the ratio of crack width to vertical differential movement of a crack is high. Results of this study imply that a SAMI will perform even better if there is some load-transfer capacity through a crack.

6. A better understanding of SAMI properties is needed through laboratory testing.

7. When a SAMI is used, the thickness of overlay becomes less critical. This may result in very economical approaches to overlay design.

REFERENCES

1. C.H. McDonald. A New Patching Material for Pavement Failures. HRB, Highway Research Record 146, 1966, pp. 1-16.
2. C.H. McDonald. Asphalt-Rubber Compounds and Their Applications for Pavement. Proc., 21st California Streets and Highway Conference, Los Angeles, 1969.
3. G.R. Morris and C.H. McDonald. Asphalt-Rubber Stress-Absorbing Membranes: Field Performance and State of the Art. TRB, Transportation Research Record 595, 1976, pp. 52-58.
4. G. Cooper and G.R. Morris. Reclaimed Rubber in Seal Coats and Research in Rubber/Asphalt Products. Proc., Arizona Conference on Roads and Streets, Univ. of Arizona, Tucson, 1974.
5. B.A. Vallerga, G.R. Morris, J.E. Huffman, and B.J. Huff. Applicability of Asphalt-Rubber Membranes in Reducing Reflection Cracking. In Symposium: Prevention and Control of Reflective Cracking, Proc., Association of Asphalt Paving Technologists, Vol. 49, 1980, pp. 330-353.
6. G.F.D. Gonsalves. Evaluation of Road Surfacings Utilizing Asphalt Rubber. Arizona Department of Transportation, Phoenix, Rept. GG3, 1979.
7. G.B. Way. Prevention of Reflective Cracking in Arizona. TRB, Transportation Research Record 756, 1980, pp. 29-32.
8. N.F. Coetzee and C.L. Monismith. Analytical Study of Minimization of Reflection Cracking in Asphalt Concrete Overlays by Use of a Rubber-Asphalt Interlayer. TRB, Transportation Research Record 700, 1979, pp. 100-108.
9. E.L. Wilson. Solid SAP: A Static Analysis Program for Three-Dimensional Solid Structures. Univ. of California, Berkeley, Rept. UC-SESM 71-19, Sept. 1971.

Publication of this paper sponsored by Committee on Pavement Rehabilitation Design.

Characterizing Fatigue Life for Asphalt Concrete Pavements

J. BRENT RAUHUT AND THOMAS W. KENNEDY

The evaluation of fatigue life for asphalt concrete pavements is very difficult because of limited knowledge as to fatigue damage relations for real pavements, reliable testing data for only a limited number of mixtures, and limited information as to how the fatigue life potential of an asphalt concrete pavement varies with temperature and mixture characteristics. This paper seeks to overcome some of these difficulties by (a) proposing a typical fatigue relation for a typical asphalt concrete mixture in place, (b) presenting procedures for modifying fatigue relations with changes in temperature and mixture stiffness, (c) proposing a procedure for taking specific mixture characteristics into account, and (d) offering a simplistic method of transforming fatigue life predictions into predictions of area cracked.

The characterization of fatigue life for asphalt concrete pavements is extremely complex and has been the subject of study by a number of researchers for more than two decades. Various laboratory tests have been employed, but the most common one involves small beams subjected to repetitive loading with either constant load or constant strain. The beams have been simply supported, supported on springs, or supported on a rubber medium to simulate a base and subgrade. One characteristic shared by all beam tests and other types of common laboratory tests is that none come close to simulating actual field conditions and a realistic crack-propagation process.

Shell Laboratories attempted a more accurate simulation with wheel-tracking tests, which produced more realistic crack propagation in small asphalt concrete slabs, but may have overpredicted fatigue life because of the lack of environmental effects. More recently, a number of attempts have been made to use laboratory test curves in conjunction with elastic-layer theory to predict the occurrence of fatigue cracking distress in real pavements. Because the laboratory relations almost always grossly underpredict fatigue cracking, shift factors have been used to translate the predictions to approximate fatigue life actually measured in the field. Such fatigue curves appear to be the best available for use in predicting fatigue cracking.

The form of the fatigue relations in common use is derived from a logarithmic relation between either stress or strain and the number of load cycles to failure. The relations between the logarithm of stress or strain and the logarithm of load cycles are considered to be linear, which results in the following general equation:

$$N_i = K_1 \epsilon_i^{-K_2}$$

where

N_i = number of load cycles to failure for a loading that results in a tensile strain,
ϵ_i = calculated strain under load,
K_2 = inverse of absolute value of slope of logarithmic function, and
$K_1 = N_i \epsilon_i^{K_2}$ for any pair N_i and ϵ_i that satisfies the logarithmic function.

Both K_1 and K_2 depend primarily on material characteristics and temperature.

A very important problem with this form of fatigue life characterization is that this equation is

extremely sensitive to small variations in the value of K_2, while test results for specimens that fail in tension are quite scattered. Further, the occurrence of fatigue cracking in the field is itself quite variable, even for apparently identical sections. Considering that laboratory test results are also of limited quality, the predictions for individual sections may be expected to be poor, and statistical means for a number of sections are not likely to be especially accurate either.

Unfortunately, in view of our limited capabilities for predicting fatigue cracking, it is the most significant distress experienced by our highways and the primary generator of maintenance and repair requirements. Therefore, it must be considered in design and analysis, and we must characterize the fatigue life potential of asphalt concrete mixtures as best we can.

It is not generally feasible to conduct fatigue testing programs for specific mixes to support routine analyses or designs because of the sophisticated laboratory equipment required and very high costs for such a program; therefore, some other approach must be developed. One reasonable approach is to select a fatigue relation that is reasonably typical for asphalt concrete pavements in place and to modify that relation on some rational basis to reflect the effects on fatigue life of established characteristics of the specific mixture of interest. The purposes for this paper are then to

1. Propose a fatigue relation for a typical asphalt concrete mixture in place,
2. Present procedures for modifying fatigue relations with changes in temperature or mixture stiffness,
3. Propose a procedure based on relative mixture stiffness for taking specific mixture characteristics into account, and
4. Offer a simplistic method of transforming fatigue life predictions into predictions of area cracked.

TYPICAL FATIGUE RELATIONS FOR ASPHALT CONCRETE PAVEMENTS IN PLACE

Thirteen fatigue relations for mixture temperatures of approximately 70°F (from previous studies) are plotted in Figure 1. Descriptions of the tests (or other bases for development) are given elsewhere (1-13).

Six relations were obtained from standard laboratory beam tests (2,6-10). Two relations were also obtained from laboratory tests, but the specimens rested on elastic supports (5,11). Two other relations were produced from multiple regression analyses on American Association of State Highway Officials (AASHO) Road Test data and are related to present serviceability index (PSI) (3,4). Witczak (3) specifically related tensile strain in the bottom of the AASHO Road Test pavements to number of load repetitions to reduce the PSI to 2.5. ARE (4) related tensile strain to measured cracking, but in terms of 18-kip equivalent single-axle load (ESAL) based on PSI. Three relations were obtained from laboratory beam-test results transformed to represent field conditions (1,12,13). In general, laboratory beam-test results grossly underpredict fatigue cracking distress, while the other relations may underpredict or overpredict.

Figure 2 includes only the three relations transformed to represent field conditions and the relation by Meyer and others (2) that was derived from stress-controlled beam testing related to 20 percent class 2 and 3 cracking at the Brampton Test Road. Note also that a relation developed by Finn and others (1) to represent 45 percent measured cracking at the AASHO Road Test is essentially identical to that of Meyer and others. It can be seen from Figure 2 that these four curves are very similar, and it appears reasonable to select from this grouping a relation to be considered typical. The relation selected was the one developed by Finn and others to represent less than 10 percent cracking at the AASHO Road Test. The relation from Meyer and others, which represents 20 percent class 2 and 3 cracking at the Brampton Test Road or 45 percent cracking at the AASHO Road Test, could also be used to represent failure or need for maintenance if a higher level of damage is preferred.

MODIFYING TYPICAL FATIGUE RELATIONS WITH CHANGES IN TEMPERATURE OR MIXTURE STIFFNESS

Typical fatigue relations were selected in the previous section to represent two different levels

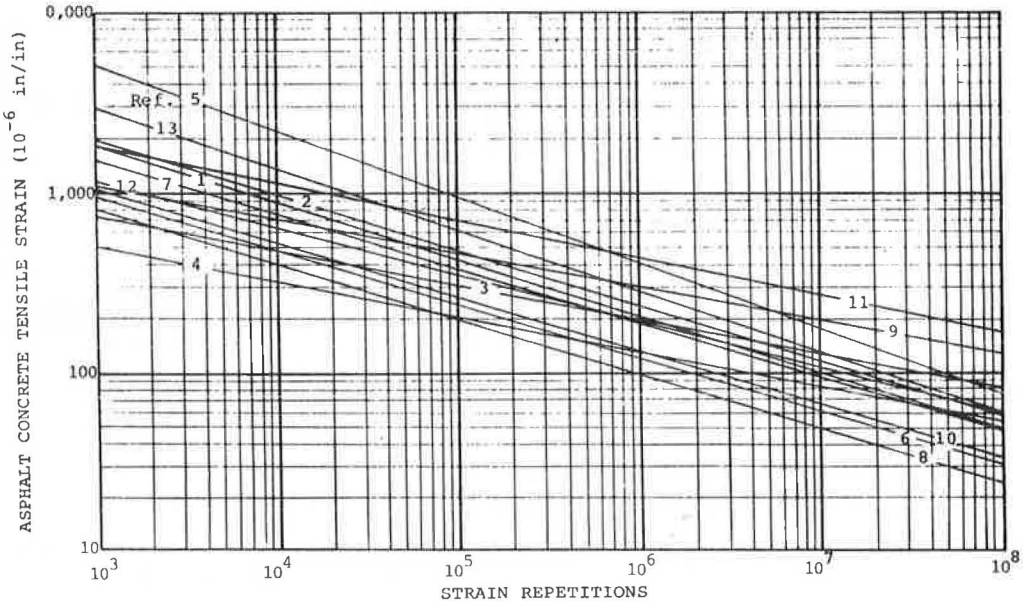

Figure 1. Fatigue relations at 70°F, including results of laboratory testing, wheel-tracking tests, and efforts to represent field conditions.

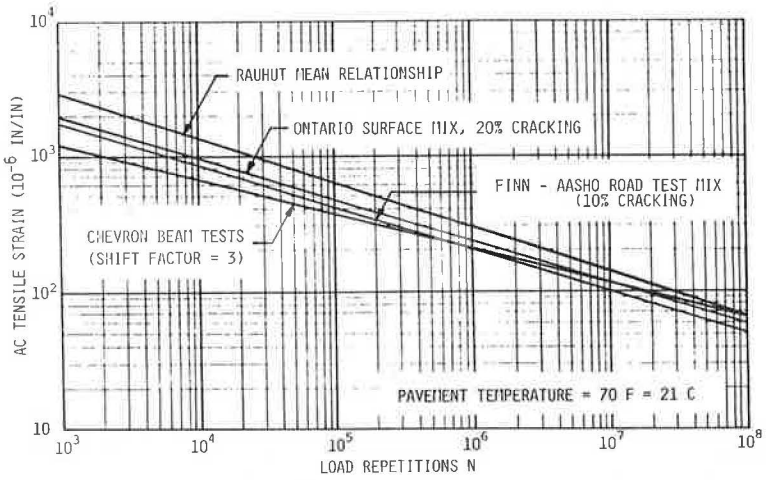

Figure 2. Fatigue relations for asphalt concrete that represent pavements at pavement temperature of 70°F.

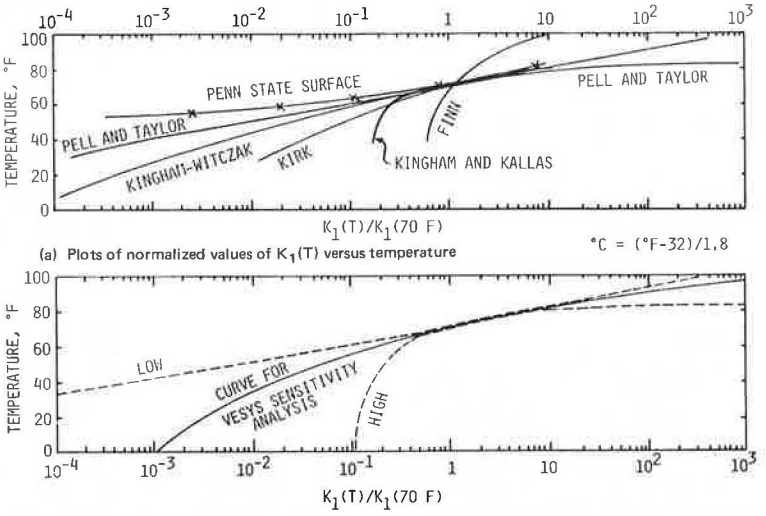

(a) Plots of normalized values of $K_1(T)$ versus temperature

(b) Plots of normalized values of $K_1(T)$ used for modifying $K_1(70°F)$ in VESYS II sensitivity analysis

Figure 3. Relation between normalized K_1 and temperature.

of fatigue cracking distress. These typical fatigue relations will require modifications to (a) represent specific mix characteristics and (b) represent changes in temperature or mixture stiffness. Procedures for the first type of modification will be provided in a subsequent section, but procedures for modifying the typical fatigue relations with temperature or mixture stiffness are the subjects of this section.

Modifications with Temperature

Witczak (3) recommended fatigue relations as functions of temperature. Rauhut and others developed procedures for varying fatigue curves with temperature, which is described and applied elsewhere (12), and these procedures were adopted by Meyer and others (2). The relation by Witczak assumes that the exponent K_2 is constant and that the multiplying coefficient K_1 varies with temperature. Rauhut and others, on the other hand, noticed some slight variations of K_2 with temperature, and this trend was included at a limited rate of change in their procedure.

The study by Rauhut was based on limited data in the literature on variations in fatigue relations with temperature for the same mixes. The data used appear elsewhere (12, Table 17) and are plotted for $K_1(T)$ normalized for $K_1(70°F)$ in Figure 3a. A curve has been added for the Finn relation (1), with $K_1(T)$ obtained by substituting values of resilient modulus for 40°, 70°, and 100°F from test results on the AASHO mix. It can be seen that the variations in $K_1(T)$ with temperature are quite different for the various sets of test results, ranging from approximately one order of magnitude for the Finn relation to many orders of magnitude for the Penn State surface mix.

Figure 3b indicates the range of variations and a curve selected on the basis of judgment to be used in converting $K_1(T)$ as a function of temperature. Meyer and others (2) developed a multiple regression equation for the curve selected as follows:

$$\log [K_1(T)/K_1(70°F)] = -2.952 + 0.000\,58T^2 \quad (1)$$

The relation for $K_2(T)$ (12) is as follows:

$$K_2(T) = K_2(70°F)[1 - 0.001(T - 70)] \quad (2)$$

By substituting 70°F for T in Equation 1, it can be readily seen that the regression curve does not pass through the value 1 when the ratio $K_1(T)/K_1(70°F)$ is 1. A somewhat more general and more accurate relation may be obtained as follows:

$$\log [K_1(T_1)/K_1(70°F)] = -2.952 + 0.000\,58T_1^2 \quad (3)$$

$$[K_1 (T_1)/K_1 (70°F)] = 10^{(-2.952 + 0.000\,58T_1^2)} \quad (4)$$

Similarly,

$$[K_1 (T_2)/K_1 (70°F)] = 10^{(-2.952 + 0.000\,58T_2^2)} \quad (5)$$

Dividing Equation 4 by Equation 5 and taking logarithms gives the following:

$$\begin{aligned}\log [K_1 (T_1)/K_1 (T_2)] &= \log [10^{(-2.952 + 0.000\,58T_1^2)} \\ &\quad \div 10^{(-2.952 + 0.000\,58T_2^2)} \\ &= \log 10 (-2.952 + 0.000\,58T_1^2 + 2.952 \\ &\quad - 0.000\,58T_2^2) \\ &= 0.000\,58 (T_1^2 - T_2^2)] \end{aligned} \quad (6)$$

Figure 4 (3) is a copy of a plot that shows the Kingham-Witczak relations in solid lines for a wide range of temperatures. Superimposed on this plot are relations generated by Equations 2 and 6 for identical temperatures based on the Kingham-Witczak relation at 70°F. As can be seen, the Witczak and Rauhut modifications for temperature are quite similar above around 60°F, but differ rather dramatically for the colder temperatures. This would be expected, considering the differences between the Kingham-Witczak relation (Figure 3a) and the typical relation selected for previous work (Figure 3b).

Figure 4. Comparison of Witczak fatigue relations for various temperatures and Witczak's 70°F fatigue relation modified with temperature by using Equations 2 and 6.

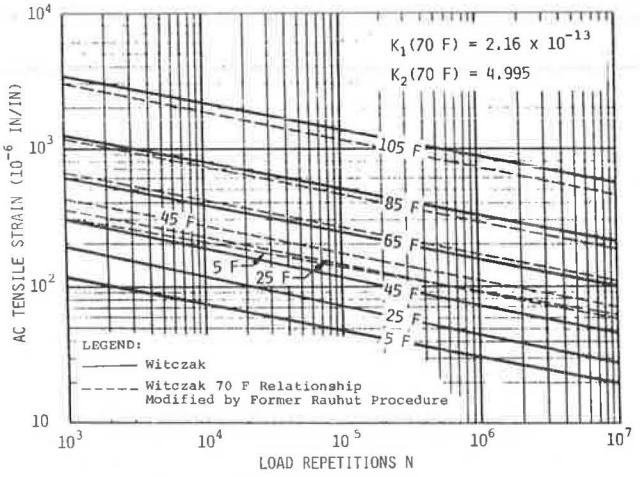

It may be seen that Equation 6 reaches a limit at a temperature of 0°F, as the values of temperature are squared. The effects of freezing mixture temperatures on fatigue relations are really not known, but such a limit appears reasonable as fatigue life potential is correlated strongly to mixture stiffness, which tends to reach an upper limit with decreasing temperature at around 20°F. Equation 6 is recommended for modifying K_1 with temperature as (a) it represents a relatively typical variation with temperature (a compromise within the broad range of variation shown in Figure 3a), and (b) the data for temperatures below freezing are very limited, but the only known data (13) are more consistent with the results from Equations 2 and 6 than with the Kingham-Witczak relation.

Equation 2 was developed during a period when the approach of considering K_2 constant and varying K_1 to account for temperature effects was generally accepted. It was noted by Rauhut at that time that there were sometimes considerable variations in K_2, and Equation 2 was developed to introduce this trend. However, much of the data then available indicated relatively constant values of K_2, so the trend was introduced at a very limited rate. There is a fairly close correlation between K_1 and K_2 that is documented in Figure 5, which was extracted from various sources (3,11, 14,15). (Note that variations of log K_1 along the abscissa of Figure 5, in general, represent variations in sample temperature.) Values of $K_2(T)$ and $K_1(T)$ obtained by application of Equations 2 and 6 to the typical relation for 10 percent cracking were also plotted. As can be seen, the Kingham-Witczak relation plots as a horizontal line because of the assumed constant value of K_2, and this appears to be inconsistent with the clear correlation established by the preponderance of test data. Also, the Finn relation, modified by Equations 2 and 6, plots almost horizontal, as Equation 2 only included a moderate rate of change with temperature.

In order to obtain the best representation of variation of $K_2(T)$ with $K_1(T)$, it was decided to

Figure 5. Combined relations between K_2 and K_1 from various studies.

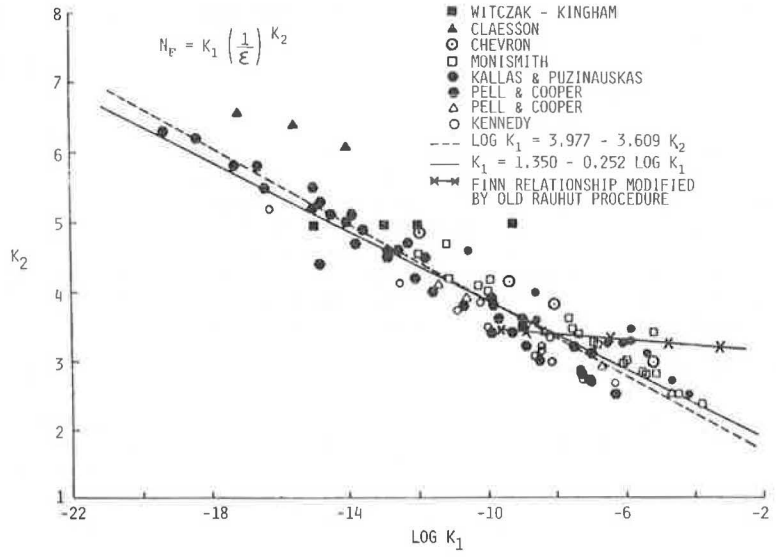

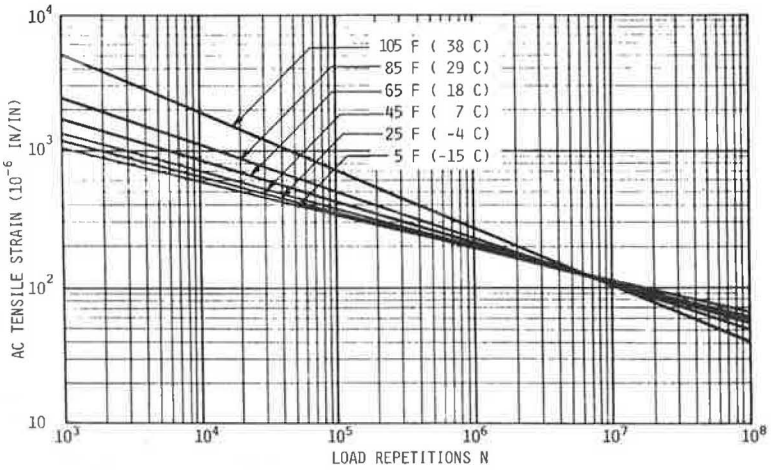

Figure 6. Fatigue relation for 10 percent cracking selected as typical, plotted for different temperatures (using new transformation relation).

use the regression equation from Figure 5 in lieu of Equation 2 for calculating K_2:

$$K_2 = 1.350 - 0.252 \log K_1 \quad (7)$$

Study of Figure 5 indicates that most of the flexure data lies above the regression line and the rotating cantilever and indirect tensile test data below. As the typical values of $K_1(70°F)$ and $K_2(70°F)$ of 7.87×10^{-7} and 3.29, respectively, appear to represent typical flexural test data better than the general regression line in Figure 5, the line was simply transformed to better represent the specific test results (at the same slope) by using Equation 7 to calculate K_2 for the known K_1 and adding the difference ΔK_2 of 0.40 between actual and calculated K_2 to the equation, i.e.,

$$K_2(T) = 1.75 - 0.252 \log K_1(T) \quad (8)$$

By using values of $K_1(T)$ calculated by Equation 6 for the typical relation and calculating consistent values of $K_2(T)$ with Equation 8, the relations plotted in Figure 6 are obtained. As can be seen by comparing the general distribution of the relations with temperature in Figure 4 to the distribution in Figure 6, changes in predicted fatigue life with changes in temperature will be considerably reduced by use of Equation 8 in lieu of Equation 2 (and indeed there is almost no change for strains approximating 0.0001). The question then arises as to which is most accurate.

The preponderance of test data now available, including results for 11 mixes (8), indicates that K_2 does vary with temperature or stiffness but at different rates for different mixes and perhaps different types of tests and procedures. However, it is not really known how either $K_1(T)$ or $K_2(T)$ vary in a field pavement with temperature, as all field relations have either been extrapolated from laboratory data by shifting the curves to approximate measured cracking levels as functions of calculated strains and repetitions of loads or either directly or implicitly based on ride quality measured at the AASHO Road Test instead of fatigue cracking. Although we may only hope to limit the magnitudes of errors to be expected because of our limited state of knowledge, our best judgment (based on available data) indicates that $K_2(T)$ is best predicted by Equation 8.

The procedure for modifying the fatigue relations with temperature adopted is the use of Equation 6 to calculate values of $K_1(T)$ for specific values of seasonal pavement temperature and Equation 8 to calculate consistent values of $K_2(T)$.

Modifications with Mixture Stiffness

Although modifications to the fatigue relations for some applications may best be made with temperature as described previously, it may be more useful to modify them with mixture stiffness for other applications.

Table 1 provides dynamic moduli, fatigue relations at various dynamic moduli, the initial strain for each fatigue relation that will cause failure at 1 million load repetitions, identification of the source for the data, and other values of use in subsequent developments. These data were studied and plotted in various formats for use in developing a means of converting the fatigue relation from one stiffness to another. It was found that plots of the logarithm of the ratio of an arbitrary fatigue coefficient $K_1(E)$ to $K_1(E = 500$ ksi) against the logarithm of the ratio of the corresponding dynamic modulus to 500 ksi approximated straight lines. Plots of these relations for each of the first six mixtures that appear in Table 1 are shown in Figure 7. Specific points have been included for plots 1, 2, and 5 to illustrate slight nonlinearities. In drawing the straight lines, emphasis was given to fit for the higher values of stiffness where the relation was most linear.

The general equation for any of the lines plotted in Figure 7 is as follows:

$$\log [K_{1i}/K_1 (E = 500 \text{ ksi})] = 0 + S \log (E_i/500 \text{ ksi})$$

where K_{1i} equals K_1 consistent with arbitrary value of dynamic modulus E_i, and S is the slope of the line (S will be negative in each case).

By moving S within the logarithm as an exponent and carrying $K_1(E = 500$ ksi) to the other side of the equation,

$$K_{1i} = K_1 (E = 500 \text{ ksi}) (E_i/500 \text{ ksi})^S \quad (9)$$

For generality, K_{1i} can be divided by another arbitrary base value, K_{1j}, so that any known value of K_1 that represents any specific mixture stiffness may be used to obtain others. The result of this division is

$$K_{1i} = K_{1j} (E_i/E_j)^S = K_{1j} (E_j/E_i)^{-S} \quad (10)$$

The values of slope for the plots in Figure 7 have also been entered on that figure and are ex-

Table 1. Fatigue relations for asphalt that vary with material stiffness.

Plot No.[a]	Reference No.	Dynamic Modulus E (ksi)	Log (E/500 ksi)	K_2	Initial Strain ϵ Leading to Failure at 10^6 Load Repetitions	$K_1 = 10^6 \epsilon^{K_2}$	$K_1 = K_1$ (E = 500 ksi)	Log [K_1/K_1 (E = 500 ksi)]	K_2/K_2 (E = 500 ksi)
1	1	100	-0.70	3.291		3.11×10^{-6}	3.95	0.60	1.0
		200	-0.40	↑		1.72×10^{-6}	2.20	0.34	
		500	0	Assumed		7.87×10^{-7}	1.00	0	
		800	0.20	Constant		5.27×10^{-7}	0.67	-0.17	
		1200	0.38	↓		3.73×10^{-7}	0.47	-0.32	
		2000	0.60	3.291		2.41×10^{-7}	0.31	-0.51	1.0
2	16	100	-0.70	5.26	4.8×10^{-4}	3.52×10^{-12}	39.8	1.60	1.027
		200	-0.40	4.95	3.4×10^{-4}	6.77×10^{-12}	76.5	1.88	0.967
		300	-0.22	5.12	2.3×10^{-4}	2.36×10^{-13}	2.7	0.42	1.0
		500	0	5.12	1.9×10^{-4}	8.86×10^{-14}	1.0	0	1.0
		1000	0.30	5.12	1.4×10^{-4}	1.86×10^{-14}	0.21	-0.68	1.0
		2000	0.60	5.12	1.1×10^{-4}	5.39×10^{-15}	0.061	-1.22	1.0
3	3	60	-0.92	5.00	8.2×10^{-4}	3.71×10^{-10}	2613	3.42	1.0
		150	-0.52		4.8×10^{-4}	2.55×10^{-11}	180	2.25	
		200	-0.40		3.6×10^{-4}	6.05×10^{-12}	42.6	1.63	
		300	-0.22	↑	2.5×10^{-4}	9.77×10^{-13}	6.9	0.84	
		500	0	Assumed	1.7×10^{-4}	1.42×10^{-13}	1.0	0	
		600	0.08	Constant	1.5×10^{-4}	7.59×10^{-14}	0.54	-0.27	
		1000	0.30	↓	0.9×10^{-4}	5.90×10^{-15}	0.04	-1.38	
		1500	0.48		0.6×10^{-4}	9.16×10^{-16}	0.0064	-2.19	
		2000	0.70	5.00	0.4×10^{-4}	9.02×10^{-17}	0.000 64	-3.20	1.0
4	11	40	-1.10	3.22	3.1×10^{-4}	5.20×10^{-6}	566	2.75	0.843
		75	-0.82	3.31	2.8×10^{-4}	1.63×10^{-6}	178	2.25	0.866
		150	-0.52	3.40	2.5×10^{-4}	5.66×10^{-7}	62	1.79	0.890
		300	-0.22	3.66	2.3×10^{-4}	4.46×10^{-8}	4.9	0.69	0.958
		500	0	3.82	2.1×10^{-4}	9.18×10^{-9}	1.0	0	1.0
		600	0.08	3.93	2.1×10^{-4}	3.25×10^{-9}	0.35	-0.45	1.029
		900	0.26	4.12	1.9×10^{-4}	4.76×10^{-10}	0.05	-1.28	1.079
		1500	0.48	4.28	1.8×10^{-4}	8.63×10^{-11}	0.009	-2.03	1.120
		4000	0.90	4.78	1.6×10^{-4}	7.13×10^{-13}	0.000 08	-4.10	1.251
5	14	100	-0.70	6.10	7.0×10^{-4}	5.65×10^{-14}	253	2.40	0.967
		200	-0.40	6.10	5.1×10^{-4}	8.18×10^{-15}	36.7	1.56	0.967
		300	-0.22	6.10	4.4×10^{-4}	3.32×10^{-15}	14.9	1.17	0.967
		500	0	6.31	3.7×10^{-4}	2.23×10^{-16}	1.0	0	1.0
		700	0.15	6.54	3.2×10^{-4}	1.44×10^{-17}	0.064	-1.19	1.036
		1000	0.30	6.54	2.8×10^{-4}	6.01×10^{-18}	0.023	-1.57	1.036
6	17	50	-1.00	2.59	1.4×10^{-4}	1.02×10^{-4}	21 030	4.33	0.710
		100	-0.70	2.85	1.3×10^{-4}	7.87×10^{-6}	1628	3.22	0.781
		250	-0.30	3.27	1.1×10^{-4}	1.16×10^{-7}	24	1.38	0.896
		500	0	3.58	1.0×10^{-4}	4.83×10^{-9}	1.0	0	1.0
		1000	0.30	4.07	9.5×10^{-5}	4.22×10^{-11}	0.0087	-2.06	1.115
		4000	0.90	5.07	9.0×10^{-5}	3.16×10^{-15}	6.55×10^{-7}	-6.18	1.389
	15	114	-0.64	2.66	2.4×10^{-5}	5.01×10^{-7}	786	2.90	0.729
		204	-0.39	3.20	3.7×10^{-5}	3.07×10^{-9}	4.8	0.66	0.877
		500	0	3.65	2.8×10^{-5}	6.37×10^{-10}	1.0	0	1.0
		584	0.67	3.73	2.7×10^{-5}	1.29×10^{-11}	0.02	-1.69	1.022

[a] Figure 7.

tremely variable, as might be expected from review of the similar information in Figure 3a. Although a value of the slope S for the particular mixture stiffness should be used when available for the transformations possible through application of Equation 9, it will be necessary, as for temperature, to select a slope that may be used as typical. The mean value for the six values of slope shown in Figure 7 is -3.84. However, it might also be reasonable to give more credence to the three lines that are very close together. If plots 3, 4, and 5 are given twice as much weight as the other three plots, the mean value is then -4.09. As this is a rather arbitrary decision in view of the variability, a value of -4 for the slope S was selected for convenience. Equation 10 then becomes

$$K_{1i} = K_{1j} (E_j/E_i)^4 \quad (11)$$

Attempts to obtain better functions through regressing the data in Table 1 for plots 3, 4, and 5 did not result in functions that predicted any better than Equation 11. As no marked improvement was gained by the regression equations and they tended to stray from the origin and perform poorly in that vicinity, Equation 11 was selected for modifying K_1 with mixture stiffness. Although it may be used for any E_j, best results will be obtained for E_j as near 500 ksi as available.

Where specific fatigue test data are available, a mixture-specific value of the negative of slope S may be obtained and substituted for the value -4 assumed in Equation 11.

COMPARISONS OF FATIGUE CRACKING PREDICTIONS FOR FATIGUE CONSTANTS MODIFIED WITH TEMPERATURE AND WITH MIXTURE STIFFNESS

Procedures have been proposed for modifying the fatigue coefficient K_1 on the basis of temperature and on the basis of mixture stiffness by using Equations 6 or 11, respectively. Once a modified

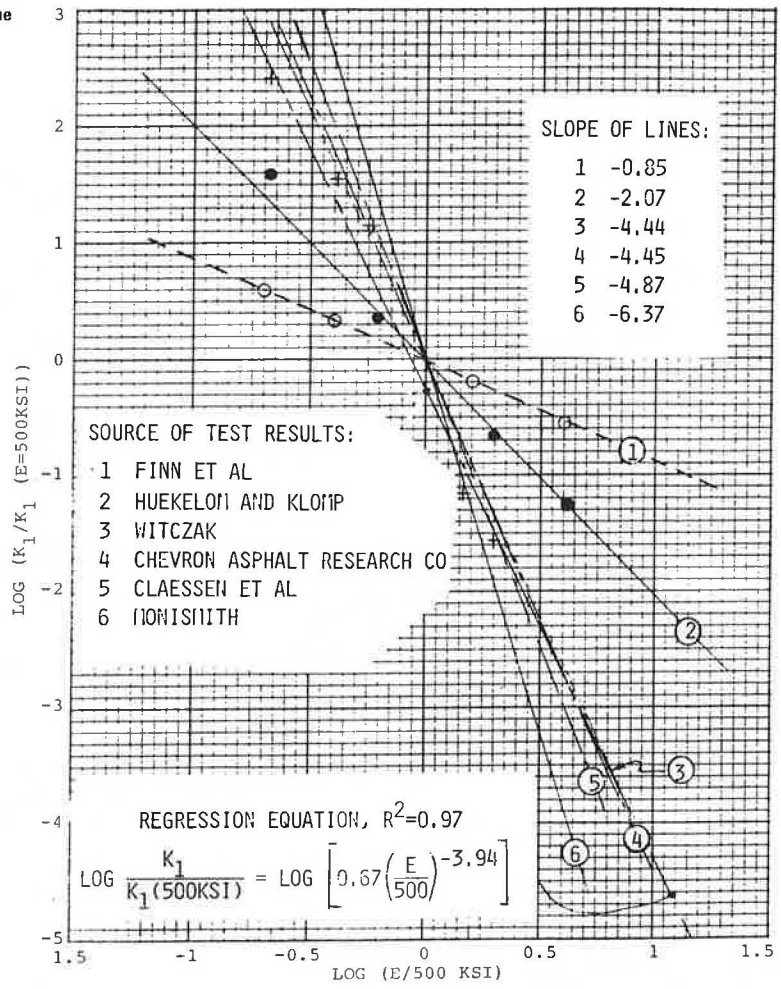

Figure 7. Plot of logarithms of ratio of K_1 for an arbitrary value of dynamic modulus E to K_1 when E is 500 ksi against E(ksi)/500.

value of K_1 is calculated, the exponent K_2 is obtained from Equation 8 in either case. These procedures were developed independently by selecting typical curves from widely scattered data (see Figures 3b and 7). As either procedure may reasonably be used, it will be useful to compare the resulting predictions for fatigue cracking.

Table 2 gives the results of applying these two procedures for two asphalt concrete mixtures and for three levels of tensile strain at the bottom of an asphalt concrete layer. The two mixtures were a relatively stiff mix reported by Witczak (18) and the AASHO Road Test mixture (4), which is of approximately average stiffness. Mixture stiffnesses related to mix temperatures were available and are included for each mix.

In view of the approximate nature of the relations used (Equations 6, 8, and 11), it is rather surprising that the differences in predicted load repetitions to 10 percent cracking are relatively small. For the 36 combinations of strain and fatigue relations calculated, the percentages of difference only exceeded 20 percent five times, four of which were for the larger strain of 0.001. The percentages of differences were in fact 10 percent or less for 26 of the 36 predictions.

For the more typical strain levels of 0.0001 to 0.0003, only 2 of the 24 sets of calculations resulted in differences greater than 20 percent, and both were for the higher temperature of 105°F past the range of the fatigue data on which the relations were developed. The differences for only 6 of the 24 exceeded 10 percent.

It appears from these comparisons that either temperature or mixture stiffness may be used as a basis for obtaining seasonal modifications to fatigue relations once a base relation in terms of either temperature or mixture stiffness is available.

MODIFYING TYPICAL FATIGUE RELATIONS TO REFLECT SPECIFIC MIX CHARACTERISTICS

Typical fatigue relations have been selected, and means of modifying these typical relations to account for changes in temperature or mixture stiffness were then proposed. The purpose of this section is to propose a procedure for modifying typical fatigue relations to reflect the characteristics of specific mixes. A thorough treatment of the variations in fatigue characteristics as related to various mix characteristics is not possible, as sufficient data do not exist in the literature for such a development. However, it is known that the fatigue life of a pavement is affected by at least the following parameters:

1. Mixture stiffness or dynamic modulus E,
2. Air voids,
3. Asphalt content,
4. Pavement temperature,
5. Viscosity of asphalt cement, and
6. Gradation and characteristics of the aggregate.

Table 2. Calculated fatigue cracking by using fatigue constants modified on basis of temperature and mixture stiffness.

Temperature (°F)	E (ksi)	Fatigue Constants: Based on Stiffness $K_1(E_i)$	Fatigue Constants: Based on Stiffness $K_2(E_i)$	Fatigue Constants: Based on Temperature $K_1(T_i)$	Fatigue Constants: Based on Temperature $K_2(T_i)$	Predicted Load Repetitions to 10 Percent Cracking: Based on Stiffness $\epsilon = 1x10^{-3}$	Based on Stiffness $\epsilon = 3x10^{-4}$	Based on Stiffness $\epsilon = 1x10^{-4}$	Based on Temperature $\epsilon = 1x10^{-3}$	Based on Temperature $\epsilon = 3x10^{-4}$	Based on Temperature $\epsilon = 1x10^{-4}$
105	245	$1.37x10^{-5}$	2.98	$4.08x10^{-4}$	2.60	$1.19x10^{4}$	$4.31x10^{5}$	$1.14x10^{7}$	$2.57x10^{4}$	$5.89x10^{5}$	$1.02x10^{7}$
85	500	$7.87x10^{-7}$	3.29	$2.55x10^{-6}$	3.16	$5.83x10^{3}$	$3.06x10^{5}$	$1.14x10^{7}$	$7.70x10^{3}$	$3.46x10^{5}$	$1.11x10^{7}$
70	810	$1.14x10^{-7}$	3.50	$1.14x10^{-7}$	3.50	$3.60x10^{3}$	$2.44x10^{5}$	$1.14x10^{7}$	$3.60x10^{3}$	$2.44x10^{5}$	$1.14x10^{7}$
65	940	$6.30x10^{-8}$	3.56	$4.47x10^{-8}$	3.60	$3.02x10^{3}$	$2.19x10^{5}$	$1.09x10^{7}$	$2.82x10^{3}$	$2.15x10^{5}$	$1.12x10^{7}$
45	1500	$9.72x10^{-9}$	3.77	$2.46x10^{-9}$	3.92	$1.98x10^{3}$	$1.86x10^{5}$	$1.17x10^{7}$	$1.42x10^{3}$	$1.59x10^{5}$	$1.18x10^{7}$
25	2300	$1.76x10^{-9}$	3.96	$3.79x10^{-10}$	4.12	$1.33x10^{3}$	$1.57x10^{5}$	$1.22x10^{7}$	$8.68x10^{2}$	$1.24x10^{5}$	$1.14x10^{7}$
5	3300	$4.15x10^{-10}$	4.11	$1.70x10^{-10}$	4.21	$8.87x10^{2}$	$1.25x10^{5}$	$1.14x10^{7}$	$7.25x10^{2}$	$1.15x10^{5}$	$1.18x10^{7}$
105	62	$3.33x10^{-3}$	2.37	$2.81x10^{-3}$	2.39	$4.29x10^{4}$	$7.44x10^{5}$	$1.01x10^{7}$	$4.16x10^{4}$	$7.39x10^{5}$	$1.02x10^{7}$
85	200	$3.07x10^{-5}$	2.89	$1.76x10^{-5}$	2.94	$1.44x10^{4}$	$4.65x10^{5}$	$1.11x10^{7}$	$1.16x10^{4}$	$4.01x10^{5}$	$1.01x10^{7}$
70	500	$7.87x10^{-7}$	3.29	$7.87x10^{-7}$	3.29	$5.83x10^{3}$	$3.06x10^{5}$	$1.14x10^{7}$	$5.83x10^{3}$	$3.06x10^{5}$	$1.14x10^{7}$
65	600	$4.00x10^{-7}$	3.36	$3.00x10^{-7}$	3.39	$4.81x10^{3}$	$2.75x10^{5}$	$1.10x10^{7}$	$4.44x10^{3}$	$2.62x10^{5}$	$1.09x10^{7}$
45	1220	$2.22x10^{-8}$	3.68	$1.69x10^{-8}$	3.71	$2.43x10^{3}$	$2.04x10^{5}$	$1.16x10^{7}$	$2.28x10^{3}$	$1.99x10^{5}$	$1.17x10^{7}$

Note: Base values are as follows: $K_1 = 7.87x10^{-7}$, $T_2 = 70°F$, $K_2 = 3.29$, and $E_j = 500$ ksi.

There is a limited amount of data available that indicates the effects of percentage of air voids, asphalt content, and mixture stiffness on the fatigue life of specific mixes. However, the interaction of these three parameters and the others listed above are not defined, so it appears necessary to select one of these three that is believed to explain the most variation in fatigue life and to base modifications to the fatigue characterizations on changes in that parameter. It is believed that the mixture stiffness explains much more about variations in the fatigue relations than any other parameter and, fortunately, more test data are available in terms of mixture stiffness. Therefore, variations in the fatigue relation will be based on variations in mixture stiffness for a specific mix tested at a specific temperature from the stiffness measured at the same temperature for the mixture on which the typical fatigue relation is based.

Equation 11 may be used to calculate the new base value of K_1 and Equation 7 to calculate a consistent base value of K_2. These base values may then be used to obtain other mixture-specific relations for other values of temperature or mixture stiffness.

OVERALL PROCEDURE FOR YEAR-ROUND CHARACTERIZATION OF FATIGUE LIFE

By using the procedure described above, fatigue relations may be obtained for specific mixes in terms of variations in their stiffness at a specified temperature from that of a typical mixture. These relations may then be modified in terms of variations in temperature or mixture stiffness to characterize fatigue life potential during various periods or seasons of the year. The only data needed are the mixture stiffness at 70°F, which can be obtained from a single dynamic-modulus test at 70°F or from a plot of mixture stiffness versus specimen temperature.

The first step is to obtain values of K_1 and K_2 that better represent the specific mixture. This is accomplished by substituting the mixture stiffness at 70°F into Equation 11 along with $K_{1j} = 7.87x10^{-7}$ and $E_j = 500$ ksi to calculate K_{1i} for the mixture. K_2 for the mixture is then obtained by substituting K_{1i} as K_1 in Equation 8.

The second step is to select analysis seasons for the year and to establish appropriate pavement temperatures to represent each season. Winter, summer, fall, and spring are usually used, sometimes with an additional short season in colder climates to represent spring thaw. (The calculation of pavement temperatures is itself a complex procedure and is outside the scope of this paper.)

Once the seasonal pavement temperatures have been established, seasonal temperatures or mixture stiffnesses may be obtained and used in Equations 6 or 11 to obtain seasonal values of K_1. Seasonal values of K_2 may then be obtained through use of Equation 8.

These seasonal fatigue relations may then be used along with calculated strains (considering seasonal values of layer stiffnesses) to arrive at values of load repetitions to failure that represent each season. Miner's hypothesis may then be used with ratios of seasonal traffic estimates to seasonal failure repetitions to accumulate consumption of fatigue life with time or traffic.

PREDICTING FATIGUE LIFE AS AREA CRACKED

Prediction of failure in fatigue depends on the definition of failure for which the fatigue relation is based. When sufficient loads have been experienced for the linear summation of cycle ratios (Miner's hypothesis) to reach unity, a damage index (DI) is defined as unity and the pavement is considered failed.

As measurement of fatigue cracking is usually as a percentage of areal cracking, it would be more convenient to predict fatigue in terms of areal cracking than as fraction failed, as is usually currently done. As the typical fatigue relation is based on 10 percent areal cracking, we know that a predicted DI of unity corresponds to 10 percent cracking for the typical fatigue relation adopted. Review of fatigue relations by Finn and others (1) indicates that the only difference is in K_1, so division of K_1 at 45 percent cracking by that at 10 percent cracking ($1.084x10^{-6} \div 7.87x10^{-7} = 1.38$) indicates that a damage index of 1.38 will correspond to 45 percent cracking. These two points are plotted in Figure 8, and a relation that is believed to represent a reasonable distribution has been developed and plotted through these points. Comparisons with similar developments for different purposes by Von Quintus and others (19) on the basis of the same fatigue relations indicate an almost identical shape for the relation.

It is proposed that the relation below be used to transform predicted DI to percentage of areal cracking (A_c):

$$A_c = 0.19e^{3.96DI} \quad (12)$$

Inspection of Figure 8 indicates that Equation 12 will predict the first noticeable crack at the

Figure 8. Curve for transforming DI to percentage of areal cracking.

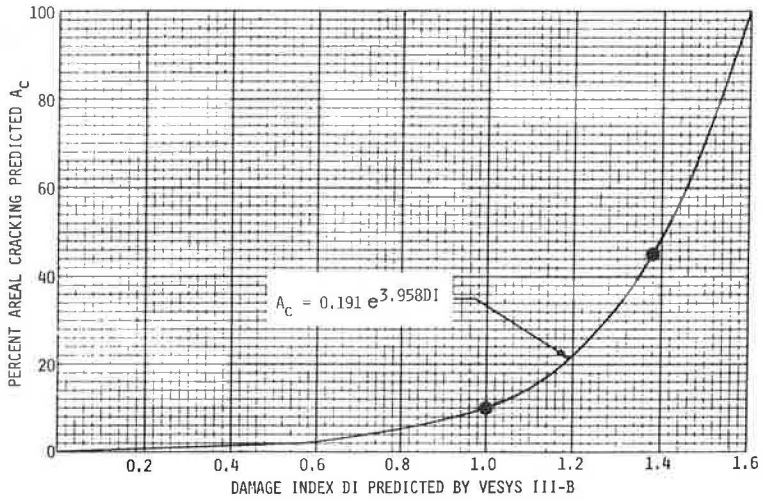

surface when the predicted damage index reaches 0.4. Ten percent cracking will be predicted at a DI of unity, 45 percent at a DI of 1.38, and 100 percent at a DI of 1.583. For constant rates of traffic (numbers and axle-load distributions), this means that 40 percent as much traffic is required to produce the first crack as is necessary to induce 10 percent cracking. Thirty-eight percent more traffic is required to progress from 10 to 45 percent cracking. For example, in the primary range of interest between 5 and 45 percent cracking, Equation 12 is believed to provide reasonable predictions for the growth of areal cracking.

SUMMARY

The evaluation of fatigue life for asphalt concrete pavements has in the past been very difficult because of limited knowledge as to fatigue damage relations for real pavements, availability of laboratory test data for only a limited set of mixtures, and limited information on the variations of fatigue life potential with pavement temperature and mixture characteristics. This paper offers procedures to overcome some of these difficulties and to improve the confidence levels at which such evaluations may be made. Although the typical fatigue relations and approximate procedures proposed are considered to offer a much greater opportunity for successful prediction of fatigue life than has been generally possible, no claims of great accuracy are made and fatigue life characterizations for specific mixtures in place should be used in the fortunate and unusual event that they should be available.

The proposed transformation from prediction of a DI to prediction of percentage of class 2 and 3 areal cracking is believed to be more meaningful to most engineers. It also offers an interval of prediction rather than relation to a single condition defined as failure. As with many fatigue-related functions, however, the rate of development of areal cracking used in developing Equation 12 is based on only one mixture and environment, and it might be expected to vary for others, as well as for other changed conditions.

Prediction of fatigue life in asphalt concrete pavements may vary considerably from actual fatigue performance in the field; however, the accuracy of such predictions has improved in the past decade due to contributions by numerous researchers. It is hoped that the procedures proposed will contribute to this positive trend.

ACKNOWLEDGMENT

Support for this work was provided by the Federal Highway Administration (FHWA) through their contract with Brent Rauhut Engineering, Inc. We are grateful for the valuable technical coordination provided by William J. Kenis, contract manager, Office of Research and Development, FHWA.

REFERENCES

1. F.N. Finn, C. Saraf, and R. Kulkarni. Development of Structural Subsystems, Final Report. NCHRP, NCHRP Project 1-10B, July 1976.
2. F.R.P. Meyer, A. Cheetham, and R.C.G. Haas. A Coordinated Method for Structural Distress Predictions in Asphalt Pavements. Proc., Association of Asphalt Paving Technologists, Vol. 47, Feb. 1978.
3. M.W. Witczak. Design of Full-Depth Asphalt Airfield Pavements. Proc., Third International Conference on Structural Design of Asphalt Pavements, Univ. of Michigan, Ann Arbor, 1972.
4. ARE, Inc. Asphalt Concrete Overlays of Flexible Pavements, Vol. 1: Development of New Design Criteria. FHWA, Rept. FHWA-RD-75-75, June 1975.
5. W. Van Dijk. Practical Fatigue Characterization of Bituminous Mixes. Proc., Association of Asphalt Paving Technologists, Vol. 44, Feb. 1975.
6. J.A. Epps and C.L. Monismith. Influence of Mixture Variables on the Flexural Fatigue Properties of Asphalt Concrete. Proc., Association of Asphalt Paving Technologists, Vol. 38, 1969.
7. C.L. Monismith, D.A. Kasianchuk, and J.A. Epps. Asphalt Mixture Behavior in Repeated Flexure--A Study of an In-Service Pavement Near Morro Bay, California. Univ. of California, Berkeley, IER Rept. TE 67-4, 1967.
8. W. Van Dijk and W. Visser. The Energy Approach to Fatigue for Pavement Design. Paper presented at Annual Meeting of Association of Asphalt Paving Technologists, Feb. 1977.
9. W.S. Smith and K. Nair. Development of Procedures for Characterization of Untreated Granular Base Course and Asphalt-Treated Base Course Materials. FHWA, Rept. FHWA-RD-74-61, Oct. 1973.
10. R.D. Barksdale. Development of Equipment and Techniques for Evaluating Fatigue and Rutting Characteristics of Asphalt Concrete Mixes. School of Civil Engineering, Georgia Institute of Technology, Atlanta, June 1977.
11. Bitumens Mix Manual. Chevron Asphalt Research Company, Richmond, CA, 1975.

12. J.B. Rauhut, J.C. O'Quin, and W.R. Hudson. Sensitivity Analysis of FHWA Structural Model VESYS IIM, Vol. 1: Preparatory and Related Studies. FHWA, Rept. FHWA-RD-76-23, March 1976.
13. P.S. Pell. Fatigue Characteristics of Bitumin and Bituminous Mixes. Proc., International Conference on Structural Design of Asphalt Pavements, Univ. of Michigan, Ann Arbor, 1962.
14. A.I.M. Claessen, J.M. Edwards, P. Sommer, and P. Uge. Asphalt Pavement Research--The Shell Method. Proc., Fourth International Conference on Structural Design of Asphalt Pavements, Univ. of Michigan, Ann Arbor, Vol. 1, Aug. 1977.
15. A.S. Adedimila and T.W. Kennedy. Fatigue and Resilient Characteristics of Asphalt Mixtures by Repeated-Load Indirect Tensile Test. Center for Highway Research, Univ. of Texas, Austin, Rept. 183-5, Aug. 1975.
16. W. Huekelom and A.J.G. Klomp. Road Design and Dynamic Loading. Proc., Association of Asphalt Paving Technologists, Vol. 33, 1964.
17. C.L. Monismith. Asphalt Mixture Behavior in Repeated Flexure. Institute of Transportation and Traffic Engineering, Univ. of California, Berkeley, Rept. TE-66-6, 1966.
18. M.W. Witczak. Development of Regression Model for Asphalt Concrete Modulus for Use in MS-1 Study. Asphalt Institute, College Park, MD, Jan. 1978.
19. H.L. von Quintus, F.N. Finn, W.R. Hudson, and F.L. Roberts. Flexible and Composite Structures for Premium Pavements, Vol. 1: Development of Design Procedure. FHWA, Nov. 1980.

Publication of this paper sponsored by Committee on Flexible Pavement Design.

Structural Design of Flexible Pavements: A Simple Predictive System

JACOB UZAN AND ROBERT L. LYTTON

During the past two decades, much effort has gone into the development of rational pavement design procedures that are intended to be integrated into a more general framework. The Federal Highway Administration has developed a computer program package known as VESYS II to predict the structural responses and hence the integrity of flexible pavements. The program is quite formidable for the local design engineer. Therefore, a simple predictive system is needed to be widely used for the structural design of flexible pavements. A simple computer program package is presented that includes (a) regression formulas for tensile strain and rut depth computations, cracking prediction, and evaluation of the rut depth variance; (b) modification and calibration of the American Association of State Highway Officials (AASHO) Road Test serviceability model, where rut depth variance replaces the slope variance; (c) seasonal (monthly) characterization of pavement materials and discrete representation of axle-load distribution; and (d) special treatment for overlay analysis. The procedure is illustrated and the results are discussed. The good agreement between the results and measured values and the simplicity of the program make it very attractive. It could be programmed on a desk (micro) computer.

During the past two decades, much effort has gone into the development of rational pavement design procedures that were intended to be integrated into a more general framework. The Federal Highway Administration (FHWA) (1) has developed a computer program package known as VESYS II (and its modifications and extensions VESYS IIM, VESYS A, and VESYS G) to predict the structural responses and hence the integrity of flexible pavements. The program is based on an advanced viscoelastic analysis that is, however, a rather significant departure from more conventional systems. The implementation and use of the VESYS package seems appropriate for a statewide study, but it appears quite formidable for the design engineer. At the same time, pavement structural subsystems have been developed for the Transportation Research Board (2). The computer programs--one for fatigue cracking and permanent deformation (named PDMAP) and one for low-temperature cracking (named COLD)--were proposed for implementation and field calibration. The PDMAP package does not include the synthesis of the two subsystems and does not predict pavement performance.

This paper presents the integration of the fatigue and permanent deformation subsystems into a computer program package. The proposed system is simple, reliable, and also general, which facilitates its use by most people who deal with pavement design and maintenance. It includes the following:

1. Modification and calibration of the American Association of State Highway Officials (AASHO) Road Test serviceability model to enable pavement performance prediction by using computed damages,
2. Cracking prediction based on the commonly used fatigue law and probabilistic considerations to express mechanistic variables into cracked areas,
3. Permanent deformation prediction based on quasi-elastic analysis,
4. Regression formulas and closed-form probabilistic solutions for evaluation of the variables involved in the performance model (the probabilistic solutions are similar to those used in VESYS G),
5. Overlay application analysis to permit pavement maintenance strategy studies, and
6. Seasonal (monthly) characterization of pavement materials and discrete representation of axle-load distribution.

SERVICEABILITY MODEL

The AASHO Road Test serviceability model relates serviceability index to variables that describe pavement damage, i.e., cracking, patching, rutting, and slope variance (3). The AASHO model reads as follows:

$$PSI = 5.03 - 1.91 \log_{10}(1 + \overline{SV}) - 1.38\,\overline{RD^2} - 0.01\sqrt{C + P} \quad (1)$$

$$R^2 = 0.84$$

where

PSI = present serviceability index,
$\overline{SV}$ = average slope variance (10^6 radian),
$\overline{RD}$ = average rut depth (in),
$\overline{C}$ = cracking (ft²/1000 ft²),
$\overline{P}$ = patching (ft²/1000 ft²), and
R = correlation coefficient.

The model was used in its original form in the VESYS IIM program. Its implementation required the prediction of all the basic variables involved: $\overline{SV}$, $\overline{RD}$, and $\overline{C}$. [The variable $\overline{P}$ (patching) was dropped from Equation 1, as it was taken into account through the variable $\overline{C}$ (cracking).] It should be noted that only two mechanistic subsystems exist for the prediction of the three variables mentioned above. Cracking and rutting are readily dealt with by the fatigue and permanent deformation subsystems, respectively, while the slope variance variable, which is the result of the variability of the material in the longitudinal direction, required additional development. Its prediction in VESYS II is based on the stochastic variation of the rut depth (1) and on assumptions that concern the spatial autocorrelation function. Rauhut and others (4,5) used an approximation for the relation between slope variance and rut depth and its variance as follows:

$$\overline{SV} \simeq k \text{ Var [RD]} \tag{2}$$

where k is the coefficient derived from linear regression with intercept forced through the origin, and Var [RD] is the rut depth variance.

The regression for all data from all four states was very poor. Substituting Equation 2 into Equation 1 corresponds, in fact, to a change of variables in Equation 1. Better results would be obtained by handling the original problem, i.e., deriving the serviceability model from raw data by using predictable variables only. The new serviceability model is then

$$PSI = a_0 + a_1 \log_{10}(1 + a_2 \text{ Var [RD]}) + a_3 \overline{RD}^{a4} + a_5 (\overline{C} + \overline{P})^{a6} \tag{3}$$

where a_0 to a_6 are the new regression coefficients. A nonlinear regression analysis was made on the four test sections of the AASHO model. The following equation was obtained by trial and error:

$$PSI = 4.436 - 1.686 \log_{10}(1 + 350 \text{ Var [RD]}) - 0.881 \overline{RD}^{2.5} - 0.031\sqrt{\overline{C} + \overline{P}} \tag{4}$$

$R^2 = 0.80$

In this equation the effect of cracking became significant, while in Equation 1 the cracking term could be dropped without affecting the correlation coefficient. Furthermore, the intercept coefficient a_0 is very close to the average value of the pavement serviceability after construction (4.44 as compared with 4.20). Therefore, the new Equation 4 might be of greater engineering significance than Equation 1, even for a lower correlation coefficient (R^2 = 0.80 as compared with 0.84).

FATIGUE SUBSYSTEM

All fatigue subsystems presented in the literature are based on (a) computing tensile stresses or strains at the bottom of the surface layer, (b) evaluating the pavement service life from the relation between number of repetitions to failure (N_f), and (c) applied stress or strain. Few fatigue subsystems extended the analysis to predict the cracked area based on field correlation (2) or probabilistic solutions (1,6).

Computation of Tensile Strain at Bottom of Asphalt Concrete

The tensile strain at the bottom of the asphaltic concrete layer has been computed for a dual wheel load with a center-to-center distance between wheels of three times the radius of contact. The computation was made by using the BISAR program of the Shell Company and at two points: under one wheel of the dual load and between the wheels. Comparison of these results for radial and tangential strains under one wheel of the dual load and between the wheels shows that, in general, the tangential strain under one wheel of the dual load is larger than the other strain components. This selection of the strain component is generally not dealt with in the VESYS IIM program (1) or the Shell method (7), since only one wheel is used for strain computations. However, it is important for the summation applied in Miner's law for fatigue analysis to select only one component of the strain tensor.

In the computer program, the strain is computed either by interpretation of tabulated values read as data or by the regression formulas for tangential strain computations that are given below (Equations 6 and 7). The regression formulas for tangential strain under one wheel of the dual load at the bottom of the first and second layer of the three- or four-layer system are as follows:

$$\begin{aligned} E_4\epsilon_1/p = {} & 0.095\,929 - 0.039\,752 \log(T_1/a) - 0.025\,642 \log(E_1/E_4) \\ & - 0.068\,359 \log(E_2/E_4) - 0.008\,391 \log(E_3/E_4) \\ & - 0.020\,938 [\log(T_1/a)]^2 + 0.020\,661 \log(T_1/a) \log(E_2/E_4) \\ & - 0.003\,075 \log(T_2/a) \log(E_1/E_4) - 0.010\,022 \log(T_2/a) \\ & \log(E_3/E_4) + 0.013\,842 \log(E_1/E_4) \log(E_2/E_4) \\ & + 0.009\,354 [\log(E_2/E_4)]^2 + 0.003\,873 \log(E_2/E_4) \\ & \log(E_3/E_4) \end{aligned} \tag{5}$$

$R^2 = 0.83$

$$\begin{aligned} E_4\epsilon_2/p = {} & 0.085\,565 - 0.063\,772 \log(T_1/a) - 0.053\,237 \log(T_2/a) \\ & - 0.003\,243 \log[(1 + T_3)/a] - 0.021\,28 \log(E_1/E_4) \\ & - 0.018\,796 \log(E_2/E_4) - 0.066\,174 \log(E_3/E_4) \\ & + 0.029\,831 \log(T_1/a) \log(T_2/a) + 0.013\,190 \log(T_1/a) \\ & \log(E_2/E_4) + 0.037\,69 \log(T_2/a) \log(E_3/E_4) \\ & + 0.010\,535 \log(T_2/a) \log(E_1/E_4) + 0.003\,481 \log(T_2/a) \\ & \log(E_2/E_4) + 0.024\,568 \log(T_2/a) \log(E_3/E_4) \\ & + 0.004\,905 \log(E_1/E_4) \log(E_2/E_4) + 0.012\,278 \log(E_1/E_4) \\ & \log(E_2/E_4) - 0.002\,551 [\log(E_2/E_4)]^2 + 0.017\,822 \\ & \log(E_2/E_4) \log(E_3/E_4) \end{aligned} \tag{6}$$

$R^2 = 0.84$

where

ϵ_1 = longitudinal (tangential) strain computed at the bottom of the upper asphaltic concrete layer under one wheel of the dual load;
ϵ_2 = longitudinal (tangential) strain computed at the bottom of the lower asphaltic concrete layer under one wheel of the dual load (applicable for an asphaltic concrete base layer or for an asphaltic overlay analysis);
p = contact pressure;

a = radius of contact;
T_1, T_2, T_3 = thicknesses of surface, base, and subbase layers, respectively; and
E_1, E_2, E_3, E_4 = elastic moduli of surface, base, subbase, and subgrade layers, respectively.

Note that the regression formulas were derived from the following values of variables: T_1/a = 0.4, 1.1, 2.2; T_2/a = 0.5, 1.3, 2.6; T_3/a = 0, 1.3, 2.6, 5.2; E_1/E_4 = 10, 60, 350; E_2/E_4 = 2, 5, 10, 60, 350; and E_3/E_4 = 1, 2, 5, 10.

Evaluation of Pavement Fatigue Life

The commonly used fatigue law that relates the applied tensile strain to the number of repetitions that cause failure is implemented in the system. The law reads

$$N_f = K_1 (1/\epsilon)^{K_2} \quad (7)$$

where

N_f = number of strain repetitions that cause failure,
ϵ = applied strain, and
K_1, K_2 = regression coefficients from laboratory or field tests.

Correction factors for rest periods or residual stress effects could be incorporated at this stage into the K_1 and K_2 coefficients. The damage caused to the structure by wheel-load repetitions is evaluated by using Miner's law, i.e.,

$$D_j = \sum_{g=1}^{j} \sum_{i=1}^{k} (n_i/N_{fi}) \quad (8)$$

where

D_j = damage caused by k different load configurations during the previous j periods,
n_i = actual number of repetitions for load i, and
N_{fi} = number of repetitions to failure determined for load i by using Equation 7.

Evaluation of Cracked Area

The cracked area is evaluated by using the approach presented by Rauhut and others (4) and Kenis (1). The pavement geometry (layer thicknesses) and material properties (elastic moduli and fatigue law parameters) are treated stochastically, and the damage factor D_j is assumed to be a normally distributed random variable whose mean and variance can be computed by using Cornell's first-order, second-moment theory [Huffert and Lai (8)]. Under these assumptions, and for each D_j mean and variance, the probability F(1) that the variable D_j reaches the value of one (or the pavement is cracked) could be computed and used to evaluate the cracked area as follows:

$$\bar{C} = 1000 [1 - F(1)] \quad (9)$$

where $\bar{C}$ is the expected cracked area (ft^2/1000 ft^2). It is used in Equation 1 or in Equation 4 to represent the cracked and patched area ($\bar{C} + \bar{P}$).

PERMANENT DEFORMATION SUBSYSTEM

The completed permanent deformation is based on the quasi-linear elastic analysis and incremental procedure proposed in three unpublished reports by J. Uzan, J.T. Christison, and K.O. Anderson [hereafter referred to as the Uzan reports (Rut Depth Prediction Using the Quasi-Elastic Approach; Prediction of Rut Depth Performance in Flexible Pavement Using Statistically Based Models; and Permanent Deformation in Asphalt Overlays on Flexible Pavements), which were done at Technion, Israel Institute of Technology, Haifa, 1979]. The procedure includes

1. Computation of the deflection bowl under loading and unloading conditions; the difference in deflection is the incremental (per repetition) residual surface deflection or rate of rutting;
2. Computation of the above rate of rutting at different stages during the pavement life; its integration enables estimation of the rut depth; and
3. For the quasi-linear elastic analysis, the moduli of elasticity under loading and unloading conditions are required.

It is shown that they are related to each other through the number of repetitions and the plastic parameters derived from repetitive loading tests.

In the actual permanent deformation, the incremental residual surface deflection is expressed as follows (from the Uzan reports):

$$d(RD)/dN = (pa/E_4) \cdot a_1 N^{a_2} \quad (10)$$

and its integration over an interval of the pavement life (i.e., the contribution of the load repetition number between n_{j-1} and n_j) is

$$\Delta RD_j = (pa/E_4) \cdot [a_1/(1 + a_2)] (n_j^{1+a_2} - n_{j-1}^{1+a_2}) \quad (11)$$

where

RD = rut depth of permanent deflection,
ΔRD_j = increment of rut depth caused by a given load during period j of the pavement life,
p = contact pressure of the dual wheel,
a = contact radius of each wheel,
a_1, a_2 = regression coefficients [functions of the pavement geometry and material properties (elastic and plastic)], and
E_4 = subgrade elastic modulus.

It should be noted that Equation 10 is similar to the rutting model by Finn and others (2). According to both the models of Finn and others (2) and VESYS, there is some evidence that the permanent deformation is well correlated to the resilient deflection of the pavement. It was therefore introduced in the model through the regression coefficients a_1 and a_2.

Two different regression models were derived:

1. The first model assumes fixed transversal distribution of wheel loads and a standard deviation of 1 ft. By using the deflection bowl and the normalized distribution, the rut depth increment per repetition in Equation 10 is computed at two locations: (a) under one wheel of the dual load that corresponds to the maximum depression, and (b) at a 2-ft distance from the first position, on both the right and the left side, which corresponds to supports of the 4-ft straight edge. The contribution of the lateral distribution to the residual incremental deflection is taken proportional to the density function of the distribution. The difference between the residual deformation at the first location (under one wheel of the dual load) and the average of the residual deformations at the second locations (on the right and the left side) is the incremental rut depth. Note that this permanent deformation definition is in accordance with the

AASHO definition and procedure for measuring rut depth. Other program packages such as VESYS do not compute the rut depth but the absolute pavement deformation, as in our second model.

2. The second model computes the permanent deformation under one wheel of the dual load. The rut depth (as measured with a 4-ft straight edge) can be evaluated by computing the deformation under the wheel and at a 2-ft distance from the wheel and is the difference between these two computations.

The two approaches are implemented in the current computer program package. The regression formulas for a_1 and a_2 are given below (Equations 12-15). The use of either the first or second model at this stage is a matter of engineering judgment until the superposition law for permanent deformation is formulated and verified.

The regression formulas for the A_1 $(=1 + a_1)$ and A_2 $(=1 + a_2)$ used in Equations 10 and 11 are given below:

1. The first case that corresponds to a given transversal distribution of wheel loads is as follows:

$$\begin{aligned}\log A_1 = {} & 0.0281 \log\alpha_2 + 0.0916 \log\alpha_3 - 0.0251 \log\alpha_4 + 0.0365 \\ & \log(1+\mu_1) + 0.1051 \log(1+\mu_2) + 0.0544 \log(1+\mu_3) \\ & + 0.0705 \log(1+\mu_4) + \log W[0.009 \log\alpha_2 + 0.0894 \log\alpha_3 \\ & - 0.039 \log\alpha_4 + 0.0425 \log(1+\mu_1) + 0.054 \log(1+\mu_2) \\ & + 0.075 \log(1+\mu_3) + 0.1025 \log(1+\mu_4)] + 0.0122 \log\alpha_1 \\ & \log\alpha_2 + 0.0255 \log\alpha_1 \log(1+\mu_2) + 0.013 \log\alpha_2 \log(1+\mu_1) \\ & - 0.1502 \log\alpha_2 \log(1+\mu_2) - 0.1752 \log\alpha_3 \log(1+\mu_1) \\ & - 0.3116 [\log(1+\mu_2)]^2 \end{aligned} \quad (12)$$

$R^2 = 0.96$

$$\begin{aligned}A_2 = {} & 0.054 + 0.0093 \log W - 1.424 \log\alpha_1 - 0.457 \log\alpha_2 + 1.428 \log\alpha_3 \\ & + 0.0265 \log\alpha_4 + 0.217 \log(1+\mu_1) - 0.4523 \log(1+\mu_2) \\ & - 0.183 \log(1+\mu_3) + 2.428 \log W \log\alpha_3 - 3.3946 \log\alpha_1 \log\alpha_2 \\ & + 1.442 (\log\alpha_2)^2 - 2.237 \log\alpha_2 \log(1+\mu_2) \end{aligned} \quad (13)$$

$R^2 = 0.94$

2. The second case is for no transversal distribution of wheel loads:

$$\begin{aligned}\log A_1 = {} & 0.0266 \log\alpha_2 + 0.055 \log(1+\mu_1) + 0.1593 \log(1+\mu_2) \\ & - 0.1084 \log(1+\mu_3) + 0.7798 \log(1+\mu_4) \\ & + \log W [0.0260 \log\alpha_2 + 0.1662 \log\alpha_4 + 0.0281 \log(1+\mu_1) \\ & + 0.1872 \log(1+\mu_2) + 0.2132 \log(1+\mu_3) + 0.8103 \log(1+\mu_4)] \\ & + 0.0293 \log\alpha_1 \log\alpha_2 + 0.0757 \log\alpha_1 \log(1+\mu_3) \\ & - 1.6121 (\log\alpha_4)^2 - 0.1072 \log\alpha_4 \log(1+\mu_2) + 0.2018 \log\alpha_4 \\ & \log(1+\mu_3) + 0.0508 [\log(1+\mu_1)]^2 + 0.0860 \log(1+\mu_1) \\ & \log(1+\mu_3) + 2.4116 [\log(1+\mu_3)]^2 \end{aligned} \quad (14)$$

$R^2 = 0.97$

$$\begin{aligned}A_2 = {} & 0.0884 - 1.1007 \log\alpha_1 - 0.9640 \log\alpha_2 - 0.2455 \log(1+\mu_2) \\ & - 1.4252 \log(1+\mu_3) + 0.6959 (\log\alpha_1)^2 - 3.220 \log\alpha_1 \log\alpha_2 \\ & - 0.9517 \log\alpha_1 \log(1+\mu_1) + 1.2965 \log\alpha_1 \log(1+\mu_2) \\ & + 6.0467 \log\alpha_1 \log(1+\mu_4) + 0.6490 (\log\alpha_2)^2 - 0.3772 \log\alpha_2 \\ & \log(1+\mu_3) + 8.0917 \log(1+\mu_2) \log(1+\mu_3) + 7.4075 \log(1+\mu_3) \\ & \log(1+\mu_4) \end{aligned} \quad (15)$$

$R^2 = 0.95$

where

$W = wE_4/pa$ = nondimensional deflection;
w = elastic deflection between wheels of the dual load;
p = contact pressure;
a = radius of contact;
T_1, T_2, T_3 = thicknesses of surface, base, and subbase layers, respectively;
E_1, E_2, E_3, E_4 = elastic moduli of surface, subbase, and subgrade layers, respectively;
$\alpha_1, \alpha_2, \alpha_3, \alpha_4$ = alpha's plastic material properties of layers; and
$\mu_1, \mu_2, \mu_3, \mu_4$ = mu's plastic material properties of layers.

The nondimensional deflection (W) was expressed as a function of the four-layer system variables as follows:

$$\begin{aligned}\log W = {} & 0.2847 - 0.2361 \log(T_1/a) - 0.0898 \log(T_2/a) \\ & - 0.2441 \log(E_1/E_4) - 0.1830 \log(E_2/E_4) - 0.0460 \log(E_3/E_4) \\ & + \log(T_1/a)\{-0.2075 \log(T_1/a) + 0.2015 \log(T_2/a) \\ & + 0.0986 \log[(1+T_3)/a] - 0.2191 \log(E_1/E_4) \\ & + 0.1246 \log(E_2/E_4) + 0.1020 \log(E_3/E_4)\} + \log(T_2/a) \\ & \{-0.1720 \log(T_2/a) + 0.1143 \log[(1+T_3)/a] + 0.0118 \\ & \log(E_1/E_4) - 0.1919 \log(E_2/E_4) - 0.0965 \log(E_3/E_4)\} \\ & + \log[(1+T_3)/a] [-0.0474 \log(E_1/E_4) + 0.0220 \log(E_2/E_4) \\ & + 0.0220 \log(E_3/E_4)] + \log(E_1/E_4) [-0.3315 \log(E_1/E_4) \\ & + 0.0145 \log(E_2/E_4) + 0.0095 \log(E_3/E_4)] + \log(E_2/E_4) \\ & [0.0216 \log(E_2/E_4) + 0.0074 \log(E_3/E_4)] \\ & + 0.0300 [\log(E_3/E_4)]^2 \end{aligned} \quad (16)$$

The rut depth variance, as required for serviceability evaluation as per Equation 4, is computed by using Cornell's first-order, second-moment theory (8) for the functions that are represented by Equation 11 and the regression formulas (Equations 12-16). It includes the effect of variation of pavement geometry (layer thicknesses) and of material properties (resilient moduli and plastic parameters of all layers).

PROGRAM DESCRIPTION

The system that has been developed to predict pavement performance includes several elements and models for describing the structure, the different materials, and the environmental and loading conditions. They are presented and discussed in the following sections.

Pavement Design Framework

The pavement design framework consists of a four-layer system with an option for selecting only the three-layer system. This is especially convenient for overlay analysis. In its early life, the three-layer system is for describing the conventional pavement while the four-layer system is used for the overlaid pavement.

The material properties required for structural analysis are the linear-elastic moduli, which are assumed temperature and/or suction dependent. Strain and rut depth computations are made by using the regression formulas (Equations 5 and 6 and 12-16).

Loads

Loads are represented by dual wheels with constant

contact radius (a = 4.5 in) and constant distance between wheels (c - c = 3a). Loads of varying intensities can be prescribed. Their contributions to fatigue life or cracking are summed by using Miner's law. Note that the sequential order of application of the loads does not affect the results. However, it does affect the rate of permanent deformation, as seen from Equations 10 or 11. In this case, the time-hardening scheme (9) is adopted for load equivalency computations that are made each month during the pavement life.

Environmental Conditions

The environmental conditions include temperature distribution of each asphalt concrete layer and temperature and suction (or moisture content) distribution of the subgrade. The analysis, and therefore the input, is made for each basic time period that has been chosen to be a monthly interval. For the asphalt concrete modulus of elasticity, which strongly depends on temperature, the following three-segment relation is assumed:

$$\text{When } T \leq 32°F,\ E_T = E_o \tag{17}$$

$$\text{When } 32°F < T \leq 77°F,\ E_T = E_o\ 10^{(T-32)\alpha_1} \tag{18}$$

$$\text{When } T < 77°F,\ E_T = E_o\ 10^{[45\alpha_1 + (T-77)\alpha_2]} \tag{19}$$

where

E_T = modulus of elasticity of asphalt concrete at temperature T (°F),
E_o = E_T at T = 32°F = 0°C, and
α_1, α_2 = material coefficients.

The temperature and suction (or moisture content) dependence of the modulus of elasticity of the subgrade are assumed as follows (10):

$$E_s = E_{sr} \cdot a_h \cdot a_T \tag{20}$$

$$a_h = \exp\,[a_5\,(h - h_s)] \tag{21}$$

$$a_T = \exp\,\{a_3\,(T - T_s)/[a_4 + (T - T_s)]\} \tag{22}$$

and

$$\ln h = a_1 - a_2 \ln w \tag{23}$$

where

E_s = subgrade modulus at temperature T and suction h or moisture content w,
E_{sr} = subgrade modulus at given reference temperature T_s and given reference suction h_s,
a_h = suction influence factor,
a_T = temperature influence factor, and
a_1, a_2, a_3, a_4, a_5 = constants.

Note that when the subgrade temperature is 32°F or less, the material is assumed to be frozen and a representative modulus of elasticity of 50 000 psi is assigned to it (2). During the frozen period, which should be specified, no rut depth computations are made, since no contribution could be made during these months.

The environmental conditions indirectly affect the material properties of granular subbase and base layers through the dependence of their moduli of elasticity on that of the subgrade. Two ratios of granular material and subgrade moduli are implemented: the Shell method (7) and the USCE method (11).

Overlay Analysis

The overlay analysis is included in the program for maintenance strategy studies. In this case, cracking involved in Equation 4 is the one that is computed in the upper layer (overlay layer). Rut depth and its variance are initialized (to zero and to the corresponding initial serviceability) and new plastic parameters (alphas and mus) of the existing pavement layers are specified. This makes it possible to take into account the changes in material properties that result from past traffic conditions. The computations are then made for the renewed pavement, and its performance is predicted.

Note that the period preceding overlay application can be subdivided into subperiods that are multiples of a year. This facility enables the designer to include changes in material properties during the pavement life that are caused by environmental and/or loading conditions (such as for cracked asphalt or any special conditions).

APPLICATION

System Description

Application of the procedure is illustrated by analyzing the pavement response of an AASHO Road Test section. The analysis presented below includes a sensitivity analysis of different pavement response components (cracking, rut depth, and its variance) to input parameter variations. The section chosen is section 581 of loop 4 in the AASHO Road Test. The input variables were collected from the literature and are summarized below:

1. Geometry: The geometry consists of 5-in asphalt concrete, 6-in base course, and 13-in subbase course on the top of the silty clay subgrade.
2. Moduli of elasticity: The asphalt concrete material is temperature dependent according to Equations 17-19, where $E_o = 1.8 \times 10^6$ psi, $\alpha_1 = 0.014$, and $\alpha_2 = 0.022$, which lead to elastic moduli as reported by Finn and others (2). The subgrade modulus is temperature and moisture dependent according to Equations 20-23, where E_{sr} = 6000 psi, $a_1 = 0$, $a_2 = -1$, $a_3 = -0.070$, $a_4 = 33.50$, and $a_5 = -0.70$, which were chosen to reduce the elastic modulus by half in the springtime period. The granular material modulus was computed by using the procedure by Barker and others (11).
3. Plastic properties: The following alphas and mus were chosen on the basis of the literature review (4,5, and Uzan reports): $\alpha_1 = 0.56$, $\mu_1 = 0.3$, $\alpha_2 = \alpha_3 = 0.9$, $\mu_2 = \mu_3 = 0.3$, $\alpha_4 = 0.80$, and $\mu_4 = 0.045$.
4. Fatigue parameters: The fatigue law from Finn and others (2) for 10 percent cracking and a corrected one ($K_1 = 0.057\,943\ E^{-0.854}$ and $0.3\ E^{-0.854}$, $K_2 = 3.291$) are implemented.
5. Environmental conditions: The asphalt temperature distribution was 48, 37, 32, 31, 35, 62, 73, 82, 87, 88, 78, and 63 for the 12 months following the onset of the test (repeated for the next 12 months). The subgrade was assumed to be frozen during the period between the second and fifth month and thawed during the sixth and seventh month.
6. Loading: The traffic is comprised of 18-kip axle loads with an assumed standard deviation of the wander of 1 ft. The traffic was not uniformly distributed throughout the test period. The actual number of repetitions was taken from the AASHO Road Test data (3).
7. Material variability: It was assumed that

Figure 1. Results of analysis of AASHO Road Test section.

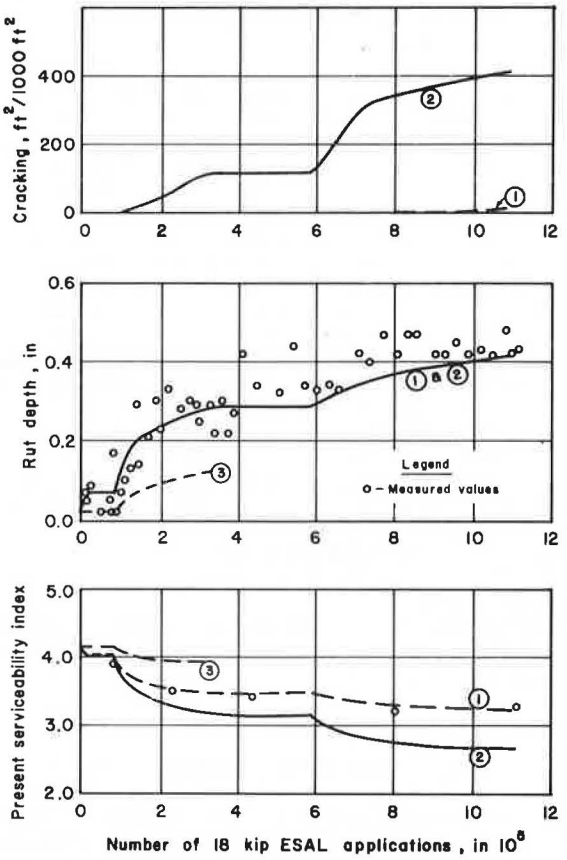

Figure 2. Results of sensitivity analysis and variation of means.

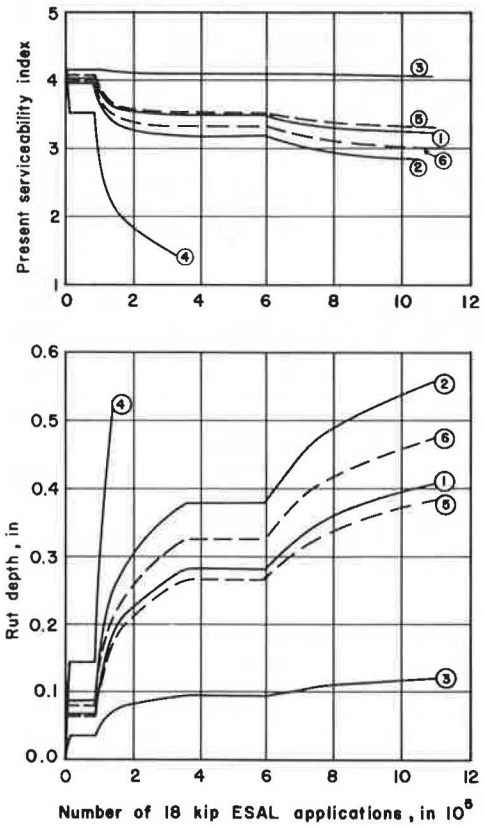

Figure 3. Results of sensitivity analysis and varying the coefficients of variation.

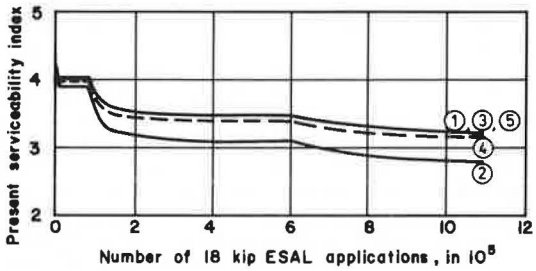

Table 1. Variable values that correspond to different curves in Figure 2.

Curve No.	α_1	μ_1	α_4	E_4 (psi)
1	0.56	0.30	0.80	6000
2	0.56	0.50	0.80	6000
3	0.70	0.30	0.80	6000
4	0.45	0.30	0.80	6000
5	0.56	0.30	0.95	6000
6	0.56	0.30	0.80	5000

the coefficient of variation of layer thicknesses, moduli of elasticity, and plastic parameters is 0.10. The regression coefficients were assumed nil for those input variables except for the subbase, base, and subgrade moduli that were fully dependent. As for the fatigue law, the coefficients of variation of the K_1 and K_2 variables were 0.3 and their regression coefficient was 0.857 (4,12).

Results

The results of the analysis are presented in Figures 1, 2, and 3, which describe the pavement performance (serviceability index, rut depth, and cracking area versus number of repetitions).

Figure 1 shows that about a 50 percent cracked area was obtained at the end of the test period when the fatigue law derived by Finn and others (2) is implemented (curve 2). Because the section did not crack, it is concluded that the fatigue law derived by Finn and others (2) in conjunction with a nonlinear computation scheme cannot be implemented in the program. The K_1 parameter was therefore corrected to correspond to minor cracking (curve 1). Figure 1 also shows the predicted performance of the pavement for the above two cases. Because the only difference is in the cracked area, the serviceability index computed by using the fatigue law (2) is lower than the index computed by using the corrected fatigue law. Measured rut depths and performance are reproduced in Figure 1 to evaluate the reliability of the prediction for the chosen input variables. It is seen that the predicted and measured shape and values are in very good agreement.

Sensitivity Analysis

The fatigue subsystem is not included in this analysis, since the section did not fail at the end of the test period. This will simplify the analysis of the rut depth and of its variance (and through these variables, the serviceability index). Moreover, we feel that the fatigue subsystem should be complemented to take into account the rest period, crack propagation, crack retardation, etc. Until then, it appears that the cracking is yet unpredictable, leading to the introduction of correction factors such as that proposed by Brown (13).

Results of the sensitivity analysis of the rut depth are presented in Figures 1 and 2, which illustrate the effect of varying only the variables that are of significance, such as α_1, μ_1, α_4, and E_4 (see Table 1). Figure 2 shows that the ranking of these variables by their effect on rut depth is similar to that reported by Rauhut and others (4,5) in their sensitivity analysis that used VESYS II. Figure 2 also shows the effect of varying these variables on the serviceability index. It is seen that the main effect is due to α_1 through its influence on the rut depth. Figure 1 illustrates the effect of the plastic properties of the base, subbase, and subgrade from the above values to perfectly elastic properties that are assumed to correspond to the overlay case (curve 3 in Figure 1). It is seen that the rut depth is reduced to less than half its value and the serviceability index remains high. This behavior corresponds with experience with overlay or step construction (Uzan report, Permanent Deformation in Asphalt Overlays on Flexible Pavements).

The rut depth variance is sensitive not only to the mean values of the input variables but also to their variance. According to Rauhut and others (4,5), the slope variance, which was replaced by the rut depth variance in Equation 3, is affected by almost the same variable variations as was the rut depth. However, this was expected to happen, since the slope variance was expressed as a function of the rut depth (Equation 2). Because this does not correspond to the current case, the sensitivity analysis is conducted only for the effect of variation of the coefficient of variation of α_1, μ_1, E_1, and E_4. Figure 3 shows the effect of varying the coefficient of variation of only one variable. Curve 1 represents the performance of the section for a 0.10 coefficient of variation; other curves correspond to an α_1's coefficient of variation of 0.2 for curve 2, a μ_1's coefficient of 0.2 for curve 3 (superimposed with curve 1), and an E_4's coefficient of 0.27 for curve 5 (also superimposed with curve 1). It is seen that the main effect is again due to varying the coefficient of variation of α_1.

From the results shown in Figures 2 and 3, it can be concluded that the pavement performance is highly affected by the α_1 plastic property.

DISCUSSION OF RESULTS

The results of the analysis presented refer to a particular section of the AASHO Road Test. The loss in serviceability in this section was mainly due to rutting and slope variance. It is seen that the fatigue law derived by Finn and others (2) from AASHO Road Test data and the PSAD program are not applicable in the present program. (This fatigue law seems appropriate only in the framework of the PDMAP program.) Because no other fatigue law is available and no cracking developed in the section, the fatigue law was therefore adjusted to correspond to minor cracking. However, note that a basic approach for fatigue analysis (based on fracture mechanics) is warranted to release from correction factors of the order of 13-18 (2) or 100 (13).

The computed rut depth versus number of repetitions is very similar to the measured one. Note that the rut depth is very sensitive to the plastic material properties of all layers, especially the upper asphaltic one. Similar results could be obtained with a different set of plastic properties. Because these properties are of primordial importance in the rut depth evaluation, their values and dependence on material and stressing variables should be investigated further. In addition, the rut depth variance was found to be primarily affected by the alpha of the upper asphaltic layer and its variation. Therefore, since there is an indication of the stress and temperature dependence of this parameter, it should be investigated carefully at stressing conditions similar to field conditions. The model for rut depth prediction is in essence similar to that developed by Uzan and others (Rut Depth Prediction Using Quasi-Elastic Approach) extended to simple statistically based models, and verified by using test sections from AASHO Road Test and Alberta and Ontario Brampton Test Road (Uzan reports, Prediction of Rut Depth Performance in Flexible Pavement Using Statistically Based Models; Permanent Deformation in Asphalt Overlays on Flexible Pavements). The results were very satisfactory. The current program is therefore expected to bring similar good results. However, information concerning material properties and performance as required by the program was not available to us.

The pavement performance predicted by the program is in very good correlation with the measured one. Note that the curvature of the serviceability index versus the number of repetitions is rather upward (sag curvature). This results from the special combination of the traffic distribution and environmental conditions.

In conclusion, the program package seems reliable and could be widely and easily implemented and programmed on a microcomputer.

REFERENCES

1. W.J. Kenis. Predictive Design Procedures, VESYS Users Manual--A Design Method for Flexible Pavements Using the VESYS Structural Subsystem. Proc., Fourth International Conference on Structural Design of Pavements, Univ. of Michigan, Ann Arbor, Vol. 1, 1977, pp. 101-130.
2. F. Finn, C. Saraf, R. Kulkarni, K. Nair, W. Smith, and A. Abdullah. The Use of Distress Prediction Subsystems for the Design of Pavement Structures. Proc., Fourth International Conference on Structural Design of Asphalt Pavements, Univ. of Michigan, Ann Arbor, Vol. 1, 1977, pp. 3-38.
3. The AASHO Road Test: Report 5, Pavement Research. HRB, Special Rept. 61E, 1962, 352 pp.
4. J.B. Rauhut, J.C. O'Quin, and W.R. Hudson. Sensitivity Analysis of FHWA Structural Model VESYS II, Vol. 1: Preparatory and Related Studies. FHWA, Rept. FHWA-RD-76-23, 1976, 261 pp.
5. J.B. Rauhut, J.C. O'Quin, and W.R. Hudson. Sensitivity Analysis of FHWA Structural Model VESYS II, Vol. 2: Sensitivity Analysis. FHWA, Rept. FHWA-RD-76-24, 1976, 132 pp.
6. P. Ullidtz. Computer Simulation of Pavement Performance. The Institute of Roads, Transport, and Town Planning, The Technical Univ. of Denmark, Lyngby, Rept. 18, 1978.
7. A.I.M. Claessen, J.M. Edwards, P. Sommer, and P. Uge. Asphalt Pavement Design--The Shell Method. Proc., Fourth International Conference on Structural Design of Asphalt Pavements, Univ. of Michigan, Ann Arbor, Vol. 1, 1977, pp. 39-74.
8. W.L. Hufferd and J.S. Lai. Analysis of N-Layered Viscoelastic Pavement Systems. FHWA, Rept. FHWA-RD-78-22, 1978, 220 pp.
9. C.L. Monismith, N. Ogawa, and C.R. Freeme. Permanent Deformation Characteristics of Subgrade Soils Due to Repeated Loading. TRB, Transportation Research Record 537, 1975, pp. 1-17.
10. E.V. Edris, Jr., and R.L. Lytton. Climatic Ma-

terials Characterization of Fine-Grained Soils. TRB, Transportation Research Record 642, 1977, pp. 39-44.
11. W.R. Barker, W.N. Brabston, and Y.T. Chou. A General System for the Structural Design of Flexible Pavements. Proc., Fourth International Conference on Structural Design of Asphalt Pavements, Univ. of Michigan, Ann Arbor, Vol. 1, 1977, pp. 209-248.
12. J.S. Lai. VESYS G--A Computer Program for Analysis of N-Layered Flexible Pavements. FHWA, Rept. FHWA-RD-77-117, 1977, 57 pp.
13. S.F. Brown. Material Characteristics for Analytical Pavement Design. In Developments in Highway Engineering (P.S. Pell, ed.), Applied Science Publishers, Ltd., London, 1978, Chapter 2, pp. 41-92.

Publication of this paper sponsored by Committee on Flexible Pavement Design.

Structural Analysis of AASHO Road Test Flexible Pavements for Performance Evaluation

DAVID R. LUHR AND B. FRANK McCULLOUGH

The structural analysis of American Association of State Highway Officials (AASHO) Road Test flexible pavements was performed for the specific purpose of developing a pavement performance model that would be implemented in a pavement management system used by the U.S. Forest Service. For this reason, a precise and highly sophisticated structural evaluation was not made. However, it was determined that the nonlinear elastic properties of unbound pavement materials and seasonal material conditions should be characterized. The use of a thin layer BISAR elastic-layer analysis helped to overcome difficulties in the structural analysis associated with the PSAD2A elastic-layer program. An equivalent layer procedure was found to give results similar to the thin layer BISAR analysis. A modified BISAR program was developed that incorporated the equivalent layer procedure and was used in the structural analysis of the AASHO Road Test pavements. Results of the analysis showed that predicted pavement deflections from the structural analysis compared very well with spring and fall deflection measurements taken at the AASHO Road Test. An evaluation of the modulus ratios of adjacent unbound pavement layers led to the conclusion that the modulus ratios are not fixed within a narrow range of values but can vary significantly depending on the state of stress in the pavement layers.

The structural analysis of flexible pavements can involve a wide range of methodologies, which range from sophisticated finite-element modeling that considers nonlinear elastic and viscoelastic properties of pavement materials to relatively uncomplicated elastic-layer techniques that have various simplifying assumptions regarding material properties, loading conditions, etc. Therefore, it is important to choose the appropriate level of sophistication for the particular situation being analyzed.

This paper describes a structural analysis of American Association of State Highway Officials (AASHO) Road Test flexible pavement sections, which was conducted as part of a cooperative research effort by the U.S. Forest Service and the University of Texas at Austin. The objective of the analysis was to calculate pavement response parameters that could be compared with AASHO Road Test pavement performance data. From this information, a pavement performance model would be developed and used to revise and improve an existing pavement management system (1).

The structural analysis in this study was not a precise and highly sophisticated evaluation of the pavement structures. Because of the number of AASHO Road Test sections to be studied, practical restrictions were necessary in the consideration of computer execution time. In addition, since the pavement performance model being developed would be included in a pavement management system, it could be assumed that a similar structural analysis would have to be employed in that system. For these reasons, a relatively simple analysis was favored. However, because of important economic comparisons made among candidate pavement materials in the pavement management system, it was felt necessary to consider the stress-sensitive properties of unbound pavement materials. Because pavement performance varies considerably, depending on climatic and seasonal conditions, it was also determined that the characterization of seasonal material properties was important in the structural analysis. These factors tended to indicate that a more sophisticated evaluation was necessary.

The following sections of this paper discuss the evaluation of different methodologies for performing the analysis. Results from this evaluation are discussed, including results from the structural analysis. A comparison is made between measured and predicted pavement deflections, and the modulus ratios for adjacent unbound pavement layers are studied.

PROCEDURE FOR NONLINEAR ELASTIC ANALYSIS

In the structural analysis of AASHO Road Test pavement sections, the asphalt layer was assumed to have linear elastic properties, whereas the granular base and subbase materials and the fine-grained subgrade were assumed to have nonlinear stress-dependent characteristics. The stress-sensitive nature of the unbound pavement materials was characterized by the following relations. For fine-grained materials,

$$M_R = A\,\sigma_d^B \quad (1)$$

where

M_R = resilient modulus of fine-grained material,
σ_d = principal stress differences ($\sigma_1 - \sigma_3$) or deviator stress (psi), and
A, B = experimentally determined coefficients that define the behavior of the fine-grained material.

For granular materials,

$$M_R = k_1 \theta^{k_2} \quad (2)$$

where

M_R = resilient modulus of granular material,
θ = first stress invariant ($\sigma_1 + \sigma_2 + \sigma_3$) or bulk stress (psi), and
k_1, k_2 = experimentally determined coefficients that define the behavior of the granular material.

Considering the relations described in Equations 1 and 2, where the modulus of an unbound pavement material varies according to the state of stress in the material, the moduli of unbound materials should vary both horizontally and vertically in the pavement structure. This type of two-dimensional variation in material moduli can be satisfactorily represented by using finite-element techniques that model nonlinear elastic material behavior (2). However, as mentioned earlier, the objective of this study was not the precise structural analysis of a layered pavement but rather to calculate pavement response parameters that could be related to pavement performance. The finite-element methodology does not lend itself to this type of objective because (a) it uses a large amount of computer execution time, which would be restrictive in the analysis of all the AASHO Road Test pavement sections; (b) the large amount of variability in pavement performance data may make the structural precision of finite-element methods superfluous in comparison; and (c) finite-element methods are too complex and consume too much computer execution time to be used routinely as part of a pavement management system.

Evaluation of Elastic-Layer Programs

An alternative way to analyze pavement structures by using nonlinear elastic material characterization is through an elastic-layer procedure. In this case, the pavement structure is divided into layers with homogeneous and isotropic material properties. This limits the modulus variation to only the vertical direction, where the modulus may change from one layer to another. A single modulus for each layer is assumed, and the stresses in each layer are determined in an interactive procedure until the relations in Equations 1 and 2 are satisfied. A computer program developed at the University of California at Berkeley [PSAD2A (3)] uses this type of procedure and was examined as a possible method to carry out the analysis of AASHO Road Test pavement sections. The PSAD2A program calculates stresses at seven horizontal locations underneath the loaded area at three depths in each layer. Figure 1 illustrates the 21 locations where stresses are calculated for each layer, with 7 locations for the subgrade. The modulus value for each location where stresses are calculated is computed from the relations in Equations 1 and 2, and the 21 modulus values are averaged to determine the stress-dependent modulus for each layer. The initial assumed modulus is compared with the calculated average modulus, and the procedure is iterated until the two moduli converge.

Two difficulties were apparent when the PSAD2A program was examined. The first involved the development of tensile stresses in the bottom of pavement layers. This is common in elastic-layer analysis, since the layer is treated as a homogeneous isotropic material. Under load, compression develops in the top of the layer and tension at the bottom. However, unbound pavement materials, particularly granular materials, have little or no mobilized tensile strength. Realizing this fact, the PSAD2A program assumes a modulus of zero when the first stress invariant (θ) becomes negative for a certain location. Often the bottom of a layer will be calculated to be in tension, which results in the seven points in the lower portion of the layer that have a modulus of zero. When the average modulus of the 21 points is calculated, the effect of the 7 moduli with a value of zero is to greatly reduce the average modulus value. This result helps to illustrate the second difficulty: The procedure for averaging the 21 modulus values has the effect of converging the solution for a condition that may not represent the behavior of the layer. The stresses are calculated from one assumed modulus for each layer, yet different modulus values are calculated for 21 points, indicating the intention to consider the two-dimensional variation in moduli for each layer, which cannot be accomplished by using elastic-layer analysis.

In an effort to alleviate the two difficulties stated above, a somewhat different approach than that used in PSAD2A was taken by using the elastic-layer methodology. An examination was made of a typical pavement structure with 7.6-cm (3-in) asphalt, 7.6-cm base, and 10-cm (4-in) subbase. First, no attempt was made to calculate the moduli at different horizontal locations in the unbound layers. Instead, only positions directly beneath the wheel loads were used to calculate stresses for the relations in Equations 1 and 2. This restriction is simply one of the limitations of using elastic-layer theory. Second, the base and subbase layers were divided into thin sublayers of 2.5-cm (1-in) thickness (Figure 2). With this small thickness, the modulus calculated from the stress condition at midlayer is probably an accurate representation of the entire sublayer. This allows the mod-

Figure 1. Locations for stress-dependent modulus calculations in program PSAD2A.

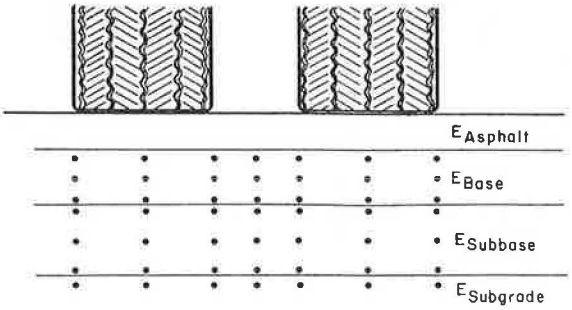

Figure 2. Locations for stress-dependent modulus calculations in thin layer BISAR analysis.

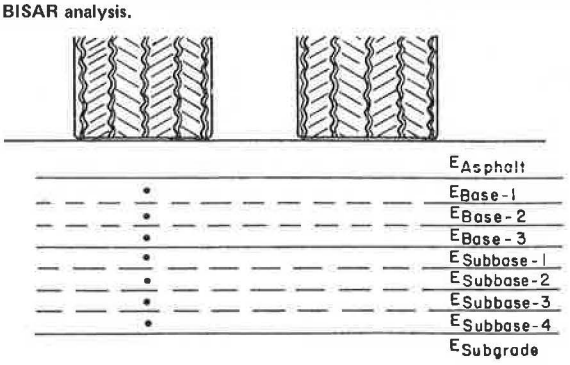

ulus to vary with depth, since it can change from sublayer to sublayer. Because the layers are thin, the problem of calculating tensile stresses in the bottom of the layers is reduced.

The structural evaluation of the pavement structure in Figure 2 was accomplished with the elastic-layer program BISAR, which was developed by Shell Research (4). The BISAR program was used because it has the capability to analyze more than five layers, and the level of friction at layer interfaces in the pavement structure can be varied. With the small thickness of the base sublayers, it was necessary to assume no friction at the asphalt-base interface. If full friction has been used at the asphalt-base interface, the thin sublayer at the top of the base would be calculated to be in tension because of the influence of the tension at the bottom of the asphalt layer. In reality, the friction at the asphalt-base interface lies somewhere between full friction and no friction. However, the assumption of no friction for analytical purposes is reasonable. Full friction was assumed for all other interfaces.

By using a fixed modulus for the asphalt and the relations in Equations 1 and 2 for the base, subbase, and subgrade, the assumed moduli for the seven locations in Figure 2 were iterated until each converged with the calculated stress-dependent modulus. If tensile stresses in any layer were greater than an arbitrary limit of 35 kPa (5 psi), the results were considered unacceptable and new moduli were assumed. Figure 3 contains the plot of moduli versus depth for the pavement structure in Figure 2 and assumes material properties for the fall season (seasonal material characterization is discussed later) and a 100-kN (22.4-kip) single-axle load. The moduli computed from the PSAD2A program are compared in Figure 3 with those from the thin layer BISAR analysis. The significantly smaller moduli calculated from PSAD2A for the base and subbase layers are mainly due to the effect of averaging in the zero modulus values from the lower positions in each layer.

It was concluded that the thin layer BISAR analysis was an appropriate method of using elastic-layer theory to model the stress sensitivity of materials in a pavement structure. Because the moduli were calculated only along the axis of load symmetry and restrictions were placed on tensile stresses, the difficulties associated with the PSAD2A program had been alleviated. However, practical limitations of computer execution time would make a thin layer BISAR analysis for all the AASHO Road Test pavement sections unfeasible. In addition, it would not be practical to incorporate this detailed a structural analysis in a pavement management system.

Figure 3. Moduli versus depth below asphalt for example pavement structure with 100-kN (22.4-kip) single-axle load.

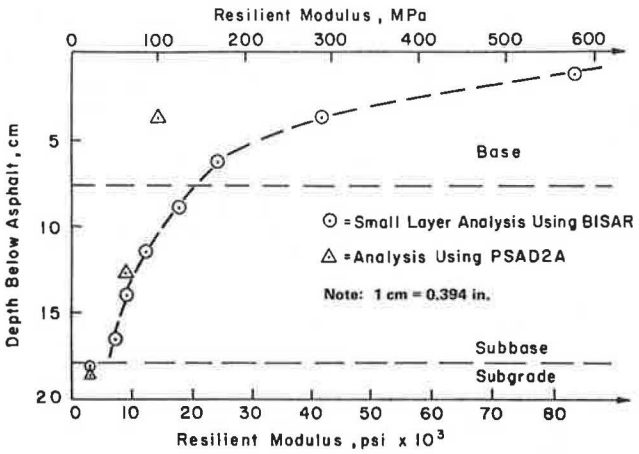

Development of an Equivalent Procedure

To develop a simpler structural analysis that still contained the advantages of the thin layer BISAR procedure, an approach that used an equivalent layer modulus was examined. This approach uses a single stress-dependent modulus for each layer instead of dividing the base and subbase into sublayers. This single modulus is equivalent to the sublayer moduli, in that the calculated stress-strain response in the asphalt and subgrade layers is the same as the response calculated with the thin sublayer analysis. For the equivalent layer analysis, it was found that if the single stress-dependent modulus for each layer is converged by using the stress condition at middepth in the layer, the calculated stress-strain response in the asphalt and subgrade will be nearly the same as for the thin layer analysis. This concept is shown in Figure 4, where the same pavement structure as in Figure 3 is examined. The moduli calculated from the small layer BISAR analysis and the equivalent layer analysis are shown, as are results from the structural analysis that include (a) surface vertical deflection, (b) asphalt tensile strain, (c) subgrade compressive strain, and (d) subgrade shear stress.

The four parameters above were selected because combined they represent most of the structural response variables used in current pavement design procedures and they cover a wide range of pavement response. If the equivalent layer analysis could produce similar results for all of these parameters, it could replace the thin layer analysis. This comparison between the thin layer analysis and the equivalent layer analysis was made for a variety of pavement structures and axle loads. The results are given in Table 1 and indicate very good agreement in nearly all cases. Based on this detailed examination, it was concluded that the equivalent layer procedure should be used to analyze the AASHO Road Test pavement sections and that it would also be appropriate for a pavement management system. A modified version of the BISAR program was developed that converges the single stress-dependent modulus for each layer in an iterative procedure by using the stress condition at middepth in the layer.

Figure 4. Example of equivalent layer analysis for pavement structure and load in Figure 3.

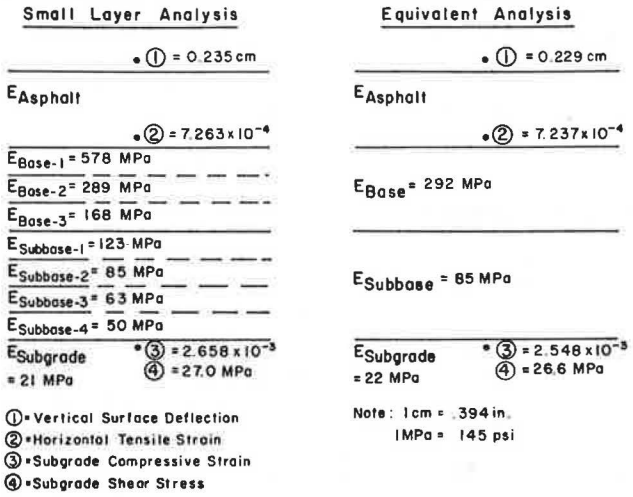

Table 1. Comparison of thin layer and equivalent layer analysis.

Pavement Thickness (cm)				Ratio[a] for			
Asphalt Concrete	Base	Subbase	Single-Axle Load (kN)	Surface Deflection	Asphalt Strain	Subgrade Strain	Subgrade Shear Stress
5	8	0	9	0.92	0.97	1.02	0.91
5	8	0	53	0.97	0.97	0.91	0.91
8	8	10	9	0.99	1.00	1.00	0.95
8	8	10	53	0.99	1.00	0.98	0.98
8	8	10	80	0.97	0.99	0.99	0.95
8	8	10	100	0.98	1.00	0.99	0.96
13	15	20	80	0.99	1.01	1.00	0.97
13	15	20	100	0.98	1.01	1.00	0.97
13	15	20	133	0.97	1.00	1.00	0.96

Note: 1 cm = 0.394 in, 1 kN = 0.225 klp.
[a]Ratio = value of equivalent analysis ÷ value of thin layer analysis.

Table 2. Elastic moduli of AASHO Road Test materials.

	Material							
	Asphalt Concrete		Base		Subbase		Subgrade	
Seasonal Moduli	kPa	psi	kPa	psi	kPa	psi	kPa	psi
March-April (spring)	4.9×10^6	0.71×10^6	$6\,900\,\theta^{0.6}$	$3\,200\,\theta^{0.6}$	$10\,000\,\theta^{0.6}$	$4\,600\,\theta^{0.6}$	$427\,000\,\sigma_d^{-1.06}$	$8\,000\,\sigma_d^{-1.06}$
May-August (summer)	1.6×10^6	0.23×10^6	$7\,800\,\theta^{0.6}$	$3\,600\,\theta^{0.6}$	$10\,800\,\theta^{0.6}$	$5\,000\,\theta^{0.6}$	$960\,000\,\sigma_d^{-1.06}$	$18\,000\,\sigma_d^{-1.06}$
September-November (fall)	3.1×10^6	0.45×10^6	$8\,700\,\theta^{0.6}$	$4\,000\,\theta^{0.6}$	$11\,700\,\theta^{0.6}$	$5\,400\,\theta^{0.6}$	$1\,440\,000\,\sigma_d^{-1.06}$	$27\,000\,\sigma_d^{-1.06}$
December-February (winter)	11.7×10^6	1.7×10^6	345 000[a]	50 000[a]	345 000[a]	50 000[a]	345 000[a]	50 000[a]

[a]Assigned values assuming frozen conditions.

ANALYSIS OF AASHO ROAD TEST SECTIONS

Seasonal Material Characterization

Because pavement performance varies according to climatic and seasonal conditions, it was appropriate to structurally analyze the AASHO Road Test pavement sections on a seasonal basis. With these results, an attempt could be made to evaluate seasonal pavement performance. To accomplish this, the material properties for the asphalt surfacing, base, subbase, and subgrade were characterized for four different seasonal periods of the year. This consisted of modulus values for the asphalt, values of A and B for the fine-grained subgrade (Equation 1), and values of k_1 and k_2 for the granular base and subbase (Equation 2). The seasonal values used in this study were developed for AASHO Road Test materials by Finn and others (5) and are listed in Table 2 (5). These seasonal material values were primarily developed from laboratory testing and are related to triaxial-type loading conditions.

Poisson's ratio was assumed constant for each material and was assigned the following values: asphalt, 0.30; granular base, 0.40; granular subbase, 0.40; and fine-grained subgrade, 0.45.

Structural Analysis

The structural analysis of the flexible pavement sections was completed by analyzing for four seasons all of the 284 combinations of flexible pavement structures and axle loads in the main AASHO Road Test experiment (6). The modified BISAR program was used to conduct the analysis by using the material properties listed in Table 2. Four stress-strain parameters were calculated for each analysis. These included tensile strain at the bottom of the asphalt layer, subgrade shear strain, subgrade compressive strain, and subgrade strain energy. An earlier evaluation of AASHO Road Test pavement sections indicated that a simple linear elastic computation of subgrade compressive strain correlated fairly well with pavement performance (7). For this reason, three of the four parameters calculated are related to subgrade response. The asphalt strain was included because it is frequently used as a predictor of asphalt cracking. Pavement deflection was specifically not included because of difficulties in predicting pavement deflection when the depth to rigid foundation (depth of roadbed) is not known (8).

All of the four parameters were calculated for positions directly beneath the wheel load in their respective layers. It is realized that sometimes maximum stresses or strains do not occur at these locations but, rather, at points between the two loads of a dual tire configuration. There were three primary reasons for calculating stresses and strains for only the locations directly beneath the load:

1. The stress-dependent modulus calculation for each layer is for the stress condition under the load. In reality, the layer moduli are different for locations between the loads, and any calculations of stresses or strains between the loads may not be accurate.
2. The purpose of the structural analysis was not the precise evaluation of stresses and strains within the pavement structure but, rather, the comparison of mechanistic parameters with pavement performance. Because conditions between the loads are probably highly correlated with conditions at the same depth under the load, the additional consideration of parameters between the loads may not make any improvement in the performance prediction.
3. The calculation of stresses and strains at other locations in the pavement structure would have greatly increased the computer time necessary for the structural analysis.

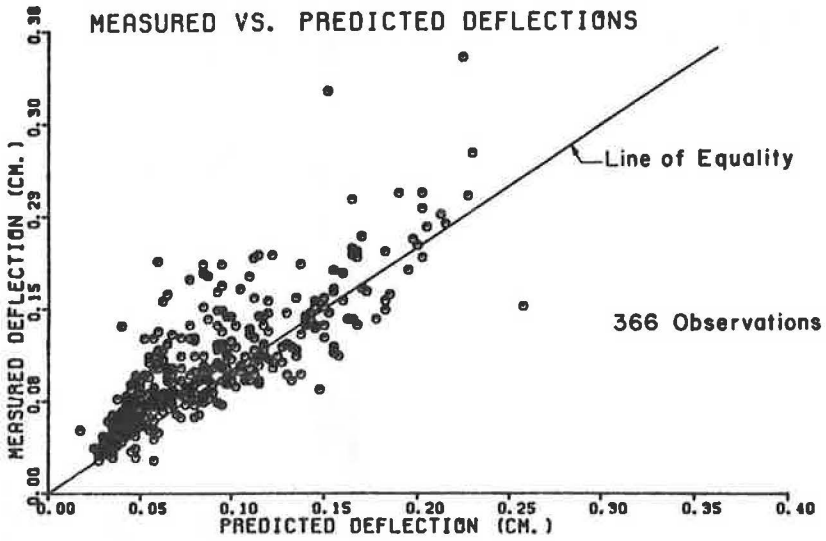

Figure 5. Measured versus predicted deflections for fall and spring seasons.

RESULTS OF ANALYSIS

The mechanistic parameters calculated from the structural analysis of AASHO Road Test pavement sections, along with other data related to axle loads and pavement performance, were used to develop a performance prediction model that was implemented in a pavement management system. The development of this performance model and associated improvements to the pavement management system is described in a separate paper (1). The results of the structural analysis with regard to deflection measurements and ratios of layer moduli are discussed in this section.

Comparison of Results with Deflection Measurements

To determine with what accuracy the material characterizations in Table 2 and the modified BISAR program represent actual pavement response, surface deflections were calculated for a large number of pavement structures and axle loads that were part of the AASHO Road Test main experiment. These predicted deflections were then compared with Benkelman beam deflection measurements taken during the AASHO Road Test. Because the depth of the roadbed for the AASHO Road Test was known (6), the problem described earlier of predicting deflection measurements without accurate knowledge of the depth of roadbed was removed. A total of 183 pavement sections from loops 2 through 6 were analyzed; they included single-axle loads from 9 to 133 kN (2-30 kips) (6). Deflection measurements were made during fall and spring seasons for each section, thereby representing the times of the year when the pavement was in its best and worst condition, respectively.

The predicted deflections are compared with the deflection measurements in Figure 5. This figure shows the accuracy of the predictions for 366 points for one spring and one fall deflection for each pavement section. Figure 5 indicates that the measured deflections are generally slightly higher than the predicted deflections. However, this trend is not serious, and the figure indicates very good correlation, considering the wide range of pavement structures, loads, and seasonal conditions being examined. The root mean square error of the predicted deflection measurements is 0.028 cm (0.011 in), which is quite reasonable when compared with the root mean square error of 0.015 cm (0.006 in) for 30 replicate deflection measurements. These replicate data give an indication of the repeatability of the deflection measurements made at the AASHO Road Test.

Evaluation of Modulus Ratios

The ratio of elastic moduli for two adjacent layers in the pavement structure has long been considered an important factor in pavement response. Therefore, it was important to examine the layer modulus ratios that were calculated by using the modified BISAR program. The current Shell pavement design procedure determines the moduli for granular base materials by using a ratio of base to subgrade modulus between 2 and 4 (9). This procedure was developed from estimates of the dynamic moduli of pavement materials by using wave velocity measurements generated from the road vibration machine. Calculated moduli from wave velocity measurements of approximately 50 pavement structures were found to have a modulus ratio that ranged from 1 to 5 for adjacent unbound pavement layers (10). Recommendations were made to use a modulus ratio of roughly 2 for structural evaluation of unbound granular layers.

The modulus ratio is generally limited by the development of tensile strains in the bottom of unbound layers. If the ratio becomes too large, the tensile strains will have the effect of decompacting the upper layer, thereby reducing the modulus of the upper layer and the modulus ratio. In this study, calculations of modulus ratios for unbound layers were made from the results of the AASHO Road Test structural analysis. The results for the three-layer pavement structures showed general agreement with the range of modulus ratios, from 1 to 5, contained in the Shell data mentioned above. The modulus ratios of base to subbase were generally lower than that of subbase to subgrade, as is shown in Figures 6 and 7. However, some very high modulus ratios were found for the two-layer pavement structures, as illustrated in Figure 8. Further examination showed that the high ratios occurred when high stresses in the pavement structure caused the base modulus to be high and the subgrade modulus to be low. This condition, therefore, occurred with the heavier loads and thinner pavement structures.

An example of this condition is shown in Figure 9, where the moduli from the thin layer BISAR analysis are plotted for a 5-cm (2-in) asphalt and 7.6-cm (3-in) base pavement structure for single-axle loads of 9 and 53 kN (2 and 12 kips). Because of the higher stresses caused by the heavier load, the

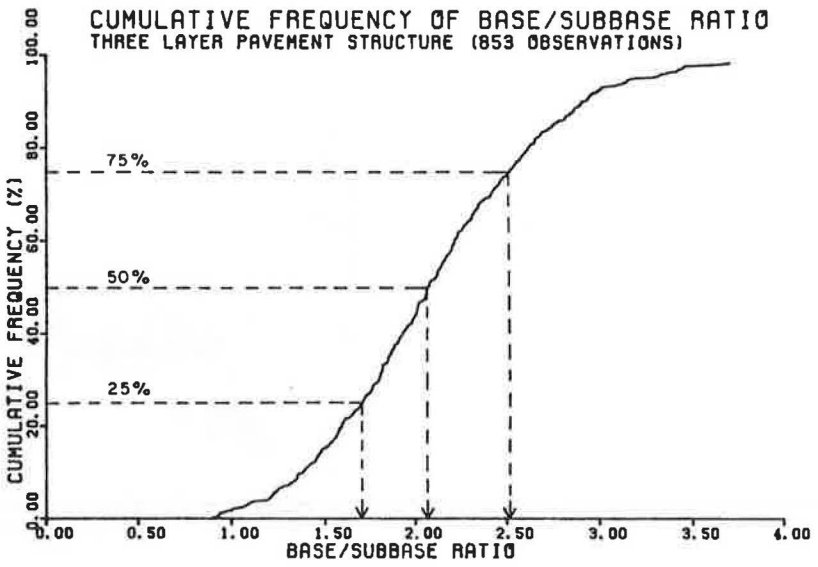

Figure 6. Modulus ratios for base and subbase layers in three-layer pavement structure.

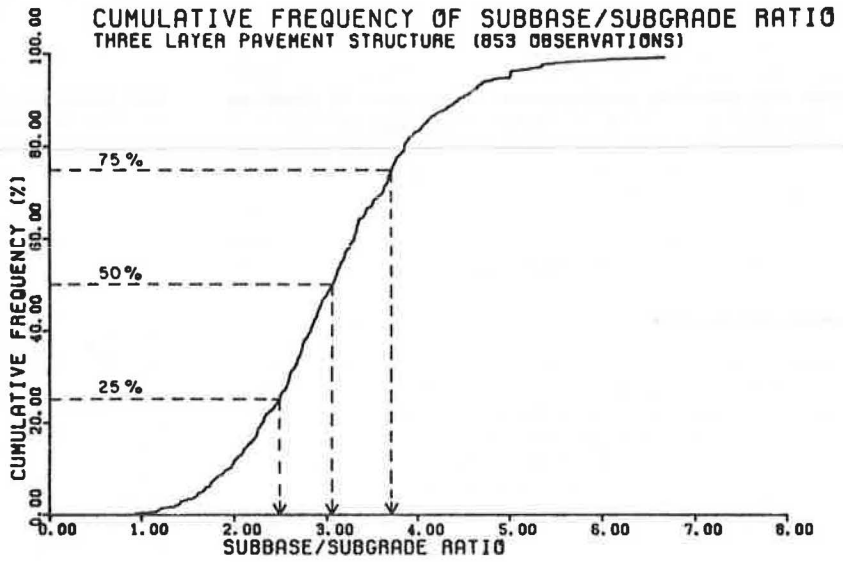

Figure 7. Modulus ratios for subbase and subgrade layers in three-layer pavement structure.

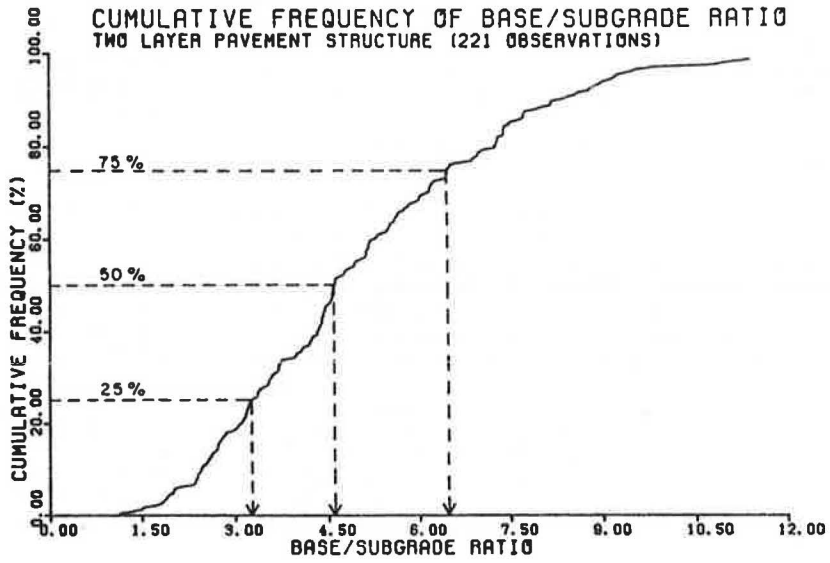

Figure 8. Modulus ratios for base and subgrade layers in two-layer pavement structure.

Figure 9. Moduli versus depth for 9- and 53-kN single-axle loads.

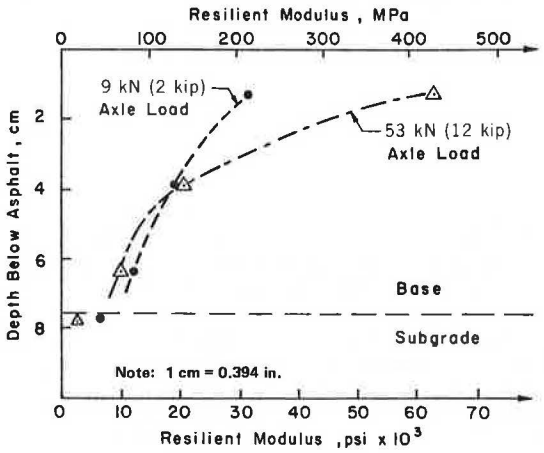

modulus of the base was higher and the modulus of the subgrade was lower than for the lighter load. This caused a higher modulus ratio for the heavy load.

It was concluded that the modulus ratios are not fixed within a certain range of values but can vary significantly, depending on the state of stress in the pavement layers. This conclusion was reinforced by the fact that the structural analysis, which was used to calculate the modulus ratios, had close agreement with actual deflection measurements.

CONCLUSIONS

This paper has presented the findings from a nonlinear elastic analysis of AASHO Road Test flexible pavement sections. The results of this analysis were not intended as a precise evaluation of pavement structures and were used in the development of a performance prediction model. Based on the findings from this study, the following conclusions are made:

1. The problems encountered when using the PSAD2A program to analyze pavement structures were solved by using a thin layer BISAR analysis;
2. An equivalent layer procedure that uses a modified BISAR program produced results very similar to the thin layer BISAR analysis;
3. The modified BISAR program and the seasonal material characterizations produced predicted surface deflections that were in good agreement with deflection measurements taken at the AASHO Road Test; and
4. Modulus ratios between adjacent unbound pavement layers are not fixed within a certain range of values but can vary significantly, depending on the state of stress in the pavement layers.

ACKNOWLEDGMENT

The research and development work discussed in this paper was conducted under a cooperative agreement between the University of Texas at Austin and the Forest Service, U.S. Department of Agriculture. The purpose of the project is to review and improve the Flexible Pavement Design chapter of the Forest Service Transportation Engineering Handbook.

REFERENCES

1. B.F. McCullough, D.R. Luhr, and A. Pelzner. An Improved Pavement Management System for Low-Volume Roads. TRB, Transportation Research Record 875, 1982, pp. 14-21.
2. L. Raad and J.L. Figueroa. Load Response of Transportation Support Systems. Transportation Engineering Journal, ASCE, Vol. 106, No. TE1, Proc. Paper 15146, Jan. 1980, pp. 111-128.
3. Asphalt Behavior in Repeated Flexure. Univ. of California, Berkeley, Rept. TE 70-5, Dec. 1970.
4. D.L. DeJonk, M.G.F. Pentz, and A.R. Korswagen. Computer Program BISAR, Layered Systems Under Normal and Tangential Surface Loads. Koninklijke /Shell-Laboratorium, Amsterdam, External Rept. ASMR-0006.73, 1973.
5. F. Finn, C. Saraf, R. Kulkarni, K. Nair, W. Smith, and A. Abdullah. The Use of Distress Prediction Subsystems for the Design of Pavement Structures. Proc., Fourth International Conference on Structural Design of Asphalt Pavements, Univ. of Michigan, Ann Arbor, Aug. 1977.
6. The AASHO Road Test: Report 5, Pavement Research. HRB, Special Rept. 61E, 1962.
7. D.R. Luhr and B.F. McCullough. Development of a Rationally Based AASHO Road Test Algorithm. TRB, Transportation Research Record 766, 1980, pp. 10-17.
8. B.F. McCullough and K.J. Boedecker. Use of Linear-Elastic-Layered Theory for the Design of CRCP Overlays. HRB, Highway Research Record 291, 1969, pp. 1-13.
9. A.I.M. Claessen, J.M. Edwards, P. Sommer, and P. Uge. Asphalt Pavement Design--The Shell Method. Proc., Fourth International Conference on Structural Design of Asphalt Pavements, Univ. of Michigan, Ann Arbor, Aug. 1977.
10. W. Heukelom and A.J.G. Klomp. Dynamic Testing as a Means of Controlling Pavements During and After Construction. Proc., First International Conference on Structural Design of Asphalt Pavements, Univ. of Michigan, Ann Arbor, 1962.

Publication of this paper sponsored by Committee on Flexible Pavement Design.

Performance Analysis for Flexible Pavements with Stabilized Base

M. C. WANG

The performance of experimental pavements at the Pennsylvania Transportation Research Facility was evaluated. These pavements contained five different types of base course: bituminous concrete, aggregate bituminous, aggregate cement, aggregate-lime-pozzolan, and crushed stone. Most of the pavements had been subjected to about 2.4 million 18-kip equivalent axle loads (EALs), which is equivalent to approximately 40-years service life. Data analyzed were pavement serviceability index and three distress manifestations--roughness, rutting, and cracking. Some existing pavement performance models were also evaluated by using the performance data. The performance data indicate that the trend of serviceability index loss with increasing EAL follows the power function developed at the American Association of State Highway Officials (AASHO) Road Test. Of the performance models evaluated--AASHO, modified Highway Research Board (HRB), and Painter's models--the AASHO model appears to predict best, although it overpredicts pavement service life. By using a curve-fitting process and regression analysis, equations that relate pavement performance indicators and structural number are formulated. These equations permit prediction of the rate of serviceability loss and pavement life required to reach a certain present serviceability index drop. Also developed are equations that relate distress with structural number and critical pavement response with pavement service life. These equations may be used to predict various distress intensities from structural numbers and also used to predict pavement life from critical response. According to the results of the analysis, the maximum compressive strain at the top of the subgrade appears to be a better factor than the maximum surface deflection for predicting pavement service life.

The American Association of State Highway Officials (AASHO) pavement performance model is widely used for design and evaluation of flexible pavements in the United States (1). This model is a result of statistical analyses of performance data obtained from the carefully designed experimental pavements at the AASHO test road. Because the data base used for the model development is related specifically only to soil and pavement materials, construction procedures, loading conditions, and environmental conditions that existed at the AASHO Road Test, the AASHO Committee on Design called for satellite studies to extend AASHO Road Test results to various environments, traffic, and construction practices (2).

The Pennsylvania Transportation Research Facility, which was constructed by using Pennsylvania's construction practices, is located near the geographical center of the Commonwealth so that the environmental conditions can be considered as representative of the entire state. Therefore, the study at the Research Facility serves the purpose to extend AASHO test results to the conditions present in Pennsylvania, although it is not the sole objective of the research. This paper presents the results of performance analyses for the experimental pavements at the Research Facility. Meanwhile, some existing pavement performance models are compared, and various equations that permit prediction of pavement performance from response variables are presented.

PENNSYLVANIA TRANSPORTATION RESEARCH FACILITY

The Pennsylvania Transportation Research Facility is a one-mile, one-lane test road. The original facility was constructed in summer 1972 and was composed of 17 test pavements of various lengths. Each pavement contained either different base-course materials with the same layer thickness or one type of base-ccurse material with different layer thicknesses, as shown in Figure 1. Of these pavement sections, section 8 was overlaid and sections 10 through 12 were replaced by eight shorter sections in fall 1975. All pavements were 12 ft wide.

The subgrade soil was a silty clay that had classifications that ranged from A-4 to A-7 according to the AASHO classification and CL according to the Unified Soil Classification. The subbase material was a crushed limestone. The base-course materials were bituminous concrete, aggregate cement, aggregate-lime-pozzolan, aggregate bituminous, and crushed stone. In the aggregate-cement base course, three types of aggregate were used--limestone, slag, and gravel. Of the aggregate-lime-pozzolan pavements, sections F and G were excluded from the analysis because they were unable to cure properly due to cold weather during construction. The wearing surface was an ID-2A bituminous concrete.

The traffic on the Research Facility was provided by a conventional truck tractor pulling a semitrailer and one or two full trailers. Scrap steel was used as the lading on the test vehicle. A total of about 2.4 million and 1.3 million applications of 18-kip equivalent axle load (EAL_{18}) had been applied to the pavements constructed in 1972 and 1975, respectively. Complete information on design, construction, and traffic operation is documented elsewhere (3,4).

MATERIAL PROPERTIES

The composition, gradation, and index properties of the constituent material of each pavement are documented in a research report (3). The modulus of elasticity of each layer was determined by using laboratory repeated-load tests on laboratory-compacted test specimens. The specimens had a diameter of 6 in and a height of 10 in. The repeated load had a frequency of 20 cycles/min and a duration of 0.1 s. The modulus values obtained for the spring weather conditions are summarized in Table 1. In the spring season, the average pavement temperature was approximately 60°F, and the average subgrade moisture content was about 23 percent. Also given in Table 1 is Poisson's ratio for each pavement constituent material. These data are obtained from other studies (5-7). Other material properties such as fatigue and viscoelastic properties are available elsewhere (8). They are not used in this paper and therefore are not included in Table 1.

The structural coefficients of the pavement materials are also included in Table 1. Of these values, the structural coefficients of the surface and subbase materials are obtained from the AASHO Interim Guide (1,2). The structural coefficients of the base-course materials are determined by using two different methods of analysis--the AASHO performance analysis and the limiting criteria approach. The first analysis was based on the use of performance data with analysis techniques similar to those used at the AASHO Road Test. The second approach was based on the limiting criteria so that the pavement deflection, maximum tensile strain at the bottom of the stabilized base, and maximum compressive strain at the top of the subgrade can be limited within permissible values. Detailed analyses are available elsewhere (9).

FIELD EVALUATION AND TESTING

Field evaluation of pavement performance was conducted periodically. Rut depth was measured biweekly every 40 ft in both wheel paths by using an A-frame that was attached to a 7-ft-long base channel. Surface cracking was surveyed and mapped biweekly. Surface roughness was measured in both wheel paths by using a MacBeth profilograph. The roughness factors obtained from the profilograph data were converted into present serviceability index (PSI) of the pavement by using the following equations:

$$PSI = 11.33 - 4.06 (\log RF) - 0.01\sqrt{C + P} - 0.21\ \overline{RD}^2 \quad (1)$$

$$RF = 63.267 + 0.686\ R \quad (2)$$

where

RF = Mays meter roughness factor,
C = area of cracking (ft²/1000 ft²),
P = area of patching (ft²/1000 ft²),
$\overline{RD}$ = average rut depth (in), and
R = profilograph readings (in/mile).

These two equations were developed by Hopkins (10) of the Pennsylvania Department of Transportation (PennDOT).

In addition, surface deflections were measured in the wheel paths by using the Benkelman beam and the

Figure 1. Plan view and longitudinal profile of test track.

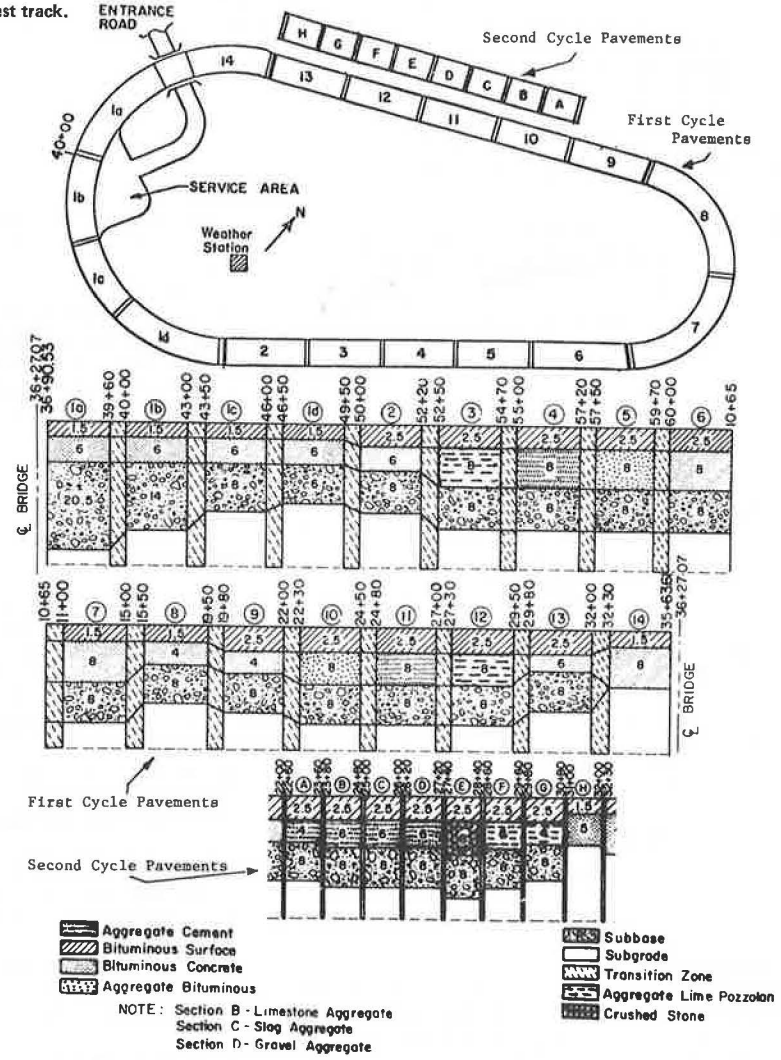

Table 1. Elastic constants and structural coefficients of pavement constituent materials for spring weather conditions.

Layer	Material	Elastic Modulus (psi 000s)	Poisson's Ratio	Structural Coefficient[a]	
				H_1 = 1.5 in	H_1 = 2.5 in
Surface	Bituminous concrete	140	0.40	0.44	0.44
Base	Bituminous concrete	320	0.35	0.35	0.32
	Limestone aggregate cement	3600	0.20	0.35	0.28
	Slag aggregate cement	3200	0.20	0.23	0.19
	Gravel aggregate cement	2500	0.20	0.21	0.17
	Aggregate-lime-pozzolan	2400	0.15	0.24	0.21
	Aggregate bituminous	100	0.35	0.26	0.24
Subbase	Crushed limestone	48	0.40	0.11	0.11
Subgrade	Silty clay	8	0.45	-	-

[a] H_1 = thickness of surface layer.

Table 2. PSI data.

Section No.	Base-Course Material[a]	Layer Thickness (in)			Structural No. (SN)	Initial PSI (PSI_o)	β	EAL (10^6) at ΔPSI =			
		Surface	Base	Subbase				0.5	1.0	1.5	2.0
1b	BC	1.5	6	14	4.30	3.35	1.36	2.04	-	-	-
1c	BC	1.5	6	8	3.64	3.45	1.95	1.74	2.70	-	-
1d	BC	1.5	6	6	3.42	3.50	1.54	1.07	2.02	2.37	2.54
2	BC	2.5	6	8	3.90	3.50	2.01	2.40	-	-	-
3	ALP	2.5	8	8	3.66	3.90	1.85	1.38	1.76	1.99	2.18
4	AC	2.5	8	8	5.98	3.85	0.95	-	-	-	-
5	AB	2.5	8	8	3.90	3.75	1.51	1.55	2.11	2.35	2.46
6	BC	2.5	8	8	4.38	3.30	1.30	2.29	-	-	-
7	BC	1.5	8	8	4.34	3.55	1.25	1.52	2.62	-	-
8	BC	1.5	4	8	2.94	3.30	2.10	0.52	0.79	1.02	1.18
9	BC	2.5	4	8	3.26	3.80	1.68	0.73	1.08	1.35	1.50
A	AC	2.5	4	8	3.18	3.75	2.13	0.63	0.92	1.10	1.21
B	AC	2.5	6	8	3.66	3.75	1.97	0.97	1.33	-	-
C	AC	2.5	6	8	3.12	3.85	2.57	0.84	1.07	1.22	1.32
D	AC	2.5	6	8	3.00	3.70	2.66	0.61	0.80	1.02	1.13
E	CS	2.5	8	8	2.86	3.70	2.25	0.28	0.49	0.64	0.77
H	BC	1.5	5	0	2.41	3.25	3.20	0.26	0.32	0.36	0.38
14	BC	1.5	8	0	3.46	3.20	1.80	0.83	1.26	1.55	-

[a]Base-course materials: BC = bituminous concrete, AC = aggregate cement, ALP = aggregate-lime-pozzolan, AB = aggregate bituminous, and CS = crushed stone.

Figure 2. Serviceability data and comparison of various models.

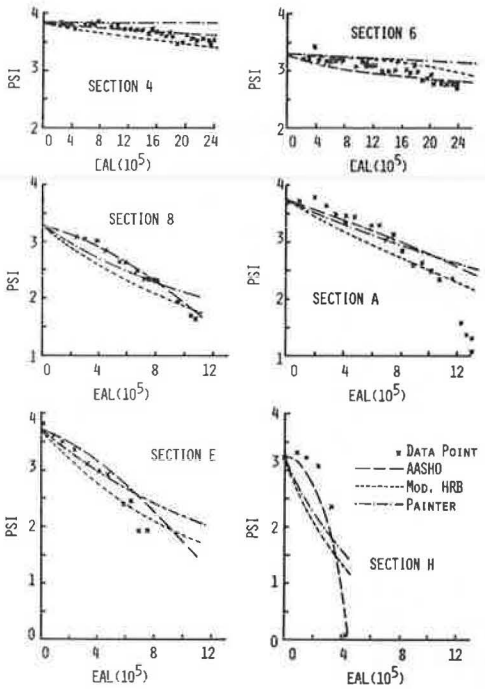

road rater. Pavement temperature profile and subgrade moisture distribution were measured by using thermocouples and moisture cells. Also, two frost-depth indicators were installed at the Research Facility to measure the depth of frost penetration. Weather data such as wind velocity, precipitation, and temperature were collected by using various meteorological gages.

PRESENT SERVICEABILITY INDEX

The complete record of PSI data for the test pavements is documented in a research report (11). Table 2 summarizes the initial PSI values and the number of 18-kip EALs required for various levels of PSI drop for all pavements except sections 1A, F, and G. These three sections are excluded because section 1A was overloaded by the equipment used for bridge construction and both sections F and G were not properly cured, as mentioned earlier. The variation of PSI with EAL for two thick pavements (sections 4 and 6), two thin pavements (sections 8 and A), one pavement with a crushed-stone base (section E), and one thin full-depth bituminous pavement (section H) is shown in Figure 2. Both Figure 2 and Table 2 demonstrate that the initial PSI values are generally low (compared with those at the AASHO test road) and vary considerably between each pavement.

Figure 2 also indicates that the serviceability loss can be described by the same power function of axle-load applications as that used at the AASHO Road Test (12):

$$c_o - P = (c_o - c_1)(W/\rho)^{\beta} \quad (3)$$

where

c_o = initial PSI,
c_1 = terminal serviceability index,
P = PSI at time t,
W = number of EALs at time t,
ρ = pavement life expressed in terms of EAL, and
β = rate of change of serviceability loss.

By fitting the power function (Equation 3) to the observed PSI versus EAL data, the two indicators of pavement performance (β and ρ) are obtained and tabulated in Table 2. Note that because of the considerable variation in the initial PSI values, the ρ values are estimated for various levels of PSI drop rather than for fixed values of terminal serviceability index. Also included in Table 2 are the type of base-course material, layer thickness, and structural number (SN) of each pavement section. SN is computed as follows:

$$SN = a_1H_1 + a_2H_2 + a_3H_3 \quad (4)$$

where H_1, H_2, and H_3 are the layer thickness (in inches) of the surface, base, and subbase, respectively; and a_1, a_2, and a_3 are the structural coefficients of the surface, base, and subbase, respectively. The structural coefficient values are obtained from Table 1.

The effect of SN on the PSI versus EAL relation can be described by available mathematical models such as the AASHO performance model (2), modified Highway Research Board (HRB) model (13), and Painter's model (14). The AASHO model is given by the following equation:

$$G/\beta = \log (EAL) - 9.36 \log (SN + 1) + \log R - 0.372 (S - 3.0) + 0.20 \quad (5)$$

where

$G = \log [(PSI_o - PSI)/(PSI_o - 1.5)]$, (5a)

PSI_o = initial PSI value,

$\beta = 0.40 + 1094(SN + 1)^{-5.19}$, (5b)

S = soil support value, and

R = regional factor.

Table 1 indicates that the subgrade soil at the Research Facility has a resilient modulus of 8000 psi. The soil support value that corresponds to this resilient modulus value is about 5.5 according to Van Til and others (1). The temperature and precipitation data at the Research Facility suggest a regional factor of 1.5. Incorporating these two values into Equation 5 yields the following equation:

$$G/\beta = \log (EAL) - 9.36 \log (SN + 1) - 0.554 \quad (6)$$

The PSI values predicted by using Equations 5a, 5b, and 6 are compared with the observed data in Figure 2. The comparison indicates that the prediction is quite good in the early stage of the pavement life. As the pavement becomes older, however, the AASHO model overpredicts pavement performance. This is in agreement with the recent findings of Darter (15).

The modified HRB performance model for flexible pavement is as follows:

$$\log (PSI_o/PSI) = EAL/[4D^8 (RS)^4] \quad (7)$$

where

$D = 0.54H_1 + 0.16r_2H_2 + 0.14H_3 + 1.00$, (7a)

r_2 = constant whose value depends on the type of base-course material, and

RS = relative strength that is used to consider the effect of regional factor; a factor of 1.5 is used in this analysis.

Painter's model relates PSI with EAL through the following equation:

$$\log (PSI_o/PSI) = F (EAL \times 10^{-6})/\log^{-1} D \quad (8)$$

where

$D = a_1H_1 + a_2H_2 + a_3H_3 - 1.52$, (8a)

and F is environmental factor; a value of 6 is used in this analysis. The predicted pavement performance by using the modified HRB and Painter's models is also shown in Figure 2. It is seen that Painter's model overpredicts performance more than the modified HRB model. Of the three performance models analyzed, the AASHO model appears to predict best, although it also overpredicts performance at the later stage of pavement life.

To improve the AASHO performance model, the pavement performance indicator (β value), which is tabulated in Table 2, is correlated with SN for all of the pavements analyzed. As shown in Figure 3, the correlation is well defined. From this correlation, the following equation is obtained:

$$\beta = 0.12 + 31.62 (SN + 1)^{-1.92} \quad (9)$$

The number of EALs (in millions) required for various levels of PSI drop (ΔPSI) tabulated in Table 2 is also correlated in Figure 4. The values of r^2 range from 0.88 to 0.95. These correlations give the following equations. For $\Delta PSI = 0.5$,

$$EAL = 2.94 \times 10^{-4} (SN + 1)^{5.42} \quad (10)$$

For $\Delta PSI = 1.0$,

$$EAL = 3.78 \times 10^{-4} (SN + 1)^{5.45} \quad (11)$$

For $\Delta PSI = 1.5$,

$$EAL = 2.23 \times 10^{-4} (SN + 1)^{6.02} \quad (12)$$

And for $\Delta PSI = 2.0$,

$$EAL = 1.06 \times 10^{-4} (SN + 1)^{6.67} \quad (13)$$

By using Equations 10 through 13, it will be possible to predict the number of EALs (in millions) required to produce a certain level of PSI drop for a given SN value. Conversely, the value of SN required to withstand a predetermined EAL can also be determined. For example, to limit PSI drop at 2 million EALs within 0.5, 1.0, 1.5, and 2.0, the pavement must have SN values of at least 4.1, 3.8, 3.5, and 3.4, respectively.

ROUGHNESS, RUTTING, AND CRACKING

Three major modes of distress manifestation are longitudinal roughness, transverse rutting, and surface cracking. Cracking can be caused by loading, thermal stress, settlement, heaving, etc. However, only load-associated cracking is treated here. Table 3 summarizes roughness, rutting, and cracking data. From these data, relations between SN and each distress manifestation are established. These relations permit prediction of either the maximum EAL to produce certain levels of distress in a given pavement or the minimum SN value so that at certain EAL the distress will not exceed a predetermined level.

Figure 5 shows the relations between SN and EAL to cause two levels of roughness, namely, 10 and 30

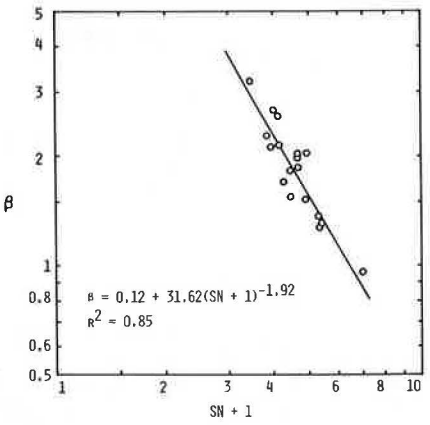

Figure 3. Pavement performance indicator (β) versus (SN + 1).

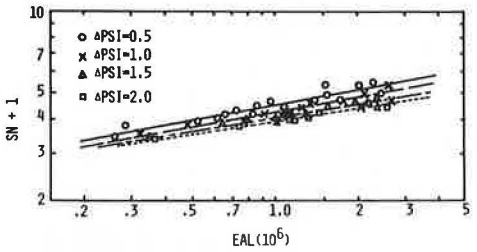

Figure 4. (SN + 1) versus EAL for four levels of PSI drop.

Table 3. Roughness, rut depth, and cracking data.

Section No.	SN	EAL (10^6) at R (in/mile) =			EAL (10^6) at RD (in) =			EAL (10^6) at C (ft^2/1000 ft^2) =		
		10	20	30	0.25	0.50	0.75	10	60	100
1b	4.30	0.92	1.80	-	1.69	-	-	-	-	-
1c	3.64	0.60	1.45	-	1.45	-	-	-	-	-
1d	3.42	0.51	1.03	1.56	1.14	1.82	2.39	1.80	-	-
2	3.90	1.10	-	-	1.68	-	-	-	-	-
3	3.66	0.70	1.29	1.58	1.41	1.93	2.27	1.26	1.80	2.15
4	5.98	1.53	-	-	2.33	-	-	-	-	-
5	3.90	0.40	0.64	0.78	1.12	1.89	2.34	2.40	-	-
6	4.38	1.54	-	-	1.60	2.53	-	-	-	-
7	4.34	0.52	1.11	1.92	1.49	2.47	-	-	-	-
8	2.94	0.13	0.27	0.40	0.63	0.95	1.17	0.39	0.98	-
9	3.26	0.23	0.49	0.82	0.56	1.02	1.40	1.04	1.31	1.46
A	3.18	0.40	0.64	0.78	0.76	1.12	1.31	1.13	1.22	-
B	3.66	0.69	0.95	1.14	1.72	-	-	-	-	-
C	3.12	0.65	0.88	1.02	0.88	1.21	1.39	1.21	1.27	1.30
D	3.00	0.47	0.65	0.76	0.80	1.14	1.26	0.75	1.20	1.23
E	2.86	0.15	0.35	0.52	0.18	0.49	0.74	0.61	0.65	0.66
H	2.41	0.13	0.21	0.27	0.29	0.32	0.35	0.36	-	-
14	3.46	0.16	0.33	0.50	1.20	1.61	-	1.00	1.35	1.50

Figure 5. (SN + 1) versus EAL for two levels of roughness.

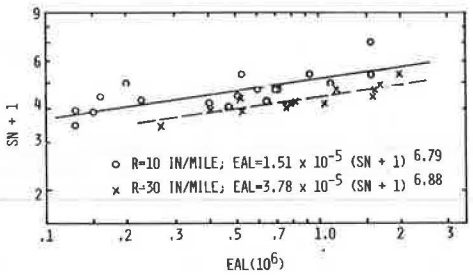

Figure 6. (SN + 1) versus EAL for three levels of rutting.

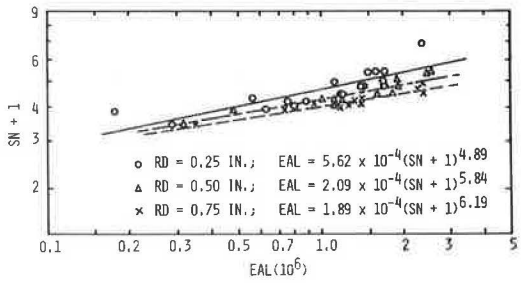

in/mile. Data points are somewhat scattered, but the trend is very clear. The values of r^2 are 0.83 and 0.90 for 10 and 30 in/mile, respectively. Equations for the two relations are given in the figure. The data indicate that, for a pavement with an SN equal to 3.5, roughness will reach 10 and 30 in/mile at an EAL of about 0.86 and 2.5 millions, respectively. Also, for a pavement to withstand 2.0 million EALs without roughness exceeding 10 and 30 in/mile, the minimum values of SN required will be about 4.6 and 3.9, respectively.

The relations between SN and EAL to cause three levels of rutting are shown in Figure 6. Equations that relate SN and EAL are given in the figure. According to this figure, for a pavement that has an SN equal to 3.5, the amount of rutting will reach 0.25, 0.50, and 0.75 in at EALs of about 0.9, 1.4, and 2.1 millions, respectively. Further, the minimum values of SN for pavements to withstand 2.0 million EALs with maximum rutting of 0.25, 0.50, and 0.75 in are about 4.4, 3.9, and 3.5, respectively.

Figure 7. (SN + 1) versus EAL for two levels of surface cracking.

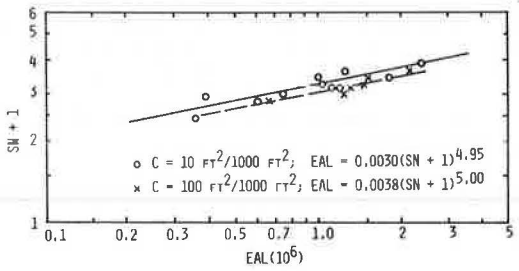

Figure 7 relates the SN and EAL required to cause two levels of cracking intensity--10 and 100 ft^2/1000 ft^2. From this relation, to limit cracking intensity within 100 ft^2/1000 ft^2 at the end of 2.0 million EALs, the SN of the pavement must be at least 2.5. For this SN value, surface cracking of 10 ft^2/1000 ft^2 will develop at EAL of about 1.5 million.

PAVEMENT RESPONSE

Critical response data, including maximum surface deflection, maximum compressive strain at the top of the subgrade, and maximum tensile strain at the bottom of the stabilized layer, are tabulated in Table 4. These critical response data were obtained from an analysis that was made by using an elastic-layer computer program together with the elastic properties tabulated in Table 1. The computer program used was the Bitumen Structures Analysis in Roads (BISAR) that was developed at Koninklijke/Shell Laboratorium in Amsterdam, The Netherlands. The traffic loading used in the analysis was an 18-kip EAL on dual wheels that had a tire pressure of 80 lbf/in^2.

The initial maximum surface deflections analyzed are in good agreement with the measured maximum Benkelman beam deflections. These deflection data are correlated with SN values in Figure 8. Two distinct relations result: one for pavements that contain bituminous concrete, crushed stone, and aggregate bituminous base, and the other for pavements with aggregate cement and aggregate-lime-pozzolan base. The r^2-value of the correlation for the aggregate cement and aggregate-lime-pozzolan pavements is 0.80 and that for the other pavements is 0.92. For a given value of SN, the deflection is

Table 4. Maximum deflection, compressive subgrade strain, and tensile strain data.

Section No.	SN	Initial Maximum Deflection (10^{-3} in)	Maximum Compressive Strain (10^{-6})	Maximum Tensile Strain (10^{-6})
1b	4.30	15.8	294.2	85.1
1c	3.64	23.0	426.6	100.2
1d	3.42	28.0	483.0	109.5
2	3.90	21.5	383.6	89.6
3	3.66	9.0	142.8	41.1
4	5.98	6.5	107.5	28.5
5	3.90	21.0	403.0	165.0
6	4.38	15.0	291.6	70.9
7	4.34	19.0	322.4	84.6
8	2.94	39.0	594.0	139.0
9	3.26	29.0	525.8	122.7
A	3.18	14.0	288.0	65.0
B	3.66	7.5	171.5	42.2
C	3.12	15.0	185.5	46.1
D	3.00	15.0	216.0	54.4
E	2.86	31.0	575.4	279.4[a]
H	2.41	40.0	844.8	209.1
14	3.46	35.0	390.9	118.1

[a]For section E, which has a crushed-stone base, maximum tensile strain at bottom of the surface layer is used.

Figure 8. Maximum surface deflection versus (SN + 1).

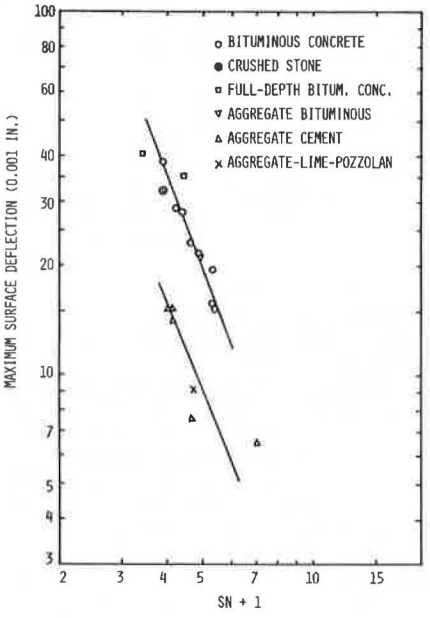

smaller for aggregate cement and aggregate-lime-pozzolan pavements than the other pavements. This is as would be expected, since aggregate cement and aggregate-lime-pozzolan have higher moduli than the other base-course materials, as shown in Table 1. Under the same intensity of loading, surface deflection decreases with increasing layer modulus value.

According to the relations in Figure 8, maximum surface deflection can be related with SN by the following equations. For pavements that contain bituminous concrete, crushed stone, and aggregate-bituminous base,

$$\delta = 0.85 + 1287.30\,(SN + 1)^{-2.58} \quad (14)$$

And for pavements with aggregate cement and aggregate-lime-pozzolan base,

$$\delta = 0.24 + 544.80\,(SN + 1)^{-2.58} \quad (15)$$

where δ is the maximum surface deflection (0.001 in). Equations 14 and 15 may be combined with Equations 10 through 13 to form relations between maximum surface deflections and EAL (in millions) required to cause predetermined PSI drops. These equations are as follows. For $\Delta PSI = 0.5$,

Bituminous concrete pavements: $EAL = 996.95\,(\delta + 0.85)^{-2.10}$ (16)

Aggregate cement pavements: $EAL = 163.85\,(\delta - 0.24)^{-2.10}$ (16a)

For $\Delta PSI = 1.0$,

Bituminous concrete pavements: $EAL = 1377.05\,(\delta + 0.85)^{-2.11}$ (17)

Aggregate cement pavements: $EAL = 224.36\,(\delta - 0.24)^{-2.11}$ (17a)

For $\Delta PSI = 1.5$,

Bituminous concrete pavements: $EAL = 3925.18\,(\delta + 0.85)^{-2.33}$ (18)

Aggregate cement pavements: $EAL = 529.34\,(\delta - 0.24)^{-2.33}$ (18a)

And for $\Delta PSI = 2.0$,

Bituminous concrete pavements: $EAL = 12\,005.39\,(\delta + 0.85)^{-2.59}$ (19)

Aggregate cement pavements: $EAL = 1294.67\,(\delta - 0.24)^{-2.59}$ (19a)

By using Equations 16 through 19a, it would be possible to estimate the EAL required to cause various levels of PSI drop for flexible pavements with different base-course materials.

The maximum strain data in Table 4 are correlated with SN in Figures 9 (compressive strain) and 10 (tensile strain). It is seen that the correlation for maximum compressive strain is much better than that for maximum tensile strain. The r^2-values for compressive strain correlations are 0.96 and 0.82 for bituminous concrete pavements and aggregate cement pavements, respectively. The equations of the correlations are as follows. For pavements with bituminous concrete, crushed stone, and aggregate-bituminous base,

$$\epsilon_v = 14.81 + 14\,805.05\,(SN + 1)^{-2.305} \quad (20)$$

And for pavements with aggregate cement and aggregate-lime-pozzolan base,

$$\epsilon_v = 5.50 + 3318.0\,(SN + 1)^{-1.875} \quad (20a)$$

In Equations 20 and 20a, ϵ_v is the maximum compressive strain (in millionths).

A comparison of Figure 8 with Figure 9 indicates that the correlation between the maximum compressive strain and SN is slightly better than the surface deflection versus SN correlation. By combining Equations 20 and 20a with Equations 10 through 13, relations between compressive strain and EAL will result. These relations permit prediction of EAL for various levels of ΔPSI from known compressive strains. It is interesting to note that Luhr and McCullough (16) also found that compressive strain gives a slightly better prediction of pavement performance. Although the maximum compressive strain is a better performance predictor than the maximum deflection, the use of the predicting equations usually requires an elastic-layer analysis to obtain compressive strain as input data. When only surface deflection data are available, it is more convenient to use Equations 16 through 19 to estimate pavement performance.

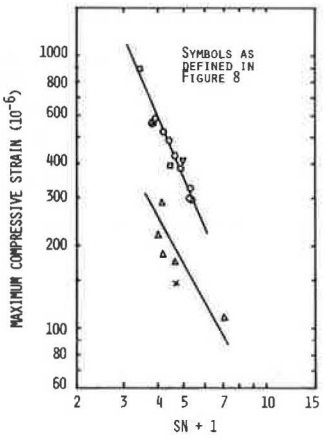

Figure 9. Maximum compressive strain at top of subgrade versus (SN + 1).

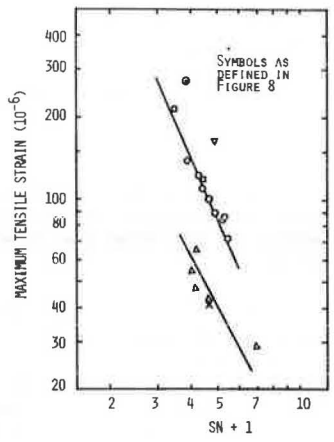

Figure 10. Maximum tensile strain at bottom of stabilized base versus (SN + 1).

SUMMARY AND CONCLUSIONS

The performance of experimental pavements at the Pennsylvania Transportation Research Facility was evaluated. Data analyzed were pavement serviceability index and three distress manifestations--roughness, rutting, and cracking. Some existing pavement performance models were evaluated by using the performance data; those evaluated were AASHO, modified HRB, and Painter's models.

The performance data indicate that the trend of serviceability index loss with increasing EAL follows the power function developed at the AASHO Road Test. Of the three performance models evaluated, the AASHO model appears to predict best, although it overpredicts pavement service life. By using a curve-fitting process and regression analysis, equations that relate pavement performance with SN, distress with SN, and performance with critical response are developed. These equations may be used to predict pavement performance from SN or critical pavement response.

ACKNOWLEDGMENT

The paper presented here is a part of the research project, A Study of Flexible Pavement Base Courses and Overlay Designs, sponsored by PennDOT in cooperation with the Federal Highway Administration (FHWA), U.S. Department of Transportation. Their support is gratefully acknowledged. The field data reported here were collected and reduced with the assistance of W.P. Kilareski, S.A. Kutz, B.A. Anani, R.P. Anderson, P.J. Kersavage, and Johannes Karundeng. This paper represents my views and does not necessarily reflect those of PennDOT or FHWA.

REFERENCES

1. C.J. Van Til, B.F. McCullough, B.A. Vallerga, and R.G. Hicks. Evaluation of AASHO Interim Guides for Design of Pavement Structures. NCHRP, Rept. 128, 1972.
2. AASHO Interim Guide for Design of Pavement Structures, 1972. AASHO, Washington, DC, 1972.
3. E.S. Lindow, W.P. Kilareski, G.Q. Bass, and T.D. Larson. Construction, Instrumentation, and Operation: Vol. 2, Interim Report on an Evaluation of Pennsylvania's Flexible Pavement Design Methodology. Pennsylvania Transportation Institute, Pennsylvania State Univ., University Park, Rept. PTI 7504, Feb. 1973.
4. W.P. Kilareski, S.A. Kutz, and G. Cumberledge. Modification, Construction, and Instrumentation of an Experimental Highway, Interim Report on a Study of Flexible Pavement Base Course and Overlay Design. Pennsylvania Transportation Institute, Pennsylvania State Univ., University Park, Rept. PTI 7607, April 1976.
5. K. Nair, W.S. Smith, and C.Y. Chang. Characterization of Asphalt Concrete and Cement-Treated Granular Base Course, Final Report. FHWA, Feb. 1972.
6. S. Kolis and R.I.T. Williams. Cement-Bound Road Materials: Strength and Elastic Properties Measured in the Laboratory. Transport and Road Research Laboratory, Crowthorne, Berkshire, England, TRRL Supplementary Rept. 334, 1978.
7. Lime-Fly Ash-Stabilized Bases and Subbases. NCHRP, Synthesis of Highway Practice 37, 1976.
8. M.G. Sharma and T.D. Larson. The Pennsylvania Pavement Research Facility: Vol. 4, Mechanical Characterization of Materials. Pennsylvania Transportation Institute, Pennsylvania State Univ., University Park, Interim Rept. PTI 7509, Aug. 1974.
9. M.C. Wang and T.D. Larson. Evaluation of Structural Coefficients of Stabilized Base-Course Materials. TRB, Transportation Research Record 725, 1979, pp. 58-67.
10. J.G. Hopkins. Pavement Roughness and Serviceability, Final Report. Bureau of Materials, Testing, and Research, Pennsylvania Department of Transportation, Harrisburg, Aug. 1975.
11. W.P. Kilareski, B. Anani, R.P. Anderson, M.C. Wang, and T.D. Larson. Remaining Life and Overlay Thickness Design for Modified Flexible Pavements. Pennsylvania Transportation Institute, Pennsylvania State Univ., University Park, Interim Rept. PTI 7905, Jan. 1979.
12. The AASHO Road Test: Report 5, Pavement Research. HRB, Special Rept. 61E, 1962.
13. P.E. Irick and W.R. Hudson. Guidelines for Satellite Studies of Pavement Performance. NCHRP, Rept. 2A, 1964.
14. L.J. Painter. Analysis of AASHO Road Test Data by the Asphalt Institute. Proc., International Conference on Structural Design of Asphalt Pavements, Univ. of Michigan, Ann Arbor, 1962, pp. 84-97.
15. M.I. Darter. Requirements for Reliable Predictive Pavement Models. TRB, Transportation Research Record 766, 1980, pp. 25-31.
16. D.R. Luhr and B.F. McCullough. Development of a Rationally Based AASHO Road Test Algorithm. TRB, Transportation Research Record 766, 1980, pp. 10-17.

Publication of this paper sponsored by Committee on Flexible Pavement Design.

Measurement and Prediction of Forward Movement and Rutting in Pavements Under Repetitive Wheel Loads

W.O. YANDELL

A three-dimensional mechano-lattice stress-strain analysis has been used to predict rutting and permanent forward displacement behavior of pavements subjected to 14 630 one-directional passes of a 226-kg (500-lb) loaded pneumatic tire under very well-controlled conditions. The two pavement sections tested consisted of crushed prospect dolerite with 10 percent clay, each placed in an indoor test track with different compactive efforts and moisture contents and a thin coating of bituminous materials. The favorable comparisons between these predictions and the measured values seem to support the mechano-lattice analysis as a pavement analysis tool.

I have been encouraged, particularly by C. L. Monismith, to compare predictions made with his mechano-lattice stress-strain analysis on pavement behavior with well-controlled practical tests. The accuracy of the mechano-lattice analysis as applied to the more complex problems of hysteretic friction has been amply verified (1-3). In this paper, the findings of the very precise repeated-rolling tests on the Sydney Test Track carried out by Sparks (4) are compared with mechano-lattice predictions. Such one-directional rolling tests of high precision are expensive and rare.

The theory of linearized elasticity has been used successfully to develop relatively rational flexible pavement design techniques. The Shell method is a good example. However, it has become apparent that a stress-strain analysis that more closely simulates pavement material behavior would allow more rigorous and reliable failure predictions. It is for this reason that I have introduced a version of the mechano-lattice analysis that simulates repeated rolling of elastoplastic materials (5-7).

SYDNEY TEST TRACK EXPERIMENTS

The Sydney Test Track was designed by Taylor in 1966 (8) with subsequent development from Sparks and Lee (9) to investigate the phenomenological aspects of flexible pavement behavior. It consists of a 25-cm (10-in) diameter loaded pneumatic tire repeatedly rolling in one direction along a test bed 4.87 m (24 ft) long by 0.91 m (3 ft) wide. Pavement structures of any thickness can be simulated by adjusting the level of the rigid base supports in each of the four 1.22-m (4-ft) long bays. The drawn rolling tire can be caused to execute lateral departures from the centerline according to any desired standard deviation.

The test sections were 15.24-cm (6-in) thick pavements compacted on a rigid foundation. The behavior of the pavements in bays 3 and 4 was simulated by the mechano-lattice analysis. These test sections consisted of crushed dolerite with 10 percent clay compacted with vibrating hammers to the dry densities, California bearing ratio (CBR) values, and moisture contents indicated in the table below (note, 1 kg/m³ = 0.062 lb/ft³):

			Optimum		
Bay	CBR (%)	Dry Density (kg/m³)	Moisture Content (%)	Dry Density (kg/m³)	(%)
3	80	6.9	6.5-6	7.0	7
4	35	6.1	5.5-5	6.7	8.5

The 227-kg (500-lb) loaded tire with a contact pressure of 690 kPa (100 psi) and a contact area of 32 cm² (5 in²) was caused to perform the normal distribution of lateral departures as repeated rolling progressed, as shown in Figure 1 by the smooth curve.

The surfaces of the test pavements were thinly coated with bituminous material, and targets were fixed to various places on the surface to enable a vernier-driven microscope to measure the lateral, longitudinal, and vertical movements of the surface at various stages throughout the test.

After the pavements were placed, two repeated-load bearing tests, each for five load repetitions, were carried out on each of the bays. These were used in this paper to determine the material properties. The results are shown in Figures 2 and 3. The rutting and permanent horizontal movement behavior was recorded throughout 14 630 one-directional passes of the loaded tire. All the information regarding these experiments was obtained from Sparks (4). Some of the same information is available elsewhere (9).

MECHANO-LATTICE ANALYSIS PREDICTION

The mechano-lattice stress-strain analysis, which

Figure 1. Lateral departures of wheel passes from centerline and approximation for mathematical prediction.

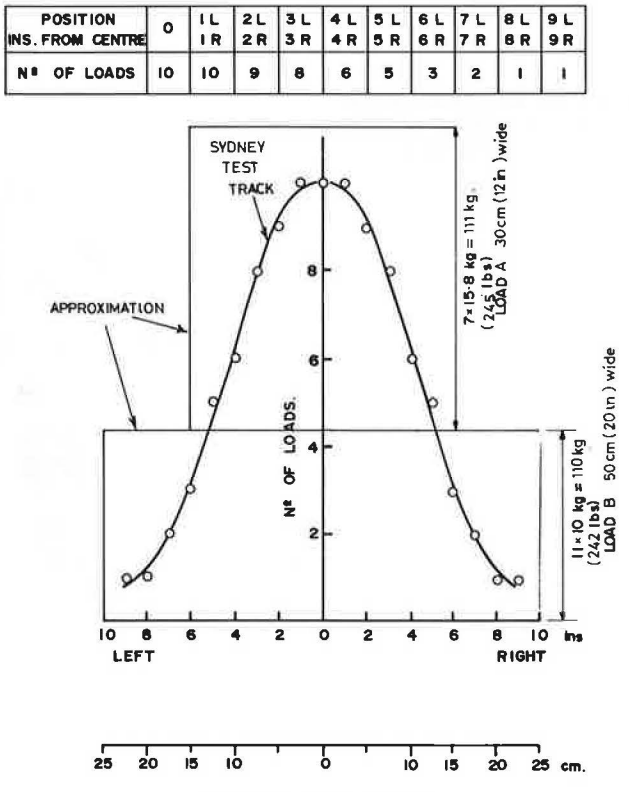

has been described elsewhere (1,5-7), is a type of mechanized finite-element analysis that was devised to simulate nonlinear and energy-absorbing materials, including elastoplastic materials.

Figure 4 shows how one of the bays in the Sydney Test Track experiment is simulated by an assembly of mechano-lattice units. One of the units is shown in the inset. The lattice unit simulates a cube of the elastoplastic road material. A unit consists of 24 elements, each of which has a larger loading to unloading compliance. This gives the simulated material the property of elastoplasticity, such that when one unit is loaded and unloaded, a residual deformation will result. When the units are connected (as shown in Figure 4) by frictionless joints at their corners, the stress-strain history of each element of each unit is taken into account as it, in simulation, moves toward, under, and away from the

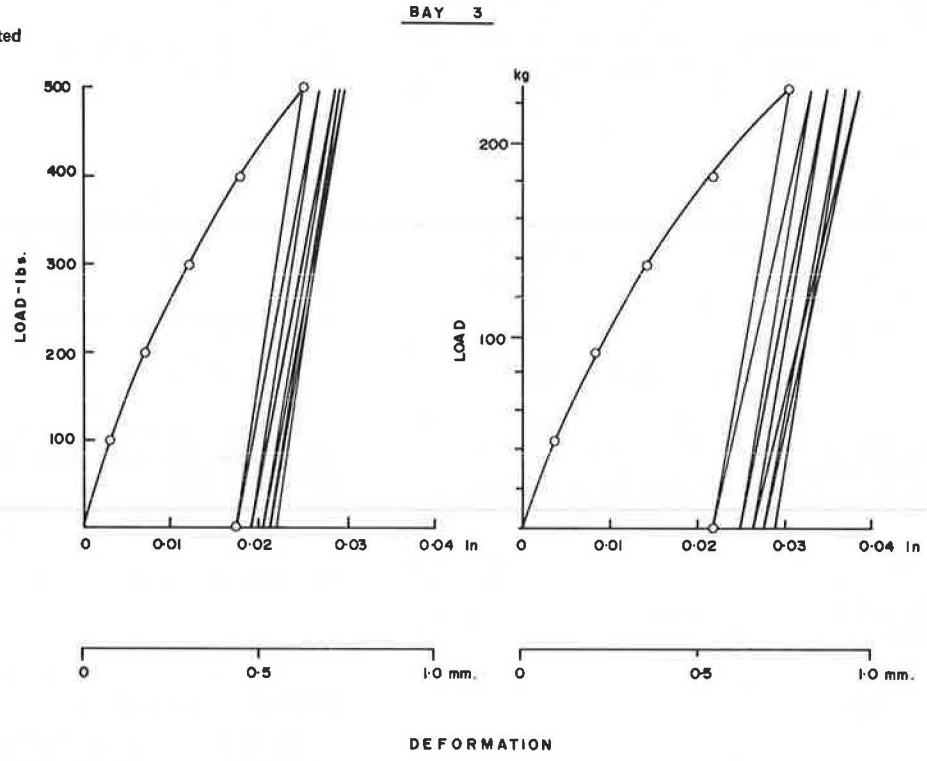

Figure 2. Load deflection results for repeated-load bearing test on compacted but untrafficked material in bay 3.

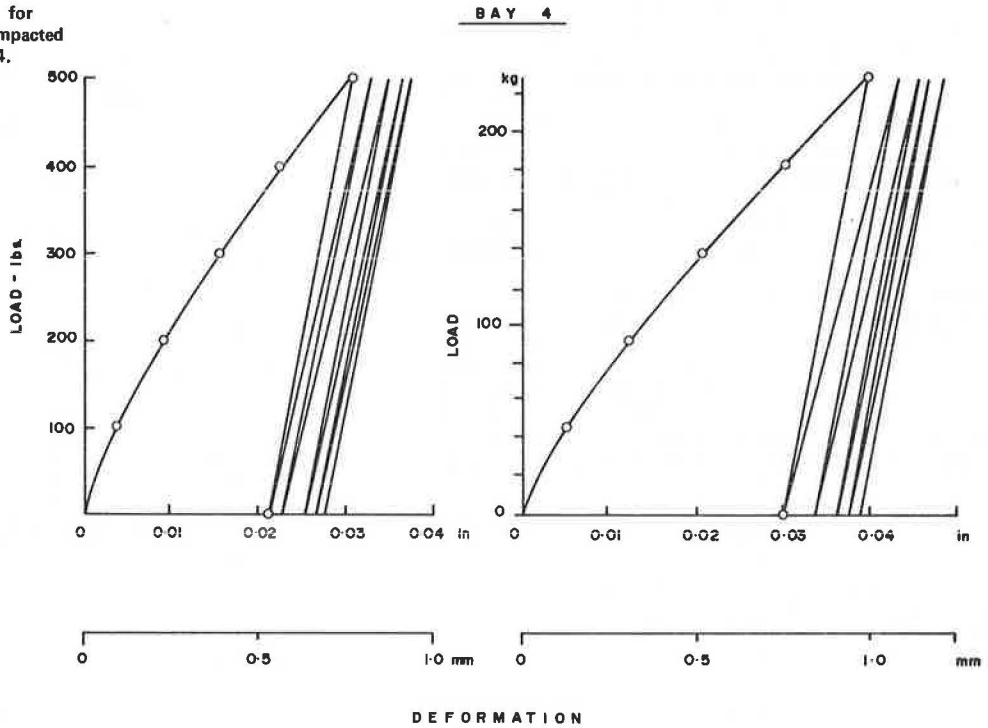

Figure 3. Load deflection results for repeated-load bearing tests on compacted but untrafficked material in bay 4.

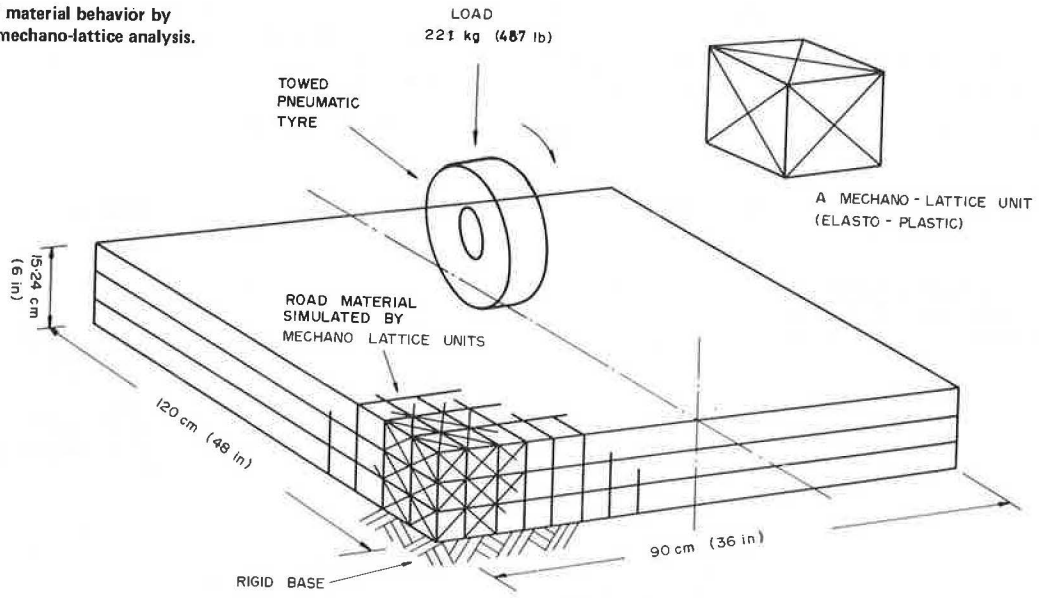

Figure 4. Simulation of material behavior by elastoplastic version of mechano-lattice analysis.

wheel load. The requirements of continuity and equilibrium are maintained in this rigorous method. The load in each diagonal and rectalinear element is determined by its length, stiffness, previous loading history, and whether its load is increasing or decreasing. The joints are moved in the direction of their unbalanced forces until equilibrium is achieved.

ROLLING RESISTANCE

To make the simulation realistic, it is necessary to take into account the fact that the test wheel is being drawn and not torque driven. Therefore, the rolling resistance will lead to a horizontal force that acts on the surface of the pavement in the direction of the wheel motion. It was assumed that such a force, which amounts to 10 percent of the normal load, should account for the rolling resistance emanating from both the road material and from the pneumatic tire. In order to show its differing effects on permanent forward movement, one case for a torque-driven wheel was also computed.

SIMULATING WHEEL LOADS

As mentioned earlier, the 5-cm (2-in) wide rolling wheel tracks sequentially about the centerline with a normal distribution. One hundred wheel passes gives one normally distributed coverage of 227-kg loads. This is possible to simulate on the computer, but it would be quite expensive. The compromise used was to simulate one-hundredth of the effect of one, 100 pass coverage by one pass of a symmetric 30-cm (12-in) wide, 111-kg (245-lb) load, called load A, plus one pass of a symmetric 50-cm (20-in) wide, 110-kg (242-lb) load, called load B, as shown in Figure 1. The contact pressures exerted by these two loads are 69 and 41 kPa (10 and 6 psi), respectively. The stress-strain behavior of the road material is elastoplastic, as shown in the inset of Figure 5, so this reduction in contact pressure by a factor of 10 will not alter the permanent deformational behavior. However, this would not be the case with an elastic perfectly plastic material or if the curved relations of the bearing tests (Figures 2 and 3) were used instead of the straight-lined assumption that appears in the inset of Figure 5 (as explained later). The above simplification would reduce resistance to rutting by a small amount due to the greater lateral shearing caused by the concentrated load of the narrow pneumatic tire compared with the wide contact region of the computer-simulated traveling load. The relatively high Poisson's ratio (0.40) would reduce this effect; however, in addition, the simulated load, being 3 percent lower than the test load, should cause, for example, a rutting underestimation of 3 percent.

REPEATED-BEARING TESTS

It is more usual to obtain the properties of a road material for life-prediction purposes by mechano-lattice analysis from repeated-load triaxial tests. However, the only information available is that of the bearing tests, the results of which are shown in Figures 2 and 3. These give surface deflection versus load for five load repetitions.

It is unfortunate that the repeated-bearing tests were not continued to a greater number of repetitions but, as can be seen in Figure 5, the sets of five points plot very nearly to parallel straight lines on the log-log plot of permanent strain versus load repetitions. There is no indication of the curvature that often, but not always, occurs as convex upward in repeated-load triaxial tests. It was therefore considered reasonable to extrapolate the straight lines to the 15 000 load repetitions necessary, as shown in Figure 5. For permanent deformation prediction purposes, the pairs of test results were averaged on the plot for 300, 800, 1800, 3800, 7300, and 14 630 wheel passes. It is necessary to the operation of the mechano-lattice analysis to transform this information to that that would emanate from a triaxial test on the same material. From the knowledge that the 227-kg loaded tire was applied to the 15.24-cm (6-in) thick pavement surface, the Young's modulus of the material in bay 3 (by using linear-elastic theory) was 70 MPa (9941 psi) and that in bay 4 was 60 MPa (8450 psi), as was the average material permanent strain equal to 0.21 of the surface deflection in centimeters (0.54 of the surface deflection in inches). The average vertical stress was calculated to be 280 kPa (40 psi). It was convenient to set the calculating unloading modulus at 105 MPa (15 000 psi). Thus, one load-unload of a simulated triaxial test would

leave a residual strain of 0.002 (see inset in Figure 5).

Thus to obtain a prediction of the rutting after n passes, one uses the following expression:

$(\epsilon_n/0.0020)$ x rut depth from one calculation pass of mechano-lattice analysis

where ϵ_n is the cumulative axial strain from the hypothetical repeated-load triaxial test as transformed from the bearing tests depicted in Figure 5. A similar expression was used for predicting forward movement.

DISCUSSION OF RESULTS

Rutting

Figures 6 and 7 show a comparison of rutting predic-

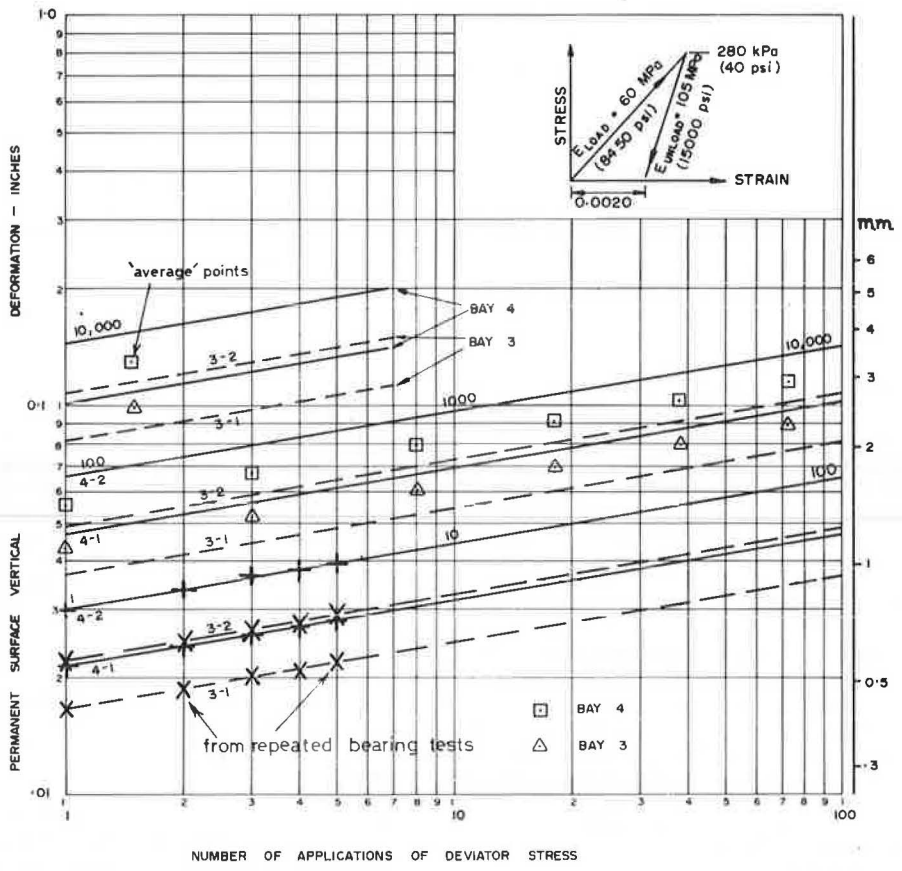

Figure 5. Extrapolation of bearing tests up to 15 000 load repetitions and load-unload hysteresis loop from a simulated triaxial test of material in bay 4.

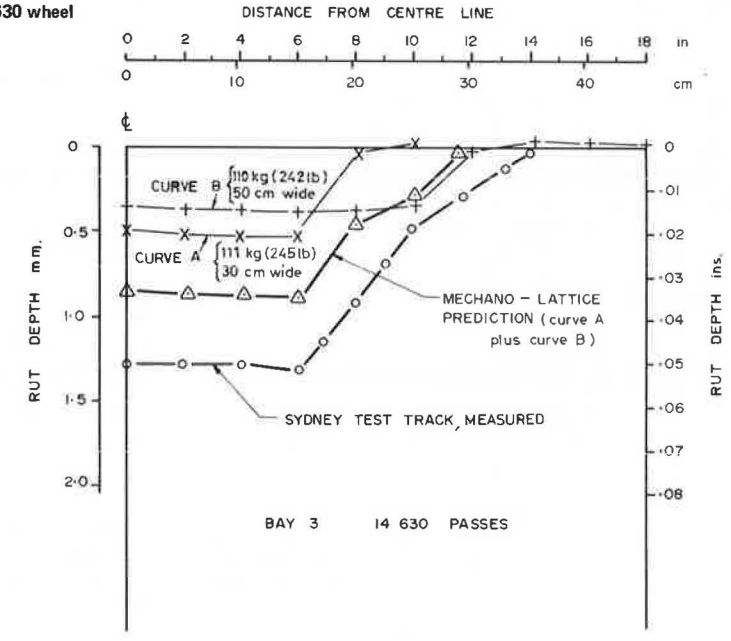

Figure 6. Measured and predicted rutting in bay 3 after 14 630 wheel passes.

tion with measurement after 14 630 passes of a 227-kg load in the central sections of bays 3 and 4, respectively. The individual effects of the 30-cm-wide, 111-kg load pass (curve A, Figure 6) and the 50-cm-wide, 110-kg load pass (curve B, Figure 6) are added to give the predicted rut shape shown. The prediction for bay 4 is very close. The comparison of rut prediction and measurement from 100 passes to 14 630 passes is shown in Figure 8. The trends are close--a fact that shows the close relation between the bearing tests and the rather lengthy repeated-rolling tests. It should be realized that the extrapolated bearing tests account for the natural decrease in plasticity with repeated loading. If the extrapolations of Figure 5 are correct, the plastic strain reduces from about 2×10^{-2} mm/mm per cycle down to 7×10^{-6} per cycle at 14 000 repetitions.

Forward Movement

The forward-movement prediction is not as successful as that of rutting, as shown in Figures 9 and 10. In bay 4, the material away from the centerline is moving in the opposite direction to the travel. The 10 percent imposed rolling resistance in the prediction is entirely responsible for the central forward movement. This can be observed in Figure 10 by comparing curve A_1 with A_2. Curve A_2 is the predicted horizontal movement of the surface at 14 630 passes without net rolling resistance (i.e., the wheel is torque driven) for the 30-cm-wide, 111-kg load.

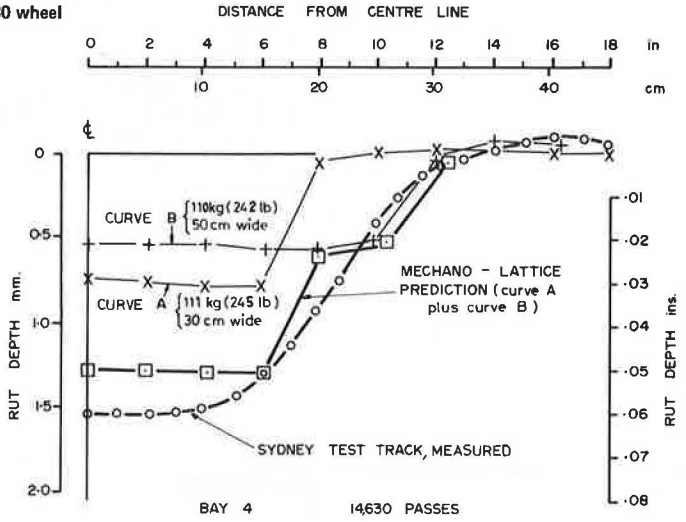

Figure 7. Measured and predicted rutting in bay 4 after 14 630 wheel passes.

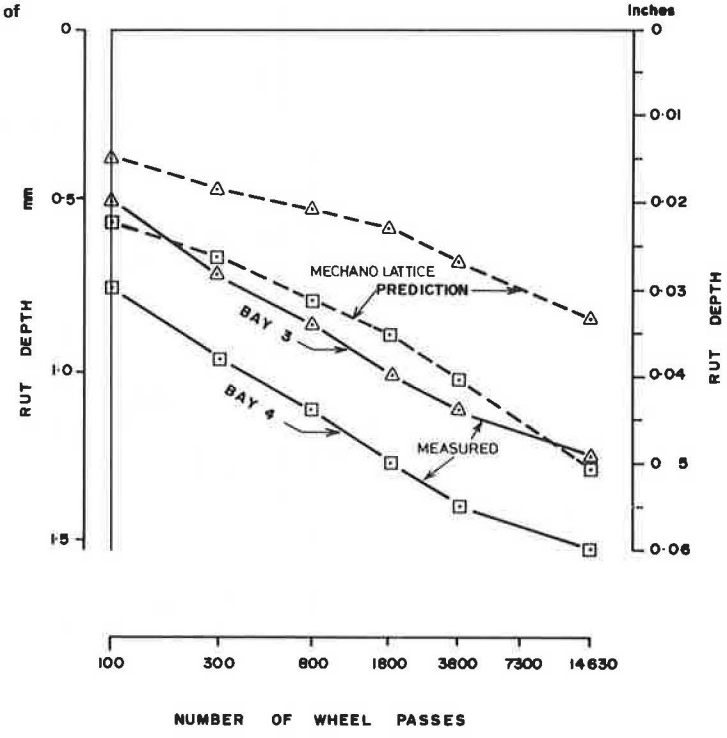

Figure 8. Measured and predicted rut invert depth over the range of 100 to 14 630 wheel passes for bays 3 and 4.

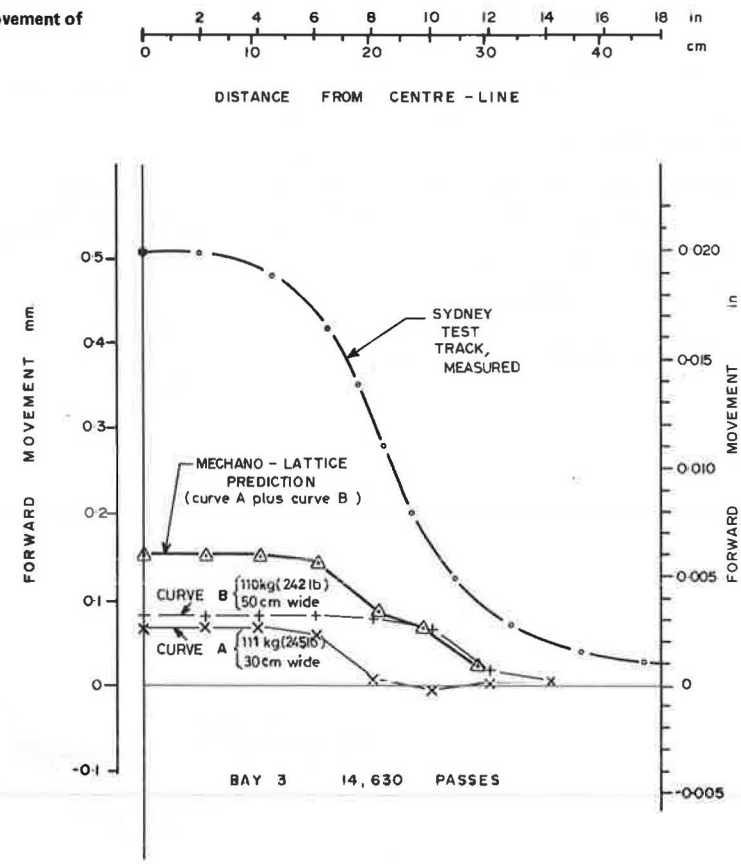

Figure 9. Measured and predicted forward surface movement of material in bay 3.

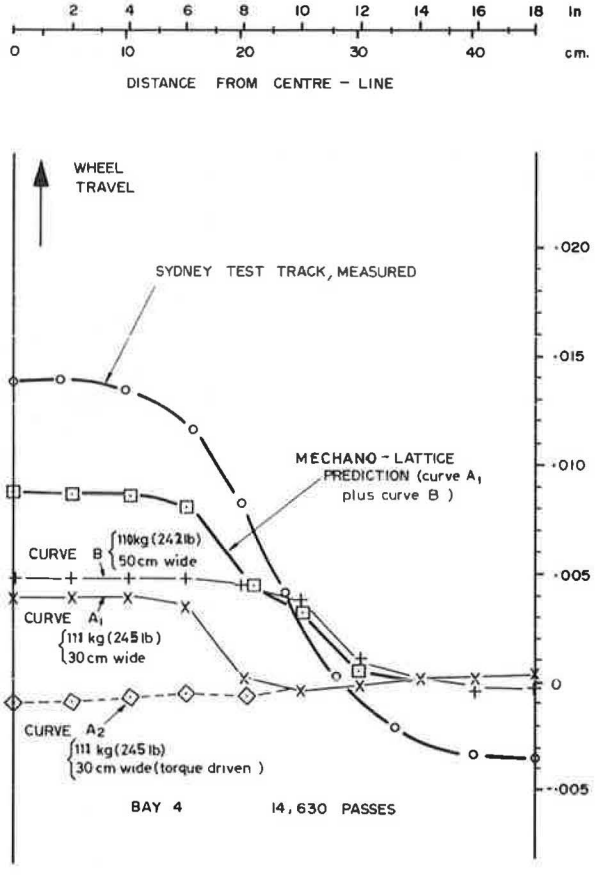

Figure 10. Measured and predicted forward surface movement of material in bay 4.

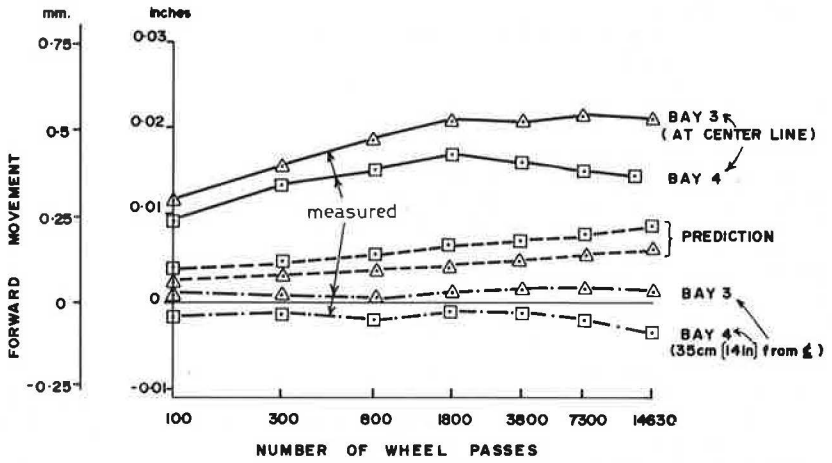

Figure 11. Measured and predicted forward surface movement over range of 100 to 14 630 wheel passes for bays 3 and 4.

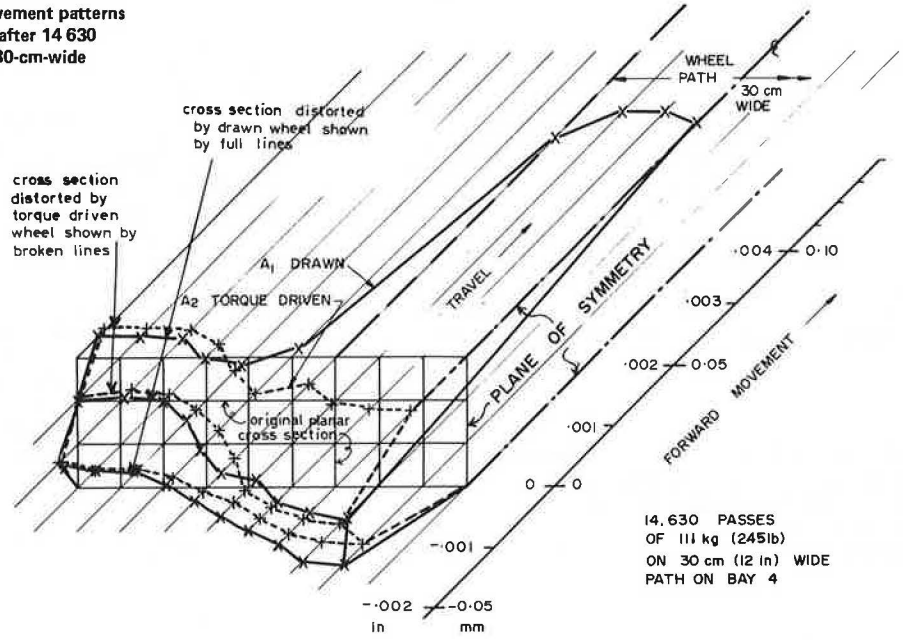

Figure 12. Predicted horizontal movement patterns for drawn and torque-driven wheels after 14 630 passes of 113-kg loaded wheel on a 30-cm-wide wheel path.

The horizontal movement of the surface trend for 100 to 14 630 passes is shown in Figure 11. Although the trends of the predictions are reasonably close to the measurement, the magnitude falls short of the measurement. A possible explanation for this can be given with reference to Figure 12. This figure shows the calculated horizontal movements of half an initially vertical cross-sectional plane after 14 630 passes of the symmetric 30-cm-wide, 111-kg load on bay 4. The full lines, curve A_1, indicate the movements associated with the tire that has a 10 percent rolling resistance (drawn). The broken lines, curve A_2, indicate the movements associated with a tire that has no net rolling resistance (torque driven). It is immediately apparent that the bulk of the material movement is opposed to the direction of wheel travel in both cases. It is only the surface material in contact with the wheel that is pushed forward in the case of the drawn wheel. The thinness of this predicted movement is limited by the coarseness of the mechano-lattice grid. If six layers of units were used instead of three in the prediction, it is obvious that a thinner layer would extend twice as far in the direction of wheel travel and thereby come closer to the actual performance.

Drawn and Torque Driven

Curves A_1 and A_2 show the difference between the effects of drawn (from the axle) and torque-driven wheels. Although deeper material will flow in the opposite direction to wheel travel, in both cases the drawn wheel will cause the material on the surface to move in the direction of travel. This was predicted and demonstrated on a miniature test in 1971 (5) in plane strain situations. This phenomenon also supports the practice of pavement engineers to have the forward wheel, on the first passes of a roller, torque driven. The trailing drawn wheel then moves the surface material forward while the torque-driven front wheel moves it backward, thereby preventing cracks from forming between the rollers and also preventing bow waves.

CONCLUSION

The prediction of rutting on a single layered pavement resting on a rigid foundation has been surprisingly accurate in view of the fact that only five load repetitions were used in the four material tests. However, if the straight-line extrapolation should instead have curved downward to some extent,

the calculated prediction would have fallen farther short of the measured values. These findings not only seem to support the validity of the elastoplastic material-simulating version of the mechano-lattice analysis, but also support the practical and theoretical work reported in 1971 (5). The dependence of horizontal flow on material properties indicates that nonhomogeniety in pavement materials can lead to lateral cracks and build up humps due to variable horizontal flow rate per wheel pass. It is believed that closer agreement of forward-movement prediction with practice would have been achieved had a finer mechano-lattice grid been used. I have analyzed many multilayered pavements by using the above method at a cost of $40/calculation pass ($1 Australian = $1.14 U.S.). This makes life predictions for as little as $160 possible.

The Sydney Test Track is being prepared for precise verification of mechano-lattice analysis of multilayered flexible pavements. However, some verification has already been achieved on real roads in less well-controlled conditions than the Sydney Test Track (7,10,11).

ACKNOWLEDGMENT

The theoretical work described here is sponsored by the Australian Research Grants Committee. The excellent practical tests conducted by Gene Sparks was supported by the Australian Road Research Board. I would like to thank Ian K. Lee, head of the Department of Civil Engineering Materials, for his continued support and good advice. I also appreciate the opportunity Bob Lytton of the Texas A&M University gave me to develop the three-dimensional version of this theoretical work while I was there in 1979.

REFERENCES

1. W.O. Yandell. A New Theory of Hysteretic Sliding Friction. WEAR, International Journal on the Science and Technology of Friction, Lubrication, and Wear, April 1971.
2. W.O. Yandell and L. Holla. Prediction of the Coefficient of Friction from Surface Texture Measurements. Proc., Seventh Australian Road Research Board Conference, 1974.
3. P. Taneerananon and W.O. Yandell. Micro-Texture Roughness Effect on Predicted Road-Tyre Friction in Wet Conditions. WEAR, International Journal on the Science and Technology of Friction, Lubrication, and Wear, Vol. 69, No. 3, 1981, pp. 321-337.
4. G.H. Sparks. Development and Use of a Machine for Examining the Behavior of Pavement Structures Under the Action of Moving Wheel Loads. Sydney Univ., Sydney, Australia, M. Eng. Sc. dissertation, March 1970.
5. W.O. Yandell. Prediction of the Behavior of Elastoplastic Roads during Repeated Rolling Using the Mechano-Lattice Analogy. HRB, Highway Research Record 374, 1971, pp. 29-41.
6. W.O. Yandell. The Influence of Residual Stresses and Strains on Fatigue Cracking. Transportation Division, ASCE (in preparation).
7. W.O. Yandell and R.L. Lytton. The Effect of Residual Stress and Strain Build Up in a Flexible Pavement by Repeated Rolling of a Tire. Texas Transportation Institute, Texas A&M Univ., College Station, Rept. RF 4087-1, Oct. 1979.
8. H. Taylor. The Design of a Road Base Test Track. Proc., Third Australian Road Research Board Conference, 1966.
9. G.H. Sparks, H. Taylor, and I.K. Lee. Development and Instrumentation of the Model Road Test Track at Sydney University. Fourth Australian Road Research Board Conference, Paper 487, 1968.
10. R. Chapman. Evaluation of Bottom Ash as a Pavement Material. School of Civil Engineering, Univ. of New South Wales, New South Wales, Australia, Master's dissertation, 1980.
11. W.O. Yandell and I.K. Lee. Applications of the Mechano-Lattice Analysis in Materials Engineering. Second Australian Conference on Engineering Materials, Sydney, July 6-8, 1981, pp. 401-422.

Publication of this paper sponsored by Committee on Strength and Deformation Characteristics of Pavement Sections.